12-2006

Modeling and Simulation of Friction-limited Continuously Variable Transmissions

Nilabh Srivastava
Clemson University, snilabh@clemson.edu

MODELING AND SIMULATION OF FRICTION-LIMITED CONTINUOUSLY VARIABLE TRANSMISSIONS

A Dissertation
Presented to
the Graduate School of
Clemson University

In Partial Fulfillment
of the Requirements for the Degree
Doctor of Philosophy
Mechanical Engineering

---

by
Nilabh Srivastava
December 2006

Accepted by:
Dr. Imtiaz Haque, Committee Chair
Dr. E. Harry Law
Dr. Cecil O. Huey Jr.
Dr. Nader Jalili

ABSTRACT

Over the last few decades, a lot of research effort has increasingly been directed towards developing vehicle transmissions that accomplish the government imperatives of increased vehicle efficiency and lower exhaust (greenhouse gaseous) emissions. These exhaust emissions can be regulated or lowered by increasing the fuel economy of a vehicle, and CVTs (continuously variable transmissions), indubitably, play a crucial role in this plan to improve the fuel economy. A continuously variable transmission is an emerging automotive transmission technology that offers a continuum of gear ratios between desired limits. A CVT offers numerous advantages over the conventional multi-step gear transmissions such as lower fuel consumption, higher vehicle efficiency, and smooth power flow from the engine to the wheels. However, the potential advantages of a CVT have not been realized completely in a mass production vehicle.

Since the belt- and the chain- type CVTs are the most commonly used CVTs, the present research outlines detailed dynamic models that give profound insight into their system characteristics, which could be exploited later to meet the goals of greater fuel economy and vehicle efficiency. The present research reports a detailed continuous one-dimensional transient-dynamic model of a metal V-belt CVT that accurately captures the various transient dynamic interactions occurring in the system, whereas the dynamics characterized by the discrete structure (that cause polygonal excitations) of the chain are captured by developing a detailed planar multibody model of a chain CVT. Moreover, belt and chain CVTs are friction-limited drives as they rely on the friction characteristic

of the contacting components in order to successfully transmit torque. Since the friction characteristic of a contact zone between two sliding surfaces may vary in accordance with the operating and loading conditions, various mathematical models of friction are introduced to understand the influence of friction characteristic on the performance of a belt/chain CVT drive. A CVT, like any other dynamical system, is susceptible to clearance formation due to continual operation, wear, and fatigue. So, a mathematical model of clearance is embedded into the CVT model (i.e. the chain CVT model) to study the influence of clearance on its dynamic performance. A considerable effort is dedicated towards comprehensive modeling of the slip dynamics and inertial coupling among band pack, belt element and the pulleys, and studying their influence on the performance of a metal V-belt CVT system. Simple trigonometric functions are also introduced in these models to capture the effects of pulley flexibility on the thrust ratio and slip behavior of a CVT system. The results discuss the influence of band pack slip, friction characteristic, clearance, and pulley flexibility on the dynamic performance, axial force requirements, and torque transmitting capacity of a belt/chain CVT drive. The results also illustrate that for certain friction (contact) conditions and clearance parameters, it is plausible for a CVT system to exhibit quasi-periodic or chaotic behavior, which severely lowers its torque carrying capacity and dynamic performance. It is also observed that the slip behavior of a CVT system is affected not only by the torque loading conditions, but also by the inertial coupling and the nonlinearities existing between the various components.

DEDICATION

I dedicate this work to my mom, my dad, my wife, and my brother. It is only because of their perpetual love, faith, support, banter, and encouragement that I have been able to accomplish this stupendous task and head towards a better future.

ACKNOWLEDGEMENTS

This dissertation not only is the culmination of all my hard work in graduate school, but also is a reflection of my relationship with many generous, thoughtful, and awe-inspiring people that I came across during my tenure as a doctoral student at Clemson University. To begin with, I am indebted to my long-time advisor and committee chair, Prof. Imtiaz Haque, for providing me with the latitude to choose a focus area of research, spending countless hours on discussing the results and dynamics of the CVT models, granting me work-flexibility, and fostering my creative thinking process. This work would not have been possible had I not been granted the freedom to pursue my own research interests, many thanks to Dr. Haque for his generosity and considerable mentoring. Throughout my doctoral work, he encouraged me to develop independent thinking and research skills. His breadth of intellectual inquisition continually stimulated my analytical thinking skills. His constant attention to the development of the computer-models of the CVTs and the text of this dissertation was invaluable. I am grateful to him for constantly providing me with vision, encouragement, and advice throughout my doctoral research work. I also would like to thank him for granting me ample opportunities to attend numerous worldwide conferences and keep myself abreast of the current research developments in automotive transmission technology.

I am also very grateful to have an exceptional doctoral committee and wish to thank Prof. Harry Law, Prof. Cecil Huey Jr., and Prof. Nader Jalili for their continual

support, encouragement, and esteemed feedback and suggestions that motivated me to achieve a high quality doctoral work.

I am grateful to Vincent Blouin for always being willing to assist me with my research problems (especially assisting me in developing a Genetic-Algorithm based optimization module for the belt CVT model) and giving valuable suggestions that could help me gain deeper insight into the CVT dynamics. I am also thankful to my friend, Yi Miao, a former graduate student of Clemson University, who helped me debug certain Visual C++ based modules for the simulation of a chain CVT drive. Among the many people who have contributed towards my development as a research scholar, I am indebted to my Master's thesis committee members at Clemson University, Prof. Georges Fadel and Prof. John Wagner, who allowed me to work in a collaborative research environment, provided invaluable critiques of my research, and fostered my predilection for research and critical thinking. I am also grateful to the departmental and university staff for rendering services cordially and efficiently, especially managing the pay stubs, official travel expenses, official supplies, thesis binding, bookkeeping, and deadlines and announcements.

In addition to my dissertation committee members, I would like to express my gratitude to all my teachers at Clemson and abroad who toiled to hone my scientific-thinking and communication skills, and have left indelible footprints on my career path while guiding me to become a thoughtful and responsible human being.

I gratefully acknowledge the enthusiasm of Dr. Haque and the U.S. Army for allowing me to work on this wonderful project and offering me financial support during the course of my research work. This research was supported by Automotive Research

Center (ARC), a U.S. Army TACOM Center of Excellence for Modeling and Simulation of Ground Vehicles at the University of Michigan. The views and conclusions contained herein are those of the author and should not be interpreted as necessarily representing the official policies or endorsements of the U.S. Army TACOM Center or the U.S. Government.

I would also like to thank all my friends for their constant support and the frolic time we had. Without them, graduation would have been a monotonous experience.

I owe a huge debt of gratitude to my mom, my dad, my younger brother, and my extended family members for their constant love, support, and banter that allow me to persevere for attaining higher levels of excellence in every realm of life.

Last but not least, I am very thankful to my wife, Bhawana, for her unfaltering dedication, encouragement, and love that helped me accomplish this stupendous task.

Everyone's cooperation and support have made my six years of graduate school at Clemson a nice and unforgettable experience. I love you all and I hope to live up to your expectations. The experience at Clemson University has been an indelible launch pad for shaping my career and will be one of the most endearing memories of my life.

TABLE OF CONTENTS

Table of Contents (Continued)

Table of Contents (Continued)

LIST OF TABLES

LIST OF FIGURES

List of Figures (Continued)

List of Figures (Continued)

List of Figures (Continued)

NOMENCLATURE

Belt CVT Model

$(\bar{n}, \bar{\tau})$, $(\mathbf{n},\boldsymbol{\tau})$	Tangential and normal coordinate system attached to the belt element
ρ	Radius of curvature of the path of the belt element
$(\hat{e}_r, \hat{e}_\theta, \hat{e}_z)$, $(\mathbf{e_r},\mathbf{e_\theta},\mathbf{e_z})$, $(\mathbf{e_{rb}},\mathbf{e_{\theta b}},\mathbf{e_{zb}})$, $(\hat{\mathbf{e}}_{\mathbf{rb}}, \hat{\mathbf{e}}_{\boldsymbol{\theta}\mathbf{b}}, \hat{\mathbf{e}}_{\mathbf{zb}})$	Rotating coordinate systems attached to the center of the pulley
ω_s	Local sliding angular velocity of the belt element
φ	Slope angle of the belt element
r	Non-deformed pitch radius of the belt element
θ	Angular position of the belt element on the pulley wrap
δs	Length of infinitesimal belt element
$\delta\chi$	Angle subtended by the belt element, δs, at its instantaneous center of curvature
β_s	Pulley half-sheave angle in the sliding plane
β	Half-sheave angle of the deformed pulley
ψ	Sliding angle of the belt element
$\bar{\mathrm{v}}$, $\mathbf{v}$	Absolute velocity of the belt element
$\bar{\mathrm{v}}_{\mathrm{rel}}$	Relative velocity between the belt element and the pulley

Nomenclature (Continued)

ω	Angular speed of the pulley
$\bar{a}$, **a**	Absolute acceleration of the belt element
L	Total length of the belt
α	Pulley wrap angle
d	Center distance between the two pulleys
μ_a	Coefficient of friction between band pack and the belt element
F	Normal force between band pack and the element
T	Tensile force in the band pack
σ_b	Linear mass density of the band pack
σ_e	Linear mass density of the belt element
Q	Compressive force in the belt elements
N	Pulley normal force
μ_b	Coefficient of friction between the belt element and the pulley
F_z	Pulley axial force
I	Rotational inertial of the pulley
τ_{in}	Input torque on driver pulley
τ_l	Load torque on driven pulley
Δ	Amplitude of pulley sheave-angle variation
β_0	Half-sheave angle of the non-deformed pulley
θ_c	Center of pulley wedge expansion

Nomenclature (Continued)

u	Axial width variation of pulley sheaves
R	Deformed pitch radius of the belt element
a	Starting coefficient of friction between either band/element or element/pulley (for continuous friction models)
μ_{bo}	Maximum coefficient of kinetic friction between belt element and the pulley
b, $\overline{\kappa}$	Growth parameter for continuous Coulomb- and Stribeck- friction characteristics
v_s	True slip velocity between the belt element and the pulley
$(\mathbf{n_b},\boldsymbol{\tau}_\mathbf{b})$	Tangential and normal coordinate system attached to the band pack
ρ_b	Radius of curvature of the path of band pack
r_b	Non-deformed pitch radius of the band pack
ξ	Slope angle of the band pack
δs_b	Length of infinitesimal band pack
$\delta\chi_b$	Angle subtended by the band pack, δs_b, at its instantaneous center of curvature
γ	Angular position of the band pack on the pulley wrap

Nomenclature (Continued)

$\mathbf{v_{be}}$	Relative velocity between band pack and the belt element
$\mathbf{v_b}$	Absolute velocity of the band pack
$\mathbf{a_b}$	Absolute acceleration of the band pack
R_b	Deformed pitch radius of the band pack
μ_{ao}	Maximum coefficient of kinetic friction between band pack and the belt element
f_r	Parameter relating kinetic friction to static friction coefficient
$\bar{\lambda}$, v_0	Stribeck-effect/lubrication-related parameter
α_2	Viscous friction coefficient for the Stribeck friction model
α_0, α_1	Stribeck friction model parameters related to static and kinetic friction
$\hat{\lambda}$	Slope parameter for approximating Coulomb friction

Multibody formalisms and Chain CVT Model

μ_0	Maximum coefficient of kinetic friction between the chain link and the pulley (or between two bodies)
μ	Coefficient of friction between chain link and the pulley (or between two bodies)

Nomenclature (Continued)

$\mathbf{F_A}$, $\mathbf{M_A}$	Active forces and moments acting on a rigid body
$\mathbf{F_P}$, $\mathbf{M_P}$	Passive forces and moments acting on a rigid body
$\mathbf{v_A}$, $\mathbf{v_P}$	Velocities of points of application of active and passive forces on a rigid body
α_k, β_k	Magnitude of forces and torques due to coupling elements between two bodies
($\mathbf{n}$, $\mathbf{t}$)	Unit normal and tangential vectors describing the contour of the body
$\mathbf{r}_D$	Relative distance between two bodies
g_N	Relative distance between two bodies (measured along the normal direction)
$\dot{g}_N, \dot{g}_T$	Relative velocity between two bodies along the contact normal and tangential directions respectively
λ_N, λ_T	Normal and tangential constraint forces
(x_c,y_c)	Coordinates of center of mass of chain link
θ	Rotational degree of freedom of chain link
(a_{cx}, a_{cy})	Linear acceleration of the center of mass of a link
(k,b,ε)	Clearance-model parameters (stiffness, damping, and link clearance respectively)
$\mathbf{I_C}$	Moment of inertia tensor of the chain link about its center of mass

Nomenclature (Continued)

Superscripts

None	Driver side parameters
$'$	Driven side parameters
$\cdot$	Time derivatives

CHAPTER 1

INTRODUCTION

Over the last few decades, environmental concerns have made it imperative for the governments of most nations to impose stringent regulations on the fuel consumption and exhaust emissions of vehicles (CAFE standards in the US, ACEA standards in Europe, etc.). "The International Energy Agency (IEA) forecasts that greenhouse emissions will have grown about 90% by 2030, mainly due to transport and especially road transport" (*Menegazzi, P., Vangraefschepe, F., "The Future of Hybrid Vehicles," IFP-Panorama 2005 Technical Report*). Emissions of carbon dioxide (CO_2), the principal greenhouse gas produced by the transportation sector, have steadily increased along with travel, energy use, and oil imports. "Globally, the transportation sector consumes 75% of total world oil imports and contributes about 25% of the world's greenhouse gases" (Ottis *et al.*, [1]). Transportation vehicles, especially passenger cars, account for a large percentage of total air-pollutant emissions, as illustrated in Figure 1.1 [2]. Consequently, automotive engineers have been progressively researching alternatives to deliver vehicles that meet the government imperatives of increased vehicle efficiency and lower emissions.

Vehicle fuel economy plays a crucial role in determining the emission of greenhouse gases. In recent years, motor fuels and combustion processes have improved and catalytic converters have come into general use. Vehicles today pollute much less than thirty years ago. Automakers are also looking into the aspects of implementing new

and renewable forms of energy production for propelling a car (e.g. solar power, fuel cells, electric power etc.). Advancements in engine design and transmission design are also being actively researched to accomplish the goals of increased vehicle efficiency and higher fuel economy.

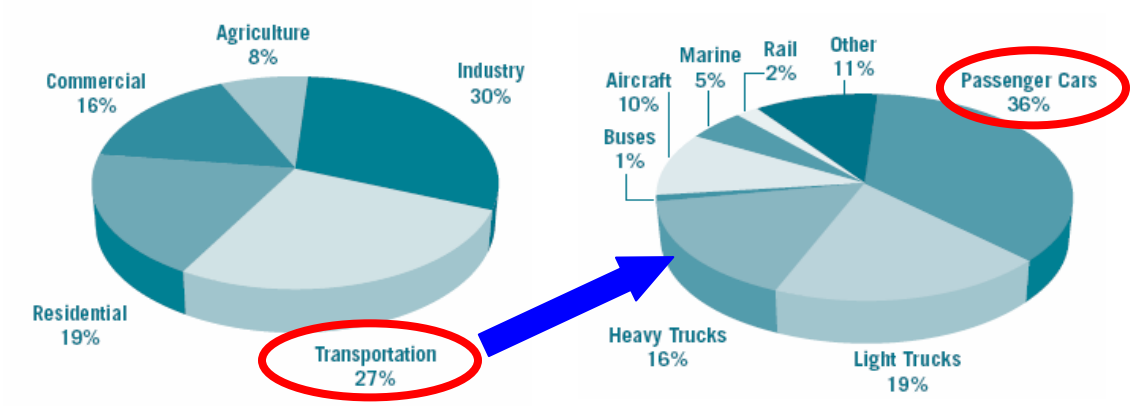

Figure 1.1: Sector-wise contribution to Greenhouse Emissions [2]

In the current competitive market, both customers and engineers are looking for a vehicle technology that can provide them with better performance at low cost. Automotive designers and engineers have been researching various transmission designs that can yield higher mechanical efficiency with low maintenance cost and low fuel consumption. Manual and automatic transmissions offer a finite number of discrete gear ratios; however, of late, continuously variable transmissions (CVT) have aroused a great deal of interest in the automotive sector due to their potential of lower emissions and better performance. A CVT is an emerging automotive transmission technology that offers an infinite number of gear ratios between two limits, which consequently allows better matching of the engine operating conditions to the variable driving scenarios. A CVT allows varying the speed ratio under load condition without the necessity to disengage the engine by means of a friction clutch. “The impact of a simple CVT can be twofold. Under one control strategy, the engine speed may be fixed and the CVT’s

changing radii can create torque multiplications, accelerations, and proper speeds under varying conditions. Another control scenario makes the engine operate at speeds within an efficient region, varying throttle position and transmission ratios to handle changing conditions. In either case, the flexibility of the CVT relative to a conventional transmission allows the engine to operate more efficiently" (Ottis *et al.* [1]). Today, many vehicle manufacturers are integrating CVTs into the driveline of their vehicles. Consequently, vehicles like Ford Fiesta, Ford Escape, Honda Civic HX, Honda Insight, Nissan Murano, Nissan Micra, Audi A8, Rover 45, Toyota Prius, etc., are increasingly catching attention of the customers and shifting the market trends to propitiate the development and use of hybrid vehicles [1, 3].

The key advantages of a CVT that interest vehicle manufacturers and customers can be summarized as:

- Higher engine efficiency
- Higher fuel economy
- Smooth acceleration without shift shocks
- Infinite gear ratios with a small number of parts
- Easy to manufacture and low cost
- Light and Compact

However, the ancillary circuitry used for controlling and changing the gear ratios leads to energy losses and also adds to the weight of the transmission and the vehicle.

The concept behind the working of a CVT dates back to 1950s, when Hub van Doorne, co-founder of DAF Company (van Doorne Automobiel Fabriek), introduced the Variomatic CVT based on a rubber V-belt design for use in heavy machinery

transmissions. The company also developed steel pushing V-belts. During the incipient design phases, the steel bands buckled because of high load transfer from the pulley. So, the engineers used movable support blocks to prevent the bands from bending. Thus came into existence the concept of push-pull torque transfer mechanism in metal V-belts.

As vehicle technology progressed over the past several decades, transmission technology also advanced. The automatic transmission (AT) has nearly replaced the manual transmission, as it is more reliable and convenient to use than the latter. However, the automatic transmission now faces stiff competition from the continuously variable transmission, which offers an infinite range of gear ratios between two limits, higher transmitting efficiency, and smoother speed-changing characteristics. These three types of transmission are functionally the same but differ in the means of achieving those functions.

1.1 Manual Transmission

A basic manual transmission can be said to be a combination of a clutch and a gear set. Figure 1.2 [4] depicts a 5-speed transmission gear box of a medium-duty passenger vehicle. There are two variations to this type of transmission: synchronized and unsynchronized. The unsynchronized transmission is more robust by nature and can handle greater loads than the synchronized transmission. However, the operator must double-clutch between shifts to match engine and transmission speed manually.

Manual transmissions in modern passenger cars use synchronizers to eliminate the need of double-clutching. Since the output shaft is splined, the collar can readily move

under the influence of gear-lever force to contact any one of the gears. A synchronizer allows the collar and the gear to make frictional contact before the dog teeth make contact. This synchronizes the speeds of the collar and the gear before the teeth start to engage.

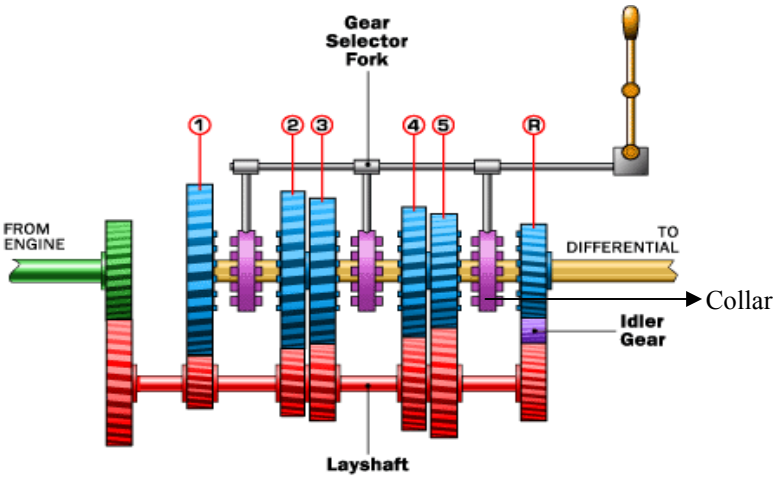

Figure 1.2: Manual Transmission [4]

1.2 Automatic Transmission

The basic components of an automatic transmission are: a torque converter that usually has a lockup clutch to prevent slippage at high speeds, a planetary gear train, and a hydraulic system/electro-mechanical controller. The torque converter connects to the crankshaft and transmits engine power to the gear train. Hydraulic pressure acting through the automatic transmission fluid produces the shift. The torque converter is a form of fluid coupling. This is a device that uses fluid and vaned rotors to transmit power between the shafts. Most cars sold in the United States since the 1950s have had automatic transmissions. Figure 1.3 [5] depicts a layout of an automatic transmission along with its components.

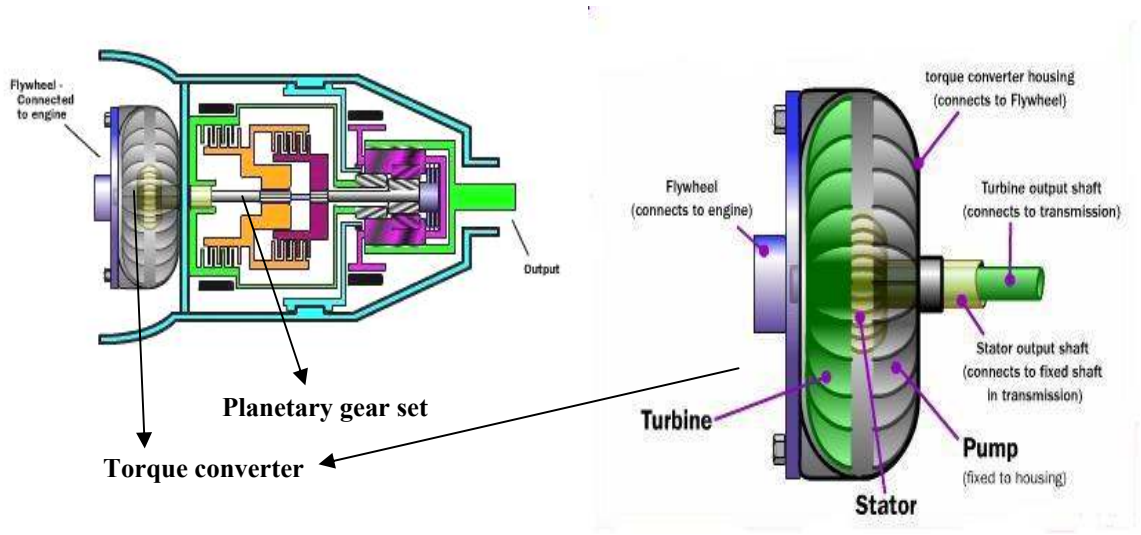

Figure 1.3: Automatic Transmission [5]

Automatic transmissions are equipped with feedback controls, which may be electronic, hydraulic, or mechanical in nature, that allow for gear selection. The shift logic is dependent on many parameters such as engine speed, hydraulic pressure, temperature, vehicle acceleration, etc. The transmission controller uses a rule-based control strategy to select the gear ratio that best suits the driving conditions. The key difference between a manual and an automatic transmission is that the manual transmission locks and unlocks different sets of gears to achieve various gear ratios, whereas in automatic transmission, the same set of gears yields different gear ratios. This is possible because of the combined action of the torque converter and compound planetary gear set. However, the multitude of parts, complex design, advanced control strategies make automatic transmissions less favorable than its counterpart i.e. the continuously variable transmission (CVT).

1.3 Continuously Variable Transmission

CVT is an emerging automotive transmission technology that offers a continuum of gear ratios between high and low extremes. Currently, three technologies coexist in the automotive market: belt CVT, toroidal CVT, and chain CVT. Figure 1.4 [6] depicts the components and basic configuration of a V-belt CVT. Figure 1.5 [7, 8] illustrates the configuration of a chain and a toroidal CVT. Belt and chain CVTs fall into the category of friction-limited CVT drives. The basic configuration of a CVT comprises two variable diameter pulleys connected by a power-transmitting device like a belt or chain. One of the sheaves on each pulley is movable. The application of an axial force to the pulley sheave initiates radial motions in the belt or chain, thereby causing the transmission ratio to vary continuously. Hydraulic actuation of pulley sheaves is commonly used in current automotive applications. However, centrifugal systems along with high power electronic solenoids are also being actively used to actuate the pulley sheaves.

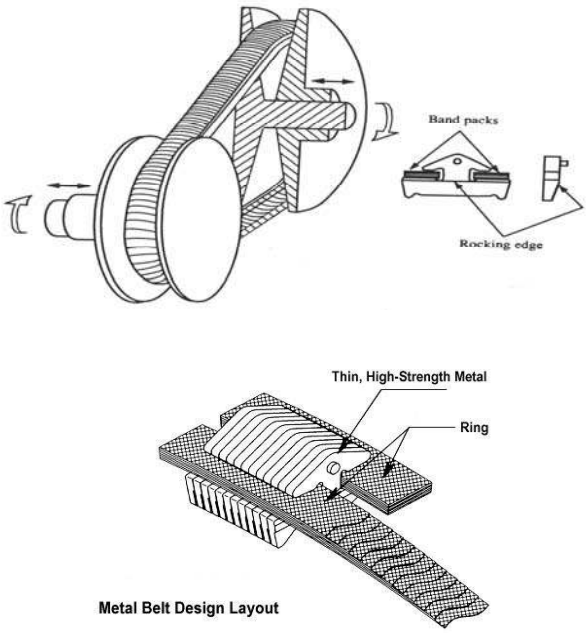

Figure 1.4: Pushing V-belt CVT arrangement [6]

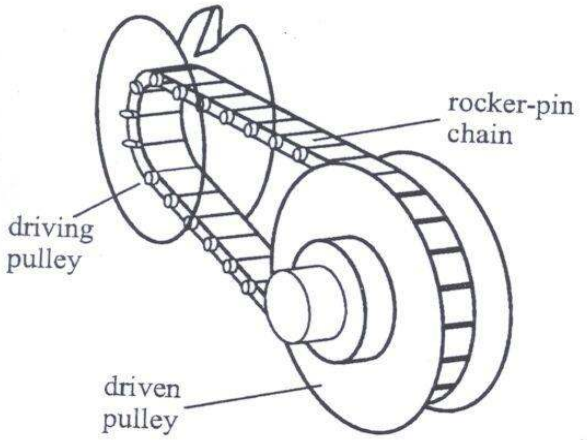

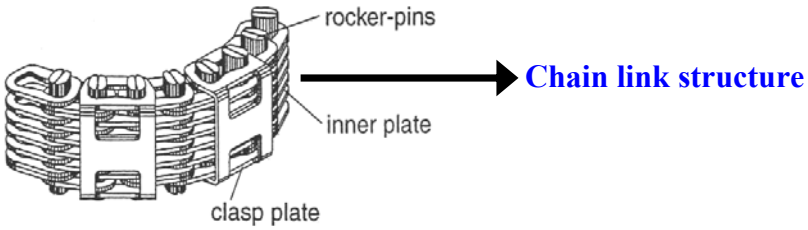

Chain CVT [7]

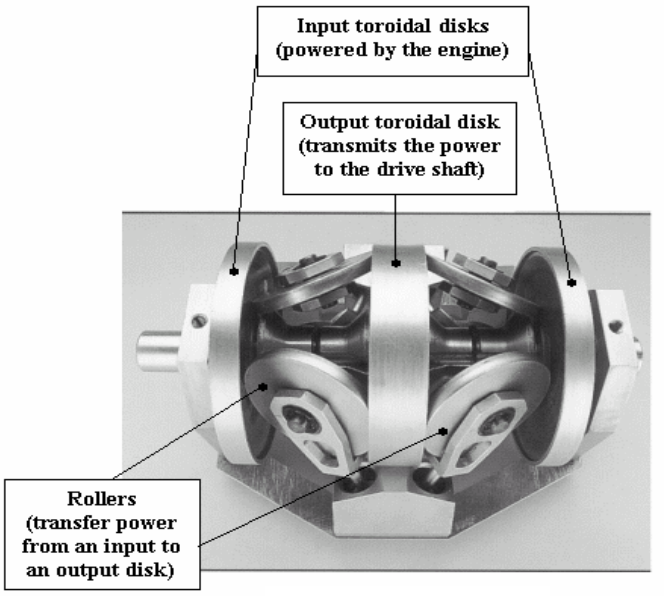

Toroidal CVT [8]

Figure 1.5: Chain and Toroidal CVTs [7,8]

The belt-type CVT can also be classified further as: push belt and pull belt. Torque is transmitted in a push-belt by compression whereas a pull-belt transmits it through tension. However, the automakers now commonly use a belt configuration which takes advantage of the push-pull effect in tandem. This leads to a high overall efficiency. However, losses are still inherent in the transmission due to power absorption by the hydraulic system for sheave-actuation and also due to belt slip. The torque capacity of a friction-driven CVT (i.e. belt or chain CVT) is limited by the strength of the belt or chain and the ability to withstand friction wear between the source and transmission medium. A lot of research is being conducted to enhance the efficiency and torque capacities of such CVTs.

The manufacturing processes for a belt/chain CVT are very cost-effective in comparison to the other transmissions. “To manufacture the bands, sheets of high-fatigue-strength maraging steel are rolled into tubes and cut into loops in a slitting operation. These small loops are stretched to size by rolling, whereupon the bands are annealed, calibrated, hardened to relieve internal stresses, and then nitrided to harden the surface. The high-tolerance elements are fabricated using techniques similar to those used to manufacture high-velocity gears or roller bearings. The steel elements are fine-blanked, hardened, deburred, and profile-shot blasted. Afterwards, they undergo a complicated sorting and selection process to match other similarly dimensioned elements” (Steven, [9]).

In addition to the advancements in belt and chain drive CVTs, significant research effort is being directed towards developing alternative designs of CVTs, e.g. spherical CVT, electric E-CVT, ball-type CVT, constant power CVT, toroidal CVT, etc [10-13].

Several car manufacturers like Mazda, Ford, and Nissan are keenly exploiting the dynamics of a toroidal CVT and its advantages in a vehicle driveline system. Research at Mazda showed a 20% improvement in fuel economy with a 3.0 liter engine over a 4-speed automatic transmission [14]. The toroidal CVT operates by transmitting power between the two pulleys by means of metal rollers, which run on a thin film of traction fluid against mating metal discs. In a half-toroidal CVT, as depicted in Figure 1.5, a large force presses a semicircular disc against the power roller, and the resulting shearing force on the squeezed oil film transmits power. Changing the effective radius of the contact point enables the gear ratio to change continuously, resulting in step-less gear shifting. A toroidal CVT adds to the other advantages of a CVT, such as:

- Transmit high torque loads due to high performance traction oil and high surface-pressure material in discs and rollers
- Higher efficiency due to the absence of complex actuating mechanisms
- Less noisy as power is transmitted through a rolling contact surface and the shearing force of oil

However, among all the CVTs, the belt- and the chain- type CVTs are the most commonly used. The primary reason for this is attributed to their design simplicity and lower manufacturing cost.

Commonly, an extension to CVT design, named as Infinitely Variable Transmission (IVT), is integrated into the vehicle driveline as it allows the transmission to drive the vehicle forwards as well as backwards. The whole arrangement is also referred as CVU, i.e. continuously variable unit. The transmission input from the engine is split into two shafts, one connected to the regular CVT and the other connected to an

epicyclic gear set. The output from the CVT shaft is connected to another shaft that connects to a different set of gear in the epicyclic gearbox. The gear that does not draw power from the engine or CVT transfers torque to the transmission output. Owing to the split in the input power, this configuration is also known as Power-Split CVT (PS-CVT). Figure 1.6 [15] depicts an input- coupled configuration of a CVU patented by Torotrak Company.

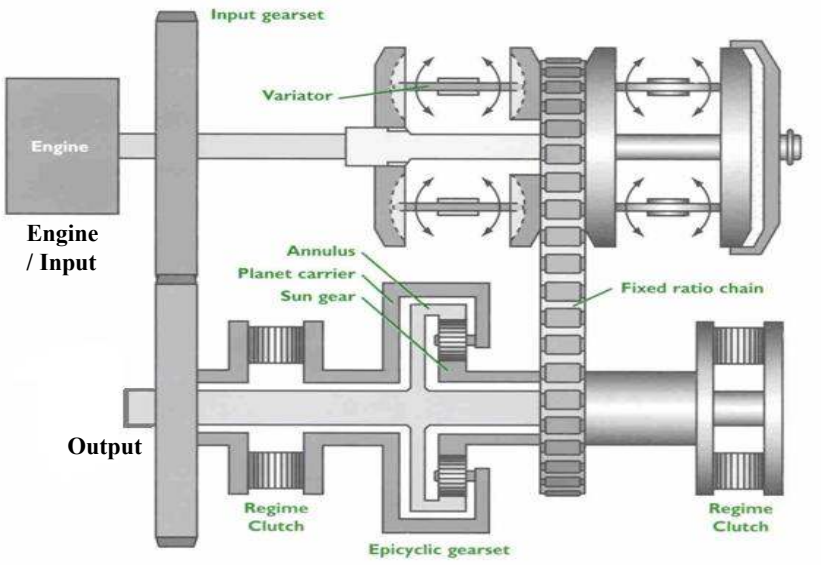

Figure 1.6: Torotrak IVT System [15]

CVT technology is also being used extensively in hybrid-vehicle transmissions. Hybrid vehicles allow separate power sources each to operate in regions of optimal efficiency, thereby granting the overall system higher efficiency. Most hybrid-electric vehicles fit into one of two fundamental categories: series or parallel. Essentially, an electric motor generates all the torque necessary to propel the automobile in series hybrid systems, and in parallel hybrid systems, a combination of an internal combustion engine and an electric motor provides the propulsion. Of the two configurations, parallel hybrid systems are more common than the series systems. The Honda-Insight and Toyota-Prius

are both charge-sustaining gasoline-electric hybrids [16] which use the parallel configuration along with regenerative braking technology to increase fuel economy. Both the cars charge their batteries from energy that would otherwise be wasted, using gasoline as their sole external source of energy. The Insight is made in both manual transmission and CVT versions. It uses the same CVT transmission design as the Honda Civic HX. However, the Prius uses an electronically-controlled power-split CVT configuration. It provides a three-way connection between the wheels, the gasoline engine and the generator/motor by the use of a planetary gear-set.

1.4 Closure

In spite of the several advantages a CVT promises, the complete potential of a CVT, in terms of the mass-production and market penetration of CVT-equipped vehicles, has not been realized so far. The expected increase in the fuel economy and enhanced drivability has not been achieved in many cases. The control logic has not been accurate enough to deliver a desired shifting behavior. However, it is indubitable that CVTs play a crucial role in the plan to improve vehicle fuel economy. Since the belt- and the chain- type CVTs are the most abundantly used CVTs, the present research aims at developing their detailed dynamic models that give insight into their system characteristics. These could be later exploited to meet the goals of higher fuel economy and higher vehicle efficiency. Moreover, as the belt and chain CVTs are friction-limited drives, their performance is significantly influenced by the friction characteristics of their contacting surfaces. Friction inherently is a non-smooth nonlinearity, which further makes the CVT a non-

smooth mechanical system. The proposed research exploits the tools of non-smooth mechanical systems to understand the influence of various friction characteristics on the behavior of the detailed dynamic models of belt and chain CVTs. To enhance the comprehensibility, this dissertation has been organized into the following chapters:

Chapter 2: It presents an extensive literature review on the work that has been done in different areas of CVT such as control systems, design, loss modeling, and dynamics. Analysis of the different aspects of a CVT that have been studied by various researchers motivates the author and, perhaps, the reader to conduct research in certain unexplored areas that can contribute towards better understanding of CVT dynamics.

Chapter 3: This chapter creates a stepwise understanding of modeling and formulation of equations of motion of a CVT system. The reader is introduced to two different CVT models: metal V-belt CVT and chain CVT. The metal V-belt model incorporates a continuous rigid-body framework for the description of the belt and also accounts for the bending of pulley sheaves. Multibody formalism is used to describe the dynamics involved in a chain CVT. A suitable clearance model is embedded into the multibody model of the chain CVT in order to capture clearance-related dynamics in the system.

Chapter 4: It discusses the friction phenomenon on a microscopic level and macroscopic level. Different models and numerical algorithms are described to capture the nonlinearities induced by friction in a system. The influence of different friction models on the dynamic response of a system is highlighted through an example of two- degree of freedom stick-slip oscillator.

Chapter 5: It presents the results of the simulation and discusses them in detail. Influence of different friction characteristics and clearance parameters on the dynamic

performance indicators of a CVT is studied. Slip behavior in a CVT is studied under the influence of both loading conditions and inertial effects. Comparisons are illustrated among the dynamic performance indicators of the two different types of CVT. The similarity in the trends or characteristics with the existing work is noted. The results are also explained on the basis of fundamental laws of physics.

Chapter 6: This is the concluding chapter and discusses the application of the present work and future research ideas.

Appendices at the end of this dissertation outline the computer programs and simulation models used to model and understand the dynamics of a CVT system.

CHAPTER 2

LITERATURE REVIEW

2.1 Previous Work

Over the past few decades, automotive transmission technology has undergone several refinements in order to meet the goals of increased vehicle performance and reduced exhaust emissions. One of the most promising technologies introduced in the automotive market is the continuously variable transmission (CVT). CVT is a power transmission device whose speed ratio can be varied continuously between two finite limits. Speed ratio is defined as the ratio of belt pitch radius on the driven pulley to that on the driver pulley, or the ratio of driver pulley speed to driven pulley speed. A few authors also use the reciprocal definition for speed ratio, i.e. ratio of driven to driver pulley speeds. There are many kinds of CVTs, each having their own characteristics, e.g. Spherical CVT, E-CVT, Hydrostatic CVT, Toroidal CVT, Power-split CVT, Belt CVT, Chain CVT, Ball-type toroidal CVT, etc. However, among all, belt and chain types are the most commonly used CVTs in automotive applications. CVT is also a promising power-transmission technology for future hybrid vehicles. As mentioned before, several car companies like Ford, Toyota, Honda, Audi, etc., have already begun to mass-produce vehicles with such types of CVT integrated into their drivelines.

Extensive research has been conducted on different aspects of a CVT e.g. performance, configuration, design, slip behavior, efficiency, vibrations, mechanics, stress or fatigue analysis, drivability, etc. The models developed to describe the dynamic

interactions in a CVT system vary in their level of complexity, their mode of analysis, and their research scope. However, since none of the models reported in the literature, barring a few, are able to accurately capture the transient-dynamic interactions occurring within a CVT system, it is imperative to develop detailed dynamic models which are comprehensive enough to be used for maximizing the potential benefits of a CVT. In addition to the many advantages a CVT promises, there are also a number of possible inherent parasitic losses associated with CVTs which account for their inefficiency. Simner [17] categorized losses within an automotive transmission into the following areas: parasitic losses, power proportional losses, inertia losses, configuration losses, and control losses. Parasitic losses occur under no-load conditions and are independent of the transmitted power. They are mainly speed- and temperature- dependent, e.g. in a manual transmission such losses can be due to oil churning, seal effects, bearing drag, etc. Further, CVT losses can be attributed to slippage, wedging action, hydraulic pumping of sheaves, other sheave actuation mechanisms, thermal effects, flexure effects, lubrication effects, fatigue and wear, etc. Akehurst [18] analyzed different loss mechanisms prevalent in a CVT, especially those occurring in a metal pushing V-belt CVT.

Since the current research primarily deals with the dynamic analysis of friction-limited CVTs i.e. belt and chain CVTs, the literature pertaining to them will be discussed. The torque capacity of a belt/chain CVT is limited by the ability of the power-transmitting device (belt/chain) to withstand the wear caused by friction between the various transmission components. Literature pertaining to loss mechanisms, mechanics, control, slip behavior, vibrations will be subsequently discussed in detail. For better

comprehensibility, the discussion is divided into several sections, where each section describes the literature on a particular aspect of CVT.

Belt Mechanics and Belt Slip:

Many papers have been published over the past two decades to describe the dynamic interactions occurring in a belt or chain CVT. The most commonly used power transmitting device in a belt-type CVT is either a steel V-belt or a rubber V-belt. A lot of work on metal and rubber V-belt is subsequently cited as they are extensively used in today's automobiles. Figure 2.1 [6, 19] depicts the layouts of a rubber V-belt and a metal V-belt.

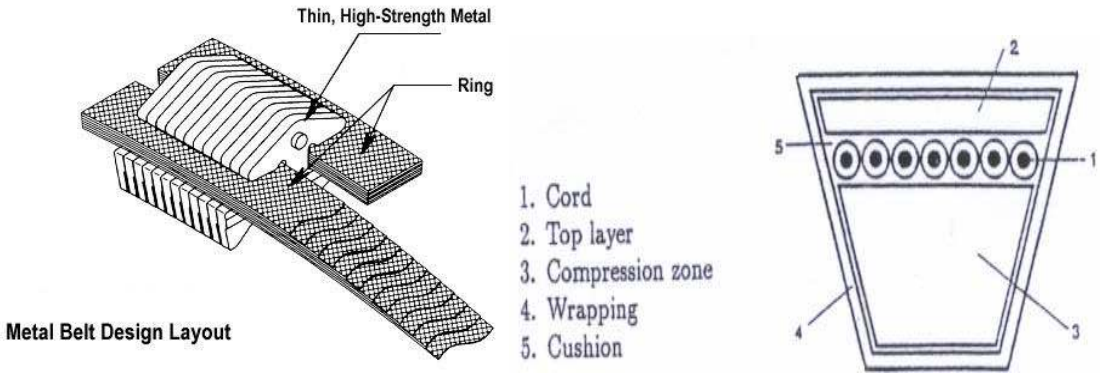

(a) (b)

Figure 2.1: Layout of (a) Metal V-belt [6] and (b) Rubber V-belt [19]

Belt drives in general do not have total slippage, so Grashof [19] divided the contact zone (or the pulley wrap region, α, α′) into sliding (or active) and adhesive (or idle) arcs. Figures 2.2 and 2.3 illustrate the geometric configuration, the sliding plane, and the simplified kinematic-description of a V-belt CVT. Only the sliding arcs, represented in the figure as (β, β′), contribute actively to the torque transmission. In the adhesive arc, the belt sticks against the pulley and the belt tension is constant. Gerbert [19] did extensive

work in understanding the mechanics of traction belts, especially metal pushing V-belt and rubber V-belt. He proposed a set of equations for describing the dynamic interactions

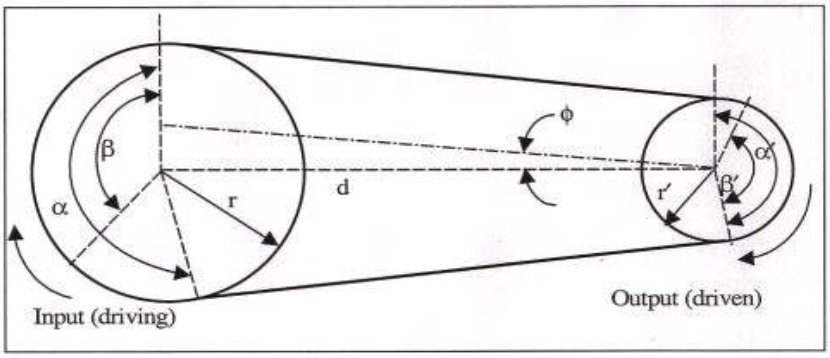

Figure 2.2: CVT Geometric Configuration

between the belt and the pulley. Since the belt is capable of moving both radially and tangentially, variable sliding angle approach was implemented to describe friction between the belt and the pulley. Previously, many researchers like Kimmich [20], Gutyar [21], Amijima [22], etc., assumed constant sliding angle over the pulley wrap to derive the equations of motion of the belt-pulley system. The variable sliding angle approach required that the equilibrium, compatibility, and constitutive equations be solved simultaneously for predicting the dynamics of a belt-pulley system. Only centripetal effects were modeled to account for the influence of belt inertia on system dynamics.

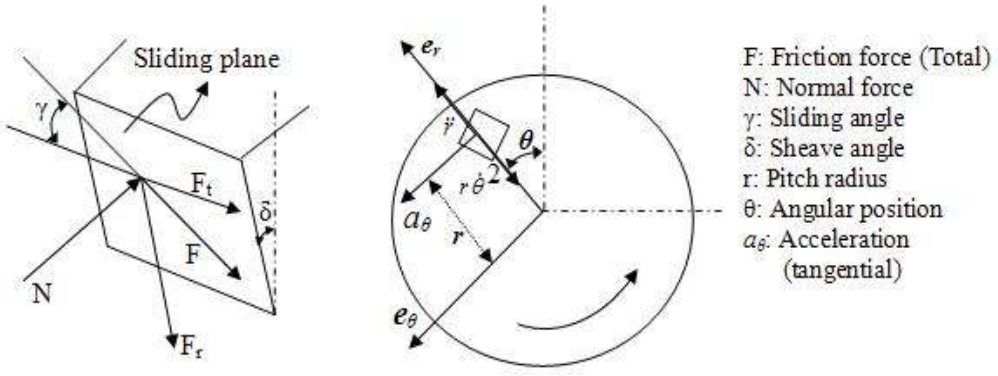

Figure 2.3: Kinematic description of the belt

Gerbert [23] did a thorough analysis to understand the slip behavior of rubber belts and developed a unified slip theory for rubber V-belts. He classified slip according to the contributions of creep, compliance, shear deflection, and flexural rigidity. The author also discussed the slip due to the poor fit between the belt and the pulley during the wedging action. Finite Element Analysis was used to calculate shear deflections in the belt and also to determine the stick-slip conditions on the belt. However, the work did not account for the influence of belt inertia, loading conditions, and belt radial variations (due to axial forces) on the slip behavior.

Gerbert [24] also studied the influence of flexural rigidity and inertia of a belt, especially a rubber V-belt, on the dynamics of a belt-pulley system. However, only centripetal effects were modeled to account for the influence of belt inertia. Owing to flexure, the belt no longer follows a straight-line motion after exiting the pulleys. As a result of the flexural effects, the contact arc becomes smaller than the nominal one, and the traction capacity of the drive increases. The author used ordinary beam theory to predict the entrance and exit slopes of the belt. The flexural rigidity has tremendous influence on the seating and unseating behavior of the belt. Rapid variation of curvature may change the direction of frictional forces, which consequently affects the torque capacity of the belt-CVT drive. Gerbert [19] also discussed power losses associated with flexure, belt compression, and temperature. He simultaneously conducted numerous experiments to support his theoretical correlations. Occasionally, it was observed that the deflection of the pulley and the compression of the belt were of the same magnitude in a metal belt CVT. Gerbert [25] studied the influence of pulley skewness on the mechanics of V-belt drives. Deflection of the pulley in the axial direction widens or shortens the

groove width, thereby influencing the motion of belt in the pulley groove. The displacement of the pulley sheaves can be attributed to the phenomena of local deflection, plate deflection, and pulley skewness. The local deflection depends on the local axial pressure. Plate theory was used to obtain global deflection of the pulley halves. The author used the influence functions derived by Ciavatti *et al.* [26] for the deformation of a transversely loaded annular plate. However, the plate equations and the belt equations need to be solved simultaneously in order to obtain the dynamic performance indicators of the belt-pulley system. Skewness of the pulley may be caused by clearances in the guiding of a movable pulley half. Gerbert [25] ignored the elastic deformations in the belt and the pulley, and studied the influence of pulley skewness on the dynamics of a stiff belt. V-belt mechanics, like any other mechanical system, is characterized by a set of differential equations. The author observed the existence of singular solutions (also known as *orthogonal points*) where the frictional forces are radially directed and all the derivatives in the differential equations vanish. The character of a solution at an orthogonal point to a great extent determines the character of the solution at other locations and other conditions. The author also observed that the axial forces for pulleys with small to medium skewness did not differ much from those in the ideal case (i.e. with parallel pulley halves). On the other hand, large skewness led to a considerable increase in axial force for low to medium torque applications. The author's conclusions, however, were not experimentally supported.

Sorge [27] introduced the concepts of deformation and elastic wedging to analyze the mechanics of rubber V-belts. The author's focus was to analyze the belt-trajectory. The study involved the theoretical problem of tension distribution and radial penetration

of a V-belt. Flexure and inertial effects were neglected. The belt deformation was related only to the axial forces and the contributions arising from Poisson effects were neglected. He incorporated the transverse elasticity of the belt and used force-deformation equations to obtain a sliding condition. The author also put considerable effort in obtaining approximate closed form solutions to the belt-pulley system. Dolan and Worley [28] extended Gerbert's work [24] to formulate closed form solutions by approximating the numerical results of both driven and driven pulleys by suitable mathematical functions. Hyperbolic and trigonometric forms were introduced to describe the tension distribution over the main active arc of contact excluding the seating and unseating regions. The authors were able to get results in close agreement to Gerbert's numerical results; however, conformity with the driver pulley system dynamics was not attained. Sorge [29] also studied the transient mechanics of rubber V-belt variators in order to understand the CVT behavior during speed-ratio shifts. The results obtained were different from those at steady state. For moderate shift speed and high angular speed, partial adhesive regions appear where the belt winds along spirals of Archimedes. Simple closed-form approximations were proposed for the purpose of speeding up the calculations for variator operative characteristics. Sorge and Gerbert [30] developed a third order rubber V-belt model considering no inertial and flexural effects. They introduced the concept of "adhesive-like" contact in V-belt mechanics. They proposed that V-belts do not stick to the pulley walls along the pulley wrap, but pass through an idle-like region where sliding occurs at extremely low relative velocity. The trajectory is nearly circular in this region and tension is almost constant. Sorge [31] also analyzed the mechanics of metal V-belts under the influence of pulley bending. The belt was considered rigid for the purpose of

model development. The author used virtual displacement approach to get approximation to belt trajectories, tension distribution, axial thrust, and slip. The author concludes that the influence of pulley deflection is important when the belt trajectory is close to the outer radius. The influence decreases near the middle radius and becomes negligible near the inner clamped radius. Therefore, he suggested the use of a mixed model at smaller radii in order to account for the deformation of both belt and pulley.

"Robertson and Tawi [32] developed a model to describe the misalignment of the belt and pulleys over a range of transmission ratios. They investigated the effects of the ratio at which zero misalignment occurred and how this ratio could be optimized to reduce maximum misalignment over the transmission ratio range" (*adopted from Akehurst's Ph.D. Thesis, [18], with permission*).

Sattler [33] analyzed the mechanics of a metal chain CVT and a V-belt CVT considering both longitudinal and transverse stiffness of the chain and belt, misalignment, and elastic deformation of the pulleys. The pulley deformation was modeled using finite-element analysis. The pulley was assumed to deform in two ways, pure axial deformation and a skew deformation. The model was also used to study efficiency aspects of belt and chain CVTs.

Micklem *et al.* [6] developed a model of steel pushing V-belt CVT based on elastohydrodynamic (EHD) lubrication theory. The author used EHD theory to model friction between various surfaces i.e. between bands, between band and element, between element and pulley. However, the author also made certain unrealistic assumptions during the course of model development, such as, uniform band tension, uniform loading and unloading arcs over the belt/pulley wraps, negligible inertial effects. Speed variation

in the belt due to deformation and compressive loads was also neglected. The author also discussed the influence of gaps between the belt elements on the slip behavior of CVT. A test rig was also designed to make measurements on the transmission. Micklem *et al.* [6, 34] proposed a viscous shear model that can predict belt slip with good accuracy over a wide range of operating conditions except when the input torque is small. They suggested that this discrepancy is due to the redistribution of gaps between the belt elements as they enter the driver pulley. The authors also reviewed the work done by Gerbert [35] and compared the results from their friction model to the results obtained by the other authors.

"Karam and Play [36] did a discrete analysis of metal V-belt drive. Due to a large number of parts, they used a numerical approach to derive global equilibrium equations from elemental part equations. The belt equations were derived using quasi-static equilibrium analysis. A lot of hypotheses and assumptions were made during the course of model development. The belt elements are always assumed to be in compression, and the bands and pulleys are assumed to be rigid. They also observed that only part of the contact arc contributed to torque transmission. Belt efficiency passes through a maximum for a speed ratio of 1. The steel bands aided power transmission at low transmission ratios, but acted against power transmission at high ratios. They later included pulley deformations in the model and observed an increase in pulley axial forces" (*adopted from Akehurst's Ph.D. Thesis, [18], with permission*).

"Asayama *et al.* [37] developed a theoretical model to describe variations in band tension and segment compression force. The authors introduced the existence of relative motion between the bands and segments, as they have a different radius of rotation, and

used this to predict changes in band tension" (*adopted from Akehurst's Ph.D. Thesis, [18], with permission*). The results were verified by conducting an experiment and a method was devised to develop a relation between belt slip limit and pulley clamping force. The equations were developed using the concepts of quasi-static equilibrium.

Kim and Lee [38] investigated the metal V-belt behavior analytically and experimentally. They proposed a speed ratio-torque load-axial force relationship to calculate belt slip. They obtained the equations of motion using quasi-static equilibrium considerations. They found that the gross slip points depend on the torque transmitting capacity of the driven side. Numerical results showed that the belt radial displacement increased in the radial inward direction for driven pulley, while that of the driver increased slightly and decreased with the increasing torque load. The effects of inertia and flexure were neglected and the band tension was assumed to be constant. Radial stiffness of belt was incorporated in order to analyze the influence of axial force on radial penetration. "Kim *et al.* [39] performed metal V-belt analysis with the objective of calculating pulley clamping forces for specific torque and transmission ratio combinations. The authors derived equations for a number of different conditions, like low ratio low load, low ratio high load, high ratio cases, and unit transmission ratio. For each of these conditions, the authors split the pulley wrap into three distinct regions: where the segment compressive force and band tension remain constant, where only the band tension changes, and where both tension and compression vary. For each of these regions and for each pulley, an axial force requirement is calculated. The total axial force at each pulley is then the sum of each of these component parts" (*adopted from Akehurst's Ph.D. Thesis, [18], with permission*). Kim and Choi [40] again investigated

the behavior of a rubber V-belt CVT analytically and experimentally. They found that as the torque load increased, the belt radial displacement increased in the radial inward direction for the driven pulley while the radial displacement decreased slightly and then increased for the driver pulley. Moreover, the relative belt displacement for the driver was negligible compared with that of driven. The experimental results were in consonance with the theoretical results except for the inlet and exit regions of the pulleys.

Sun [41] did a performance-based analysis of a metal V-belt CVT. He modeled the metal V-belt as a composite of multiple-bands and metal-blocks. The author assumed a constant value for the active arc for calculation purposes, and observed the influence of ratio change on axial forces. The equations of motion were derived on the assumption of quasi-static equilibrium. Flexural effects were neglected and the steel blocks were treated as a continuous belt subjected only to compression. The author also assumed that the deformation and creep in bands and steel blocks under torque load were the same as those without torque load. A computational scheme was devised that adapted the analysis to the computation of the metal-belt drive's performance for any specific drive-schedule.

Massouros [42] investigated elastic creep velocity of a rubber V-belt analytically and experimentally. The belt creep velocity depends not only on the structural characteristics of the belt, but also on the operational characteristics of the CVT. It also affects the torque transmission capacity of a belt drive. During the power transmission with a belt-pulley system, the velocity of the driving side of the belt is larger than the driven side. The gradual change of the velocity from the larger value to the lower value and inversely, takes place on the pulley wrap arcs by the elastic creep of the belt on the pulley. The belt creep takes place towards the moving direction in the driven pulley and

opposite to the moving direction in the driving pulley. It was observed that the belt creep velocity at each point of the arc of creep is a linear function of transmitted power and varies exponentially along the arc of creep. The belt dynamics was modeled using quasi-static equilibrium concepts.

Kobayashi *et al.* [43, 44] focused on the gap distribution between the elements and analyzed the mechanism causing microslip in a metal belt CVT. The authors also investigated the torque transmitting capacity of a metal V-belt CVT under no load conditions on driven pulley. The belt slip was calculated on the basis of mean gap (due to the redistribution of gaps among the belt elements). They showed that the slip ratio rises to a state of macroslip when the transmitted torque exceeds the slip-limit torque. The slip hypothesis made a number of assumptions: the slip was assumed to occur only on the pulley where the gaps were present and these elemental gaps were assumed to be distributed evenly in the idle sector at the entrance to the loading pulley. The authors observed the existence of active and idle arcs during different phases of transmission. Figure 2.4 [43] depicts gap redistribution phenomenon among belt elements. Radial variations of the belt due to the axial forces were neglected. The equations for calculating

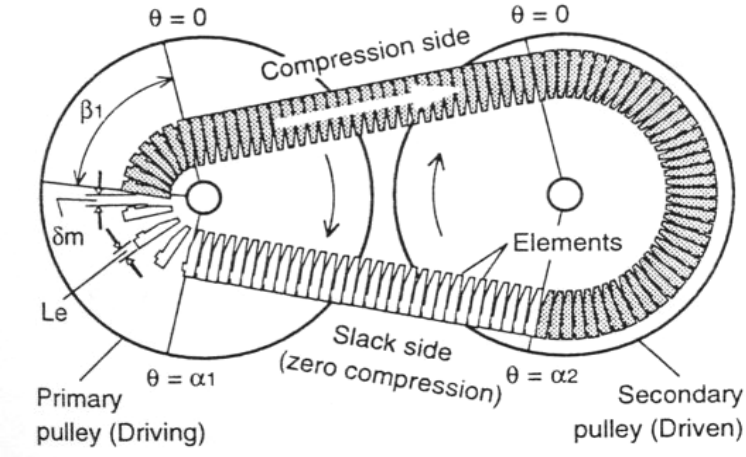

Figure 2.4: Slip mechanism due to gaps in a metal V-belt [43]

the forces were obtained from the conditions of quasi-static equilibrium. An experimental test-rig was also developed in order to verify the theoretical results. They observed that the slip ratio decreased with an increase in the pulley clamping force. They also noted the relationship between the slip-limit torque and the driven pulley clamping force at low and high pulley ratios. The authors also developed a Finite Element model of the variator mechanism to analyze the forces and stresses acting on the CVT components and to investigate the effects of belt misalignment on the band tension distribution and the belt torque capacity. It was observed that with increased belt misalignment, the maximum band tension increased whereas the torque capacity reduced.

Browne [45] investigated the torque capacity of metal belt CVTs under the conditions of quasi-static equilibrium and impending slip. Moreover, since the belt was assumed to be under the conditions of gross-slip, all the frictional forces were circumferentially directed. Only the inertial effects arising from centripetal acceleration were taken into account. It was proposed that the torque transmission capacity was limited by the maximum belt tension and the associated fatigue strength of the tension members. It was observed that for a given belt design, increasing the width with proportional changes in tension capability and mass led to a proportional increase in torque capacity. Optimization with respect to belt pitch radius yielded a 1-5 % increase in the torque capacity of the CVT system. This could be larger or smaller depending on the initial configuration of the drive.

Bonsen *et al.* [46] analyzed slip and efficiency in a metal pushing V-belt CVT. High clamping force levels reduce the efficiency of CVT. However, high clamping forces are necessary to prevent slip between the belt and the pulley. If a small amount of slip is

allowed, the clamping force level can be reduced. They investigated the variation of transmitted torque with slip. Radial slip was attributed to CVT shifting and spiral running of the belt. It was proposed that the amount of radial slip depended on the pulley deformation effects, the shifting speed, and the driver angular speed. Tangential slip was defined on the basis of redistribution of gap between the belt elements, just as in Kobayashi *et al.* [43]. It was observed that the traction coefficient (a measure of torque capacity) of a belt CVT increased with slip in the microslip regime. However, once the maximum torque capacity of the CVT was attained, the slip rose dramatically and the traction coefficient began to decrease. The friction between the belt and the pulley was modeled according to Stribeck's friction law. The force distributions were obtained using Asayama's [37] model. The authors also concluded that the traction coefficient is largely dependent on the CVT ratio and is not much influenced by pulley speed and clamping pressure. However, the CVT efficiency depends not only on the clamping pressure but also on the CVT ratio.

Amijima *et al.* [47] studied the axial force distribution on a block-type CVT analytically as well as experimentally. They observed the variation in the axial force profile as the belt progressed from the inlet to the exit of a pulley. A block V-belt CVT consists of high rigidity blocks and two tension members that fasten the blocks. Figure 2.5 [47] depicts the belt configuration for a block-type CVT.

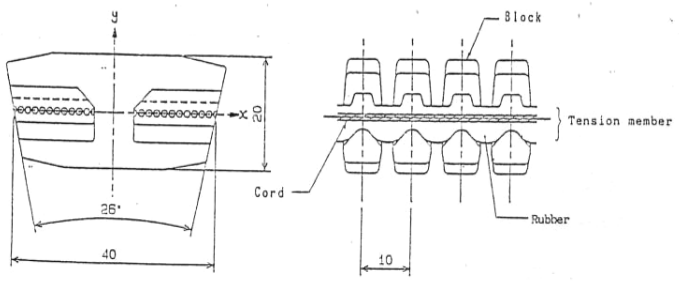

Figure 2.5: Belt configuration of a block-type CVT [47]

The authors developed a correlation to relate the angular position of the belt on the pulley to the sliding angle. The equations of motion were derived using quasi-static equilibrium and a relationship was developed to relate the two axial forces to tension, belt material properties and groove angle. The experiments yielded that the thrust force profile varies over the pulley and is maximum at the exit point. The authors observed that even under conditions of zero power transmission, the thrust pressure is not constant through the pulley contact arc when an initial tension exists in the belt. The thrust force increased with the increase in the transmitted load at any speed ratio. It was noted that usually the thrust force on the smaller pulley was higher than that on the larger pulley.

Sferra *et al.* [48] developed a unique model of metal V-belt CVT in order to simulate its transient behavior. The model includes inertial and pulley deformation effects. Discrete and continuous shifting behaviors were simulated in order to compute efficiency and power losses due to friction between the belt and the pulley halves. The results showed high loss of efficiency during shifting transients. Power losses due to other parasitic effects were not included in the model.

Chung and Sung [49] proposed a theoretical formulation for analyzing the contact behavior of a rubber V-belt drive with mono-cord construction. Based on the equilibrium equations that included the flexural rigidity of the belt, the coupling between the radial and circumferential motions was considered. The analysis was based on the work of Gerbert [19]. The tensile stress distribution, the active and idle arcs within the contact region, the sliding angle and the effects of bending rigidity on power loss were evaluated numerically.

Ide and Tanaka [50] experimentally measured the contact force between a metal pushing V-belt and the pulley sheave using ultrasonic waves. The relative change in the shape of the belt wrapping arc due to changes in the clamping force and transmitted torque is detected. The results showed that the shape of the belt wrapping arc is not co-axial with the pulley axis, and this was attributed to the asymmetrical pulley deformation. For low torques on the driver pulley, the contact force distribution exhibited peaks at the inlet and outlet of the pulleys. The peak on the outlet was higher, especially on the pulley with larger pitch radius. It was proposed that the asymmetrical pulley deformation and the self-locking of the belt on the pulley were responsible for the high peak at the pulley outlet. The authors also observed that the high peak of the contact force at the pulley outlet decreased as the driving torque increased. This was attributed to the increase in the belt compressive force and the disappearance of self-locking phenomenon of the belt on the pulley.

Ferrando *et al.* [51] designed a test bench for a V-belt CVT used in mopeds and conducted a series of tests covering the variable conditions of speed, torque, tension, and transmission ratio. The authors reviewed several models for computing pulley axial forces, as mentioned by Worley [52], Miloiu [19], and Gerbert [24, 53]. They also developed empirical models for computing axial forces and compared these models to those mentioned in the literature.

Bullinger and Pfeiffer [54] developed an elastic model of a metal V-belt CVT to determine its power transmission characteristics at steady-state. Pulley, shaft, and belt deformations were taken into account. The pulleys were modeled as elastic multibody system. Both the pulley sets have degrees of freedom associated with both rigid body

motion and elastic deformation. The pulley deformation was modeled using Finite Element Approximation and Maxwell's Reciprocal Theorem of Elasticity. The frictional constraints were modeled using the theory of unilateral constraints. The belt dynamics was specified by separate longitudinal and transverse approaches. The transversal dynamics was modeled using Ritz-approach based on B-splines. The longitudinal dynamics was described by using Lagrange coordinates. Figure 2.6 [54] depicts the multibody model used by the authors to capture the dynamic interactions in a metal V-belt CVT system.

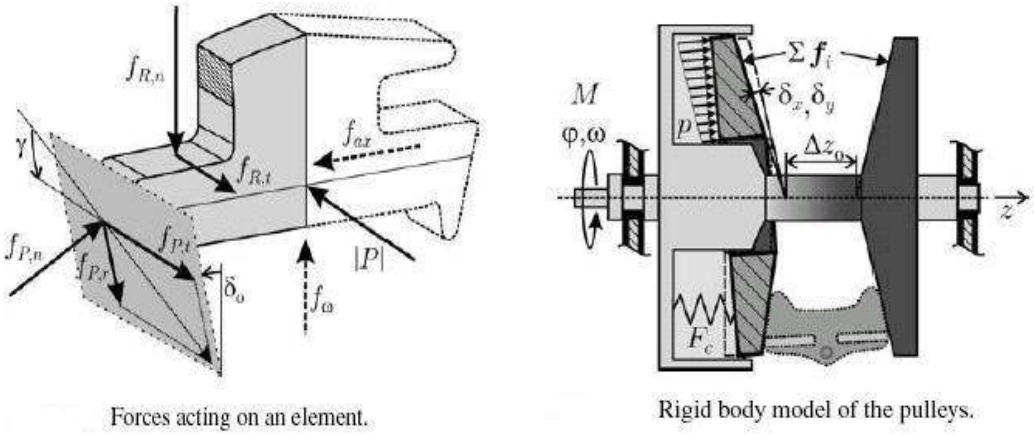

Figure 2.6: Multibody model of metal V-belt CVT [54]

Carbone *et al.* [55] did extensive work on modeling transient dynamics of a metal pushing V-belt CVT under shift ratio variations. They ignored longitudinal and transversal deformation of the belt. The radial thickness and the bending stiffness of the belt were also neglected during the analysis. Coulomb friction was used to model friction between the surfaces. Non-dimensional equations were defined to encompass different loading scenarios; however, the coupling between radial and tangential motions of the belt was not modeled in detail. The authors put considerable effort to obtain analytical solutions to the differential equations that describe the motion of belt over the driver and

driven pulley wraps. Carbone *et al.* [56] also studied the influence of clearance between the belt elements on the rapid shifting dynamics of a metal pushing V-belt CVT. The band tension and inertial effects were neglected in the analysis. The clearance between the elements was modeled as a kinematic strain of the belt. The authors noted that the power transmission is assured only if an active arc exists where the elements are pressed against each other and where compressive forces arise among the steel elements. The idle arc, where the steel elements are separated and no compression exists, does not contribute to torque transmission. On the driver pulley, a "shock" section was observed which separates the idle arc from the active arc. On the driven pulley, there is no shock section, but an "expansion wave" kind of phenomenon occurs as the clearance between the belt elements grows on the idle arc. Figure 2.7 [56] depicts the steady-state geometrical description of a metal V-belt CVT under the influence of clearance-redistribution.

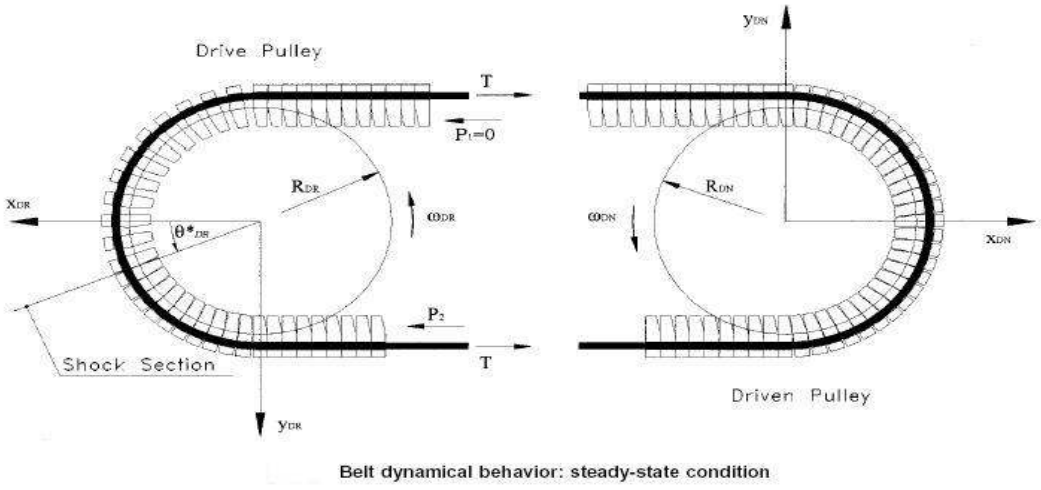

Figure 2.7: Geometrical description of belt CVT at steady-state [56]

Carbone *et al.* [57, 58] developed a one-dimensional continuous model of belt and also discussed the effect of band-element interaction on the dynamic behavior of a CVT. Flexural and inertial effects were neglected. The authors used two friction models, Coulomb friction model and a visco-plastic friction model, to model friction between the

belt and pulley. It was noted that the Coulomb friction model is unable to correctly predict the shift dynamics of CVT during slow maneuvers (i.e. creep-mode phases), but it could predict the limiting traction capacity of the belt drive and the CVT behavior in slip-mode (rapid shifting) phases. However, a visco-plastic model is able to accurately predict CVT behavior in creep-mode phases, and is also able to detect the transition from creep mode to slip mode. The authors also proposed simple relations to link shift speed to the clamping force ratio, the driver pulley speed, and the load torque. Carbone *et al.* [59] also studied the influence of pulley deformation on the shifting mechanism of a metal V-belt CVT. Coulomb friction hypothesis was used to model friction between different surfaces. Flexural effects of the belt were neglected, however pulley bending was considered. Only the inertial effects arising from centripetal acceleration of the belt were taken into account. Moreover, the continuity of the belt drive between the driver and driven pulleys was not modeled. The authors predicted that Coulomb friction model was able to accurately describe shifting behavior of CVT in creep and slip modes if the model took pulley bending effects into account. The authors used Sattler's [33] work to model pulley bending effects. They also suggested the absence of adherent arc between the belt and the pulley. Moreover, in steady state, the pressure and tension distributions were unaffected by pulley bending and depended only on the force ratio. However, pulley bending played a significant role in determining the transient response of the variator. It was shown that in creep mode, the rate of change of speed ratio continuously increases as the stiffness of the pulley decreases. The model was also able to predict the influence of angular velocity of the pulleys on the rate of change of speed ratio. The authors also proposed that during

creep-mode phases, the shift speed is almost linearly related to the logarithm of pulley clamping force ratio.

Experiments done by a number of researchers, especially those done by Fujii and Kanehara, have shown that both the tensile force in the band pack and the compressive force between the belt elements aid in torque transmission. Their work suggested that these forces vary non-uniformly over the pulley wrap, which invalidates the assumption of constant band tension made by other researchers. "Based on these original experimental findings, Fujii and Kanehara produced a number of subsequent publications each expanding to a degree on the previous work. Fujii *et al.* [60] did an experimental analysis to obtain clamping forces for different torque levels and angular speeds at a constant transmission ratio. The effect of speed on clamping force was found to be much more significant than the torque load effects. Fujii *et al.* [61] discussed experimental techniques to measure band tension and element compressive forces. The authors observed the existence of active and idle angles on the driving pulley and suggested that the magnitude of torque transmission by the bands may be up to 40~45% under some operating conditions. The authors also proposed that the band tension distributions are due to the speed differences that must exist between the bands and segments. Tension distributions are shown to decrease around the smaller of the two pulleys in the direction of belt travel" (*adopted from Akehurst's Ph.D. Thesis, [18], with permission*). Consequently, the band tension impedes torque transfer in high ratio and aids the transfer of torque in low ratio. This happens to such an extent that in low ratio, for a range of lower torque levels, the whole torque load was observed to be transferred by the band tensions alone. In the third part of their paper, Fujii *et al*. [18, 62] used a number of strain

gauged belt elements to measure forces acting in various directions on the belt element. The experiments were conducted on a constant transmission ratio CVT at low belt speeds and low clamping pressures. Time histories of pulley normal force, belt compressive force, transmitting force (i.e. tangential friction force between belt element and pulley), radial friction force, element shoulder force, etc. were recorded during the experiment. Since it was difficult to measure belt compression in the free span of the CVT system, a straight-line fit between the entry and exit conditions on each pulley was assumed. The pulley normal force was not evenly distributed about the contact arcs. It was observed that the normal force per element was lower on the pulley with the larger wrap angle; however, the element normal force exhibited peaks at the entry and exit of the pulleys, an observation noted by Ide *et al.* [50]. The authors also observed the existence of idle and active arcs in a belt running at a high transmission ratio. The radial friction force restricted the penetration of belt element into the pulley, except at the pulley exits where it acted to retain the belt element in the pulley wedge. Fushimi *et al.* [63] developed a numerical model to calculate steady-state force distributions and compared it to the results from existing experimental work. The metal V-belt is modeled using a lumped-parameter approach and consisted of three kinds of springs and two kinds of interfacial elements for one block and the ring. Fujii *et al.* [64] later extended the experimental set-up used in their fourth paper to record forces in a CVT under the conditions of varying transmission ratio. Time histories of various forces acting in a belt-pulley system were recorded. However, none of the above-mentioned papers of Fujii *et al.* included any kind of theoretical modeling of a metal V-belt CVT in order to explain the various dynamic interactions occurring in the system. Moreover, since the experiment was conducted at

low speeds and low pressures, inertial and deformation effects could not be captured in detail. However, Fujii and Kanehara co-authored a paper with Kuwabara [65] where they proposed an advanced numerical model to analyze power transmitting mechanism in a metal pushing V-belt CVT. The forces acting in the system were estimated not only at steady states but also during transitional states where the speed ratio was changing. The band tension is not assumed to be constant. The model takes into account the various dynamic interactions occurring among bands, elements and the pulleys. It was observed that bands transmitted negative power under over-drive conditions (i.e. when the pitch radius on driven pulley is smaller than the driver pulley radius). So, in order to meet load, the blocks transmit power more than the nominal. Much greater thrust was needed to shift the speed ratio during transitional state in comparison to the requirements in steady-state. The authors also observed that the thrust ratio (ratio of driver axial force to driven axial force) slightly increases with increase in coefficient of friction between the belt and the pulley. Coulomb friction was used to model friction between all the surfaces. The influence of flexure and belt inertia was neglected during the course of model development. Figure 2.8 depicts some of the steady-state results from Fujii *et al.* [65] that highlight the combined role of band pack and element forces in successful torque transmission.

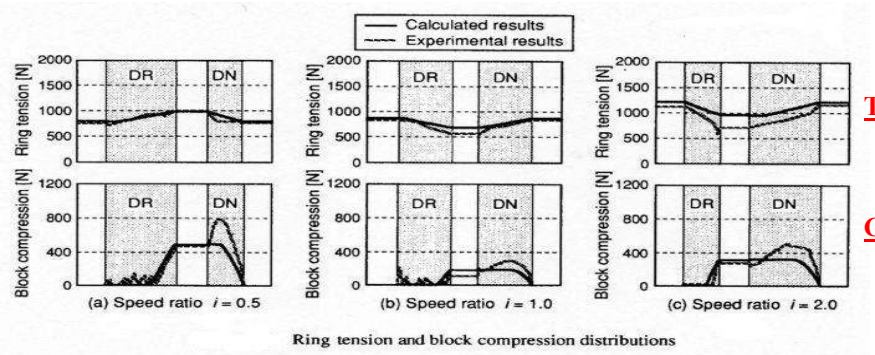

Figure 2.8: Steady-state Tensile and Compressive Forces in belt CVT [65]

Katsuya *et al.* [66] also obtained the equations of motion of the belt but they assumed the presence of friction only in circumferential direction. Kanehara, Fujii, and Oono [67] developed a macroscopic power transmitting model of a metal V-belt CVT at steady-state. They introduced mean coefficients of friction between the blocks and the pulleys, and between the blocks and the rings (or bands). The analysis was based on classical Euler's theory for conventional V-belts; however, the existence of idle and active arcs was taken into consideration. So, the torque transmission of the CVT was characterized by means of six mean coefficients of friction. The simulation, in effect, focused on changes in ratio and the effect of up-shift and downshift conditions on the friction coefficients between the components. Fujii and Kanehara co-authored a paper with Fujimura [68, 69] where they used mean coefficients of friction, as in their previous work, and shifting gradients to reveal the shifting mechanism of a metal V-belt CVT. Shifting gradient is a non-dimensional parameter which was defined as the radial increment of a block sitting on a pulley in radial direction per unit block path. The experimental results showed that the thrust force and the sliding speed significantly influenced the mean coefficients of friction. The authors also observed that the shifting gradient was influenced neither by pulley speed nor by torque ratio. Torque ratio is defined as the ratio of transmitted torque to the maximum transmittable torque. It was observed that the shifting gradient increased with increasing the thrust of a pulley in which the belt pitch radius was increasing. It also decreased with increasing thrust of a pulley in which belt pitch radius is decreasing. However, the authors did not include the influence of belt tensile and compressive forces on the shifting gradient of the variator. Fujii and Kanehara later co-authored a paper with Kataoka [70] where they analyzed shift

mechanisms of the variator and characterized friction between the blocks and the pulleys. The authors concluded that the shifting gradient is governed not only by the elastic deformations of the blocks (from the pulley thrusts), but also by the ring tension and block compression. The authors developed quasi-static equilibrium equations (neglecting detail inertial effects) to estimate target pulley thrusts at steady and transitional states. They also modeled the dynamic behavior of a belt block at the entrance of the pulleys. The driving and driven pulley thrusts were calculated by considering the forces acting on the blocks at the pulley entrance, which agreed with the experimental results at not only steady state but also transitional state. The frictional performance of CVT fluids and the frictional characteristics between the blocks and a pulley were evaluated by applying the mean coefficient of friction as a friction parameter. It was found from the experiments that the estimated coefficient of friction of CVT fluids was not constant with respect to the operating conditions. It varied due to the relative sliding between the blocks and the pulley and due to the normal pressure acting on the V-surface of the block. Miyawaza *et al.* [71] developed a discrete model in order to analyze the power transmitting mechanism of a dry hybrid V-belt CVT at both steady and transitional states. Block tilting and pulley deformation effects were included in the analysis. The model could consider seating/unseating behavior of the belt in the pulley groove, belt deformation, and radial penetration in the pulley groove simultaneously. A dry hybrid V-belt consists of a pair of tension members and many lateral H-shaped blocks. Blocks are connected to each other by tension members. The tension members are inserted into the grooves between two arms of the blocks, as shown in Figure 2.9 [71]. Since blocks are subjected to high pulley thrust to generate sufficient frictional forces, they have a hybrid structure utilizing a

strong core made of aluminum alloy. The belt is modeled using a lumped-parameter approach and consists of 5 springs and 1 interface element (which monitors the stick-slip transitions between the block and the pulley).

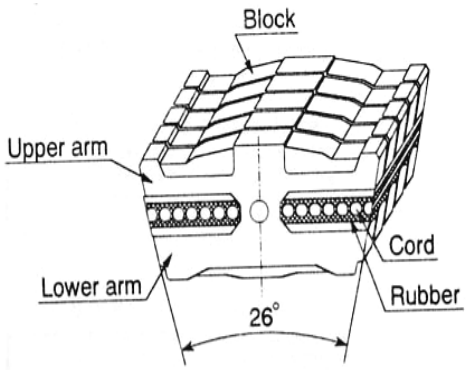

Figure 2.9: A dry hybrid V-belt assembly [71]

The authors assumed that the block arms do not bend in the analysis and they also neglected the influence of inertial effects on the dynamics of the belt-pulley system. The authors noted the absence of idle arcs on both driver and driven pulleys even when the transmitting torque was low. The coefficient of friction, block tilting, and pulley deformation affect the resultant pulley thrust. It was observed that at a speed ratio of 0.5, the pulley thrust ratio decreased 20% from the nominal value due to block tilting. However, the influence of block tilting on transmitting force and belt tension distributions was insignificant. At low speed ratios, a dramatic decrease of pulley thrust ratio was found when pulley deformation was considered. The authors also concluded that larger the coefficient of friction between belt and pulley, the lesser the pulley thrust force required for power transmission.

Shieh and Chen [72] developed a rigorous three-dimensional finite element procedure to analyze contact phenomena in belt transmission systems. They adopted a transformation matrix method (Chen and Yeh [73]) to satisfy geometric conditions on the

contacting surfaces and also used modified elements with incremental Wilson displacement modes (Wilson *et al.* [74]) to improve the accuracy due to bending at the end zones of the contact area of the belt-pulley interface. The influence of friction coefficients on the deformation, normal and tangential contact forces was studied in detail. Shieh and Chen [75] also studied the influence of angular speed on the frictional contact behavior of a rubber V-belt drive system. The authors used the finite element formulation from their earlier work to calculate the deformations and contact forces in the V-belt drive. However, in this work, an incremental restricted variational principle was established with the centrifugal force term to simulate the V-belt drive system operating at an angular speed. The authors observed that the normalized tangential and normal contact forces decreased as the angular speed increased. This affected the maximum transmitted torque endured by the V-belt drive system. The authors also investigated the power loss phenomenon by calculating the friction angle (sliding angle) distribution over the whole contacting arc of the belt. An increase in the friction angle increased the inward radial deformation of the V-belt which accounts for the power loss of the operating V-belt drive system.

Srivastava and Haque [76] developed a detailed transient dynamic model of a metal pushing V-belt block-type CVT. The goal was to understand the transient behavior of a belt element as it traveled from the inlet to the exit of either of the two pulleys. The inertial coupling due to the radial and tangential motions of the belt was modeled in detail. Flexural effects were neglected and the contact between the belt and the pulley was modeled using continuous Coulomb friction theory. It is evident from their work that not only the configuration and loading conditions, but also the inertial forces, influence

the dynamic performance of a CVT, especially the slip behavior and torque capacity. Srivastava *et al.* [77] also highlighted the significance of providing the CVT with a feasible set of initial operating conditions to initiate torque transmission. The authors suggested that CVT, being a highly nonlinear system, needs a specific set of operating conditions, which can be found using an efficient search mechanism, in order to successfully meet load requirements. The authors used Genetic Algorithms (GA) to capture this feasible set and also highlighted its efficiency in capturing this set by comparing it to the results generated by Design of Experiments (DOE). The optimization objective function was suitably chosen to maximize torque transmission capacity of the CVT system. Srivastava and Haque [78] developed a metal pushing V-belt CVT model in steady-state to study its microslip behavior and define its operating regime. They discussed the influence of torques and axial forces on the slip behavior of the belt. Slip is based on the redistribution of gaps among the belt elements and the formation of inactive arcs, as proposed by Kobayashi *et al.* [43]. The model is able to predict the maximum transmittable torque before the belt undergoes gross slip. The authors also observed that even under steady-state conditions, the CVT operates in a definite regime of axial forces and torques, which may be different from the operating regime under transient conditions. They predicted the minimum axial force necessary to initiate torque transmission and also the maximum axial force that the CVT can sustain (based on the slip behavior of the belt and not on the effects of stress, wear, or fatigue). The operating regimes for axial forces and torques were obtained by running numerous simulations with different transmission ratios.

Design issues, Losses and Efficiency:

Hsieh and Yan [79] discussed the efficiency-based design aspects of a CVT. The authors worked on differential transmissions and used the concepts of kinematic graph, static equilibrium and frictional loss for analyzing the mechanical efficiency of a CVT. They also performed optimization of the CVT using design constraints on velocity ratios to maximize mechanical efficiency.

Huang and Hu [80] studied the influence of a CVT on the fuel consumption levels of a vehicle. The authors did a design analysis of a CVT with the objectives of maximum motor speed and minimum fuel consumption. They devised a computational algorithm using surface fitting techniques for engine performance data and simulated annealing methods for optimization purposes. The CVT configuration sufficed to their research purposes and the necessary equations were developed.

Several design configurations have also been proposed for a continuously variable transmission like a split torque transmission by Hanachi [81], a geared-neutral variable transmission by Linzell *et al.* [82], and a double planetary gear train-CVT by Mucino *et al.* [83]. Hanachi [81] developed a computer-based mathematical model to represent a split-torque geared-neutral transmission. The equations of motion were derived using Lagrange's non-holonomic form. His work includes an engine-model, a transmission, a differential and a simple vehicle model. Slip inside the continuously variable unit was not taken into account; however, clutch slip was modeled using the assumptions of Couette flow and hydrodynamic lubrication.

Mucino *et al.* [83] proposed a design configuration that provides a power/torque split function. The key feature i.e. the power-split phenomenon, allows the CVT to carry

larger portion of input power at higher speeds. The authors implemented a simple design methodology, used kinematics and transmission ratio limits to design the planetary gear set.

Kluger *et al.* [84] presented an overview of current manual, automatic, and continuously variable transmission efficiencies. The authors also qualitatively discussed loss mechanisms in these transmissions and suggested design improvements to enhance transmission efficiency. As the belt-type CVTs require pressures of up to 3 MPa, the pumping power requirements represent a very large portion of the overall CVT power loss. The authors suggested the use of radial ball pump or a radial piston pump for sheave actuation in order to reduce pumping losses. The authors also discussed losses in a toroidal CVT and attributed those to the normal force generation and reaction, contact patch losses, and final drive effects. The authors found that manual transmission is the most efficient transmission among all three technologies. However, since the technology is quite mature, there is very little room for improvement in terms of efficiency and fuel economy. Kluger *et al.* [85] also discussed the mechanisms, forces, and efficiencies of different types of CVT, especially the push belt CVT, the variable diameter elastomer belt type CVT, the toroidal CVT, the nutating type CVT, and the epicyclic CVT. The amount of power which can be transmitted by a push belt type CVT is dependent on either the tensile strength of the bands or the transverse buckling strength of the belt elements. The dynamics within the steel bands play a crucial role in determining the maximum torque that can be transmitted. The authors suggested that the torque transmission is due to both pushing forces in the belt elements and friction forces between the elements and the bands. Singh and Nair [86] developed mathematical models

of different CVTs by using existing literature and later normalized the information to allow comparison of different CVT concepts (toroidal, chain, belt, hydrostatic) on an equitable basis. The models were used to compute the efficiencies of individual CVTs at selected points covering the entire operating envelope. The authors conclude that the rubber belt CVT, in general, is the most efficient among all. The PIV chain CVT is inefficient for low torques and traction CVT is less efficient than chain and belt CVTs in under-drive ratios.

Gerbert [87] also incorporated arc correction factors in V-belt transmission design. He used Euler's equation for calculating the belt tension and introduced new factors to the list of existing ISO factors for belt drives with speed ratios different from unity. These factors account for the decrease in the torque capacity of a belt drive due to the reduction of contact arc at any of the pulleys.

Micklem *et al.* [88] also studied the influence of wedging action on the torque transmission aspects of a CVT. Their work discussed a semi-empirical model to explain the belt torque loss under conditions of no load and loading on the driven pulley. Measurements showed that the loss is dependent on the secondary pulley clamping force and on the belt configuration. It was shown that in overdrive ratio, the torque loss imposed severe limitations on the maximum efficiency of transmission. Experiments were conducted on the transmission using a test rig with 1.1-litre petrol engine. The results predicted a relationship between the torque loss and the driven clamping force.

Akehurst [18] did extensive theoretical and experimental work on investigating the loss mechanisms associated with an automotive metal V-belt CVT. The author developed mathematical models to describe torque loss mechanisms within the belt drive.

Radial friction effects were neglected in the analysis except in the entry and exit regions of the pulley. The author also assumed that all the bands shared the tension load evenly. The main torque loss event is proposed to occur due to bands sliding relative to each other and the segment, and segments sliding relative to the pulley. Two further loss models were developed to describe losses as the segments travel around the pulley contact arc. These losses were due to the measured pulley deflections causing the segments to contact the pulley past ideal exit and entry points (wedge loss) and to penetrate further into the pulley than the ideal radius of the belt (penetration loss). The wedge loss is similar to an earlier empirical model developed by Micklem *et al.* [88]. Tangential belt slip was investigated based on the redistribution of gaps between the belt elements, as proposed by Kobayashi *et al.* [43]. In addition to the torque loss associated with the belt, the author studied other parasitic losses involved in the transmission system, like, seal and bearing drag losses, pump losses, clutch drag losses, meshing losses, churning and windage losses. In steady state, it was observed that the losses in high ratio at low speeds are lower than low ratio losses, due in part to the reduced pump losses. However, as the speeds increased, the high ratio losses exceeded those in low ratio. This was attributed to the increased belt torque losses, and final drive losses. Also, it was noted that in both ratios the torque loss increased with output torque loading. However, in low ratio conditions, the torque loss under no load conditions was higher than when the transmission was lightly loaded. The author also studied the influence of temperature on the loss mechanisms of the transmission (especially, the effects of cold temperatures). It was shown that the torque loss through the transmission varied

significantly with respect to temperature, and with bulk fluid temperatures in excess of 65 deg. Celsius, the torque loss through the transmission increased rapidly.

Saito [89] developed a simulation method allowing simultaneous evaluation of the dynamic behavior and the stress simulation for estimating the durability of a metal pushing V-belt for a CVT system. The influence of pulley stiffness on the dynamic behavior of a CVT was taken into account in the analysis. It was found that raising the pulley flexural stiffness contributed to the ring impact stress at the pulley entrance and exit, which increased the overall stress amplitude. The ratio of movable and fixed pulley rigidity had little influence on ring stress amplitude. There were cases, however, when changes in misalignment due to rigidity ratio caused ring edge contact to occur. The author also concluded that it is necessary to pay careful attention to ring impact stress and edge contact when determining pulley specifications that allow belt durability.

Gerbert [19] identified four major failure modes in rubber V-belts: cord rupture due to high torques, cord separation at moderate torques, radial cracks, and abrasion. Of these, cord separation mode was the most prevalent. It was attributed to the shear stresses occurring in the belt. Radial cracks start at the bottom of the belt and propagate towards the cord layer. They were attributed to the compressive stresses in the belt under low-torque applications. The author also observed that abrasion was more prevalent in drives with locked-center distance than in drives with variable center distance.

Childs *et al.* [90] did an experimental study on the power transmission efficiency of a V-belt, the wedge angle of which did not match its pulley groove. The experiments were run on a V-belt drive at a unit speed ratio. Unequal belt tensions in the strands between the pulleys, caused by power transmission, gave rise to a fractional angular

speed loss. On the other hand, sliding of belt into and out of the pulley grooves and belt bending hysteresis gave rise to torque loss. This occurred even when there is no torque transmission. The authors developed belt bending theory and ran experiments to observe how a belt's wedge angle changed with radius and material properties. They suggested that the Poisson ratio of the belt in the transverse direction should equal 0.25 for the least overall belt bending distortion effects. The authors proposed that belts with wedge angle smaller than the pulley groove suffered larger losses in comparison to a well-fitting belt. It was found that for greatest efficiency the wedge angle of the belt when bent to the pitch radius of the pulley should equal the groove wedge angle to within ± 1 degree. Childs *et al.* [91] also studied the influence of small pulley radii on the power transmission losses in V-belt drives. At low levels of torque, the fractional speed loss in the active arc region is caused by extension of the tension member and radial movement of belt within the pulley groove. Moreover, this speed loss is proportional to the transmitted torque. The influence of the radial and circumferential slip on the dynamics of a V-belt drive has already been discussed earlier in this chapter. Torque losses in V-belt drives were found experimentally to vary little with transmitted torque. They are caused by hysteresis losses (flexure of belt) and sliding (wedging of belt into and out of the pulley). Gerbert [19] also studied torque loss and related it to belt tension, stiffness, and coefficient of friction (all correlations were presented in dimensionless form). However, Childs *et al.* developed a new sliding theory (different from Gerbert's) to predict torque loss in V-belt drives. The authors experimentally observed optimum torques for maximum efficiency. At low torques, efficiency was reduced by torque losses which remain constant as torque was reduced; at higher torques, greater slip reduced efficiency. At lower tensions, slip reduced

the torques that could be transmitted while at higher tensions torque losses became excessive. The authors observed that the fractional speed loss was not only dependent on the transmitted torque but also on the total belt tension. The fractional speed loss increased with the reduced belt tension more on the small- than on the large- radii pulleys. Pulley radius also strongly influenced the maximum tension ratio that can be supported around a pulley without excessive power loss. It was also suggested that the hysteresis torque loss increased with decreasing pulley radius. The torque loss in a belt drive was independent of the transmitted torque but was linearly related to the total belt tension. The rate of increase of torque loss with the total belt tension was found to be inversely related to the pulley radius.

Gerbert [19] studied the influence of thermal effects on the performance and the life of a rubber V-belt drive by developing a simple heat transfer model based on conduction and convection effects. He proposed that heat is generated at the surface of the belt due to friction i.e. sliding between the belt and the pulley. Heat is also generated inside the belt due to hysteresis. The author suggested that thermal effects due to hysteresis significantly influence the life of a belt drive.

"Abo *et al.* [92] investigated the rate of heat generation in a metal V-belt CVT with respect to the slip speeds between the mating components. They modeled belt slip based on the redistribution of gaps among the belt elements, as discussed by Kobayashi *et al*. [43]. Any slip speed between the segments and the bands was assumed to occur only on the pulley with the smallest radius. The slip between the neighboring bands in a band pack is calculated in a similar way. All the energy loss due to the slipping contacts was assumed to be converted into heat energy, since noise and vibration energy are likely to

be small. Simulation results indicated that at constant belt speeds belt heat generation is greatest when the belt ratio is low. Losses also increase if the input torque is large or the belt speed is high. The simulation results were validated using a test rig facility. The heat generation measured experimentally, by recording the temperature rise of a known volume of lubricant, was assumed to be due to the bearings and the belt mechanism" (*adopted from Akehurst's Ph.D. Thesis, [18], with permission*).

A lot of research effort is also being put into investigating the influence of different lubricants on the performance of a belt/chain CVT. Lubrication also affects the torque loss mechanism due to the associated thermal effects and also modifies contact conditions between the belt and the pulley. "Peiffer *et al.* [93] describe a range of methods developed by Shell for testing different blends of CVT fluids to meet desired performance characteristics. The CVT fluids also have to perform many tasks in the transmission such as, allowing judder free clutch performance, providing good low temperature pumping action and starting performance, reducing losses in gears and bearings, yielding high pump and variator efficiencies. High pump efficiency requires the fluid to have almost constant viscosity-temperature behavior and excellent air release properties, so that the pumped volume does not change due to excessive leakage or changes in the fluid density. The variator efficiency demands on the fluid are more contradictory; a fluid capable of giving high metal to metal friction characteristics allows the clamping pressure to be reduced, thus reducing the pump losses, but at the same time this may increase the power loss due to friction within the other belt components. A number of the fluids tested produced friction vs. slip characteristics that increase with sliding speed, a beneficial characteristic in the functioning of the variator" (*adopted from*

Akehurst's Ph.D. Thesis, [18], with permission). Narita *et al.* [94] investigated the influence of lubricating oil on the torque capacity and the efficiency of a metal V-belt CVT. In order to analyze the friction characteristics of each of the contacting parts in the CVT, the authors used block-on-disc type friction testing machine. The contact surfaces between the block and the pulley was assumed to be under boundary lubrication conditions, and the transmission ratio was kept constant. It was found from the experiment that the torque capacity of the CVT correlates with the friction coefficient under high contact pressure (200 MPa) and relatively high sliding velocity (0.1 m/s) in the friction testing machine. The authors also found that the transmission efficiency decreased as the load decreased and it also decreased with the torque capacity. At a constant speed ratio, when the pulley thrust was higher, the efficiency was lower. Further, the efficiency decreased at lower torque ratios. The authors also investigated friction loss between the bands and the elements, and between the elements and the pulleys. The friction loss between the block and the pulley increased at a high torque ratio (high load) due to an increase in the sliding velocity. The friction loss between the block and the band at low load was greater than that between the block and the pulley. So, the authors suggested that it is necessary to improve the efficiency at low load to reduce the friction coefficient at low contact pressure.

Noise and Vibrations:

Vibration of power transmission belts has been investigated for many years and is still a challenging area of research. The problem, to a certain extent, belongs to a class referred to as axially moving material vibration. Yue [95] studied the effect of moving contact

between the belt and the pulleys on the vibration properties of the belt-drive. Due to the flexural rigidity of the belt, the free span of the belt between the pulleys is not a straight line. A theory of shape and length of the free span of a non-vibrating flexible belt was developed by Gerbert [24]. In a vibrating belt, the contact point moves along the pulley wrap, which implies that the length of the free span of the belt between the pulleys is not constant but varies with the vibration. This phenomenon is more commonly observed in rubber V-belts than in metal belts. The author introduced the concept of initial vibrating length. Different pitch radii and vibrating amplitudes affected the vibrating length of the belt. Increasing vibrating length led to an increase in the fundamental natural frequency of the belt. The author also noted that the cyclic variation of the belt length did not behave as a parametric excitation.

Kong and Parker [96] modeled the belt as an axially moving beam wrapped on fixed pulleys. For the axially moving beam model, the span boundary conditions are typically specified as simply supported or clamped, and the beam is assumed to remain straight in steady state. However, in real world applications like CVTs, the beam wraps around two fixed pulleys. This induces initial curvature in the steady state for non-vanishing bending stiffness, and the beam-pulley contact points are not on the common tangent between the pulleys. The authors proposed two different models to model such effects under steady state conditions. The first method assumed that the beam-pulley contact points were fixed on the common tangent line between the two pulleys. The second method eliminated this restriction. Instead, the contact points were not specified a priori but were calculated from a steady-state analysis of the beam in free spans. Bending of a moving beam around the bounding pulleys causes a non-trivial steady solution about

which the system vibrates. This steady curvature tends to increase the beam natural frequencies. The fixed boundary model overestimated the natural frequencies, especially for large bending stiffness. For the undetermined boundary model, as the bending stiffness increased, some natural frequencies decreased when the bending stiffness was small because of increased free span length in this range. For fixed boundary model, increasing beam speed increased the curvature, which made the system stiff. For the undetermined boundary model, increasing beam speed increased the curvature as well as the free span length, which made the system soft.

Thurman and Mote [97] studied the free, periodic, nonlinear oscillation of an axially moving strip. The oscillations were determined by the approximate solution of two, coupled, nonlinear, partial differential equations. One equation described the longitudinal dynamics, and the other the transversal dynamics. The authors incorporated the essence of Lindstedt and Krylov-Bogoliuboff methods to obtain accurate periodic solutions efficiently. The authors concluded that the existence of axial transport velocity reduced the fundamental period of oscillation and increases the relative importance of nonlinear terms in the equations of motion.

Chung and Sung [98] did an analytical and experimental study on the vibration of a rubber V-belt CVT during speed-ratio shifts. The major components were modeled as an instantaneous flexible four-bar linkage for analyzing the belt-CVT vibration behavior. The free span of axially moving belt was considered as the flexible coupler link, while the variable-diameter driving and driven sheaves were modeled as the crank and rocker links, respectively. The authors used mixed-variational principle to derive the equations of motion of the system. The boundary and initial conditions were determined from the

physical configuration of a practical CVT system. The length of the free span of the belt was obtained from contact analysis. A parametric study on the natural frequencies of the belt was then performed by using assumed-modes method. The authors observed that the natural frequencies of both tight- and slack- sides decrease as the CVT accelerates. Moreover, in steady state, higher belt tensions led to higher natural frequencies. Also, the natural frequency of the belt decreased with increasing transport velocity.

Leamy and Wasfy [99] developed an explicit time integration finite element model to study the effect of belt bending on the dynamic and steady-state responses of belt drives. Three-node beam elements based on torsional-spring formulation were used to model the belt. The pulleys were assumed to be rigid. Frictional contact between the pulleys and the belt was modeled using a penalty formulation with the frictional contact governed by a Coulomb-like tri-linear friction law. The authors observed that both belt creep and belt tension increased with the belt's bending stiffness. The bending stiffness also increased the tangential friction force and the normal force on the belt near the entry and exit sections of the pulley. The belt wrap angle around the pulley decreased as the belt bending stiffness increased. The belt natural frequencies increased only slightly with the bending stiffness. The authors predicted that the belt wear is expected to increase as the belt bending stiffness increases. Leamy *et al.* [100] also developed belt drive models to predict the drive's dynamic response to harmonic excitation. They put in considerable effort to model nonlinear belt response in frictional contact at the belt-pulley interface. The authors proposed two different models to solve the problem and identified a single dimensionless parameter Ω that governed the dynamic response. The authors suggested that a quasi-static model for belt-pulley interaction will remain accurate for belt drive

systems for which $\Omega < 1/3$. For $\Omega > 10$, they suggested that the frictional support acts effectively as an anechoic termination.

Moon and Wickert [101-102] developed a model to study radial boundary vibrations of misaligned V-belt drives. The authors assumed impending slip conditions and neglected inertial effects. The model was used to predict two quantities which described the motion of the belt at its boundary with the pulley sheave: the critical rotation angle of the sheave and the elevation of the belt across its span. These quantities were subsequently related to the frequency and the amplitude of the boundary excitation. Both pulley eccentricity and pulley misalignment can excite the motion of the belt on its boundary with the sheave. In the case of eccentricity, the excitation observed was usually sinusoidal and it occurred with the rotation of the sheave. However, the motion was low enough in frequency to generate substantial structural vibration of the belt. Parallel offset misalignment, on the other hand, produced a sawtooth-like stick-slip motion at a frequency that depended on the critical angle and the operating speed. Periodic bursts of vibration and noise resulted, and were associated with fine-scale slippage of the belt in the pulley groove.

Abrate [103] presented a state-of-the-art review on the vibration analysis of power transmission belts. Axial, transverse, and torsional vibrations of a power transmission belt were discussed. The author discussed the influence of belt tension, transport velocity, bending rigidity, support flexibility, pulley and belt imperfections, etc. on the vibration characteristics of the belts. The author also discussed the noise transmission phenomenon in power transmission belts [104].

Pfeiffer *et al.* [105] developed simplistic models to analyze self-induced vibrations in a pushing V-belt CVT. The free span length of the belt was assumed to be constant in the analysis. It was shown that the certain friction characteristics, especially those having negative gradient with respect to relative velocity, could induce self-excited vibrations in the belt. The friction characteristic and the elasticity of the pulley sheaves also determined the working area where vibrations occurred. The authors also observed that increasing pulley stiffness decreased belt vibration, but failed to eliminate them completely. Figure 2.10 [105] depicts the excitation mechanism proposed by the authors.

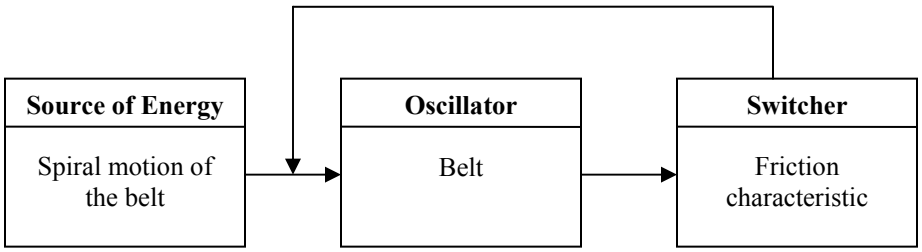

Figure 2.10: Self-excitation mechanism in a metal V-belt CVT [105]

Imamura *et al.* [106] experimentally studied the noise reduction in a continuously variable transmission. The authors proposed that the main cause of the CVT sound was the contact of CVT belt and the pulley. They proposed that the natural frequencies of the pulley should be tuned in order to reduce CVT sound. It was also shown that damping materials, when attached to the pulleys, reduced CVT noise considerably.

Control:

The control aspects for achieving a desired gear ratio profile or an actuation force are also an inevitable part of CVT research. The development of an optimum CVT control strategy is not an easy task owing to two partially opposite features that have to be

satisfied: the reduction of fuel consumption and the requirement of appropriate drivability. An accurate and fast control of the rate of change of speed ratio is a prerequisite for meeting these goals. The advanced control strategy also needs an accurate model of the transmission shifting dynamics in order to foresee the actual clamping forces needed to change the axial position of the pulleys and the CVT speed ratio.

In order to achieve minimum fuel consumption relative to various levels of desired drive torque, both engine speed and engine torque should be controlled simultaneously, which requires an integrated engine-transmission control. The purpose of the integrated CVT-engine control is to realize the optimal engine operation for minimum fuel consumption while also satisfying driver's demand. For optimal engine operation, the engine should be operated on the optimal operating line (OOL). In Figure 2.11 [18, 107], an OOL for minimum fuel consumption is shown on the engine characteristic map. The OOL for the minimum fuel consumption can be obtained from the SFC contours and iso-power curves. The optimal engine operation point is defined as the point where the optimal engine power curve crosses with the OOL. Minimum fuel consumption can be achieved by operating the engine on the optimal operation point by simultaneous TVO (throttle valve opening) and CVT ratio control, i.e. an integrated control.

An engine-CVT integrated control was suggested by Takiyama *et al.* [108]. The authors developed an algorithm to control the vehicle velocity from the difference between the desired and actual velocity and the CVT ratio from the difference between the desired and actual engine speed. However, they neglected the transient characteristics of powertrain, which resulted in poor performance when the vehicle acceleration varied.

Later, Takiyama [109] modified the control algorithm using decoupling theory and taking into account the effects of air-fuel ratio to attain higher fuel economy.

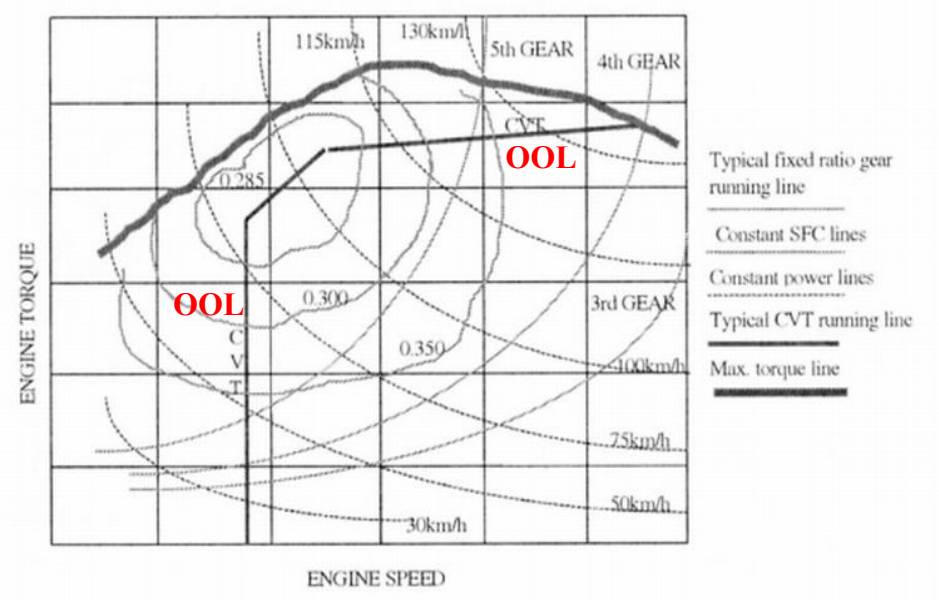

Figure 2.11: Typical Operating Map of a CVT Vehicle [18]

Sakaguchi *et al.* [110] developed an integrated engine-CVT control from the viewpoint of minimizing powertrain losses. The authors suggested that in an integrated engine-CVT control, it is necessary to consider powertrain losses in order to determine the target engine torque. Yasuoka *et al.* [111] developed an integrated engine-CVT control algorithm to obtain the demanded drive torque for optimum fuel economy. The authors used the engine torque to compensate for the drive torque response delay caused by the CVT response lag. The authors calculated the target torque by assuming that the accelerator pedal travel represents the demanded drive torque and used the target gear ratio as the CVT ratio. Kim *et al.* [112] developed an integrated engine-CVT control algorithm by considering the powertrain loss and the inertia torque due to the CVT ratio change during the transient state. They also proposed some compensation algorithms to reduce the effect of the CVT ratio response lag on the drive torque. The authors

conducted experiments to conclude that the optimal engine speed compensation algorithm gives better engine operation around the OOL, compared to optimal torque compensation, while showing nearly the same acceleration response. Kim *et al.* [113] experimentally investigated the response characteristics of a parallel hybrid electric vehicle (HEV) CVT and developed a ratio control algorithm integrated into a hydraulic control system. Based on the ratio control algorithm, the effect of CVT system dynamics on the HEV engine operation is investigated by hardware in the loop simulation. The simulation showed that the engine performance could be improved by using closed loop control, where variable control gains were used depending on the shift direction and the CVT speed ratio by considering nonlinear characteristics of ratio-control hydraulic valves and CVT belt-pulley dynamics. In order to maintain a steady-state speed ratio, an optimal pulley thrust is required. Decreasing clamping forces in the variator improves the efficiency of a CVT; however, it also increases the risk of belt wear due to excessive slippage. Bonsen *et al.* [114, 115] developed a gain-scheduling PI controller to measure and control slip in a CVT while minimizing clamping forces and preventing destructive belt slip. However, the slip control system was designed for quasi-static ratio control, which does not hold in dynamic driving situations. Saito and Lewis [116] developed a simulation technique for a metal pushing V-belt CVT with feedback thrust controllers. Multi-body formalisms were used to model the belt, and a modified PI controller was used to adjust pulley thrusts until a desired speed ratio was obtained. Some other interesting control algorithms proposed in the literature include Setlur *et al.* [117], Cho *et al.* [118], Pfiffner *et al.* [119, 120], etc.

Chain CVT:

In addition to the belt CVT, a lot of research effort is being directed towards understanding the dynamics and power transmission characteristics of chain CVTs. A chain-drive CVT consists of two variable diameter pulley sets connected to each other by means of a rocker-pin chain. A rocker-pin chain consists of inner plates, clasp plates, and rocker pins, as depicted in Figure 2.12 [7].

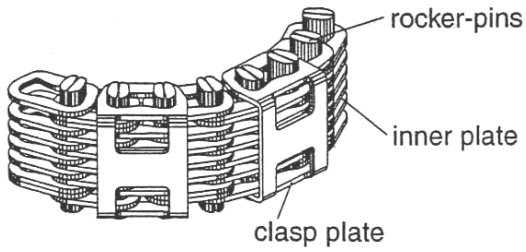

Figure 2.12: Chain link configuration [7]

All plates transmit tractive power, while the clasp plates also orientate the rocker pins perpendicular to the direction of motion of chain. Unlike a belt, the contact forces between chain and pulley are discretely distributed. This leads to impacts as chain links enter and leave the pulley. Hence, excitation mechanisms exist, which are strongly connected to polygonal action of chain links. This results in vibrations of the whole system, thereby influencing the dynamic behavior of the CVT system. Fawcett [121] did an extensive review on the existing literature related to belt and chain drives. The papers from different sources were grouped into three sections, as: dynamics of axially moving materials, chain-drive dynamics, and belt-drive dynamics. Most of the literature discussed by the author was related to the dynamics of roller chain drives, rubber V- and flat belts, and toothed belts. In contrast to roller chain drives, CVT chain drives transmit power exclusively through frictional forces in the contact zones between the bolts of the

chain and the cone sheaves of the pulleys. Every contact has two possible states, sticking or slipping, depending on the relatively velocity of the contacting surfaces. The possible transitions between them lead to mechanical system with time variant structure. Sauer [7] developed a finite-element method (FEM) based, static model for a CVT chain drive with elastic pulley-sets and a chain described link by link. The model gives a good theoretical description of the torque transfer behavior of CVT chain drives.

Srnik and Pfeiffer [7, 122-123] studied the dynamic behavior of a chain CVT drive for high torque applications. They developed a planar model of chain CVT with three-dimensional contact between chain link and pulley. The work dealt with multi-body formalisms and finite element modeling. In order to consider the discrete structure of the chain, which causes polygonal action, the chain is modeled link by link. The chain links are, thus, modeled as kinematically decoupled rigid bodies, which are interconnected by force elements, as proposed by Fritz and Pfeiffer [124]. Each link has three degrees of freedom, which is the maximum number of degrees of freedom in a plane. The pulley set is modeled as an elastic multibody system. Neglecting its own dynamics, the pair of rocker pins was modeled as one single, massless spring acting exclusively perpendicular to the plane of the model. The model was run at the conditions of constant driver pulley speed and constant driven pulley load torque. The researchers used Coulomb's friction law as well as a time sparing continuous approximation to calculate the contact forces. The computational cost was high in order to determine exact contact conditions between the links and the pulley, when a discontinuous friction model was used. The authors used methods developed by Pfeiffer and Glocker [125] for systems with time variant structure to get time histories from the chain CVT model. The simulation results showed the

influence of the cone pulley's deformation on the power transmission. They also show the repercussion of polygonal action between the chain links. The results also mention about the influence of chain's pitch on the vibrational behavior of transmission. The authors proposed that an unintegrated chain pitch reduced vibration amplitudes but also included a wider excitation band. The authors note that the sheave's deformation has a decisive influence on the contact kinematics and kinetics between a chain link and the pulley sheave. They also concluded that the efficiency of chain drive with flexible sheaves is lower than the one with rigid sheaves. This was attributed to substantially higher radial movements of chain link in the pulley groove under the influence of pulley flexibility.

Sedlmayr and Pfeiffer [126-129] studied the spatial dynamics of chain CVT drives. The authors modeled the links and the pulleys as elastic bodies and also included pulley misalignment effects. Even a small pulley misalignment was observed to yield significant tensile forces in the chain. Therefore, the authors decided to work on a chain model which took spatial effects into account. The pulley deformation was modeled using static FEM approximation and Reciprocal Theorem of Elasticity. Both pulley sets have one rotational, two translational in-plane, and one axial out-of-plane degrees of freedom. The pulleys also have other degrees of freedom related to elastic deformation. The pulley misalignment is dependent on the speed ratio and the length of chain. In order to limit the contact pressure between pins and sheaves the disc curvature radius is chosen not to be lower than a lower bound, which was 1.7 m for their model. Each chain link represents an elastic body, having three translational rigid body degrees of freedom. The links also have a few more degrees of freedom to describe the orientation and

deformation of pins. The links are kinematically connected between pairs of rocker pins. The elasticity and the translational damping of the joint are taken into account by the link force element, whereas the rotational damping and the axial friction between the pair of pins are considered in the joint force element. In the link force element each plate is taken into account as a spring. The effect of moving contacts relative to the plate spring reference points between a rocker pin and an adjoining plate are modeled as an exponentially varying contact torque. Edge bearing effects between the ends of the pins and the sheaves were observed, owing to the influence of shear, torsional, and bending deformations of rocker pins. The authors noted that due to the bending forces, the pulley misalignment induced a large gradient of the tensile forces in the spans. On entering the pulley, the shape of a pin changed abruptly because of suddenly growing contact forces. The authors also suggested that CVT chains without clasp plates are more flexible in shear direction and thus have lower tensile forces. The authors suggested that the tensile forces of a plate could be reduced by using longer rocker pins and more plates. However, this was not a good solution because with the same cross section of the pins, due to pin bending, the load splitting on the plates became worse. However, the tensile forces can be reduced by changing the design of a plate. Tensile forces were much less for a softer and lighter plate. The authors also did a comparative study on the efficiencies of metal V-belts and chains, and concluded that CVT chain drives have higher efficiencies especially with curved pulleys. A comparative study on the dynamics and performance of metal V-belt CVT and chain CVT was done by Lebrecht *et al.* [130]. Pausch *et al.* [131] analyzed the nonlinear dynamics of a chain drive CVT applied in an automotive drive train system.

Maier and Pfeiffer [132] developed a method to assess noise emission from the driveline components of a hybrid vehicle. Multibody models of the entire gearbox, the chain CVT, and other driveline components were used. The authors used complex nonlinear stiffness functions in the analysis to model excitation mechanisms arising from impact and friction in the chain CVT system and toothing forces in the gearbox. A method to calculate the A-rated equivalent continuous force level of the bearing forces, which is proportional to the sound, was also discussed. Stepanenko and Sankar [133] investigated limit cycle behavior induced by clearances in kinematic chains. They developed a new dynamic model of nonlinear element with clearance and analyzed its influence on the dynamics of power kinematic chains. Tenberge [134] developed a fast computational algorithm to compute dynamic indicators of chain CVT from a mathematical model which includes deformations, loadings, and other inertial effects at constant and variable speed ratios.

2.2 Research Objective

To the best of the author's knowledge and efforts, of the literature reviewed so far, very few research contributions have been made in understanding the influence of belt acceleration effects on the performance of a metal V-belt CVT (Srivastava *et al.* [76-78], Pfeiffer *et al.* [7, 54, 122, 126] , Fujii *et al.* [60-65]). Most of the models developed in literature only dealt with the inertial effects arising from centripetal acceleration. The literature review discussed in the previous section reveals the following opportunities of

research, which form the research objectives, for better understanding of the dynamic interactions in a CVT system:

- It is imperative to develop models that explore the transient behavior of a CVT system in detail as most of the CVTs operate in this mode. Most of the models of metal V-belt CVTs existing in the literature are based on steady-state quasi-static equilibrium analysis which neglects the influence of inertial effects on a CVT's performance. In addition to neglecting the influence of inertial effects on the performance of a CVT, a lot of the existing models neglect the dynamic interactions between the band pack and the belt element. It has been reported by some of the authors (Fujii *et al.* [61, 63, 65], Kobayashi *et al.* [43], Srivastava *et al.* [76-78], etc.) that the bands, under certain conditions, can contribute significantly to the torque capacity of a metal V-belt CVT. Moreover, it has been extensively showed in the literature that pulley flexibility significantly influences the thrust ratio and torque capacity of a CVT system. Hence, **a significant opportunity for research lies in the development of detail transient-dynamics model of a metal V-belt CVT that captures the influence of inertial effects, belt-band interactions, and pulley flexibility on its slip behavior and dynamic performance**. The transient-dynamics model developed by Srivastava *et al.* [76-77] is further extended in this research to incorporate the influence of pulley flexibility and band pack slip on the system dynamics.
- Belt- and chain- type CVTs fall into the class of non-smooth mechanical systems due to the presence of friction- and clearance- based nonlinearities. Almost all the models, except a few [6, 58, 105, 136], mentioned in the literature use Coulomb friction

theory to model friction between the contacting surfaces. The non-smoothness imposed by this friction characteristic arises from the discontinuous transitions between the stick and slip phases of the motion. However, depending on different operating or loading conditions and design configurations, the friction characteristic of the contacting surface may vary. For instance, in case of a fully lubricated CVT, the friction characteristic of the contacting surface may bear a resemblance to Stribeck curve [135] rather than to a continuous Coulomb characteristic. Moreover, very high forces in the contact zone may further lead to the conditions of elasto-plastic-hydrodynamic lubrication, which may yield a different friction characteristic. It has also been briefly mentioned in some the papers (Pfeiffer *et al.* [105], Togai *et al.* [136]) that certain friction characteristics induce self-excited vibrations in the CVT system. However, it is not clear whether such phenomenon is an artifact of the friction model or the real behavior of the system. It is, thus, necessary to **study the influence of different friction characteristics on the performance of transient-dynamic models of belt and chain CVTs**. Boundary lubrication and EHD lubrication models will be used to study the influence of friction under lubrication on the dynamics of belt and chain CVT systems. It is also important to note that although an exact knowledge of the friction characteristic in a CVT system can only be obtained by conducting experiments on a real production CVT, these mathematical models give profound insight into the probable behavior of a CVT system under different operating or loading conditions.

- Clearance is another non-smooth nonlinearity (may be piecewise linear) that has significant impact on the torque capacity and efficiency of a CVT system. As

mechanical systems wear, clearances between mating surfaces develop that can fundamentally change the behavior of the system and also induce unnecessary noise and vibrations. A CVT is no exception, and over continual operation it is susceptible to form clearances between its components. Moreover, it is quite possible for a CVT to have clearances among its various components during the assembly process. These clearances influence the dynamic behavior, torque capacity, and life of a CVT. Clearance inherently is a non-smooth nonlinearity (may be piecewise linear), which makes the CVT system non-smooth too. Significant amount of research [41, 43, 46, 56, 76-78] has been done on modeling clearance effects through gap redistribution theory in a metal V-belt CVT under quasi-static equilibrium conditions. Although some intensive research has been done on understanding the dynamics of chain CVTs (Pfeiffer et al. [7, 123, 129]), literature on the influence of clearance on the dynamics of CVT chains is scarce. So, another objective of this proposed research is to **develop a detailed multibody model of chain CVT, which incorporates a clearance model for studying clearance-related nonlinear effects in a chain CVT system**.

2.3 Research Contributions

- As mentioned before, most of the research related to modeling the transient dynamics of a metal V-belt CVT ignore the influence of inertial effects on the performance of a CVT. Srivastava *et al.* [76-77] previously developed detailed transient models considering the influence of both inertial effects and loading conditions on the slip behavior of a metal belt CVT. The transient-dynamics model developed by Srivastava

et al. [76-77] is further extended in this research to incorporate the influence of pulley flexibility and band-element slip on the dynamic performance of a metal V-belt CVT.

- Of all the literature surveyed so far and to the best of author's knowledge, only a few [58, 105, 136] have briefly discussed the influence of different friction characteristics on the dynamic performance of a CVT. The friction between the belt/chain and the pulley is usually modeled using Coulomb friction theory. However, as discussed earlier, the friction characteristic of the contact zone between two surfaces may vary depending on the loading condition and the design configuration. Since it is experimentally cumbersome to measure exact friction characteristics of the contacting surfaces in a CVT system, different literature-based mathematical models of friction are incorporated in these transient-dynamic CVT models in order to gain an insight into the influence of friction on the dynamic performance of a CVT.
- Although a lot of research has been done on developing multi-body formalisms for a chain CVT, literature related to the influence of clearance between chain links in a chain-drive CVT is scarce. Clearances among chain links have significant impact on the torque transmission capacity and efficiency of a chain- drive CVT. A clearance-model is developed and embedded into a planar multibody model of chain CVT in order to observe the influence of clearance between chain links on the dynamic performance of a chain CVT.
- A novel comparative analysis, based on the dynamics of stick-slip oscillators, is presented as an aid to understand some of the complex nonlinear phenomena in a CVT system.

- A comparative study based on the dynamic performance and torque transmissibility of a chain- and a belt- CVT is also presented. Although the results of the belt and the chain CVT models have not been experimentally verified, the trends discussed not only are comparable to those existing in the literature, but also are in consonance with the physics of the transmission.

2.4 Closure

Continuously variable transmission is an emerging technology as it offers a number of advantages over the automatic and manual transmission. A lot of research is available in the area of CVTs and new methods are constantly being devised in order to realize the full potential of a CVT. However, the recent designs and dynamic analyses of CVTs have not been able to foster its cause. It is incumbent on the researchers to explore the dynamics in detail in order to attain the proposed advantages of a CVT in a real production vehicle. The review of the previous work in this area has fostered the interest of author to develop models of some commonly used CVTs, i.e. the chain and belt CVTs, which accurately capture the detailed dynamic interactions occurring within the system. The detailed dynamic models discussed in this dissertation characterize friction-driven CVTs in a broader context by taking into account the effects of various nonlinearities on their performance. These models could be later exploited to design efficient controllers, identify loss mechanisms in a CVT system, analyze noise and vibration behavior of a CVT, characterize its operating regime and torque carrying capacity, optimize CVT to maximize vehicle performance and fuel economy, gain insight into CVT dynamics, etc.

CHAPTER 3

MODEL DEVELOPMENT AND FORMULATION OF EQUATIONS

3.1 Metal V-belt CVT Configuration

The basic configuration of a metal V-belt CVT consists of two variable diameter pulleys connected by a power-transmitting device i.e. a metal V-belt. The pulley centers are a fixed distance apart. The pulley on the engine side is called the primary or the driver pulley. The other on the final drive (or the wheel side) is the secondary or the driven pulley. Since one of the sheaves on each pulley is movable, the application of an axial force on the movable pulley sheave allows the belt to move radially in the pulley groove. In addition to the radial motion, the belt also moves tangentially around the pulley under the influence of an applied torque. The metal V-belt is made of two series of thin steel bands holding together thin trapezoidal elements. The elements are connected to each other by a system of pegs and holes, a peg in the forward face of an element connected to a hole in the rear face of the element in front. Usually, an initial gap exists between the elements of the belt as they are not tightly pressed together.

Torque is transferred from the driver to the driven pulley by the pushing action of the elements. As the belt moves, an element is carried forward on the driver pulley due to the friction forces generated from the pulley. This forward motion of the element generates compressive forces as it pushes on the element ahead of it. On the driven side, the belt transfers torque to the driven pulley through friction. Due to the presence of friction between the band pack and the elements, the tensile forces in the bands also vary

as the belt moves on the driver and driven pulleys. Thus, the operation of such a CVT is based on both the pulling and pushing mechanisms of the composite-structured belt. Figure 3.1 [6] illustrates the basic arrangement of a metal V-belt CVT. The band pack runs over the belt elements, whereas the belt element contacts not only the band pack, but also the pulley sheave.

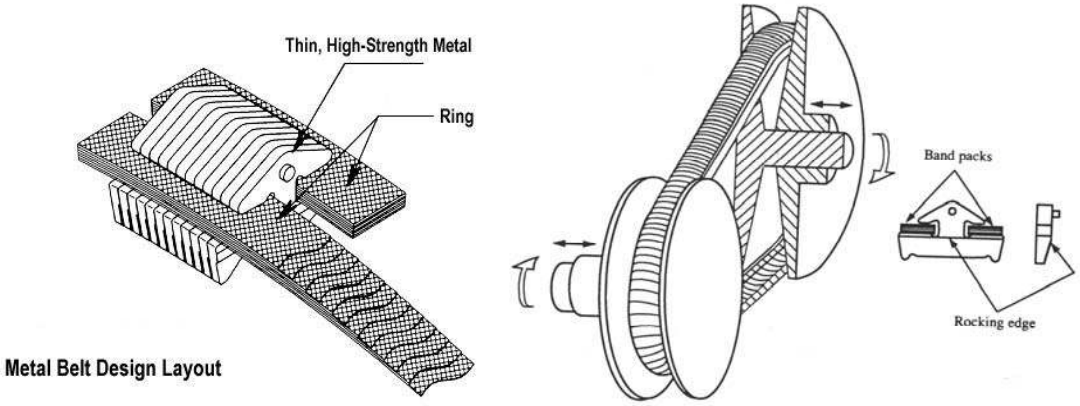

Figure 3.1: Basic Metal V-belt CVT arrangement [6]

3.2 Transient Model Development for a Metal V-belt CVT

3.2.1 System Consideration

Unlike flat belts, metal V-belts exhibit a complex dynamic behavior because of their ability to move both radially and tangentially in the pulley groove. The belt thus traces a noncircular path owing to this bi-directional sliding motion. The belt-CVT model presented in this dissertation is exposed to the external conditions of a constant driver angular speed, a constant input torque applied to the driver pulley, and a constant load torque on the driven pulley. The model starts off from the initial configuration and runs to

obtain the various dynamic indicators describing the belt-pulley interactions. The system boundary is limited to only the pulleys and the belt.

3.2.2 Assumptions

The assumptions made in the analysis are:

- Bending and torsional stiffness of the belt are neglected
- Continuous Coulomb friction model is used to model friction between a belt element and the pulley
- Pulley misalignment effects are neglected, however, pulley deformations are modeled using Sferra's model [48].
- The band pack can only sustain tensile forces, whereas a belt element can only undergo compression
- The belt is considered as an inextensible strip with zero radial thickness and infinite axial stiffness
- The center of mass of an element and the band pack coincide, which implies that the radial changes for an element is the same as that for the band pack
- Arcs subtended by the band pack and the element are equal
- Elements and bands are treated as a continuous belt
- Empirical relations to model torque-loss effects are not incorporated in the model
- The element dimensions are small in comparison to the radii of the pulleys
- Impending slip conditions exist between the band pack and the element
- The pressure distribution between the belt element and the pulley is constant over the wrap angle

- Belt mass density remains constant

The elastic deformation of the pulley sheave is described on the basis of Sferra's model [48]: simple trigonometric functions are used to describe the varying pulley groove angle and the local elastic axial deformations of the pulley sheaves. Figure 3.2 depicts the model for pulley deformation.

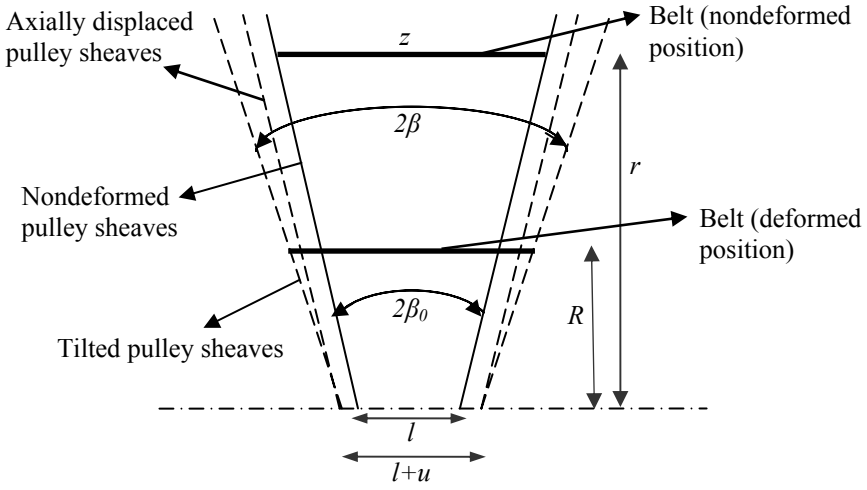

Figure 3.2: Pulley deformation model

Figure 3.3 depicts the free-body diagrams of a belt segment engaged with the primary pulley. The kinematic description involves two coordinate systems; **(n, τ)** that is attached to the belt and describes its path (ρ is the radius of curvature of the path of the belt element), and ($\hat{e}_r, \hat{e}_\theta, \hat{e}_z$) which is a rotating coordinate system attached to the center of the pulley i.e. point O. The point labeled C is the center of curvature of the belt path which changes with time. ω_s is the local sliding angular velocity of the belt element, defined later in the section.

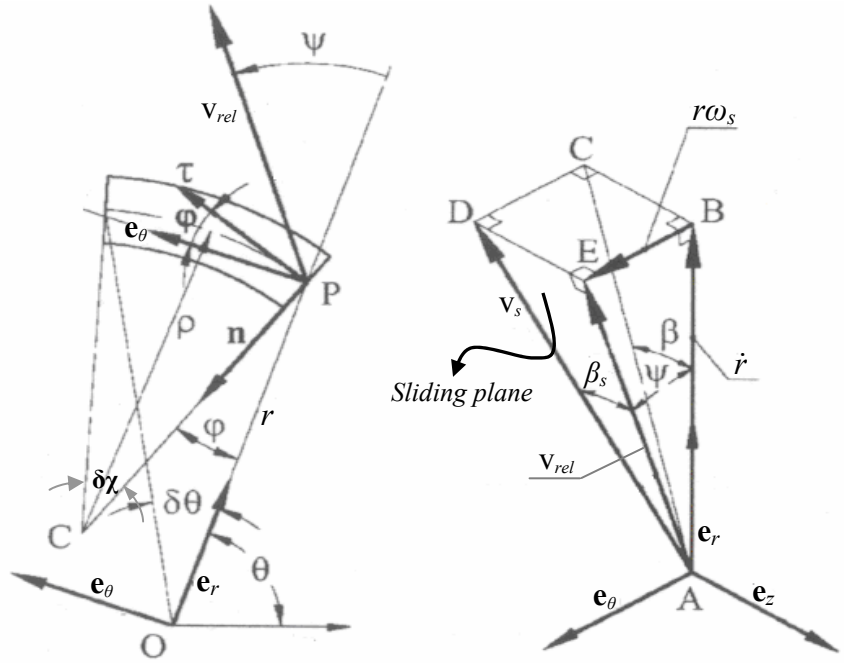

(a): Kinematic description of the belt

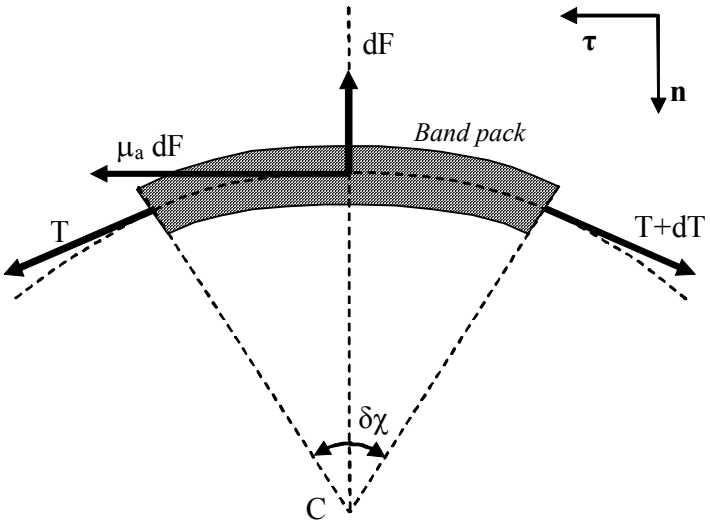

(b): Free body diagram of driver band pack

Figure 3.3: Free body diagrams of driver system

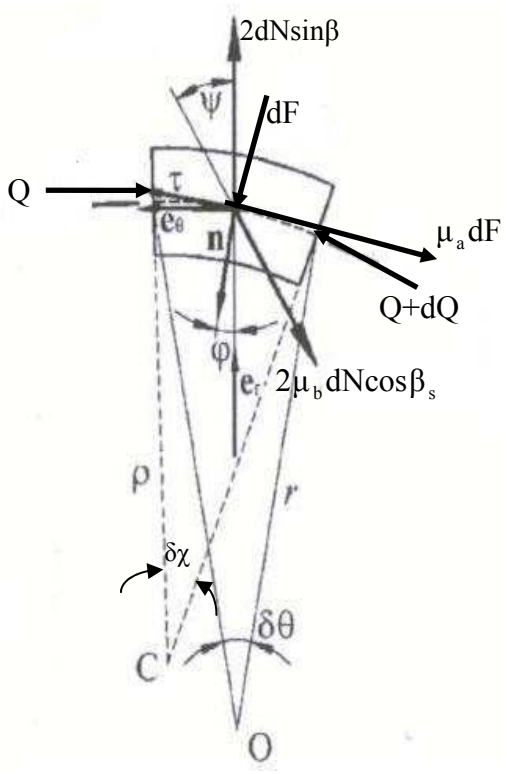

(c): Free body diagram of driver belt element

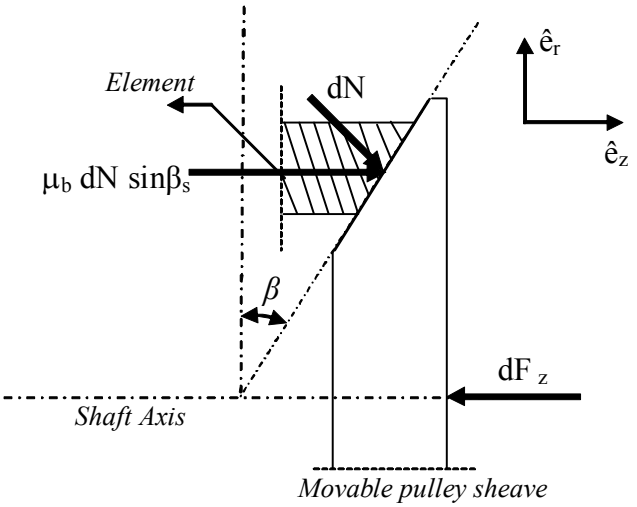

(d): Forces on driver pulley sheave

Figure 3.3: Free body diagrams of driver system (contd.)

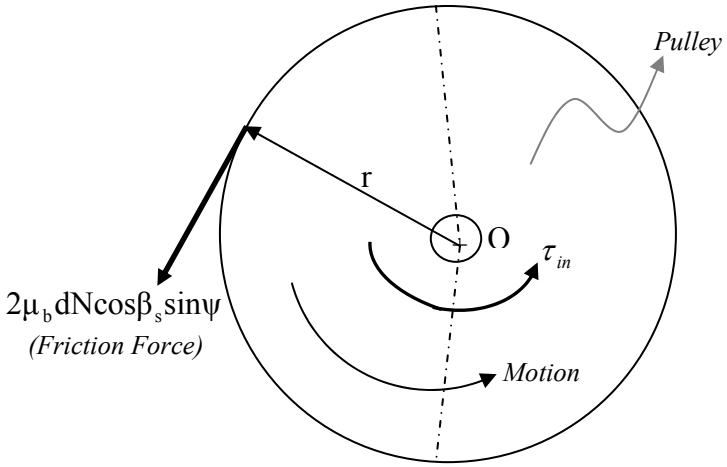

(e): Forces and torques on driver pulley

Figure 3.3: Free body diagrams of driver system (contd.)

3.2.3 Driver System Analysis

From the kinematic description of the belt (i.e. Figure 3.3 (a)), the following geometrical relationships can be derived:

$$\left.\begin{aligned} &\tan\varphi = \frac{1}{r}\frac{\partial r}{\partial \theta} \\ &\delta s = \frac{r}{\cos\varphi}\delta\theta \\ &\frac{1}{\rho} = \frac{\cos\varphi}{r}\left(1 - \frac{\partial\varphi}{\partial\theta}\right) = \frac{\delta\chi}{\delta s} \\ &\tan\beta_s = \tan\beta\cos\psi \end{aligned}\right\} \qquad (1)$$

The plane ADE in the 3-D view (refer to Figure 3.3 (a)) is the actual sliding plane where the belt slides. The belt slides tangentially and also moves radially in the pulley groove. The planes ABE and ABC are the rotational plane and the pulley wedging-angle, β, plane respectively. The angle β_s represents the pulley wedging-angle in the sliding plane of the belt.

The constraint of inextensibility of the belt implies that the time rate of change of the length of any infinitesimal belt element must be zero, i.e.

$$\begin{aligned} &\frac{d}{dt}\delta s = 0 \quad i.e. \\ &\frac{d}{dt}\left(\frac{r\delta\theta}{\cos\varphi}\right) = 0 \end{aligned} \tag{2}$$

Since the rate of change of the angular location and the speed of a belt element may not be constant or infinitesimal, its temporal variation can not be neglected in the above equation. However, (2) can be further simplified as,

$$\delta s = \frac{r\delta\theta}{\cos\varphi}$$

Taking natural logarithm of both sides of the above equation and differentiating the resulting expression with respect to time yields,

$$\frac{1}{\delta s}\frac{d}{dt}\delta s = \frac{\dot{r}}{r} + \dot{\varphi}\tan\varphi + \frac{1}{\delta\theta}\frac{d}{dt}\delta\theta$$

Since the belt element is inextensible, one finally gets a constraint equation as,

$$\frac{\dot{r}}{r} + \dot{\varphi}\tan\varphi + \frac{1}{\delta\theta}\frac{d}{dt}\delta\theta = 0$$

For an infinitesimal time step, tangent approximation reduces the abovementioned constraint equation as,

$$\left.\begin{aligned} &\frac{\dot{r}}{r} + \dot{\varphi}\tan\varphi + \frac{1}{\delta\theta}\delta\left(\frac{d\theta}{dt}\right) = 0 \\ &\frac{\dot{r}}{r} + \dot{\varphi}\tan\varphi + \frac{\delta\dot{\theta}}{\delta\theta} = 0 \\ &\frac{\dot{r}}{r} + \dot{\varphi}\tan\varphi + \frac{\delta\dot{\theta}/\delta t}{\delta\theta/\delta t} = 0 \\ &\frac{\dot{r}}{r} + \dot{\varphi}\tan\varphi + \frac{\ddot{\theta}}{\dot{\theta}} = 0 \end{aligned}\right\} \tag{3}$$

Also, for an infinitesimal time step,

$$\tan\varphi \approx \frac{\dot{r}}{r\dot{\theta}} \tag{4}$$

Incorporating the above approximation into the final equation of (3) results into a constraint equation for belt inextensibility, as:

$$\dot{r}\left(\dot{\theta}+\dot{\varphi}\right)+r\ddot{\theta}=0 \tag{5}$$

Belt Kinematics:

Friction between a belt element and the pulley is modeled using continuous Coulomb friction theory. In order to accurately predict the magnitude and direction of friction force, it is necessary to evaluate the relative velocity between a belt element and the pulley. Moreover, it is also necessary to calculate belt acceleration in order to observe the influence of inertial effects on the dynamics of a metal V-belt CVT.

The velocity of an infinitesimal belt element of length δs can be expressed as:

$$\bar{v} = \lim_{\delta t \to 0} \frac{\delta s}{\delta t}\ \bar{\tau}$$

$$\bar{v} = \lim_{\delta t \to 0} \frac{\delta s}{\delta \theta}\frac{\delta \theta}{\delta t}\ \bar{\tau}$$

$$\bar{v} = \lim_{\delta t \to 0} \sqrt{r^2 + \left(\frac{\delta r}{\delta \theta}\right)^2}\ \frac{\delta \theta}{\delta t}\ \bar{\tau}$$

$$\bar{v} = \sqrt{\dot{r}^2 + r^2\dot{\theta}^2}\ \bar{\tau}$$

Introducing (4) and the coordinate transformation between $(\bar{\tau},\bar{n})$ and $(\hat{e}_r,\hat{e}_\theta)$, i.e.

$$\begin{Bmatrix}\bar{\tau}\\ \bar{n}\end{Bmatrix} = \begin{bmatrix}\sin\varphi & \cos\varphi\\ -\cos\varphi & \sin\varphi\end{bmatrix}\begin{Bmatrix}\hat{e}_r\\ \hat{e}_\theta\end{Bmatrix} \tag{6}$$

in the above expression for belt velocity, yields

$$\bar{v} = \dot{r}\,\hat{e}_r + r\dot{\theta}\,\hat{e}_\theta \tag{7}$$

So, the relative velocity between a belt element and the pulley can be readily obtained as:

$$\left.\begin{aligned} &\bar{\mathrm{v}}_{\mathrm{rel}} = \dot{r}\,\hat{e}_r + r\omega_s\,\hat{e}_\theta \\ &\omega_s = \dot{\theta} - \omega \\ &\text{Also, } \tan\psi = \frac{r\omega_s}{\dot{r}} \end{aligned}\right\} \tag{8}$$

The acceleration of a belt element can be obtained from differentiating the velocity of the belt element, as:

$$\bar{a} = \frac{d\bar{\mathrm{v}}}{dt} = \left(\ddot{r} - r\dot{\theta}^2\right)\hat{e}_r + \left(r\ddot{\theta} + 2\dot{r}\dot{\theta}\right)\hat{e}_\theta \tag{9}$$

Since the belt is treated as an inextensible strip, the total length of the belt (refer to Figure 3.4) must be constant. The constraint of constant belt length can be mathematically expressed as:

$$\left.\begin{aligned} &\frac{dL}{dt} = 0, \quad \text{where} \\ &L = \int_0^{\alpha} \frac{r\,d\theta}{\cos\varphi} + \int_0^{\alpha'} \frac{r'\,d\theta'}{\cos\varphi'} + 2d\cos\varepsilon \\ &\varepsilon = \sin^{-1}\left(\frac{r'-r}{d}\right) \end{aligned}\right\} \tag{10}$$

Since the flexural effects of the metal belt are assumed to be negligible, it is reasonable to assume that the belt always exits and enters the pulley tangentially. Had this assumption been not made, the complexity of the problem would have increased as the wrap angles α, α' would no longer be known quantities. The constraint equation (10) kinematically couples the driver and driven systems to each other.

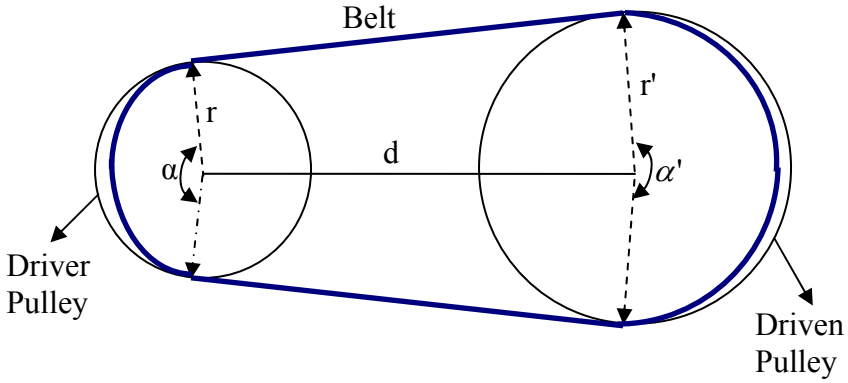

Figure 3.4: Belt-drive geometrical description

The wrap angles are given by the following relations:

$$\left.\begin{aligned}\alpha &= \pi - 2\sin^{-1}\left(\frac{r' - r}{d}\right)\\ \alpha' &= \pi + 2\sin^{-1}\left(\frac{r' - r}{d}\right)\end{aligned}\right\} \tag{11}$$

<u>Governing Equations of Motion</u>:

<u>Band pack</u>:

Summation of forces in the tangential and normal directions (refer to Figure 3.3 (b)) for the band pack yields the following equations respectively:

$$\sum F_\tau :\rightarrow \mu_a dF - dT = \sigma_b ds(\bar{a}.\bar{\tau})$$

$$\sum F_n :\rightarrow -dF + Td\chi = \sigma_b ds(\bar{a}.\bar{n})$$

Using (1), (6), and (9), for an infinitesimal time step, the above equations for band pack can be simplified to obtain:

$$\sum F_\tau :\rightarrow \mu_a \dot{F} - \dot{T} = \sigma_b r\dot{\theta}\left[\left(\ddot{r} - r\dot{\theta}^2\right)\tan\varphi + \left(2\dot{r}\dot{\theta} + r\ddot{\theta}\right)\right] \tag{12}$$

$$\sum F_n :\rightarrow \frac{T}{\rho} - \frac{\dot{F}\cos\varphi}{r\dot{\theta}} = \sigma_b\left[-\left(\ddot{r} - r\dot{\theta}^2\right)\cos\varphi + \left(2\dot{r}\dot{\theta} + r\ddot{\theta}\right)\sin\varphi\right] \tag{13}$$

Belt Element:

Similarly, summation of forces in the tangential and normal directions (refer to Figure 3.3 (c)) for the belt element yields the following equations respectively:

$$\sum F_\tau :\rightarrow \dot{Q} - \mu_a \dot{F} + 2\dot{N}\{\sin\beta \sin\varphi - \mu_b \cos\beta_s \sin(\varphi+\psi)\} = \sigma_e r\dot{\theta}\left[\left(\ddot{r} - r\dot{\theta}^2\right)\tan\varphi + \left(2\dot{r}\dot{\theta} + r\ddot{\theta}\right)\right] \tag{14}$$

$$\sum F_n :\rightarrow -\frac{Q}{\rho} + \frac{\cos\varphi}{r\dot{\theta}}\left[\dot{F} - 2\dot{N}\{\sin\beta\cos\varphi - \mu_b \cos\beta_s \cos(\varphi+\psi)\}\right] = \sigma_e\left[-\left(\ddot{r} - r\dot{\theta}^2\right)\cos\varphi + \left(2\dot{r}\dot{\theta} + r\ddot{\theta}\right)\sin\varphi\right] \tag{15}$$

It is to be noted in the above equations that the acceleration of the belt element is the same as that of the band pack as their center of masses coincide.

Driver Pulley:

Neglecting the sheave inertial effects and summing the forces on the movable pulley sheave in the axial direction results in the following equation:

$$F_z = \int_0^\alpha dN\left(\cos\beta + \mu_b \sin\beta_s\right) \tag{16}$$

Summing all the moments acting on the driver pulley yields,

$$\sum M_0 :\rightarrow I\dot{\omega} = \tau_{in} + \int_0^\alpha 2\mu_b r \cos\beta_s \sin\psi dN \tag{17}$$

Pulley Deformation Modifications:

Simple trigonometric functions, in accordance with Sferra's model [48], are used to describe the variations in the pulley groove angle and the axial width of the pulley groove. Since the belt has infinite rigidity in the axial direction, the width of belt is constant. The following equations describe pulley deformation effects in Figure 3.2:

$$\beta = \beta_0 + \frac{\Delta}{2}\sin\left(\theta - \theta_c + \frac{\pi}{2}\right)$$
$$u = 2r\tan(\beta - \beta_0) \tag{18}$$

The belt pitch radius on the deformed pulley sheave is given as:

$$\begin{aligned} R\tan\beta &= r\tan\beta_0 - \frac{u}{2} \\ &= r(\tan\beta_0 - \tan(\beta - \beta_0)) \end{aligned} \tag{19}$$

The amplitude of the variation in the pulley groove angle, Δ, is always much smaller than unity; however, it is not constant during speed-ratio changing phases due to the variations in the pulley axial (clamping) forces. Sferra *et al.* [48] proposed the following correlations for the variation Δ and the center of the pulley wedge expansion θ_c.

$$\Delta = \frac{0.000045\tau_{in}}{\left(\frac{r}{r'}\right)^{0.55}}$$
$$\theta_c = \frac{\pi}{3}\frac{r}{r'} + \frac{23\pi}{180} \tag{20}$$

Since $\Delta << 1$ (i.e. $|\beta - \beta_0| << 1$), Taylor series expansion of $\tan\beta$ around β_0 gives,

$$\tan\beta = \tan\beta_0 + \frac{\Delta}{2\cos^2\beta_0}\sin\left(\theta - \theta_c + \frac{\pi}{2}\right) \tag{21}$$

Moreover, $u \approx r\Delta\sin\left(\theta - \theta_c + \frac{\pi}{2}\right)$

Using (21) and the approximation of $\Delta << 1$, the following relation for the belt pitch radius on a deformed pulley can be easily deduced:

$$R = r\left(1 - \Delta\frac{1+\cos^2\beta_0}{\sin 2\beta_0}\sin\left(\theta - \theta_c + \frac{\pi}{2}\right)\right) \tag{22}$$

Taking natural logarithm on both sides of (19) and differentiating the resulting expression with respect to time yields the following relation:

$$\frac{\dot{R}}{R}+\frac{\dot{\beta}}{\cos^2\beta\tan\beta}=\frac{\dot{r}}{r}-\frac{\dot{\beta}}{(\tan\beta_0-\tan(\beta-\beta_0))\cos^2(\beta-\beta_0)}$$

Differentiating (18) w.r.t time to get $\dot{\beta}$ and using the assumption $|\beta-\beta_0|<<1$, one gets,

$$\dot{R}=\frac{R\dot{r}}{r}-\omega R\Delta\frac{1+\cos^2\beta_0}{\sin 2\beta_0}\cos\left(\theta-\theta_c+\frac{\pi}{2}\right) \tag{23}$$

So, equations (22) and (23) give the modified position and velocity of the belt by taking into account the pulley deformation effects.

3.2.4 Driven System Analysis

The dynamic interactions between the belt and the driven pulley are analogous to those between the belt and the driver pulley. The belt transfers torque to the driven pulley in order to sustain the load torque. Figure 3.5 depicts the free-body diagrams of a belt segment engaged with the driven pulley.

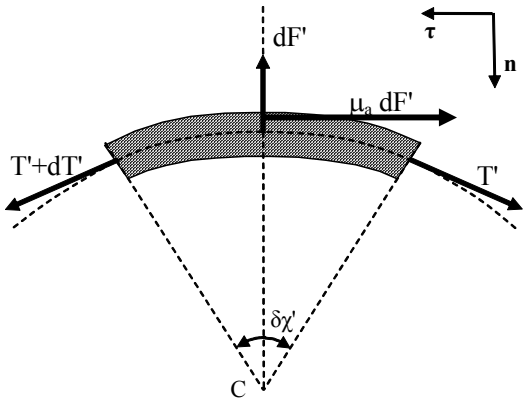

(a): Free body diagram of driven band pack

Figure 3.5: Free body diagrams of driven system

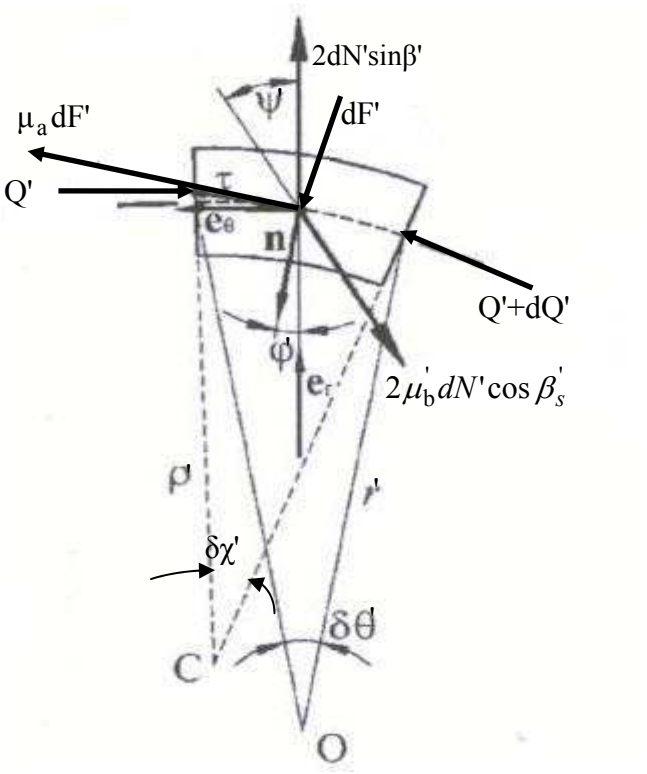

(b): Free body diagram of driven belt element

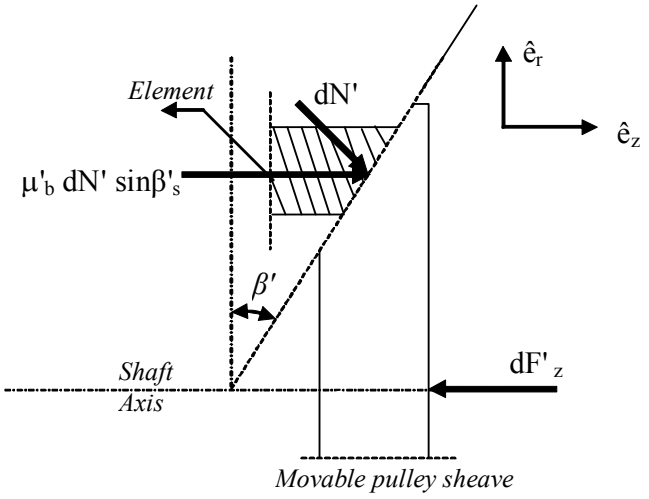

(c): Forces on driven pulley sheave

Figure 3.5: Free body diagrams of driven system (contd.)

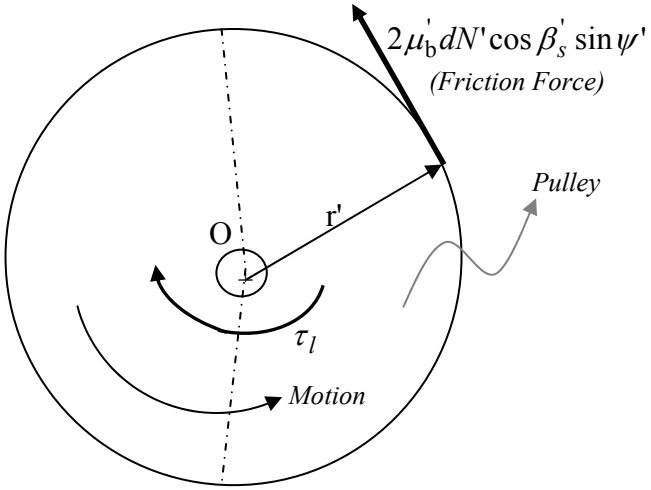

(d): Forces and torques on driven pulley

Figure 3.5: Free body diagrams of driven system (contd.)

Governing Equations of Motion:

It is evident from the free body diagrams of the driven system that except for a few equations, the rest of the governing equations of motion of the driven system are identical to the equations of driver system. For brevity purposes, only the equations which are dissimilar to the driver system equations will be mentioned.

Band pack (tangential equation):

$$\sum F_\tau :\rightarrow -\mu_a \dot{F}' + \dot{T}' = \sigma_b r' \dot{\theta}' \left[\left(\ddot{r}' - r' \dot{\theta}'^2 \right) \tan\varphi' + \left(2\dot{r}' \dot{\theta}' + r' \ddot{\theta}' \right) \right] \tag{24}$$

Belt Element (tangential equation):

$$\sum F_\tau :\rightarrow \dot{Q}' + \mu_a \dot{F}' + 2\dot{N}' \left\{ \sin\beta' \sin\varphi' - \mu'_b \cos\beta'_s \sin(\varphi' + \psi') \right\} = \sigma_e r' \dot{\theta}' \left[\left(\ddot{r}' - r' \dot{\theta}'^2 \right) \tan\varphi' + \left(2\dot{r}' \dot{\theta}' + r' \ddot{\theta}' \right) \right] \tag{25}$$

Driven Pulley:

$$\sum M_0 :\rightarrow I' \dot{\omega}' = -\tau_l + \int_0^{\alpha'} 2\mu'_b \, r' \cos\beta'_s \sin\psi' dN' \tag{26}$$

The driven system is kinematically coupled to the driver system through the constraint of constant belt length i.e. equation (10). The influence of pulley deformation on the driven system dynamics can be incorporated in a way similar to the driver pulley deformation analysis. The coefficient of friction between the belt element and the pulley surface is given by the continuous Coulomb friction theory, i.e.

$$\mu_b = a + (\mu_{bo} - a)(1 - e^{-|v_S|/b}) \tag{27}$$

where, a, b are constants and v_s is the slip velocity. It is to be noted that the relative velocity as given by equation (10) is not the actual sliding velocity of the belt element. Since the belt slides on the sliding plane (refer to Figure 3.3(a)), the actual sliding (relative) velocity, v_s, between the belt element and the pulley is, in fact, given by,

$$v_S = \dot{r}\sqrt{\sec^2\psi + \tan^2\beta}, \quad \tan\beta_s = \tan\beta\cos\psi$$

3.2.5 Solution Procedure for the Equations of Motion of the CVT Model

A CVT allows the engine to run within a constant range of speed where maximum fuel economy can be achieved. There are two different ways to analyze the dynamics of a CVT: (a) allow a constant axial force on the driver pulley and observe the system dynamics under torque loading conditions (Srivastava and Haque [76-77]), and (b) allow the driver pulley speed to be constant (say, the one which corresponds to the maximum fuel economy) and observe the system dynamics under torque loading conditions.

There are fourteen primary unknowns (seven each for driver and driven) in the CVT model, as: $[R, \theta, T, Q, F, N, \omega]$. The rest of the unknowns can be obtained using these primary unknowns. The analysis presented in the subsequent subsections is based

on the loading scenario (b) i.e. constant driver pulley speed with an input torque on driver pulley and a load torque on driven pulley.

It can be observed from the previous section (i.e. section 3.2) that the CVT dynamics is governed by a complex system of integro-differential equations along with some kinematic constraint equations. However, under certain assumptions, it is possible to simplify the model without compromising the dynamics involved in the system. In addition to the assumptions mentioned in section 3.2.2, the following assumptions are made in the analysis:

- Uniform pressure distribution, i.e. $\left(\frac{1}{r}\frac{dN}{d\theta}\right)$, between the belt and the pulley
- Assume φ is negligible and $\dot{\varphi} << \dot{\theta}$

It is reasonable to assume φ to be a small quantity as it implies that the rate at which belt pitch radius changes is smaller than the rate at which belt traverses around the pulley. Moreover, the rate at which the slope angle (φ) changes is perhaps smaller than the rate at which the angular position (θ) of the belt element changes.

DRIVER System Solution Procedure:

Under the abovementioned assumptions, (16) can be approximated as:

$$F_z = \frac{\dot{N}\alpha}{\dot{\theta}}\left(\cos\beta + \mu_b \sin\beta_s\right) \tag{28}$$

Moreover, since the driver pulley speed, ω, is constant, one gets,

$$\dot{N} = -\frac{\tau_{in}\dot{\theta}}{2\mu_b r\alpha\cos\beta_s \sin\psi} \tag{29}$$

The following relations can also be derived from (1),

$$\rho \approx r$$
$$\varphi \approx \frac{\dot{r}}{r\dot{\theta}} \qquad (30)$$
$$\ddot{\theta} = -\frac{\dot{r}\dot{\theta}}{r}$$

The radius of curvature of the belt is the same as the belt pitch radius, which is reasonable to assume except at the inlet and exit regions of the pulley.

Solving the differential equation in (30) yields,

$\theta = \int_0^{t_1} \frac{c_1 dt}{r}$, t_1 is the time taken to traverse the entire pulley wrap.

The above equation implies that the belt traces a complex non-circular trajectory over the pulley wrap. However, for an infinitesimal instant of time it can be assumed that the belt follows a circular path, as illustrated by the slightly exaggerated path in Figure 3.6.

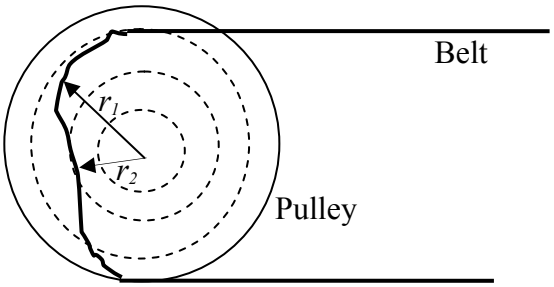

Although the belt trajectory is non-circular, the belt position, for an infinitesimal instant of time, can be assumed to be located by constant radius vectors, as r_1 and r_2.

Figure 3.6: Belt trajectory

The constraint of constant belt length i.e. equation (10), which relates the driver to the driven system, reduces to the following form:

$$\dot{r}\alpha + \dot{r}'\alpha' = 0 \qquad (31)$$

The driver band pack and element equations reduce to the following forms:

Driver Band pack:

$$\begin{aligned}\dot{T} &= \mu_a \dot{F} - \sigma_b \dot{r}\ddot{r} \\ T\dot{\theta} - \dot{F} &= \sigma_b\left(-r\ddot{r}\dot{\theta} + r^2\dot{\theta}^3 + \dot{r}^2\dot{\theta}\right)\end{aligned} \tag{32}$$

Driver Belt Element:

$$\begin{aligned}\dot{Q} - \mu_a \dot{F} + 2\dot{N}\left(\varphi \sin\beta - \mu_b \cos\beta_s \sin\psi - \varphi\mu_b \cos\beta_s \cos\psi\right) &= \sigma_e \dot{r}\ddot{r} \\ -Q\dot{\theta} + \dot{F} - 2\dot{N}\left(\sin\beta - \mu_b \cos\beta_s \cos\psi + \varphi\mu_b \cos\beta_s \sin\psi\right) &= \sigma_e\left(-r\ddot{r}\dot{\theta} + r^2\dot{\theta}^3 + \dot{r}^2\dot{\theta}\right)\end{aligned} \tag{33}$$

Since the driver pulley speed is a constant, the driver system has only six unknowns. Equations (29), (30), (32), (33) can be solved simultaneously to obtain the time histories of other unknown driver system parameters. Later appropriate modifications are introduced in the form of pulley bending equations in order to take flexural effects into account. The driver axial force can be computed from equation (28). Knowing the driver system parameters, the driven system solution procedure can be initiated using the constraint equation (31).

DRIVEN System Solution Procedure:

The following equations along with equation (31) and the pulley bending equations describe the dynamic interactions between the belt and the driven pulley:

$$\begin{aligned}\rho' &\approx r' \\ \varphi' &\approx \frac{\dot{r}'}{r'\dot{\theta}'} \\ \ddot{\theta}' &= -\frac{\dot{r}'\dot{\theta}'}{r'}\end{aligned} \tag{34}$$

Driven Band pack:

$$\begin{aligned}\dot{T}' &= \mu_a \dot{F}' - \sigma_b \dot{r}'\ddot{r}' \\ T'\dot{\theta}' - \dot{F}' &= \sigma_b\left(-r'\ddot{r}'\dot{\theta}' + r'^2\dot{\theta}'^3 + \dot{r}'^2\dot{\theta}'\right)\end{aligned} \tag{35}$$

Driven Belt Element:

$$\begin{aligned}&\dot{Q}'-\mu_a\dot{F}'+2\dot{N}'\left(\varphi'\sin\beta'-\mu'_b\cos\beta'_s\sin\psi'-\varphi'\mu'_b\cos\beta'_s\cos\psi'\right)=\sigma_e\dot{r}'\ddot{r}'\\&-Q'\dot{\theta}'+\dot{F}'-2\dot{N}'\left(\sin\beta'-\mu'_b\cos\beta'_s\cos\psi'+\varphi'\mu'_b\cos\beta'_s\sin\psi'\right)\\&\qquad=\sigma_e\left(-r'\ddot{r}'\dot{\theta}'+r'^2\dot{\theta}'^3+\dot{r}'^2\dot{\theta}'\right)\end{aligned}\tag{36}$$

Driven Axial Force:

$$F'_z=\frac{\dot{N}'\alpha'}{\dot{\theta}'}\left(\cos\beta'+\mu'_b\sin\beta'_s\right)\tag{37}$$

Driven pulley speed:

$$I'\dot{\omega}'=-\tau_l+2\mu'_b r'\cos\beta'_s\sin\psi'\frac{\dot{N}'}{\dot{\theta}'}\alpha'\tag{38}$$

All of the above equations describing driven system can be simultaneously solved to obtain the time histories of driven system parameters and the driven pulley axial force.

3.3 Transient Model of Metal V-belt CVT: Belt-Band Slip Dynamics

In addition to the push mechanism, the pulling action in the band pack also contributes significantly to the torque transmission mechanism in a metal V-belt CVT. Srivastava *et al.* [76-78], Fujii *et al.* [61-65], Kobayashi *et al.* [43-44], under the assumption of impending belt-band slip, have already highlighted the significance of tensile force in the band pack in determining the maximum torque transmitting capacity of a metal V-belt CVT. Although the model presented in the earlier section captures the inertial dynamics between a belt element and the pulley in detail, it is unable to take into account the slip dynamics arising from the inertial interactions between the band pack and the belt element. The band pack was assumed to be always in state of impending slip, as in the

case of Euler's flat-belt theory, and also experienced the same acceleration as the belt element. The slip between the band and the belt element may further reduce the torque capacity and enhance the losses in the system. The model, subsequently discussed in this section, not only takes into account the inertial coupling between belt element and the pulley, but also accounts for the slip dynamics between the band pack and the belt element. The loading conditions are the same as the previous model, i.e. a constant driver angular speed, a constant input torque applied to the driver pulley, and a constant load torque on the driven pulley.

3.3.1 Assumptions

The assumptions made in the analysis are:

- Bending and torsional stiffness of the belt are neglected
- Pulley misalignment effects are neglected, however, pulley deformations are modeled using Sferra's model [48].
- The band pack can only sustain tensile forces, whereas a belt element can only undergo compression
- Elements and bands are treated as a continuous belt
- Line contact between the belt and the pulley is parallel to the pulley axis
- The element and band dimensions are small in comparison to the radii of the pulleys
- Belt elements and bands are inextensible
- Belt length is constant
- Negligible elastic deformations in the belt
- Belt mass density remains constant

Figure 3.7 depicts the free-body diagrams of a belt segment engaged with the driver pulley. The kinematic description involves the following coordinate systems; (**n**, **τ**) that is attached to the belt element and describes its path (ρ is the radius of curvature of the path of the belt element), ($\mathbf{n_b}$, $\boldsymbol{\tau_b}$) that is attached to the band pack and describes its path (ρ_b is the radius of curvature of the path of the band pack), and ($\hat{\mathbf{e}}_r, \hat{\mathbf{e}}_\theta, \hat{\mathbf{e}}_z$) and ($\hat{\mathbf{e}}_{rb}, \hat{\mathbf{e}}_{\theta b}, \hat{\mathbf{e}}_{zb}$) that are rotating coordinate systems attached to the center of the pulley i.e. point O. The points labeled C and D are the instantaneous centers of curvature of the paths of belt element and band pack respectively. ω_s is the local sliding angular velocity of the belt element.

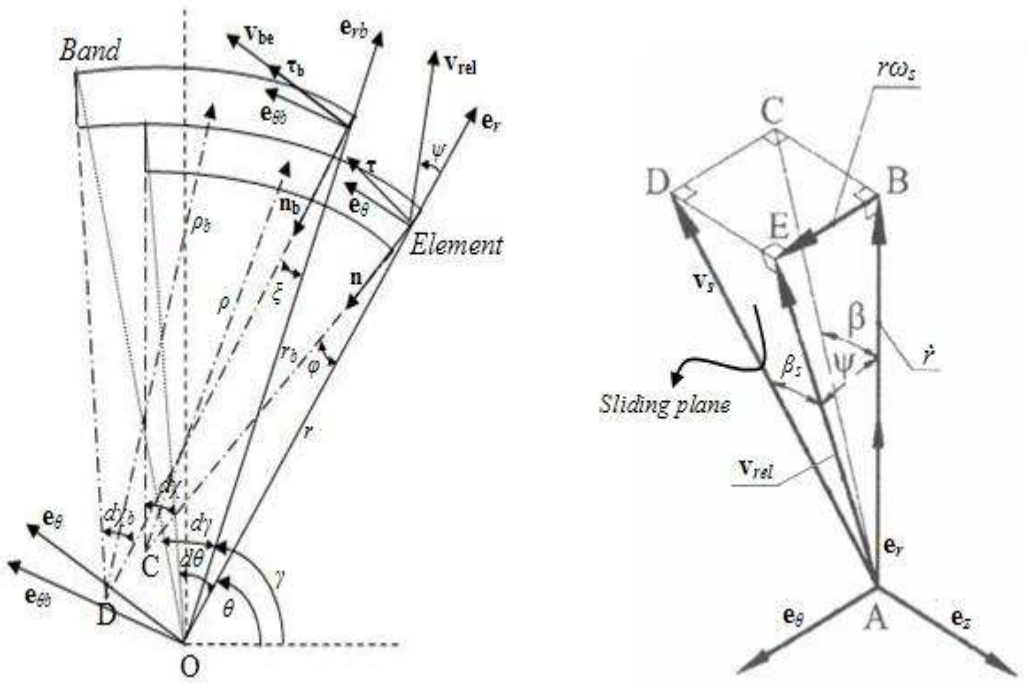

(a) Kinematic description of the belt

Figure 3.7: Free body diagrams of driver system – Band/Belt Slip

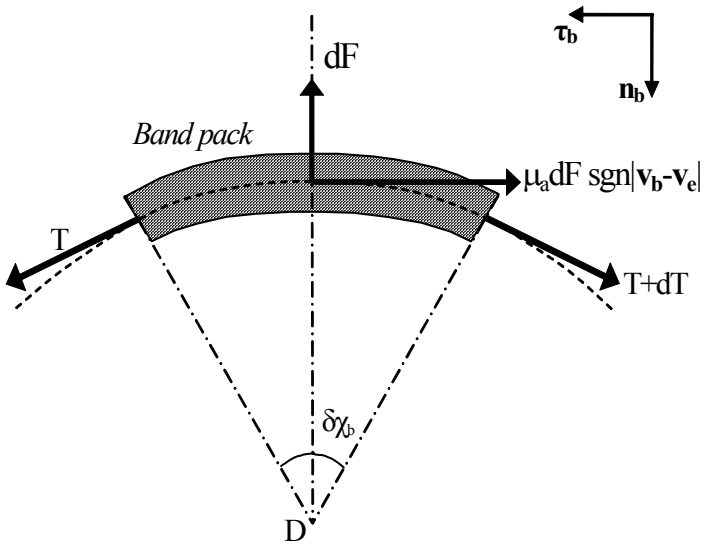

(b) Free body diagram of driver band pack

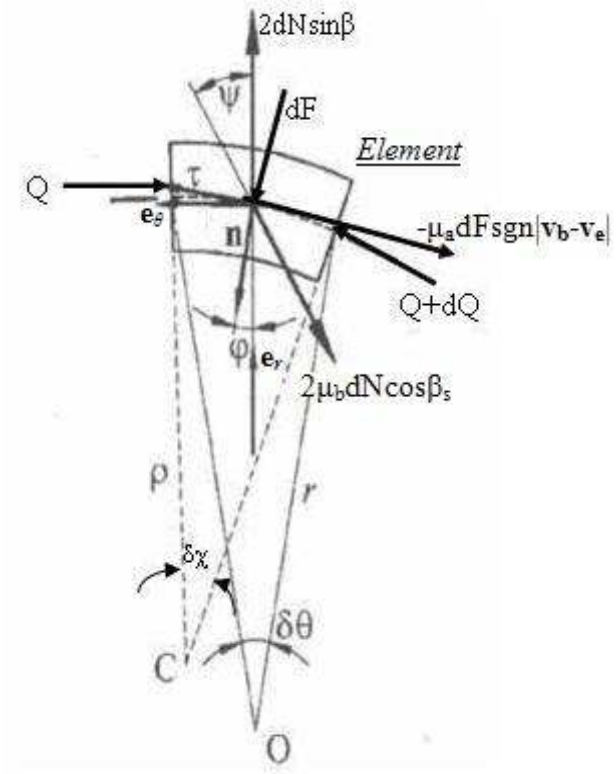

(c) Free body diagram of driver belt element

Figure 3.7: Free body diagrams of driver system – Band/Belt Slip (contd.)

The free body diagrams for the forces and torques acting on the driver pulley are analogous to those depicted in Figure 3.3 (d) and (e). Similar free-body analysis can be

done on a belt segment engaged with the driven pulley under the influence of a load torque, τ_l.

3.3.2 Driver System Analysis

From the kinematic description of the belt (refer to Figure 3.7(a)), the following geometrical relationships can be derived:

$$\left.\begin{aligned}
&\tan\varphi = \frac{1}{r}\frac{\partial r}{\partial \theta} \\
&\tan\xi = \frac{1}{r_b}\frac{\partial r_b}{\partial \gamma} \\
&\frac{1}{\rho} = \frac{\cos\varphi}{r}\left(1-\frac{\partial\varphi}{\partial\theta}\right) = \frac{\delta\chi}{\delta s} \\
&\frac{1}{\rho_b} = \frac{\cos\xi}{r_b}\left(1-\frac{\partial\xi}{\partial\gamma}\right) = \frac{\delta\chi_b}{\delta s_b} \\
&\tan\beta_s = \tan\beta\cos\psi
\end{aligned}\right\} \tag{39}$$

Moreover, the constraint of inextensibility of the belt element and the band pack implies that the time rate of change of the length of any infinitesimal piece of the belt element and the band must be zero, i.e.

$$\begin{aligned}
&\frac{d}{dt}\delta s = 0,\ \delta s = \frac{r\delta\theta}{\cos\varphi} \\
&\frac{d}{dt}\delta s_b = 0,\ \ \delta s_b = \frac{r_b\delta\gamma}{\cos\xi}
\end{aligned} \tag{40}$$

Now, for an infinitesimal time step, introducing tangent approximation further reduces (40) to,

$$\begin{aligned}
&\frac{\dot r}{r} + \dot\varphi\tan\varphi + \frac{\ddot\theta}{\dot\theta} = 0 \\
&\frac{\dot r_b}{r} + \dot\xi\tan\xi + \frac{\ddot\gamma}{\dot\gamma} = 0
\end{aligned} \tag{41}$$

Also, for an infinitesimal time step,

$$\tan\varphi = \frac{\dot{r}}{r\dot{\theta}}$$
$$\tan\xi = \frac{\dot{r}_b}{r_b\dot{\gamma}} \tag{42}$$

Incorporating (42) into (41) yields the following constraint equations for the inextensibility of the belt element and the band pack,

$$\dot{r}(\dot{\theta}+\dot{\varphi}) + r\ddot{\theta} = 0$$
$$\dot{r}_b(\dot{\gamma}+\dot{\xi}) + r_b\ddot{\gamma} = 0 \tag{43}$$

In addition to these inextensibility constraints, the constraint of constant belt length (31), under the assumption of negligible flexural effects in the belt, kinematically couples the driver and the driven system dynamics. Moreover, it is necessary to evaluate the relative velocity between the band pack and the belt element in order to determine the friction force between these two bodies. The relative velocity between the band pack and the belt element is given as,

$$\mathbf{v_{be}} = \mathbf{v_b} - \mathbf{v} = \dot{r}_b\,\hat{\mathbf{e}}_{\mathbf{rb}} + r_b\dot{\gamma}\,\hat{\mathbf{e}}_{\boldsymbol{\theta}\mathbf{b}} - \dot{r}\,\hat{\mathbf{e}}_{\mathbf{r}} - r\dot{\theta}\,\hat{\mathbf{e}}_{\boldsymbol{\theta}} \tag{44}$$

Since the band pack slides on the surface of the element, the relative velocity (and the friction force) must act purely in the tangential direction, consequently yielding the following constraint equation that couples the band pack dynamics to the motion of the belt element,

$$\mathbf{v_{be}} \bullet \mathbf{n_b} = (\mathbf{v_b} - \mathbf{v}) \bullet \mathbf{n_b} = 0 \tag{45}$$

Using (42) and the following coordinate transformations, i.e.

$$\begin{Bmatrix}\boldsymbol{\tau}_\mathbf{b}\\ \mathbf{n_b}\end{Bmatrix} = \begin{bmatrix}\sin\xi & \cos\xi\\ -\cos\xi & \sin\xi\end{bmatrix}\begin{Bmatrix}\hat{\mathbf{e}}_{\mathbf{rb}}\\ \hat{\mathbf{e}}_{\boldsymbol{\theta}\mathbf{b}}\end{Bmatrix}$$
$$\begin{Bmatrix}\hat{\mathbf{e}}_{\mathbf{r}}\\ \hat{\mathbf{e}}_{\boldsymbol{\theta}}\end{Bmatrix} = \begin{bmatrix}\cos(\gamma-\theta) & -\sin(\gamma-\theta)\\ \sin(\gamma-\theta) & \cos(\gamma-\theta)\end{bmatrix}\begin{Bmatrix}\hat{\mathbf{e}}_{\mathbf{rb}}\\ \hat{\mathbf{e}}_{\boldsymbol{\theta}\mathbf{b}}\end{Bmatrix} \tag{46}$$

in equation (45), the following constraint equation can be obtained,

$$\xi = \gamma - \theta + \varphi \tag{47}$$

It is to be noted that equation (47) is a holonomic constraint that couples the band pack dynamics to the belt element dynamics. So, using (47), the relative velocity between the band pack and the belt element can be further expressed as,

$$\mathbf{v_{be}} = \mathbf{v_b} - \mathbf{v} = (\dot{r}_b \sin\xi + r_b\dot{\gamma}\cos\xi - \dot{r}\sin\varphi - r\dot{\theta}\cos\varphi)\ \boldsymbol{\tau}_\mathbf{b} \tag{48}$$

Knowing the velocities of the belt element and the band pack, the following expressions for the acceleration of the belt element and the band pack can be readily obtained,

$$\begin{aligned}\mathbf{a} &= \frac{d\mathbf{v}}{dt} = (\ddot{r} - r\dot{\theta}^2)\,\hat{\mathbf{e}}_\mathbf{r} + (r\ddot{\theta} + 2\dot{r}\dot{\theta})\,\hat{\mathbf{e}}_{\boldsymbol{\theta}} \\ \mathbf{a_b} &= \frac{d\mathbf{v_b}}{dt} = (\ddot{r}_b - r_b\dot{\gamma}^2)\,\hat{\mathbf{e}}_{\mathbf{rb}} + (r_b\ddot{\gamma} + 2\dot{r}_b\dot{\gamma})\,\hat{\mathbf{e}}_{\boldsymbol{\theta}\mathbf{b}}\end{aligned} \tag{49}$$

It is to be noted that the acceleration of the band pack is not the same as the acceleration of belt element, as the band pack is allowed to slip over the belt element, contrary to the impending slip conditions mentioned in the previous model.

In addition to the aforementioned assumptions, the following assumptions are also made in the analysis to aid the solution procedure,

- Uniform pressure distribution ($dN/rd\theta$) between the belt element and the pulley
- Assume φ, ξ, are negligible and $\dot{\varphi}, \dot{\xi} << \dot{\theta}, \dot{\gamma}$

It is reasonable to assume φ, ξ to be negligible quantities as it implies that the rate at which the belt pitch radius changes is smaller than the rate at which belt traverses the pulley wraps. Moreover, it is plausible that the rate at which the slope angles (φ, ξ) change is smaller than the rate at which the angular positions of the belt element and band (θ, γ) change.

Now, summation of forces in the normal and tangential directions, ($\mathbf{n_b}$, $\boldsymbol{\tau_b}$), (refer to Figure 3.7(b)) for the driver band pack yields the following equations respectively,

$$\sum F_{nb} \rightarrow Td\chi_b - dF = \sigma_b ds_b(\mathbf{a_b} \bullet \mathbf{n_b})$$
$$\sum F_{\tau b} \rightarrow -dT - \mu_a dF \operatorname{sgn} | \mathbf{v_{be}} | = \sigma_b ds_b(\mathbf{a_b} \bullet \boldsymbol{\tau}_\mathbf{b})$$

Under the assumption of small ξ and $\dot{\xi}$, for an infinitesimal time step, the equations of motion for the driver band pack can be simplified to obtain,

$$\begin{aligned} &\dot{T} = -\mu_a \dot{F} \operatorname{sgn} | \mathbf{v_{be}} | - \sigma_b \dot{r}_b \ddot{r}_b \\ &T\dot{\gamma} - \dot{F} = \sigma_b \left(- r_b \ddot{r}_b \dot{\gamma} + r_b^2 \dot{\gamma}^3 + \dot{r}_b^2 \dot{\gamma} \right) \\ &\tan \xi \approx \xi \approx \frac{\dot{r}_b}{r_b \dot{\gamma}}, \quad \ddot{\gamma} = -\frac{\dot{r}_b \dot{\gamma}}{r_b}, \ \rho_b \approx r_b \end{aligned} \tag{50}$$

Similarly, summation of forces in the normal and tangential directions, ($\mathbf{n}$, $\boldsymbol{\tau}$), (refer to Figure 3.7(c)) for the driver belt element yields the following equations respectively,

$$\sum F_n \rightarrow -Qd\chi - 2dN\{\sin\beta\cos\varphi - \mu_b \cos\beta_s \cos(\varphi + \psi)\} + dF(\mathbf{n_b} \bullet \mathbf{n}) + \mu_a dF(\boldsymbol{\tau}_\mathbf{b} \bullet \mathbf{n}) = \sigma_e ds(\mathbf{a} \bullet \mathbf{n})$$
$$\sum F_\tau \rightarrow dQ + \mu_a dF \operatorname{sgn} | \mathbf{v_{be}} | (\boldsymbol{\tau}_\mathbf{b} \bullet \boldsymbol{\tau}) + dF(\mathbf{n_b} \bullet \boldsymbol{\tau}) + 2dN\{\sin\beta\sin\varphi - \mu_b \cos\beta_s \sin(\varphi + \psi)\} = \sigma_e ds(\mathbf{a} \bullet \boldsymbol{\tau})$$

Under the assumptions of small $\xi, \dot{\xi}$, $\varphi, \dot{\varphi}$, for an infinitesimal time step, the equations of motion for the driver belt element can be simplified to obtain,

$$\begin{aligned} &\dot{Q} + 2\dot{N}\{\varphi\sin\beta - \mu_b \cos\beta_s \sin\psi - \mu_b \varphi \cos\beta_s \sin\psi\} + \dot{F}\{(\xi - \varphi)\cos(\gamma - \theta) - (1 + \xi\varphi)\sin(\gamma - \theta)\} \\ &+ \mu_a \dot{F} \operatorname{sgn} | \mathbf{v_{be}} | \{(1 + \xi\varphi)\cos(\gamma - \theta) - (\xi - \varphi)\sin(\gamma - \theta)\} = \sigma_e \dot{r}\ddot{r} \\ &- Q\dot{\theta} - 2\dot{N}\{\sin\beta - \mu_b \cos\beta_s \cos\psi + \mu_b \varphi \cos\beta_s \sin\psi\} + \dot{F}\{(\xi - \varphi)\sin(\gamma - \theta) + (1 + \xi\varphi)\cos(\gamma - \theta)\} \\ &+ \mu_a \dot{F} \operatorname{sgn} | \mathbf{v_{be}} | \{(1 + \xi\varphi)\sin(\gamma - \theta) + (\xi - \varphi)\cos(\gamma - \theta)\} = \sigma_e(-r\ddot{r}\dot{\theta} + r^2\dot{\theta}^3 + \dot{r}^2\dot{\theta}) \end{aligned} \tag{51}$$

Equation (51) can be further reduced to the following form by using the holonomic constraint equation (47) and the assumption of small slope angles ξ and φ,

$$\dot{Q}+2\dot{N}\{\varphi\sin\beta-\mu_b\cos\beta_s\sin\psi-\mu_b\varphi\cos\beta_s\sin\psi\}+\mu_a\dot{F}\,\mathrm{sgn}\,|\,\mathbf{v_{be}}\,|=\sigma_e\dot{r}\ddot{r}$$
$$-Q\dot{\theta}-2\dot{N}\{\sin\beta-\mu_b\cos\beta_s\cos\psi+\mu_b\varphi\cos\beta_s\sin\psi\}+\dot{F}=\sigma_e(-r\ddot{r}\dot{\theta}+r^2\dot{\theta}^3+\dot{r}^2\dot{\theta}) \qquad (52)$$
$$\tan\varphi\approx\varphi\approx\frac{\dot{r}}{r\dot{\theta}},\quad \ddot{\theta}=-\frac{\dot{r}\dot{\theta}}{r},\ \rho\approx r$$

In addition to the equations for belt element and band pack, summing the forces and torques on the driver and driven pulleys yields further equations ((28), (29), (37), (38)) for the CVT system. In order to take into account the influence of elastic deformations of the pulley sheaves on the thrust ratio and slip behavior of a CVT, equations analogous to equations (18)-(23) are introduced in the model. Thus, there are eighteen primary unknowns (nine each for driver and driven) in this CVT model, as: [$R,R_b,\theta,\gamma,T,Q,F,N,\omega$]. Since the driver pulley speed is maintained as a constant, the driver system has only eight unknowns. It is to be noted from the aforementioned equations that the motion of a belt element is tightly coupled not only to the motion of the pulley, but also to the motion of the band pack. The equations for the driver system can be simultaneously solved to obtain the time histories of the eight unknown driver system parameters. Later, appropriate modifications are introduced in the form of the pulley bending equations to take the flexural effects into account.

Similar analysis of a belt segment engaged with the driven pulley under load torque conditions yields the equations for the driven system dynamics. Knowing the driver system parameters, the driven system solution procedure can be initiated using the constraint equation (31). The coefficient of friction between the various contacting surfaces of this CVT system is governed by the following equation:

$$\mu_{a,b}=\mu_{ao,bo}(1-e^{-\bar{\kappa}|\mathbf{v_{be,s}}|})(1+(f_r-1)e^{-\bar{\lambda}|\mathbf{v_{be,s}}|})$$

3.4 Transient Model of a Chain CVT using Multibody Formalisms

3.4.1 Chain CVT Configuration

A chain CVT consists of two variable-diameter pulleys connected to each other by means of a rocker-pin chain. A rocker-pin chain consists of inner plates, clasp plates, and rocker pins. All plates transmit tractive power, while the clasp plates also orientate the rocker pins perpendicular to the direction of motion of chain. Figure 3.8 [7] depicts the components of a chain CVT drive.

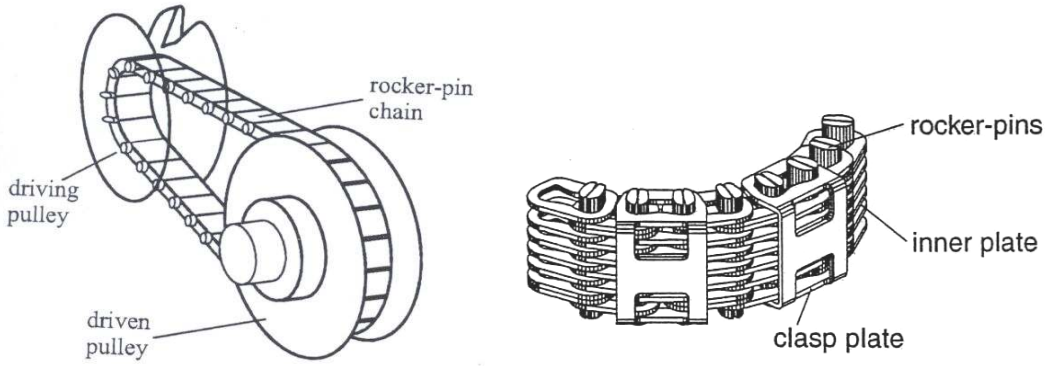

Figure 3.8: Components of a chain CVT [7]

The rocker pins transmit the frictional and normal load between the pulleys and the chain on their spherical end faces. They also join the plates and roll on each other on their arched inner rocker surface when the chain bends. Moreover, unlike a belt, the contact forces between chain and pulley are discretely distributed. This leads to impacts as the chain links enter and leave the pulley. Hence, excitation mechanisms exist, which are strongly connected to polygonal action of chain links. This results in vibrations of the whole system, which influences the dynamic behavior of the system. CVT chain drives transmit power exclusively through these frictional forces occurring in the contact zones between the bolts of the chain and the conical pulley sheaves. The pulley sheaves also

undergo elastic deformation due to high forces in the contact zones. Each contact has two possible states: stick or slip, depending on the relative velocity between the chain link and the pulley. The possible transitions between them lead to a mechanical system with time variant structure. However, the time variance of the system can be eliminated by using the continuous Coulomb friction theory to model friction between the link and the pulley, as:

$$\mu = a + (\mu_0 - a)(1 - e^{-|v_{rel}|/b})$$

The application of such a friction characteristic neglects the effects from stiction in a chain CVT model, as the tangential constraints are always active in contact. In order to capture the dynamic interactions between the chain link and the pulley realistically, it is necessary to model the chain CVT drive as a discrete multibody model. The multi-body modeling of chain CVT not only captures the dynamic interactions realistically, but also helps in understanding excitation mechanisms associated with the polygonal action of the chain links. Had the chain been modeled as a continuous rigid body as done in the case of belt-CVT, these excitation mechanisms would never have been captured, thereby eluding the real system dynamics. The subsequent sections discuss the various principles of multibody dynamics (Pfeiffer and Glocker [125]) that are relevant to the model development.

3.4.2 Multibody Formalism: Formulation of Contact Kinematics and Dynamics

Equations of Motion of Multibody System with Bilateral Holonomic Constraints

Let us consider a system of rigid or elastic bodies under the influence of forces with a few constraint conditions. Some of these constraints may act permanently on the system,

which results in a time-independent reduction of the degrees of freedom of the system. Such constraints are called bilateral constraints. On the other hand, there can be a few unilateral constraints which influence the system depending on the contact conditions, consequently, leading to a state-dependent system with varying number of degrees of freedom. Such contact conditions arise from collisions, contact or separation, stick-slip transitions with respect to Coulomb friction, etc. A typical body, *i*, in an *n*-multibody system under holonomic bilateral constraints is shown in Figure 3.9 [125].

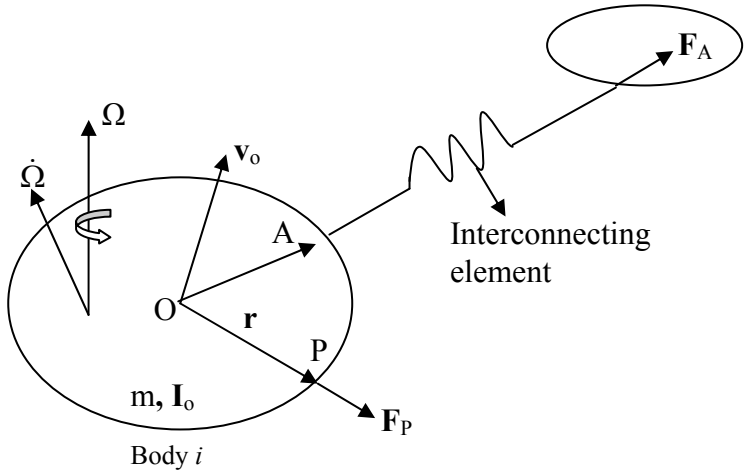

Figure 3.9: Bilaterally-constrained multibody system [125]

In the above figure, O denotes the center of mass of body *i* with mass m and inertia matrix $\mathbf{I}_O$, **r** denotes a position vector of a point on the body from O, $\mathbf{v}_O$ is the absolute velocity of the center of mass of body and **Ω** is the absolute angular velocity of the body. The forces and moments acting on the body are divided into two sets: the subscript 'A' denotes active forces and moments (i.e. those which produce power), whereas the subscript 'P' denotes passive forces and moments (i.e. those which produce no power).

The equations of motion of body *i* in an *n*-body system can be written using Newton-Euler equations, as:

$$\left\{\begin{pmatrix}\dot{\mathbf{p}}\\ \dot{\mathbf{L}}\end{pmatrix}-\begin{pmatrix}\mathbf{I} & \mathbf{0}\\ \tilde{\mathbf{r}}_{\mathbf{OA}} & \mathbf{I}\end{pmatrix}\begin{pmatrix}\mathbf{F}_{\mathbf{A}}\\ \mathbf{M}_{\mathbf{A}}\end{pmatrix}-\begin{pmatrix}\mathbf{I} & \mathbf{0}\\ \tilde{\mathbf{r}}_{\mathbf{OP}} & \mathbf{I}\end{pmatrix}\begin{pmatrix}\mathbf{F}_{\mathbf{P}}\\ \mathbf{M}_{\mathbf{P}}\end{pmatrix}\right\}_i = \mathbf{0} \quad ,i=1\ldots n,\ \dot{p},\dot{L}\in\Re^3 \tag{53}$$

The linear and angular momenta (**p**, **L** respectively) of each body *i* can be further expressed as,

$$\begin{pmatrix}\dot{\mathbf{p}}\\ \dot{\mathbf{L}}\end{pmatrix}=\begin{pmatrix}m\mathbf{I} & \mathbf{0}\\ \mathbf{0} & \mathbf{I}_{\mathbf{O}}\end{pmatrix}\begin{pmatrix}\dot{\mathbf{v}}_{\mathbf{O}}\\ \dot{\boldsymbol{\Omega}}\end{pmatrix}+\begin{pmatrix}\mathbf{0}\\ \tilde{\Omega}\mathbf{I}_{\mathbf{O}}\Omega\end{pmatrix} \tag{54}$$

In these equations, a quantity say $\tilde{\mathbf{a}}$ is a 3x3 skew-symmetric matrix which helps to express the cross product **a** x **b** by a matrix-vector multiplication $\tilde{\mathbf{a}}\mathbf{b}$. Also, **I** represents the 3x3 identity matrix.

The kinematic equations for the body *i* are:

$$\begin{pmatrix}\mathbf{v}_{\mathbf{A}}\\ \boldsymbol{\Omega}\end{pmatrix}=\begin{pmatrix}\mathbf{I} & -\tilde{\mathbf{r}}_{\mathbf{OA}}\\ \mathbf{0} & \mathbf{I}\end{pmatrix}\begin{pmatrix}\mathbf{v}_{\mathbf{O}}\\ \boldsymbol{\Omega}\end{pmatrix}$$
$$\begin{pmatrix}\mathbf{v}_{\mathbf{P}}\\ \boldsymbol{\Omega}\end{pmatrix}=\begin{pmatrix}\mathbf{I} & -\tilde{\mathbf{r}}_{\mathbf{OP}}\\ \mathbf{0} & \mathbf{I}\end{pmatrix}\begin{pmatrix}\mathbf{v}_{\mathbf{O}}\\ \boldsymbol{\Omega}\end{pmatrix} \tag{55}$$

Assuming the system has only *f* degrees of freedom due to 6*n*-*f* bilateral holonomic constraints, one can choose a set of *f* generalized (velocity) coordinates $\dot{\mathbf{q}}$, which describe the system uniquely and fulfill each of the constraints. Introducing the concept of Jacobian to transform from system coordinates to generalized coordinates yields,

$$\begin{pmatrix}\dfrac{\partial\mathbf{v}_{\mathbf{S}}}{\partial\dot{\mathbf{q}}}\\ \dfrac{\partial\boldsymbol{\Omega}}{\partial\dot{\mathbf{q}}}\end{pmatrix}=\begin{pmatrix}\mathbf{J}_{\mathbf{S}}\\ \mathbf{J}_{\mathbf{R}}\end{pmatrix} \quad ;\begin{pmatrix}\mathbf{J}_{\mathbf{S}}\in\Re^{3,f}\\ \mathbf{J}_{\mathbf{R}}\in\Re^{3,f}\end{pmatrix} \tag{56}$$

In the above equation, $\mathbf{J}_S$ and $\mathbf{J}_R$ are the Jacobian of translation of point S of the body and the Jacobian of rotation of the body. S can represent any point (O, A, P) on the body *i*.

Moreover, the absolute accelerations of the body *i* can be expressed in terms of generalized coordinates as:

$$\begin{pmatrix} \dot{\mathbf{v}}_O \\ \dot{\boldsymbol{\Omega}} \end{pmatrix} = \begin{pmatrix} \mathbf{J}_O \\ \mathbf{J}_R \end{pmatrix} \ddot{\mathbf{q}} + \begin{pmatrix} \tilde{\mathbf{j}}_O \\ \tilde{\mathbf{j}}_R \end{pmatrix} \tag{57}$$

where the extraneous terms of absolute acceleration have been collected in $\begin{pmatrix} \tilde{\mathbf{j}}_O \\ \tilde{\mathbf{j}}_R \end{pmatrix}$.

Now, the total virtual power of the multibody system can be obtained as:

$$\sum_{i=1}^{n} \left\{ \begin{pmatrix} \delta\mathbf{v}_O \\ \delta\boldsymbol{\Omega} \end{pmatrix}^T \left[\begin{pmatrix} \dot{\mathbf{p}} \\ \dot{\mathbf{L}} \end{pmatrix} - \begin{pmatrix} \mathbf{I} & \mathbf{0} \\ \tilde{\mathbf{r}}_{OA} & \mathbf{I} \end{pmatrix} \begin{pmatrix} \mathbf{F}_A \\ \mathbf{M}_A \end{pmatrix} - \begin{pmatrix} \mathbf{I} & \mathbf{0} \\ \tilde{\mathbf{r}}_{OP} & \mathbf{I} \end{pmatrix} \begin{pmatrix} \mathbf{F}_P \\ \mathbf{M}_P \end{pmatrix} \right] \right\}_i = \mathbf{0} \tag{58}$$

Using equations (55) and (56) and noting the arbitrariness of the selection of generalized coordinates, one gets:

$$\sum_{i=1}^{n} \left\{ \begin{pmatrix} \mathbf{J}_O \\ \mathbf{J}_R \end{pmatrix}^T \begin{pmatrix} \dot{\mathbf{p}} \\ \dot{\mathbf{L}} \end{pmatrix} - \begin{pmatrix} \mathbf{J}_A \\ \mathbf{J}_R \end{pmatrix}^T \begin{pmatrix} \mathbf{F}_A \\ \mathbf{M}_A \end{pmatrix} - \begin{pmatrix} \mathbf{J}_P \\ \mathbf{J}_R \end{pmatrix}^T \begin{pmatrix} \mathbf{F}_P \\ \mathbf{M}_P \end{pmatrix} \right\}_i = \mathbf{0} \tag{59}$$

Selecting index P according to Jourdain principle of lost power i.e.

$$\sum_{i=1}^{n} \left\{ \begin{pmatrix} \mathbf{J}_P \\ \mathbf{J}_R \end{pmatrix}^T \begin{pmatrix} \mathbf{F}_P \\ \mathbf{M}_P \end{pmatrix} \right\}_i = \mathbf{0} \tag{60}$$

one finally gets the following dynamical equation for the multibody system:

$$\sum_{i=1}^{n} \left\{ \begin{pmatrix} \mathbf{J}_O \\ \mathbf{J}_R \end{pmatrix}^T \begin{pmatrix} \dot{\mathbf{p}} \\ \dot{\mathbf{L}} \end{pmatrix} - \begin{pmatrix} \mathbf{J}_A \\ \mathbf{J}_R \end{pmatrix}^T \begin{pmatrix} \mathbf{F}_A \\ \mathbf{M}_A \end{pmatrix} \right\}_i = \mathbf{0} \tag{61}$$

Using (54) and (57), equation (61) can be reduced in the following form:

$$\mathbf{M(q,}\,\mathrm{t}\mathbf{)}.\ddot{\mathbf{q}} - \mathbf{h(q,}\,\dot{\mathbf{q}}\mathbf{,}\,\mathrm{t}\mathbf{)} = \mathbf{0} \quad \in \Re^{\mathbf{f}} \tag{62}$$

where **M** is a symmetric positive-definite mass matrix and **h** is a vector containing gyroscopic terms and other terms arising from all the active forces and moments.

It is quite common to model contact between two touching/neighboring bodies using force elements that are governed by some characteristic force laws. Figure 3.10 depicts the interconnection between bodies *i* and *j* using a force coupling.

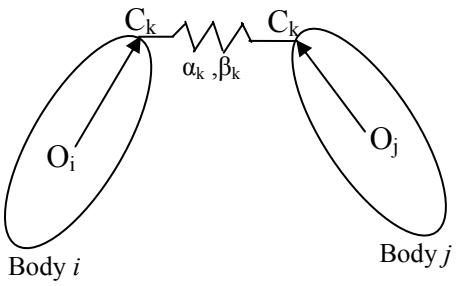

Figure 3.10: Force coupling between two bodies

The line of action of the force due to the coupling is defined by the connection points between the two bodies and is formally given by the unit vectors $\mathbf{e}_i$ or $\mathbf{e}_j$ ($\mathbf{e}_i$ = - $\mathbf{e}_j$) with respect to body *i* or body *j*. Let the forces and torques due to the coupling element be given by the following laws:

$$\begin{aligned} \mathbf{F}_i &= \boldsymbol{e}_i \alpha_k, \quad \mathbf{F}_j = \boldsymbol{e}_j \alpha_k \\ \mathbf{M}_i &= \boldsymbol{e}_i \beta_k, \quad \mathbf{M}_j = \boldsymbol{e}_j \beta_k \end{aligned} \tag{63}$$

It is to be noted that these forces and torques due to the coupling element are active. Incorporating these into equation (62) and introducing corresponding Jacobians, one gets,

$$\mathbf{M}\ddot{\mathbf{q}} - \mathbf{h} - \mathbf{J}_{Ai}^{T}\mathbf{F}_i - \mathbf{J}_{Aj}^{T}\mathbf{F}_j - \mathbf{J}_{Ri}^{T}\mathbf{M}_i - \mathbf{J}_{Rj}^{T}\mathbf{M}_j = 0$$

Using (49),

$$\mathbf{M}\ddot{\mathbf{q}} - \mathbf{h} - \sum_i \left(\boldsymbol{w}_A \alpha_k\right)_i + \sum_i \left(\boldsymbol{w}_R \beta_k\right)_i = 0 \tag{64}$$

where

$$\boldsymbol{w}_{Ai} = \mathbf{J}_{Ai}^{T}\boldsymbol{e}_i + \mathbf{J}_{Aj}^{T}\boldsymbol{e}_j, \boldsymbol{w}_{Ri} = \mathbf{J}_{Ri}\boldsymbol{e}_i + \mathbf{J}_{Rj}\boldsymbol{e}_j$$

$\boldsymbol{w}_{Ai}$, $\boldsymbol{w}_{Ri}$ are unit vectors in the configuration space (i.e. space of generalized coordinates, $\mathbf{R}^f$) in the direction of the corresponding force or torque laws.

Contact Kinematics:

Equation (64) describes the dynamics of a multibody system with bilateral contacts under the influence of active forces, torques, and force couplings. In order to take into account various unilateral contacts occurring in the multibody system, it is necessary to understand contact kinematics and dynamics so that equation (64) can be modified to include all the system constraints. The beginning of contact is indicated by the vanishing relative distance between two bodies and the end of contact is dependent on the relative acceleration between the same two bodies. Since the chain CVT model presented in this research is a discrete planar multibody system, all the contact events are assumed to occur in planar sections of the two contacting bodies. Figure 3.11 depicts two separated bodies undergoing contact. The contact forces, as shown in the figure, come into existence when the relative distance between the two bodies vanishes. The contact forces are also equal and opposite, as per Newton's III law of motion. From the figure, it can be noted that for contact to occur:

$$\mathbf{n_1^T}(s_1)\mathbf{t_2}(s_2) = 0 \quad \& \quad \mathbf{r_D^T}(s_1, s_2)\mathbf{t_1}(s_1) = 0 \tag{65}$$

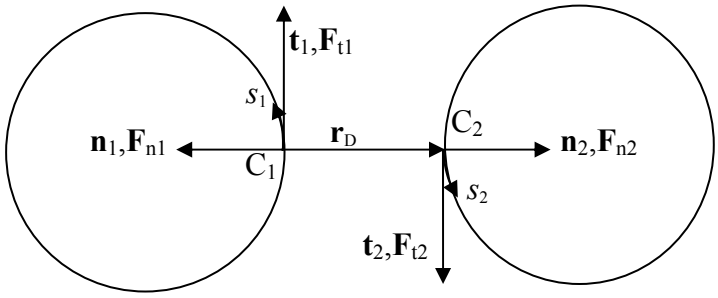

Figure 3.11: Contact configuration

The solution (s_1,s_2 i.e. the contour parameters) of the equation (65) generates the configuration shown in Figure 3.11 where the normal and tangential vectors of both the

bodies are antiparallel to each other, and the distance vector $\mathbf{r}_D$ is perpendicular to both the surfaces. The distance g_N between the two bodies can be written as:

$$g_N = \mathbf{r}_D^T \mathbf{n}_2 = -\mathbf{r}_D^T \mathbf{n}_1 \tag{66}$$

g_N is positive for separation and is zero when the two bodies come in contact. For vanishing distance $g_N = 0$, the relative velocity of the body-fixed points C_1 and C_2 in the tangential and normal directions are respectively given as:

$$\begin{aligned} \dot{g}_T &= \mathbf{t}_1^T(\mathbf{v}_{c1} - \mathbf{v}_{c2}) = \mathbf{t}_1^T \mathbf{v}_{c1} + \mathbf{t}_2^T \mathbf{v}_{c2} \\ \dot{g}_N &= \mathbf{n}_1^T(\mathbf{v}_{c1} - \mathbf{v}_{c2}) = \mathbf{n}_1^T \mathbf{v}_{c1} + \mathbf{n}_2^T \mathbf{v}_{c2} \end{aligned} \tag{67}$$

Introducing the respective Jacobians to transform the relative velocities in terms of generalized coordinates yields,

$$\begin{aligned} &\dot{g}_N = \boldsymbol{w}_N^T \dot{\mathbf{q}} + \hat{w}_N, \quad \dot{g}_T = \boldsymbol{w}_T^T \dot{\mathbf{q}} + \hat{w}_T \\ &\text{where} \\ &\boldsymbol{w}_N = \mathbf{J}_{c1}^T \mathbf{n}_1 + \mathbf{J}_{c2}^T \mathbf{n}_2 \quad , \boldsymbol{w}_T = \mathbf{J}_{c1}^T \mathbf{t}_1 + \mathbf{J}_{c2}^T \mathbf{t}_2 \\ &\hat{w}_N = \hat{\mathbf{j}}_{c1}^T \mathbf{n}_1 + \hat{\mathbf{j}}_{c2}^T \mathbf{n}_2 \quad , \hat{w}_T = \hat{\mathbf{j}}_{c1}^T \mathbf{n}_1 + \hat{\mathbf{j}}_{c2}^T \mathbf{n}_2 \\ &\text{The Jacobians can be obtained from :} \\ &\mathbf{v}_{c1,c2} = \mathbf{J}_{c1,c2} \dot{\mathbf{q}} + \hat{\mathbf{j}}_{c1,c2} \end{aligned} \tag{68}$$

The relative acceleration of the contacting bodies in normal and tangential directions can be easily obtained by deriving (68) with respect to time.

$$\ddot{g}_N = \boldsymbol{w}_N^T \ddot{\mathbf{q}} + \widetilde{w}_N, \quad \ddot{g}_T = \boldsymbol{w}_T^T \ddot{\mathbf{q}} + \widetilde{w}_T \tag{69}$$

It can be noted from these equations that contact between two bodies can be maintained if g_N and $\dot{g}_N$ are equal to zero all the time. This can be further ensured by allowing $\ddot{g}_N = 0$. So, a transition from continual contact to separation requires that $\ddot{g}_N > 0$. Moreover, depending on whether $\dot{g}_T$ is zero or not, stick-slip transition times can be determined. So, the following conditions can be written for slip or stick phenomenon under contact.

$$\begin{aligned}&\text{Slip}:\\&g_N = 0,\ \dot{g}_N = 0,\ \ddot{g}_N = 0,\ \dot{g}_T \neq 0,\ \ddot{g}_T \neq 0\\&\text{Stick}:\\&g_N = 0,\ \dot{g}_N = 0,\ \ddot{g}_N = 0,\ \dot{g}_T = 0,\ \ddot{g}_T = 0\end{aligned} \tag{70}$$

Equations of Motion of Multibody System with Multiple-Contact Configurations:

In order to accommodate unilateral constraints, equation (64) must be modified. Referring to Figure 3.11 for a case of contact under Coulomb friction, it is noted that the active tangential friction force depends on the passive normal force while sliding; however, this force becomes passive under sticking conditions. The contact forces can be incorporated in equation (61) by introducing the corresponding Jacobians and Lagrange multipliers. So, the equation of motion of a multibody system under the contact configuration of Figure 3.11 can be written as:

$$\begin{aligned}&\sum_{i=1}^{n}\left\{\begin{pmatrix}\mathbf{J_O}\\ \mathbf{J_R}\end{pmatrix}^T\begin{pmatrix}\dot{\mathbf{p}}\\ \dot{\mathbf{L}}\end{pmatrix}-\begin{pmatrix}\mathbf{J_A}\\ \mathbf{J_R}\end{pmatrix}^T\begin{pmatrix}\mathbf{F_A}\\ \mathbf{M_A}\end{pmatrix}\right\}_i - \mathbf{J}_{\mathbf{C1}}^{\mathbf{T}}\left(\mathbf{F_{N1}}+\mathbf{F_{T1}}\right)-\mathbf{J}_{\mathbf{C2}}^{\mathbf{T}}\left(\mathbf{F_{N2}}+\mathbf{F_{T2}}\right)=\mathbf{0}\\&\sum_{i=1}^{n}\left\{\begin{pmatrix}\mathbf{J_O}\\ \mathbf{J_R}\end{pmatrix}^T\begin{pmatrix}\dot{\mathbf{p}}\\ \dot{\mathbf{L}}\end{pmatrix}-\begin{pmatrix}\mathbf{J_A}\\ \mathbf{J_R}\end{pmatrix}^T\begin{pmatrix}\mathbf{F_A}\\ \mathbf{M_A}\end{pmatrix}\right\}_i - \left(\mathbf{J}_{\mathbf{C1}}^{\mathbf{T}}\mathbf{n_1}+\mathbf{J}_{\mathbf{C2}}^{\mathbf{T}}\mathbf{n_2}\right)\lambda_N-\left(\mathbf{J}_{\mathbf{C1}}^{\mathbf{T}}\mathbf{t_1}+\mathbf{J}_{\mathbf{C2}}^{\mathbf{T}}\mathbf{t_2}\right)\lambda_T=\mathbf{0}\end{aligned} \tag{71}$$

Using (62) and (68),

$$\mathbf{M}\ddot{\mathbf{q}} - \mathbf{h} - \boldsymbol{w}_{\mathbf{N}}\lambda_N - \boldsymbol{w}_{\mathbf{T}}\lambda_T = \mathbf{0} \tag{72}$$

Let us consider a system with n_C contact points and introduce the following four index sets to describe the kinematical state of each of the contacts:

$I_C = \{1, 2, ..., n_C\}$

$I_G = \{ i \in I_C \mid g_{Ni} = 0 \}$ with n_G elements

$I_N = \{ i \in I_G \mid \dot{g}_{Ni} = 0 \}$ with n_N elements

$I_T = \{ i \in I_N \mid \dot{g}_{Ti} = 0 \}$ with n_T elements

So, if one neglects collision dynamics, equation (72) can be rewritten as,

$$\mathbf{M}\,\ddot{\mathbf{q}} - \mathbf{h} - \sum_{i \in \mathbf{I_N}} \left(\boldsymbol{w}_{\mathbf{N}} \lambda_N + \boldsymbol{w}_{\mathbf{T}} \lambda_T \right)_i = \mathbf{0} \tag{73}$$

In order to solve equation (73), $2n_N$ additional equations are required. Using Coulomb's friction law, one can express the tangential forces of the sliding contacts (elements of $I_N \setminus I_T$), as,

$$\lambda_{Ti} = -\mu_i \lambda_{Ni} sign(\dot{g}_{Ti}), \quad \lambda_{Ni} \geq 0, \forall i \in I_N \setminus I_T$$

The remaining $n_N + n_T$ equations are obtained by imposing some conditions on the relative accelerations of the bodies in contact.

$$\begin{aligned} \ddot{g}_{Ni} &= \boldsymbol{w}_{\mathbf{Ni}}^{\mathbf{T}} \ddot{\mathbf{q}} + \widetilde{w}_{Ni} \quad \forall i \in I_N \\ \ddot{g}_{Ti} &= \boldsymbol{w}_{\mathbf{Ti}}^{\mathbf{T}} \ddot{\mathbf{q}} + \widetilde{w}_{Ti} \quad \forall i \in I_T \end{aligned} \tag{74}$$

Expressing (73) and (74) in matrix notation, one gets,

$$\begin{aligned} &\mathbf{M}\,\ddot{\mathbf{q}} - \mathbf{h} - \left(\mathbf{W_N} + \mathbf{W_S}\hat{\boldsymbol{\mu}}_{\mathbf{S}} \mid \mathbf{W_T} \right) \begin{pmatrix} \boldsymbol{\lambda}_{\mathbf{N}} \\ \boldsymbol{\lambda}_{\mathbf{T}} \end{pmatrix} = \mathbf{0} \quad \in \Re^{\mathbf{f}} \\ &\begin{pmatrix} \ddot{\mathbf{g}}_{\mathbf{N}} \\ \ddot{\mathbf{g}}_{\mathbf{T}} \end{pmatrix} = \begin{pmatrix} \mathbf{W}_{\mathbf{N}}^{\mathbf{T}} \\ \mathbf{W}_{\mathbf{T}}^{\mathbf{T}} \end{pmatrix} \ddot{\mathbf{q}} + \begin{pmatrix} \widetilde{\boldsymbol{w}}_N \\ \widetilde{\boldsymbol{w}}_T \end{pmatrix} \quad \in \Re^{\mathbf{n_N + n_T}} \end{aligned} \tag{75}$$

where

$$\hat{\boldsymbol{\mu}}_{\mathbf{S}} = \{-\mu_i sign(\dot{g}_{Ti})\}, \quad i \in I_N \setminus I_T$$

Equation (75) can be further condensed in matrix form to get:

$$\begin{aligned} &\mathbf{M}\,\ddot{\mathbf{q}} - \mathbf{h} - \left(\mathbf{W} + \mathbf{N_S} \right) \boldsymbol{\lambda} = \mathbf{0} \quad \in \Re^{\mathbf{f}} \\ &\ddot{\mathbf{g}} = \mathbf{W}^{\mathbf{T}} \ddot{\mathbf{q}} + \widetilde{w} \quad \in \Re^{\mathbf{n_N + n_T}} \\ &\mathbf{N_S} = \left(\mathbf{W_S}\hat{\boldsymbol{\mu}}_{\mathbf{S}} \mid \mathbf{0} \right), \mathbf{W} = \left(\mathbf{W_N} \mid \mathbf{W_T} \right) \end{aligned} \tag{76}$$

Further, simplification of equation (76) further yields:

$$\ddot{\mathbf{g}} = \mathbf{W}^{\mathbf{T}} \mathbf{M}^{-\mathbf{1}} (\mathbf{W} + \mathbf{N_S}) \boldsymbol{\lambda} + (\mathbf{W}^{\mathbf{T}} \mathbf{M}^{-\mathbf{1}} \mathbf{h} + \widetilde{w}) \quad \in \Re^{\mathbf{n_N + n_T}} \tag{77}$$

Equation (77) is a linear system with $n_N + n_T$ equations and $2(n_N + n_T)$ unknowns ($\ddot{\mathbf{g}}, \boldsymbol{\lambda}$). The system is completely solvable for the following three cases:

- Case 1: Under the situation of continuous contact and stick for all time t, the relative acceleration vector vanishes, thereby, yielding a completely solvable linear system for $\boldsymbol{\lambda}$.
- Case 2: Slip without stick phenomenon (implying $n_T = 0$)
- Case 3: Slip with stick phenomenon

For the last two cases, Pfeiffer *et al.* [125] developed a unique Linear Complementarity Problem (LCP) to detect transitions between the following states: contact – slip – stick – separation.

3.4.3 Application of Multibody Formalisms: Planar Chain CVT Model

The theory outlined in the previous section is used to model the various dynamic interactions in a chain-drive CVT. It is necessary to model the chain CVT drive as a multibody system in order to accurately capture the excitation dynamics and the polygonal effects arising from its discrete structure. As illustrated in Figure 3.8, the chain-drive CVT consists of two pulleys and a chain. The system is subjected to an input torque on the driver pulley and a resisting load torque on the driven pulley. The basic assumptions involved in the model development are:

- The chain links are rigid i.e. they undergo negligible elastic deformations
- Friction between the pulley and the links are governed by continuous Coulomb friction theory
- Dynamic effects due to out-of-plane or spatial motion of the chain links are neglected

- Pulley misalignment effects are neglected; however, pulley flexibility effects are incorporated using Sferra's model [48] (as mentioned in the analysis of belt CVT).
- The interactions between the rocker pins of neighboring links and between a rocker pin and a plate can all be accounted for by modeling the chain link as a planar rigid body.

The modeling of various components of a chain-drive CVT is discussed subsequently.

Model of chain links: The chain in the CVT is modeled link by link to account for its discrete structure. Each chain link represents a rigid body with 3 degrees of freedom in a plane (i.e. (x_C, y_C, θ) : 2 translations of the center of mass of the link and 1 rotation about an axis passing through the link's center of mass). Moreover, the chain links are kinematically decoupled. The chain links are connected to each other by force elements which take into account the elasticity and damping of the links and joints. In case of contact between a link and a pulley, additional normal and tangential forces act on the bolt of the link and therefore on the link. These contact forces correspond with the associated contact forces acting on the pulley. Figure 3.12 depicts the free-body diagram of a chain link. The spring in the force element is governed by a non-linear force-deformation law (kind of hardening spring) in order to take into account the dynamic effects due to clearance between the links. The equations of motion of links not in contact with the pulley are governed by (54), (57), and (61). The active forces and torques acting on the link arise from the forces in the force-element. However, these must be modified when the links contact the pulleys.

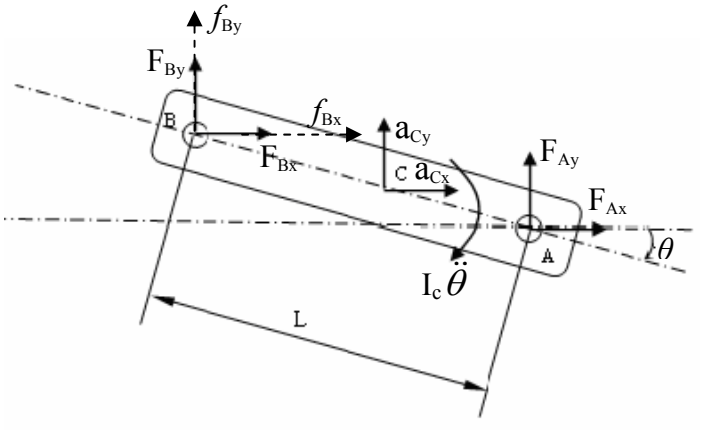

(a)

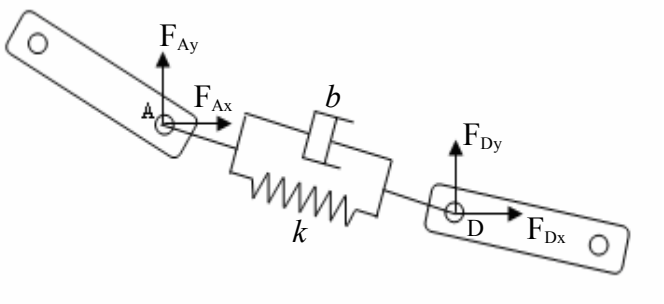

(b)

Figure 3.12: Free body diagram of a chain link

The Jacobian matrix between the system coordinates and the configuration (or generalized) coordinates of a link at its center of mass can be obtained as,

$$\mathbf{v_C} = \begin{pmatrix} \dot{x}_C \\ \dot{y}_C \\ 0 \end{pmatrix}, \boldsymbol{\Omega} = \begin{pmatrix} 0 \\ 0 \\ \dot{\theta} \end{pmatrix}, \dot{\mathbf{q}} = \begin{pmatrix} \dot{x}_C \\ \dot{y}_C \\ \dot{\theta} \end{pmatrix}$$

$$\mathbf{J} = \begin{pmatrix} \mathbf{J_C} \\ \mathbf{J_R} \end{pmatrix} = \begin{pmatrix} \dfrac{\partial \mathbf{v_C}}{\partial \dot{\mathbf{q}}} \\ \dfrac{\partial \boldsymbol{\Omega}}{\partial \dot{\mathbf{q}}} \end{pmatrix} = \begin{pmatrix} 1 & 0 & 0 \\ 0 & 1 & 0 \\ 0 & 0 & 0 \\ 0 & 0 & 0 \\ 0 & 0 & 0 \\ 0 & 0 & 1 \end{pmatrix} \tag{78}$$

So, equation of motion of a link not in contact with pulley is:

$$\mathbf{J}^{\mathbf{T}} \begin{pmatrix} m\mathbf{I} & \mathbf{0} \\ \mathbf{0} & \mathbf{I_C} \end{pmatrix} \mathbf{J}\,\ddot{\mathbf{q}} + \mathbf{J}^{\mathbf{T}} \begin{pmatrix} \mathbf{0} \\ \widetilde{\boldsymbol{\Omega}}\mathbf{I_C}\boldsymbol{\Omega} \end{pmatrix} = \mathbf{J}^{\mathbf{T}}_{\mathbf{A,B}} \begin{pmatrix} \mathbf{F} \\ \widetilde{\mathbf{r}}_{\mathbf{A,B}}\mathbf{F} \end{pmatrix} \tag{79}$$

Similarly, Jacobian matrices for the link at the points of application of the active force **F** (A, B in the figure) can be obtained through the velocities of the corresponding points of the link, i.e., $\mathbf{J}_A$ can be obtained through an expression for velocity at point A, $\mathbf{v}_A$. The active forces, **F**, and the torques acting on the link due to these forces are obtained by computing the forces in the springs and dampers of the force-elements connected to that particular link. These forces and torques further depend on the position and velocity of the end points of the link and its successor. It is to be noted that if (79) is summed for all the links in the system, one gets an equation of the same form as (62). Now, modifications similar to (73) are introduced in (79) to account for the contact between this link and the pulley. So, the equation of motion for all the links under unilateral contact conditions can be written as:

$$\mathbf{M}\ddot{\mathbf{q}} - \mathbf{h} - \left(\mathbf{W}_N + \mathbf{W}_S\hat{\boldsymbol{\mu}}_S \mid \mathbf{W}_T\right)\begin{pmatrix}\boldsymbol{\lambda}_N\\ \boldsymbol{\lambda}_T\end{pmatrix} = \mathbf{0}$$

where (80)

$$\hat{\boldsymbol{\mu}}_S = \{-\mu_i sign(\dot{g}_{Ti})\}$$

$\boldsymbol{\lambda}_N$, $\boldsymbol{\lambda}_T$ are the normal and the sticking constraint forces of the links that are in contact with the pulley and $\dot{g}_{Ti}$ is the tangential relative velocity between the link, *i*, and the pulley. $\mathbf{W}_N$ represents a matrix with coefficients of relative acceleration (in the normal direction) between the links and the pulley in the configuration space. $\mathbf{W}_S$ represents a matrix with coefficients of relative acceleration (in the tangential direction) between the links and the pulley in the configuration space when the links are slipping on the pulley sheave, whereas $\mathbf{W}_T$ represents a matrix with coefficients of relative acceleration (in the tangential direction) between the links and the pulley in the configuration space when the

links are sticking to the pulley sheave. It is to be noted that the relative velocity and accelerations are computed at the contact points where the links contact the pulley.

It has been previously stated that the time variance of the model due to contact-slip-stick-separation transitions can be eliminated by assuming the friction between the bolt of the chain link and the pulley to be governed by continuous Coulomb theory. Under this theory, the tangential constraints include no stiction as the frictional forces are assumed to be vanishingly small for negligible relative velocity between the link and the pulley. Figure 3.13 depicts the continuous Coulomb friction model. The model illustrates that at low relative velocity between two surfaces, the frictional force is also low. However, in reality, zero relative velocity between two surfaces implies a stick situation where frictional force can vary from - μN to μN (μ represents the coefficient of friction between two surfaces, and N represents the normal force between the same two surfaces). This phenomenon relates to the microslip theory.

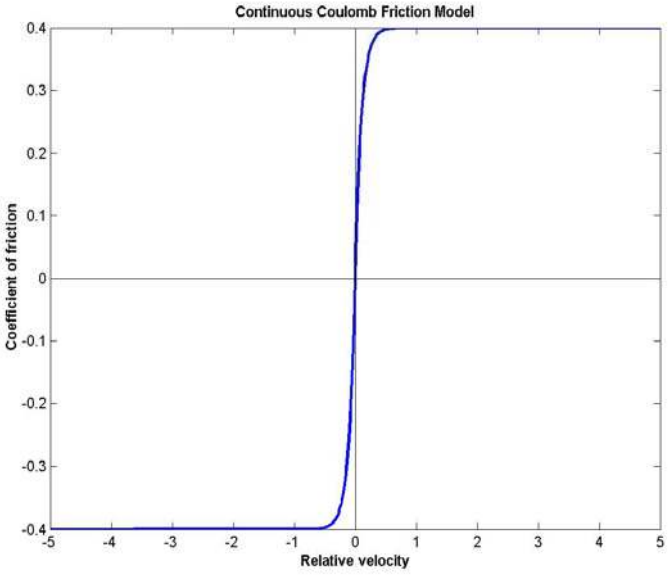

Figure 3.13: Continuous Coulomb Friction Model
(*e.g.: a = 0.003,b = 0.1,* $\mu_{bo} = 0.4$)

The continuous Coulomb friction theory is able to capture the microslip physics under the assumption that low relative velocity leads to low frictional force. This assumption relates to the macroslip theory. It shows that the frictional force increases with relative velocity until it reaches the saturation limit. Under the assumption of continuous Coulomb friction model, the equation (80) for all the links becomes:

$$\begin{aligned}&\mathbf{M}\ddot{\mathbf{q}} - \mathbf{h} - \left(\mathbf{W_N} + \mathbf{W_S}\hat{\boldsymbol{\mu}}_\mathbf{S}\right)\boldsymbol{\lambda}_\mathbf{N} = \mathbf{0}\\ &\text{where}\\ &\hat{\boldsymbol{\mu}}_\mathbf{S} = \{-\mu_i(\dot{g}_{Ti})sign(\dot{g}_{Ti})\}\\ &\boldsymbol{\lambda}_\mathbf{T} = \mathbf{0}\end{aligned} \tag{81}$$

So, the continuous Coulomb friction theory obviates the determination of exact switching conditions (from LCP algorithm [125]) between the stick and slip phases of motion.

Model of Pulleys: Each pulley is modeled as a rigid body with one degree of freedom i.e. the rotational degree of freedom (ϕ). A pulley is also loaded with the frictional and normal forces between the rocker pins of the links and the pulley and an external moment. An input torque is applied to the driver pulley and a load torque on the driven pulley. These contact forces arise from unilateral constraints, which may be active or passive. The equation of motion of pulley with contact based on continuous Coulomb friction is given by a scalar equation as:

$$\begin{aligned}&J_P\ddot{\phi} = h_P - \left(\mathbf{W_{Np}} + \mathbf{W_{Sp}}\hat{\boldsymbol{\mu}}_\mathbf{S}\right)\boldsymbol{\lambda}_\mathbf{Np}\\ &\text{where}\\ &\hat{\boldsymbol{\mu}}_\mathbf{S} = \{-\mu_i(\dot{g}_{Ti})sign(\dot{g}_{Ti})\}\\ &h_P \text{ contains external torques}\\ &\mathrm{J_p} \text{ is the pulley rotational inertia}\end{aligned} \tag{82}$$

Although elastic deformations of the chain links have been assumed to have a negligible effect on the CVT's performance, the variation of the local groove width

caused by the elastic deformation of the pulleys significantly influences the thrust ratio, the slip behavior, and the performance of a chain CVT [7, 31, 33, 48, 59, 127]. However, since one of the goals of this research was to study the influence of friction characteristic on CVT dynamics, a detailed finite-element modeling of pulley sheaves was evaded. Hence, instead of a detailed finite-element formulation of pulley sheaves, simple trigonometric functions (as outlined by Sferra *et al.* [48]) are used to describe the varying pulley groove angle and the local elastic axial deformations of the pulley sheaves. The analysis, which consequently takes pulley flexibility into account, is similar to that outlined in the section on metal V-belt CVT model.

Contact Dynamics Model:

A chain link contacts a pulley at the ends of a rocker pin. As the plates move, the rocker pins of adjacent links also interact with each other. Assuming negligible dynamic interaction between a pair of rocker pins, these rocker pins are modeled as a single bolt. So, every link is associated with one bolt through which it contacts the pulley sheaves. The bolt is represented as a linear massless spring. The contact planes of the bolts are the end faces of the springs. The surfaces of the bolt are loaded with the normal and frictional contact forces. Figure 3.14 illustrates the free diagram for the interactions between the bolt and a pulley. It is necessary to quantify this bolt spring force, F_b, in order to derive the contact forces. The bolt spring force is given in accordance with Pfeiffer's model [6]. It depends on the bolt length, l_b, and stiffness, K_b, as well as on the local distance between the pulley sheaves, z. Since the pulley sheaves also bend, additional axial width variation (refer to Figure 3.2) affects the bolt force. So, the bolt force, F_b, is given as:

$$F_b = \begin{cases} K_b(l_b - z - u) & \forall (z+u) \le l_b \\ 0 & \forall (z+u) > l_b \end{cases} \tag{83}$$

In this figure, $\mathbf{F}_r$ and $\mathbf{F}_t$ represent the components of the resultant friction force vector $\mathbf{F}_f$ between a chain link and the pulley, which act in the plane of the pulley sheave, and **N** is the normal force between the link and the pulley, and β is the pulley half-sheave angle. Summing the forces in the axial i.e. z-direction, one gets,

$$N = F_r \tan\beta + \frac{F_b}{\cos\beta} \tag{84}$$

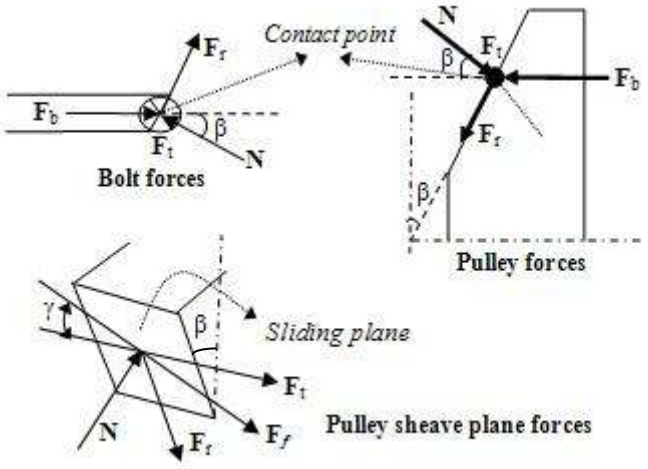

Figure 3.14: Free body diagram for bolt-pulley interactions

As before, the use of continuous Coulomb friction theory eliminates the stiction constraints and hence, the total friction force is given as,

$$\mathbf{F_f} = -\mu \mathbf{N} \frac{\dot{\mathbf{g}}}{|\dot{\mathbf{g}}|} \tag{85}$$

It is to be noted that the chain link slips in the plane of the pulley sheave. The slip angle, γ, defines the plane in which the friction force acts. It is the angle which the resultant friction force vector, $\mathbf{F}_f$, makes with the tangential direction vector on the pulley. So, in order to get the friction force vector, it is crucial to keep a track of the relative velocity vector between the chain link and the pulley. Inserting (85) into (84) gives the normal force (**N** or $\boldsymbol{\lambda}_N$) in terms of the bolt force, as $\mathbf{F}_r$ is just the radial component of the total

friction force $\mathbf{F}_f$. The relative acceleration and the relative velocity between the link and the pulley can be obtained using contact kinematics as depicted in Figure 3.15. Once the normal forces are known, they can substituted in (81) and (82) to get the time histories of the generalized coordinates of the system.

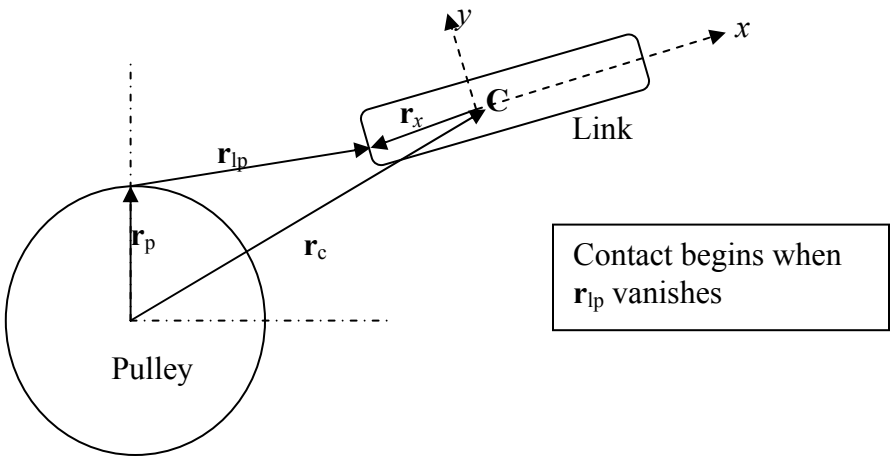

Figure 3.15: Contact Kinematics between a link and a pulley

Model for clearance between links:

As mentioned before, the chain links are modeled as rigid bodies connected to each other by means of force elements i.e. springs and dampers. Due to continual operation, wear or fatigue, a chain-drive CVT is susceptible to form clearances between the chain links. Moreover, it is quite possible for a chain CVT to have clearances among its various components during the assembly process. Link clearance, as depicted in Figure 3.16 (a), drastically influence the dynamic behavior of the chain CVT as it affects the transmitted torque and also causes early failure of the system owing to high noise and vibrations. Figure 3.16 (b) also depicts the force-deformation law in the spring which accounts for the clearance (ε) between the chain link elements. It is obvious from the figure that the clearance among the links influences the total transmitted force in the chain-drive CVT.

As the clearance gap closes, the spring force increases. Moreover, losses can be associated with link-clearance as the torque transmitted for such CVTs is less than that for a chain CVT with no link-clearance. Clearance can also induce non-desirable or perilous nonlinear phenomena in a system, the most common being self-excited vibrations.

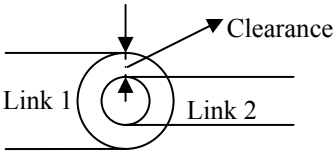

(a)

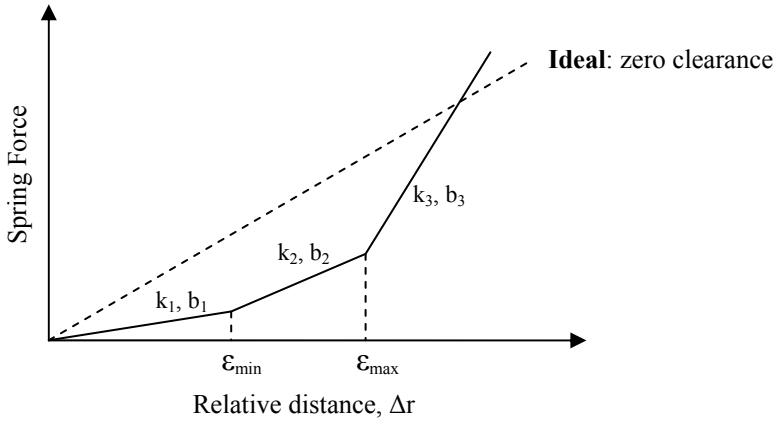

(b)

Figure 3.16: Model for clearance between the chain links

3.5 Mathematical Modeling of Friction

Of all the literature surveyed so far, only a few [58, 105, 136] have briefly cited the influence of friction characteristics on the dynamics of a metal- and chain- drive CVT. Most of the work has been developed using Coulomb friction theory to describe friction between the contacting surfaces of a CVT. The friction phenomenon described by this

law is inherently discontinuous in nature. It is common engineering practice to introduce a smoothening function to represent the set-valued friction law. However, certain friction-related phenomena like chaos, limit-cycles, hysteresis, etc., are neither easy to detect nor easy to explain on the basis of classical Coulomb-Amonton friction theory. It is well-known that the stick-slip transitions in a friction-driven system can induce self-excited vibrations [105, 136] in the system and influence its dynamic performance. Hence, it is useful to introduce several mathematical models that possibly describe friction phenomenon in the contacting zone of such CVTs under different loading conditions. A real production CVT operating inside a vehicle is a well-lubricated system, and, under such circumstances, it is possible that the friction characteristic in the contacting zone resembles Stribeck friction [135] rather than Coulomb friction. Moreover, since the contact pressures generated over the contact arc are huge, the friction characteristic may further deviate to resemble that of elasto-plastic-hydrodynamic contact. In addition to the continuous Coulomb friction model (refer to Figure 3.13), other friction models, as illustrated in Figure 3.17, were used in this research to characterize friction between the belt/chain and the pulley. These models not only capture kinetic-friction dynamics, but also capture dynamics related to stiction and lubrication.

It is evident that governing equations of a chain-drive CVT possess time-varying structure due to the possible transitions between stick and slip phases of the contact. However, without significant loss of accuracy [7], it is possible to evade this time-variance in the system by assuming the friction between the bolt of the chain link and the pulley to be approximated by a smooth nonlinear function. Although mathematical models of friction give an insight into the dynamic behavior of a friction-limited drive

under different operating conditions, an exact friction characteristic of a friction-driven system can only be obtained by conducting experiments on the system.

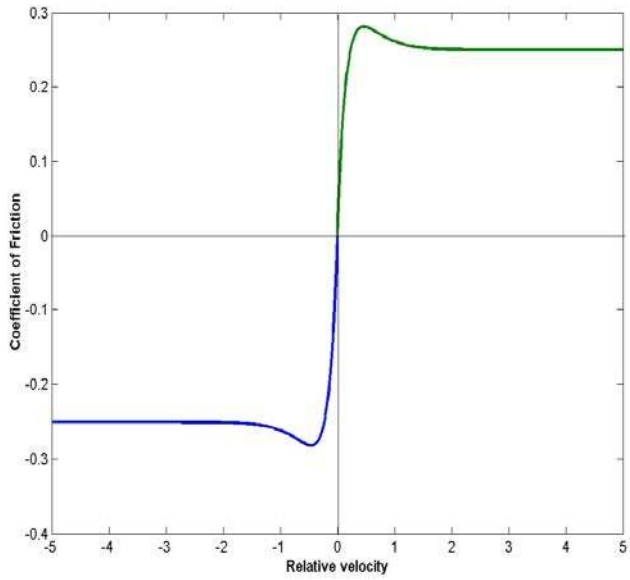

(a) Analytical Friction Model: $\mu = \mu_0 \left(1 - e^{-\kappa|v|}\right)\left(1 + (f_r - 1)e^{-\bar{\lambda}|v|}\right)$

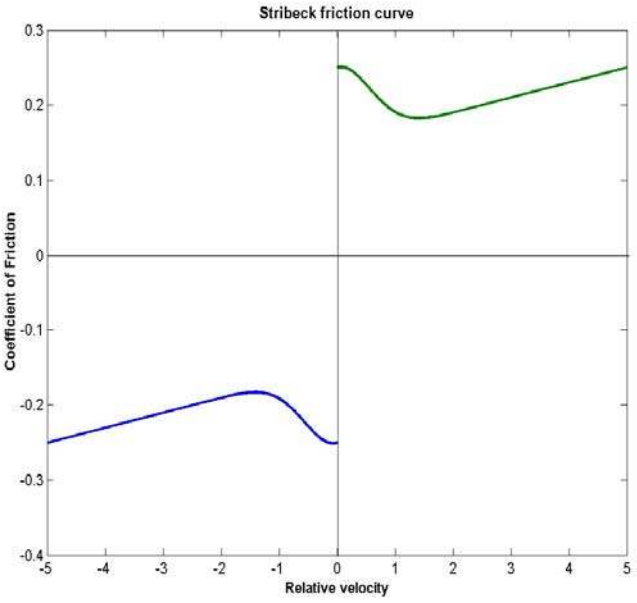

(b) Stribeck Friction model: $\mu = \alpha_0 + \alpha_1 e^{-\left(v/v_0\right)^2} + \alpha_2 v$

Figure 3.17: Mathematical models for friction

3.6 Closure

The chapter discusses models for two different configurations of a CVT: metal V-belt type and chain type. The belt CVT model takes the inertial and pulley flexural effects into account, and uses kinematic constraints to link the driver dynamics to the driven dynamics. Multibody formalisms are used to capture the discrete structure of the chain-drive CVT. Continuous Coulomb friction theory is used to model friction between the power transmitting device and the pulley. Clearance effects from the chain links are modeled using a piecewise-linear force-deformation law in the interconnection elements. In addition to the continuous Coulomb friction model, other friction characteristics were introduced to model friction between the belt/chain and the pulley in order to understand self-excited vibration phenomenon and other associated dynamic effects in such systems. Since it is difficult to monitor friction experimentally during the running conditions of a complex nonlinear system (e.g. a CVT), these mathematical models of friction give insight into the different dynamic maneuvers that a system can exhibit under different contact-zone loading conditions. The models of the metal pushing V-belt CVT and the chain CVT take into account the effects arising from the belt/chain-pulley inertial interactions, belt-band inertial interactions, pulley flexibility, clearance, and contact-zone friction characteristics on the performance of a CVT system. These models give profound insight into the dynamics of a CVT system, which could be exploited further to design efficient controllers and reduce associated losses.

CHAPTER 4

DRY FRICTION MODELING AND NON-SMOOTH MECHANICAL SYSTEMS

4.1 Dry Friction

Dry friction plays a significant role in the dynamic behavior of a mechanical system. It is a nonlinearity which is abundant in nature, machines, and other processes. Continuously variable transmissions (CVTs) are friction-limited drives. The torque transmitting capacity and the dynamic performance of a CVT are greatly influenced by the friction characteristics of the various contacting surfaces. However, the presence of dry friction can also induce chaotic phenomena and self-sustained vibrations in the CVT, which possibly degrade the system performance [137]. Dry friction, from a tribologist point of view, is a resisting force which opposes the relative motion between the contacting surfaces of two or more solid bodies.

Leonardo da Vinci formulated the earliest laws of friction and stated that the friction force is independent of the area of contact and is proportional to the applied normal load. The relation between the normal contact force and the tangential friction force was later experimentally studied by Amontons. Coulomb considered the influence of sliding speed and direction and stated that the friction coefficient is almost independent of the sliding velocity; however, the friction force opposes the sliding direction. Coulomb's law can be stated as:

$$F_T = -\mu F_N sign(v_{rel}), \quad v_{rel} \neq 0$$

The bodies stick to each other when the relative velocity between the contacting surfaces vanishes. Under the conditions of stick, the friction force adjusts itself accordingly to make equilibrium with the externally applied forces. The bodies remain sticking as long as equilibrium is ensured. Coulomb also developed the concept of limiting static friction. It is only when the externally applied forces exceed the value of the static friction force that the bodies begin to slide on each other. So, Coulomb's law can be reformulated as:

$$\begin{aligned} -\mu_s F_N \le F_T \le \mu_s F_N \quad & , v_{rel} = 0 \qquad \text{(Stick)} \\ \mathrm{F_T} = -\mu_k F_N sign\,(v_{rel}), \quad & v_{rel} \neq 0 \qquad \text{(Slip)} \end{aligned} \tag{1}$$

μ_k is the coefficient of friction in the slip phase, which Coulomb referred to as the coefficient of kinetic friction, and μ_s is the coefficient of static friction.

Coulomb's law is an idealization of the complex physical contact behavior. The surfaces of solid bodies which appear macroscopically smooth are in fact rough on a microscopic level. On a microscopic level, the surface of each body can be imagined to consist of a range of protuberances that is interposed against an inverted range on the other contacting surface, as depicted in Figure 4.1 [138]. These protuberances are also referred to as surface asperities. True contact between two surfaces occurs only where the asperities touch each other.

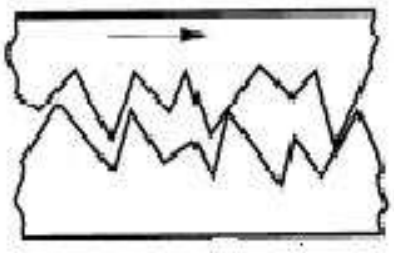

Figure 4.1: Microscopic friction phenomenon [138]

The true contact area is therefore much smaller than the apparent area of contact. Moreover, the true contact area is proportional to the total normal load. The asperities

deform to generate the contact area necessary to take up the total normal load. These asperities are also sheared when the contacting surfaces move tangentially over each other, consequently giving rise to the friction force. Even when the bodies are macroscopically sticking to each other, there is always a microscopic tangential relative displacement between the contacting surfaces. This pre-sliding displacement is caused due to elasto-plastic deformation of the asperities which continues until the external forces overcome the maximum static friction force.

Lubricant between the surfaces significantly influences the friction characteristics of the contacting surfaces [135]. For a small relative velocity, the surfaces slide with asperities loosely meshing with each other (even if the surfaces are lubricated). This low-velocity friction regime is called boundary lubrication. Increasing the relative velocity increases the separation between the surfaces and allows partial lubrication which diminishes friction. Film thickness is a vital parameter in friction under lubrication. For low velocities, the lubricant acts as a surface film and the shear strength of this film determines the friction between the surfaces. At higher velocities and low pressures, a fluid layer of lubricant builds up on the surface due to hydrodynamic effects. Friction is then determined by the shear forces in the fluid layer. These shear forces depend on the viscous character of the lubricant as well as on the shear velocity distribution in the fluid film. At high velocities and pressures, the lubricant layer builds up under elasto-hydrodynamic effects. In such contact conditions, the lubricant transforms into an amorphous solid phase due to high pressures in the contact zone. The shear forces of this solid phase turn out to be practically independent of the shear velocity. The shear strength of a solid lubricant film at low velocities is generally higher than the shear forces of the

corresponding fluid film built up at higher velocities. As a result, the friction coefficient in lubricated systems normally decreases when the velocity increases from zero. The decrease of friction due to increasing sliding velocity is referred to as Stribeck effect. When the thickness of the film is large enough, which occurs under the conditions of full lubrication, to completely separate the bodies in contact, the friction coefficient may increase with velocity as the hydrodynamic effects become significant. Figure 4.2 depicts a typical Stribeck friction curve [135].

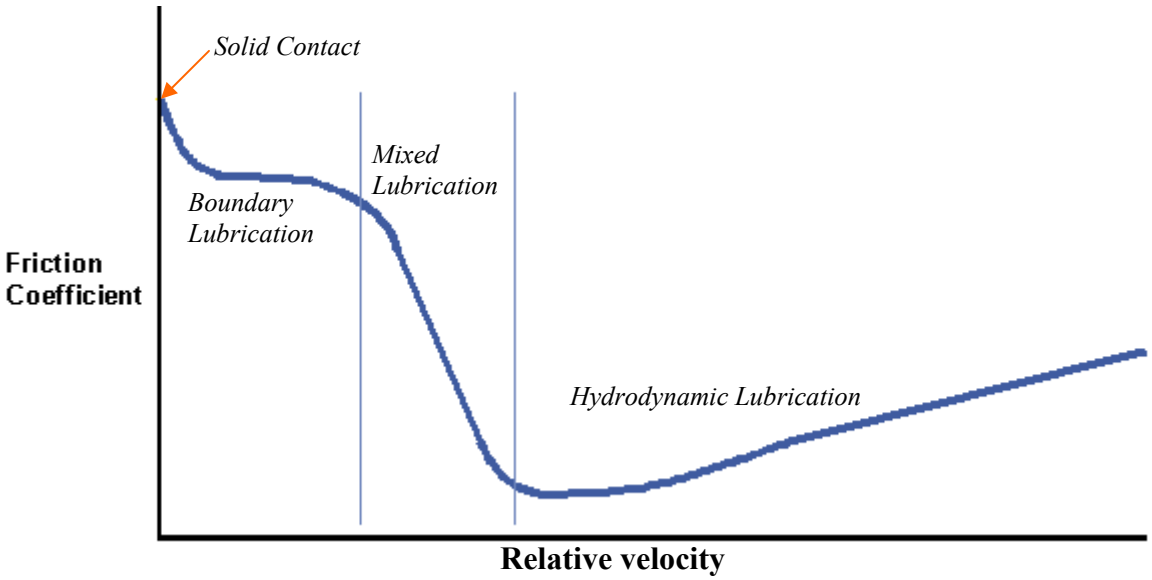

Figure 4.2: Stribeck friction curve

The friction coefficient is thus dependent on the relative velocity of the contacting surfaces. For most practical purposes, Coulomb's law aptly describes the friction characteristic between two contacting surfaces. However, it fails to describe other non-linear phenomena associated with friction, for instance, chaos and self-excited vibrations. Experimental studies have also confirmed the presence of hysteresis in friction-based systems, which can be attributed to dissimilar variations in the friction force during acceleration and deceleration phases of motion. The hysteresis phenomenon, as depicted

by Figure 4.3 [139, 140], can also not be dealt with by the classical Coulomb's law. The hysteresis loop becomes wider as the velocity variations become faster.

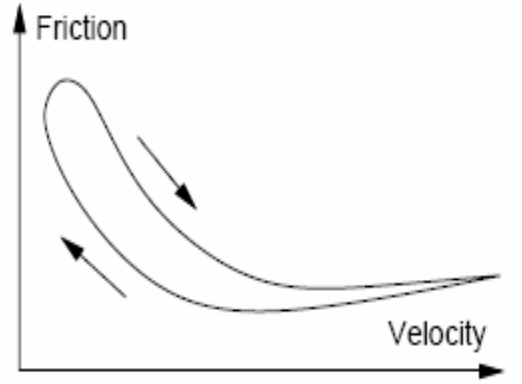

Figure 4.3: Hysteresis induced by Friction [139,140]

Many different models, as illustrated in Figure 4.4 [135, 141], are proposed in literature for the mathematical description of dry friction. It is necessary to understand the variations in the dynamic performance of a system under the influence of different friction characteristics of the contacting surfaces.

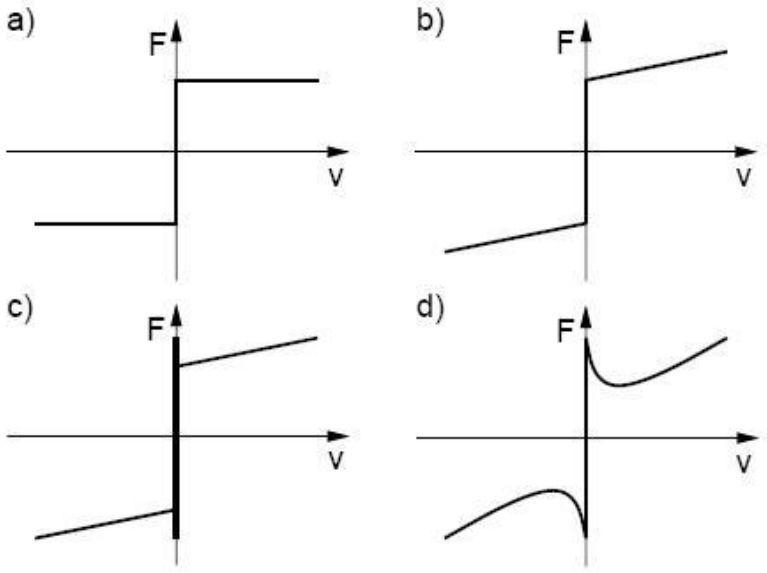

(a) Coulomb (b) Coulomb + Viscous (c) Stiction + Coulomb + Viscous (d) Stribeck

Figure 4.4: Models of Friction [135]

The discontinuity at the origin, as depicted in Figure 4.4, is unrealistic for the purposes of simulation. The common approach to overcome this discontinuity is to approximate the stick-phase by some smooth function, as was mentioned in the previous chapter (refer to Figures 3.12 and 3.16). Moreover, the *signum* function can be further approximated as,

$$sign\,(v) = \frac{2}{\pi}\tan^{-1}(\hat{\lambda} v) \tag{2}$$

The higher the slope parameter ($\hat{\lambda}$), the better is the approximation of the stiction phenomenon. Such friction models result in smooth ordinary differential equations for the equations of motion of the system. All the standard integration routines can therefore be directly applied and the existence and uniqueness of the solution is guaranteed. However, there are a few disadvantages associated with such smooth friction models. The smooth friction model fails to capture the dynamics of stick phase accurately. The friction force is vanishingly small at zero velocity. The model thus allows the body to accelerate even though the external forces on the body are less than the peak stiction force. Moreover, the steep slope of the approximating non-linear friction model yields a stiff differential equation for vanishing relative velocity, which becomes inconvenient from a numerical point of view.

Friction, as can be noted from equation (1), induces set-valued forced laws for describing the dynamics of a friction-driven system. Such dynamical models of system with dry friction result in Filippov-type differential equations. Filippov systems form a class of non-smooth systems described by differential equations with a discontinuous right-hand side. Non-smooth systems exhibit several interesting nonlinear phenomena, like grazing bifurcation, discontinuous bifurcation, nonlinear complementarity conditions, etc., which possibly are lost when the set-valued friction laws are

approximated by smoothening functions. The subsequent sections (Leine and Nijmeijer [143]) discuss Filippov systems and the dynamics associated with them.

4.2 Filippov Systems and Differential Inclusions

Filippov [142] analyzed differential equations with discontinuous right-hand side and introduced new solution concepts for such equations on the basis of convex-analysis. Consider a dynamical system described by a set of ordinary differential equations, as,

$$\dot{\mathbf{x}}(t) = \mathbf{f}(t, \mathbf{x}(t)), \quad \mathbf{x}(t) \in \Re^n \tag{3}$$

where **x**(t) is a state vector and **f**(t, **x**(t)) is the vector field or the right-hand side vector describing the time derivative of the state vector. The solution to (3) is guaranteed to exist if the vector field is linearly bounded, continuous, and locally Lipschitz. However, if the vector-field is discontinuous in **x**, Filippov's theory governs the existence and uniqueness of solutions. Filippov extended the notion of a solution to (3) by replacing the right-hand side **f**(t, **x**) by a set-valued function **F**(t, **x**) such that **F**(t, **x**) = **f**(t, **x**) for all **x** where **f** is continuous. However, at the points of discontinuity, a suitable choice of **F**(t,**x**) is incorporated. The differential equation in (3) is then replaced by the following differential inclusion:

$$\dot{\mathbf{x}}(t) \in \mathbf{F}(t, \mathbf{x}(t)), \quad \mathbf{x}(t) \in \Re^n \tag{4}$$

So, differential inclusions can be regarded as convexification of discontinuous differential equations.

Filippov stated that an absolute continuous function **x**(t) : $[0, \tau] \to \Re^n$ is said to be a solution of (3) if for almost all t $\in [0, \tau]$ it satisfies (4) where **F**(t, **x**(t)) is the closed

convex hull of the limits of **f**(t, **x**(t)). The 'almost all' value of t includes all t in the interval $[0,\tau]$ except those with Lebesgue measure 0 (i.e. the points of discontinuity). So, the existence of a solution to the differential inclusion (4) is guaranteed if **F**(t, **x**(t)) is nonempty, bounded, closed, convex, and upper semi-continuous. The differential inclusion (4) can be further expressed as [143]:

$$\dot{\mathbf{x}}(t) \in \mathbf{F}(t,\mathbf{x}(t)) = \begin{cases} \mathbf{f}_{-}(t,\mathbf{x}(t)), & \mathbf{x} \in V_{-} \\ \overline{co}\{\mathbf{f}_{-}(t,\mathbf{x}(t)),\ \mathbf{f}_{+}(t,\mathbf{x}(t))\}, & \mathbf{x} \in \Sigma \\ \mathbf{f}_{+}(t,\mathbf{x}(t)), & \mathbf{x} \in V_{+} \end{cases} \tag{5}$$

$$\overline{co}\{\mathbf{f}_{-},\ \mathbf{f}_{+}\} = \{(1-q)\mathbf{f}_{-} + q\mathbf{f}_{+},\ \forall q \in [0,1]\}$$

Here, the state space $\boldsymbol{R}^{n}$ is split in two subspaces V_{-} and V_{+} where the function **f**(t, **x**) is continuous, smooth, and linearly bounded, and Σ is the switching boundary where the **f**(t, **x**) is discontinuous. Σ is a hypersurface and is defined by a scalar switching boundary function h(**x**). The state **x** is in Σ when h(**x**) = 0, in V_{-} when h(**x**) < 0, and in V_{+} when h(**x**) > 0. The switching boundary need not necessarily be smooth, autonomous, and a singleton. It is possible for a differential inclusion to have non-unique solutions. Filippov, however, also proposed a couple of conditions under which the uniqueness of the solution of differential inclusion (5) is guaranteed.

Theorem [142] : Let a function f(t, x) in a domain D be discontinuous only on a set M of measure zero. Let there exist a summable function g(t) such that for almost all points (t,x) and (t,y) of the domain D, one has $|f(t, x)| \leq g(t)$ and for $|x-y| < \varepsilon$, $\varepsilon > 0$,

$(x - y) \cdot (f(t, x) - f(t, y)) \leq g(t) |x-y|^2$

Then equation (3) has a unique solution in forward time (also referred to as right uniqueness) in the domain D.

Filippov also derived other uniqueness conditions based on the geometrical interpretation of the differential inclusion. The set **F**(t,**x**) is a linear segment joining the end points of the vectors $\mathbf{f}_-$ and $\mathbf{f}_+$. Let P be a plane tangent to the hypersurface h(**x**) at the point **x** on the hypersurface (i.e. the switching boundary). If for $t_1 < t < t_2$, the line segment **F**(t,**x**) lies on one side of the tangent plane P, the solutions for these *t* pass from one side of the surface to the other. If this line segment intersects the plane P, the intersection point is the end point of the vector $\mathbf{f}^0$(t,**x**) which determines the velocity of the motion along the hypersurface in the **x** space. So, the function **x**(t) satisfying $\dot{\mathbf{x}} = \mathbf{f}^{\mathbf{0}}(t, \mathbf{x})$ is assumed to be the solution of equation (3). If $\mathbf{f}^0 \neq \mathbf{f}_-$ and $\mathbf{f}^0 \neq \mathbf{f}_+$, the solution obtained is known as the *sliding-mode* solution. If the whole of the segment with the ends $\mathbf{f}_-$ and $\mathbf{f}_+$ lies in the plane P, the velocity of the motion along the hypersurface is not determined uniquely. Figure 4.5 [142] illustrates the geometrical interpretation of Filippov's solution concept.

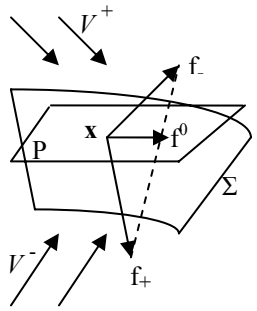

Figure 4.5: Geometrical interpretation of Differential Inclusion [142]

Filippov concluded that the solution of the differential equation (5) with an initial condition $\mathbf{x_0} \in \Sigma$ is locally unique in forward time if

1. $\mathbf{n(x_0)}^T \mathbf{f}_-(t_0, \mathbf{x_0}) \,.\, \mathbf{n(x_0)}^T \mathbf{f}_+(t_0, \mathbf{x_0}) > 0, \quad \forall \mathbf{n(x)} \in \partial h(\mathbf{x})$, i.e. transversal intersection, or

if,

2. $\mathbf{n}(\mathbf{x_0})^T \mathbf{f}_{-}(t_0, \mathbf{x_0}) > 0$ & $\mathbf{n}(\mathbf{x_0})^T \mathbf{f}_{+}(t_0, \mathbf{x_0}) < 0, \quad \forall \mathbf{n}(\mathbf{x}) \in \partial h(\mathbf{x})$, i.e. attractive sliding mode.

It is to be noted that the hypersurface h(**x**) need not be smooth, so, it is necessary to introduce the concept of generalized differential in the aforementioned conditions for defining the normal **n**(**x**) to the hypersurface. For smooth switching boundary, one gets $\partial h(\mathbf{x}) = \nabla h(\mathbf{x})$.

Although, it is quite common to approximate a discontinuous nonlinearity by a smoothing function, the method poses inherent disadvantages. The major disadvantages of introducing a smoothing approximation for the nonlinearity are the loss of possible limit sets and the occurrence of stiff differential equations. However, the smooth-approximation model always guarantees the existence and uniqueness of solutions. The following example illustrates the loss of limit set when a discontinuous nonlinearity is approximated by a smooth function.

Example [143]: Consider the discontinuous system:

$$\begin{aligned} \dot{x}_1 &= x_2 \\ \dot{x}_2 &= a + b\ sign\ (x_2), \quad a \le b \end{aligned} \tag{6}$$

The smoothened system can be represented as:

$$\begin{aligned} \dot{x}_1 &= x_2 \\ \dot{x}_2 &= a + b\,\frac{2}{\pi}\tan^{-1}(\lambda x_2), \quad a \le b, \lambda >> 1 \end{aligned} \tag{7}$$

The smoothened system in equation (7) does not have an equilibrium position for $a \neq 0$. However, the original discontinuous system in equation (6) has a set of equilibria ($x_1 \in R,\ x_2 = 0$). Moreover, the smoothened system is quite stiff because of very steep slope near the origin. So, it is evident that even though the approximation is

mathematically consistent, the true physical characteristics of the system may not be captured by the smoothened system. The subsequent sections discuss other methods to solve the differential inclusion without any loss of the physical characteristics of the system. Nonetheless, the most common engineering practice is to approximate a discontinuous nonlinearity in system by a smooth function.

4.3 Switch Model of Friction

Leine *et al.* [143] developed a numerical technique, i.e. the Switch Model, for integrating differential equations with sliding modes without suffering from stiff differential equations. They introduced an interval of low relative velocity i.e. $|v_{rel}| < \eta$, known as the 'stick band', which approximates the stick mode. The Switch Model introduces a vector field in the stick band such that the state of the system is pushed to the middle of the stick band, thereby avoiding numerical instabilities. Let the switching boundary consist of an attractive sliding mode, a repulsive sliding mode, and transversal intersections from V_- to V_+ and vice-versa. The Switch model constructs a 'band' with a very small thickness 2η around Σ, namely the subspace U (attractive) **U** Q (repulsive) **U** T_- **U** T_+ (transversal), as shown in Figure 4.6 [143] (**U** denotes the union of sets). The subspaces for a smooth switching boundary h(**x**) can be expressed as,

$$\begin{aligned} U &= \{\mathbf{x} \in \Re^{\mathbf{n}} \mid \mathbf{n}^{\mathbf{T}}\mathbf{f}_{+} < 0 \wedge \mathbf{n}^{\mathbf{T}}\mathbf{f}_{-} > 0\} \\ Q &= \{\mathbf{x} \in \Re^{\mathbf{n}} \mid \mathbf{n}^{\mathbf{T}}\mathbf{f}_{+} > 0 \wedge \mathbf{n}^{\mathbf{T}}\mathbf{f}_{-} < 0\} \\ T_{+} &= \{\mathbf{x} \in \Re^{\mathbf{n}} \mid \mathbf{n}^{\mathbf{T}}\mathbf{f}_{+} > 0 \wedge \mathbf{n}^{\mathbf{T}}\mathbf{f}_{-} > 0\} \\ T_{-} &= \{\mathbf{x} \in \Re^{\mathbf{n}} \mid \mathbf{n}^{\mathbf{T}}\mathbf{f}_{+} < 0 \wedge \mathbf{n}^{\mathbf{T}}\mathbf{f}_{-} < 0\} \end{aligned} \tag{8}$$

The symbol, Λ, in (8) denotes the intersection of sets. The subspace U ends when the vector field in V_- or V_+ becomes parallel to Σ. In the subspace U the vector field is chosen such that the solution is pushed to the middle to the band. This is established by setting $\dot{h}(\mathbf{x}) = -\tau_a^{-1} h(\mathbf{x})$, where τ_a is a time constant that determines how fast the solution will be attracted towards the switching boundary $h(\mathbf{x}) = 0$. Since the solution is in the sliding mode region, one also has,

$\dot{\mathbf{x}}(t) = \alpha \mathbf{f}_+ + (1-\alpha)\mathbf{f}_-$.

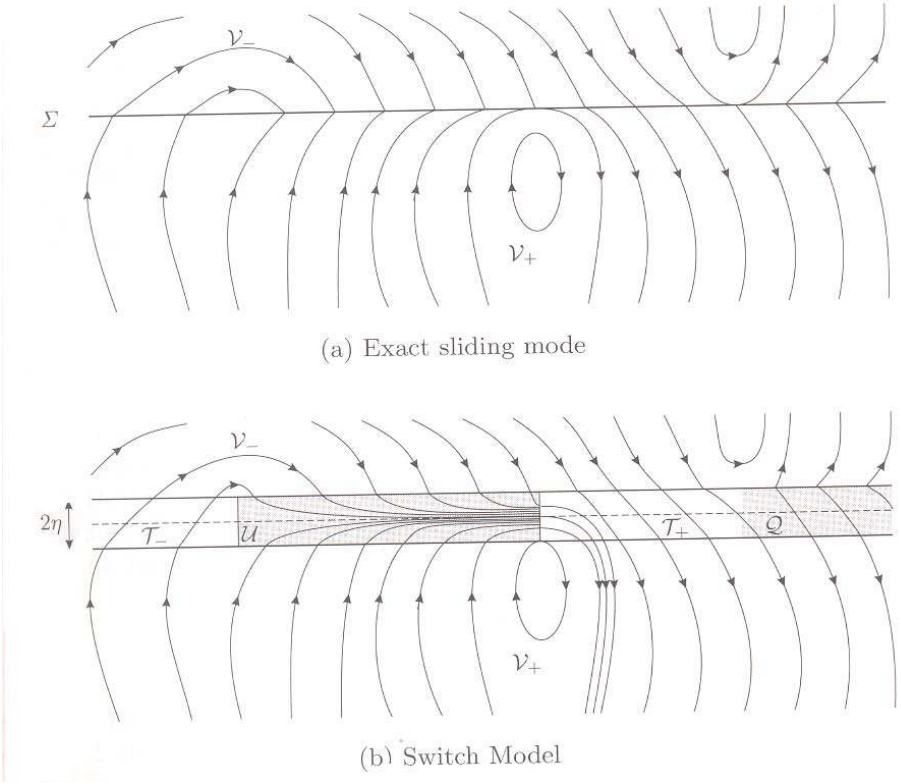

Figure 4.6: Switch Model Approximation [143]

From the aforementioned two equations, one gets

$$\alpha = \frac{\mathbf{n}^T \mathbf{f}_- + \tau_a^{-1} h}{\mathbf{n}^T (\mathbf{f}_- - \mathbf{f}_+)}$$

The vector field in the transition spaces T_- and T_+ is $\mathbf{f}_-$ and $\mathbf{f}_+$. As stated before, for forward time, the solution is unique for attractive and transversal intersection modes. However, the solution exhibits non-uniqueness for a repulsive sliding mode, Q. So, one arbitrarily assigns the vector field in Q to be $\mathbf{f}_+$. Therefore, the pseudo-code for a Switch Model can be written as:

*Calculate h(**x**),* $\mathbf{f}_-(t, \mathbf{x})$, $\mathbf{f}_+(t, \mathbf{x})$

If $|h|>\eta$ *then*

If $h> \eta$ *then*

$$\dot{\mathbf{x}}(t) = \mathbf{f}_+, \quad \mathbf{x}(t) \in V_+$$

else

$$\dot{\mathbf{x}}(t) = \mathbf{f}_-, \quad \mathbf{x}(t) \in V_+$$

end

else

$$\dot{\mathbf{x}}(t) = \mathbf{f}_+, \quad \text{if} \quad \mathbf{x}(t) \in T_+$$

$$\dot{\mathbf{x}}(t) = \mathbf{f}_-, \quad \text{if} \quad \mathbf{x}(t) \in T_-$$

$$\dot{\mathbf{x}}(t) = (1-\alpha)\mathbf{f}_- + \alpha\,\mathbf{f}_+, \quad \& \quad \alpha = \frac{\mathbf{n}^{\mathrm{T}}\mathbf{f}_- + \tau_a^{-1}h}{\mathbf{n}^{\mathrm{T}}(\mathbf{f}_- - \mathbf{f}_+)} \quad \text{if} \quad \mathbf{x}(t) \in U$$

$$\dot{\mathbf{x}}(t) = \mathbf{f}_+, \quad \text{if} \quad \mathbf{x}(t) \in Q$$

end

The Switch Model maintains the continuity of the state vector and yields a set of non-stiff ordinary differential equations. The only disadvantage of such a model is the increasingly complex logical structure with the increasing number of switching boundaries. The Switch Model is therefore practically not feasible for mechanical systems with a large

number of frictional contacts. However, extensive literature has been published [143-147] in the area of finding efficient solutions for multibody systems with a large number of unilateral contacts, for instance, Linear Complementarity Problem (LCP), Non-Linear Complementarity Problem (NLCP), Augmented Lagrangian Method, etc. Although these algorithms are able to aptly capture the transitional dynamics of a multibody system with unilateral contacts, they are quite expensive and unwieldy to use.

4.4 Friction and Chaos

Since some of the friction characteristics vary continuously with respect to velocity (as in the case of Stribeck friction), friction-driven systems may undergo bifurcations [148, 149], where the system makes transitions from one limit set to another, thereby exhibiting different dynamic behavior. A bifurcation point (with respect to μ) is a solution $(\mathbf{x}^*, \mu^*)$ of $\dot{\mathbf{x}} = \mathbf{f}(\mathbf{x}, \mu)$, where the number of equilibria or (quasi-) periodic solutions changes when μ passes μ^*. Both smooth and non-smooth characterization of friction-based systems are capable of exhibiting bifurcations, however, the dynamics become richer and more complex in the non-smooth case. A friction-driven system is also capable of undergoing self-excited vibrations and chaotic behavior. Extensive work [150-153] has been done on formulating and understanding chaotic behavior of 1- and 2- degree of freedom systems subjected to friction constraints and periodic forcing functions. Chaos and routes to chaos have been commonly identified in systems which exhibit bifurcations. For a system to be classified as chaotic, the phase-space of the system must be 3-dimensional or higher and must have the following properties [154]:

- Sensitive dependence on initial conditions
- Topologically mixing
- Periodic orbits must be dense

Sensitivity to initial conditions implies that two points in such a system may move along vastly different trajectories in their phase space, even if the difference in their initial configurations is very small, as depicted in Figure 4.7. As a result of this sensitivity, the behavior of systems that exhibit chaos appears to be random, even though the model of the system is deterministic.

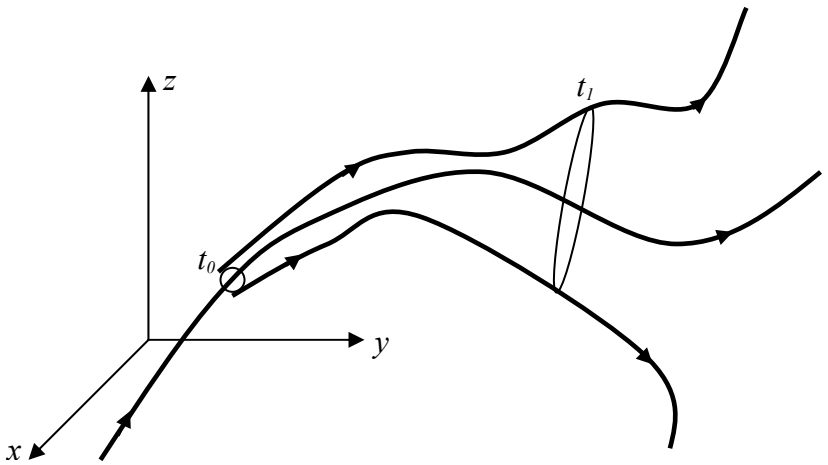

Figure 4.7: Chaos – Divergence of Orbits from Sensitivity to Initial Conditions

A system is *topologically mixing* if it evolves over time so that any given region or open set of its phase space eventually overlaps with any other given region. Since the phase space is of a finite size, this usually means that the phase space will become thoroughly mixed together after a fairly short time. A subset A of a topological space X is called *dense* (in X) if, intuitively, any point in X can be "well-approximated" by points in A. Formally, A is *dense* in X if for any point x in X, any neighborhood of x contains at least a point from A. Although extensive literature is available on simple chaotic systems with 1- or 2- degrees of freedom, literature on chaotic phenomena in multibody systems is scarce.

Although the exact representation of stick-slip dynamics is based on the theory of differential inclusions, it is quite common to use smooth functions to approximate the friction behavior. The smoothened systems introduce stiff differential equations, and may also exhibit some drifting behavior (due to the loss of possible limit sets), yet they play a significant role in understanding the stick-slip dynamics of a friction-based system. Moreover, bifurcation studies, Poincaré sections, Lyapunov exponents, cell-mapping methods, chaotic analysis, etc., may be readily done by incorporating the tools widely used for analyzing the nonlinear dynamics of smooth mechanical systems. In essence, models of physical reality are smooth or non-smooth depending on the abstraction level one chooses to describe a particular system. The subsequently discussed example of a 2-degree of freedom (DOF) stick-slip oscillator highlights the influence of different friction characteristics on the dynamics of the system.

4.5 2-DOF Stick-Slip Oscillator

Consider two masses lying on a moving belt and connected to each other by means of spring and dampers. The belt moves with constant velocity and the friction characteristic between the masses and the belt is described by two different mathematical models. Figure 4.8 depicts the configuration of the concerned oscillator. Both the masses move along the coordinates x_1, x_2 due to the friction forces F_1, F_2 existing between them and the belt that moves with a constant velocity v. The masses are connected to each other and to fixed supports by means of springs and dampers of stiffnesses k_1, k_2 and damping coefficients c_1, c_2 respectively.

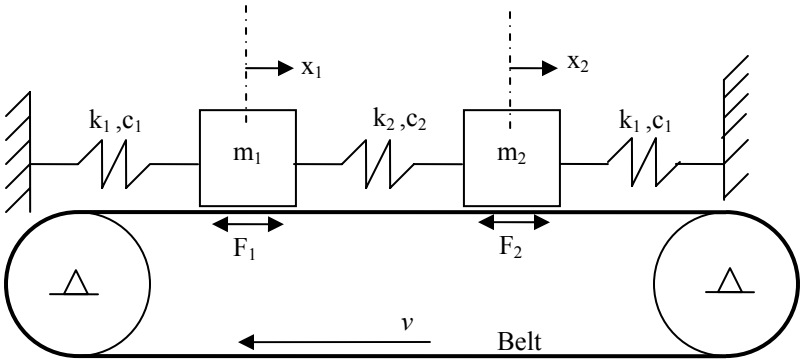

Figure 4.8: 2-DOF Stick-Slip Oscillator

The equations of motion of the system can be written in matrix form, as:

$$\begin{bmatrix} m_1 & 0 \\ 0 & m_2 \end{bmatrix}\begin{Bmatrix} \ddot{x}_1 \\ \ddot{x}_2 \end{Bmatrix}+\begin{bmatrix} c_1+c_2 & -c_2 \\ -c_2 & c_1+c_2 \end{bmatrix}\begin{Bmatrix} \dot{x}_1 \\ \dot{x}_2 \end{Bmatrix}+\begin{bmatrix} k_1+k_2 & -k_2 \\ -k_2 & k_1+k_2 \end{bmatrix}\begin{Bmatrix} x_1 \\ x_2 \end{Bmatrix}=\begin{Bmatrix} F_1 \\ F_2 \end{Bmatrix}$$
$$\begin{Bmatrix} F_1 \\ F_2 \end{Bmatrix}=\begin{Bmatrix} -\mu m_1 g \operatorname{sgn}|\dot{x}_1 - v| \\ -\mu m_2 g \operatorname{sgn}|\dot{x}_2 - v| \end{Bmatrix} \quad (9)$$

The above equation is of the form of $\mathbf{M}\ddot{\mathbf{x}}+\mathbf{C}\dot{\mathbf{x}}+\mathbf{K}\mathbf{x}=\mathbf{F}$, and can be readily represented in the state-space form as:

$$\dot{\mathbf{q}}=\mathbf{A}\,\mathbf{q}+\mathbf{B},$$

where, (10)

$$\mathbf{q}:=[q_1,q_2,q_3,q_4]^T=[x_1,x_2,\dot{x}_1,\dot{x}_2]^T,\ \mathbf{A}=\begin{bmatrix} \mathbf{0} & \mathbf{I} \\ -\mathbf{M}^{-1}\mathbf{K} & -\mathbf{M}^{-1}\mathbf{C} \end{bmatrix},\ \mathbf{B}=[\mathbf{0}\ \mathbf{M}^{-1}]^T\mathbf{F}$$

It is evident from (10) that a 2-DOF stick-slip oscillator has a 4-dimensional phase-space representation and also possesses a discontinuous right-hand side (i.e. the forcing vector). Hence, the oscillator represented by (10) falls under the category of non-smooth mechanical systems, in particular Filippov systems. The non-smooth system (10) has two switching boundaries i.e. $\dot{x}_1=v, \dot{x}_2=v$. This non-smooth system can be approximated by introducing smoothening functions, as mentioned in equation (2). The smooth approximation of the stick-slip oscillator dynamics is given by:

$$\begin{bmatrix} m_1 & 0 \\ 0 & m_2 \end{bmatrix}\begin{Bmatrix} \ddot{x}_1 \\ \ddot{x}_2 \end{Bmatrix}+\begin{bmatrix} c_1+c_2 & -c_2 \\ -c_2 & c_1+c_2 \end{bmatrix}\begin{Bmatrix} \dot{x}_1 \\ \dot{x}_2 \end{Bmatrix}+\begin{bmatrix} k_1+k_2 & -k_2 \\ -k_2 & k_1+k_2 \end{bmatrix}\begin{Bmatrix} x_1 \\ x_2 \end{Bmatrix}= \begin{Bmatrix} -2\mu m_1 g \tan^{-1}\left(\lambda(\dot{x}_1-v)\right)/\pi \\ -2\mu m_2 g \tan^{-1}\left(\lambda(\dot{x}_2-v)\right)/\pi \end{Bmatrix} \tag{11}$$

Using Laplace transform on equation (9), a transfer function matrix can be obtained that relates the outputs (x_1, x_2) to the inputs (friction force). Let u_1 and u_2 be the inputs that represent the friction force between the belt and the masses m_1 and m_2 respectively. Assume for simplicity that $m_1 = m_2 = m$. So, the transfer function matrix, **G**(**s**), for the system is given by the following relationship,

$$\left.\begin{aligned} &\begin{Bmatrix} X_1(s) \\ X_2(s) \end{Bmatrix} = \mathbf{G(s)}\begin{Bmatrix} U_1(s) \\ U_2(s) \end{Bmatrix}, \quad \text{where} \\ &\mathbf{G(s)} = \begin{bmatrix} \mathrm{G}_{11}(s) & \mathrm{G}_{12}(s) \\ \mathrm{G}_{21}(s) & \mathrm{G}_{22}(s) \end{bmatrix} \\ &\mathrm{G}_{11}(s) = \mathrm{G}_{22}(s) = \frac{ms^2+(c_1+c_2)s+(k_1+k_2)}{(ms^2+(c_1+c_2)s+(k_1+k_2))^2-(c_2s+k_2)^2} \\ &\mathrm{G}_{12}(s) = \mathrm{G}_{21}(s) = \frac{c_2s+k_2}{(ms^2+(c_1+c_2)s+(k_1+k_2))^2-(c_2s+k_2)^2} \end{aligned}\right\} \tag{12}$$

Since the inputs are friction forces, which are nonlinear and discontinuous, the stability analysis of this stick-slip oscillator is not trivial. However, preliminary investigation on the stability analysis can be done using the Theory of Describing Functions [155]. Friction forces are described by signum functions, which act as relays. The describing function for an ideal relay that describes the friction forces in (9) can be written as:

$$N(j\omega, A) = \frac{4\mu mg}{\pi A}\angle 0^0, \quad A = amplitude$$

Stability analysis of a nonlinear system is based on the possible intersections of the transfer function $G(j\omega)$ and the describing function $-1/N$ [155]. Figure 4.9 illustrates the

Nyquist plot for the individual components of the transfer matrix **G**($j\omega$), and also the polar plot for the function -1/N.

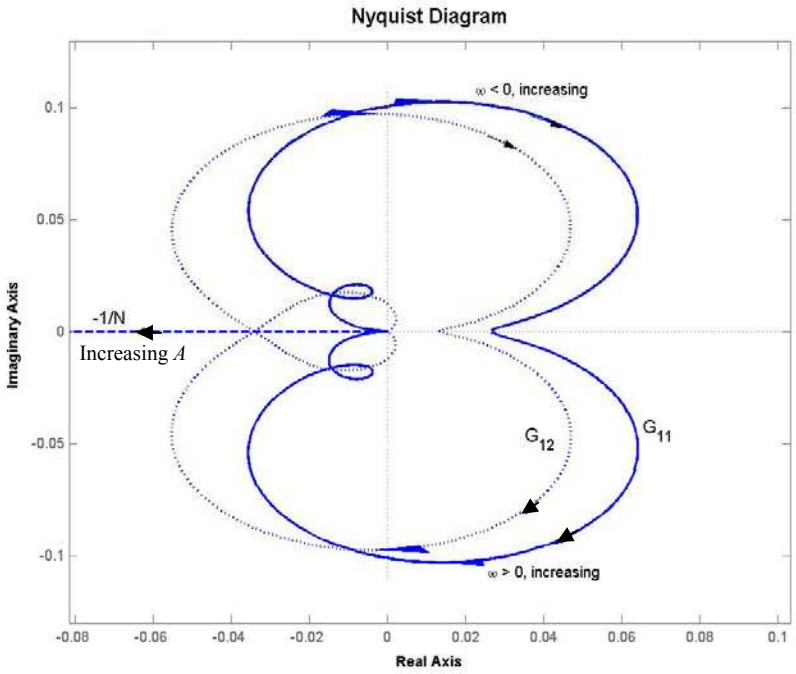

Figure 4.9: Nyquist plot of **G**($j\omega$) and -1/N

It can be noted from the figure that although the transfer function $G_{11}(j\omega)$ does not intersect with the function $-N^{-1}$, the cross-transfer function $G_{12}(j\omega)$ intersects with it. Since the given stick-slip oscillator is a double input-double output system, the stability of the system from this Nyquist plot analysis is not much discernible (contrary to the case of a single input-single output system). Hence, further investigations are inevitably made to analyze the stability of this nonlinear stick-slip oscillator.

Further, preliminary analysis of the phase portrait and trajectory behavior can be done by calculating the divergence of the vector field (i.e. **Aq**+**B**) in (10). The divergence of this vector field is given as,

$$\nabla \bullet (\mathbf{Aq} + \mathbf{B}) = \nabla \bullet \dot{\mathbf{q}} = -\frac{(c_1 + c_2)(m_1 + m_2)}{m_1 m_2} - Y$$

$$Y = \frac{2m_1 \lambda g \mu}{\pi(1 + \lambda^2 (q_3 - v)^2)} + \frac{2m_2 \lambda g \mu}{\pi(1 + \lambda^2 (q_4 - v)^2)} + \frac{2m_1 g}{\pi} \tan^{-1}(\lambda(q_3 - v)) \frac{\partial \mu}{\partial q_3} \quad (13)$$

$$+ \frac{2m_2 g}{\pi} \tan^{-1}(\lambda(q_4 - v)) \frac{\partial \mu}{\partial q_4}$$

The divergence of the vector field essentially represents the compressibility of the phase volume. It is evident from (13) that for constant coefficient of friction, as in Coulomb-Amontons law, the phase volume decreases with time (as the divergence is always negative). This implies that the system is dissipative and the system would, most probably, reach a stable fixed point. However, it can again be noted from equation (13) that the compressibility of phase a volume can also vary depending on the gradient of friction characteristic (as in the case of Stribeck friction). Consequently, this allows the system to exhibit periodic or chaotic behavior.

The smoothened oscillator system (11) is examined for different nonlinear phenomena under the influence of two different friction characteristics: (a) constant coefficient of friction (i.e. the classical Coulomb-Amontons friction model, $\mu = \mu_0$), (b) Stribeck friction model i.e. $\mu = \mu_0 \left(1 - e^{-b|\mathrm{v_{rel}}|}\right)\left(1 + (f_r - 1)e^{-a|\mathrm{v_{rel}}|}\right)$.

The simulation is run for a number of initial conditions i.e. ($\mathbf{x_0}, \dot{\mathbf{x}}_\mathbf{0}$) and the following parameters, (k_1, k_2) = 25; (c_1, c_2) = 1; (m_1, m_2) = 1; v = 3.5; $\mu_0 = 0.25, f_r = 6.5, \lambda = 10^4$; a = 1; b = 5; g = 9.81.

Case 1: $\mu = \mu_0$

The equilibrium point of the smoothened system is obtained by setting the time derivatives of the states in (11) to zero. The equilibrium point for the system defined by

the abovementioned parameters is given by (x_1^*, x_2^*) = (0.098, 0.098). Linearizing (11) about this equilibrium point yields,

$$\begin{bmatrix} m_1 & 0 \\ 0 & m_2 \end{bmatrix}\begin{Bmatrix} \ddot{\hat{x}}_1 \\ \ddot{\hat{x}}_2 \end{Bmatrix}+\begin{bmatrix} c_1+c_2 & -c_2 \\ -c_2 & c_1+c_2 \end{bmatrix}\begin{Bmatrix} \dot{\hat{x}}_1 \\ \dot{\hat{x}}_2 \end{Bmatrix}+\begin{bmatrix} k_1+k_2 & -k_2 \\ -k_2 & k_1+k_2 \end{bmatrix}\begin{Bmatrix} \hat{x}_1 \\ \hat{x}_2 \end{Bmatrix}= \begin{Bmatrix} -2\mu_0 m_1 g \lambda \dot{\hat{x}}_1/(\pi(1+\lambda^2 v^2)) \\ -2\mu_0 m_2 g \lambda \dot{\hat{x}}_2/(\pi(1+\lambda^2 v^2)) \end{Bmatrix} \tag{14}$$

It is to be noted that (14) describes the dynamics of the system perturbed around the equilibrium point. So, $(\hat{x}_1, \hat{x}_2)$ are the perturbed system variables. Equation (14) can be further simplified as,

$$\begin{bmatrix} m_1 & 0 \\ 0 & m_2 \end{bmatrix}\begin{Bmatrix} \ddot{\hat{x}}_1 \\ \ddot{\hat{x}}_2 \end{Bmatrix}+\begin{bmatrix} k_1+k_2 & -k_2 \\ -k_2 & k_1+k_2 \end{bmatrix}\begin{Bmatrix} \hat{x}_1 \\ \hat{x}_2 \end{Bmatrix}+\begin{bmatrix} c_{11} & -c_2 \\ -c_2 & c_{22} \end{bmatrix}\begin{Bmatrix} \dot{\hat{x}}_1 \\ \dot{\hat{x}}_2 \end{Bmatrix}=\begin{Bmatrix} 0 \\ 0 \end{Bmatrix}$$
$$c_{11}=c_1+c_2+(2\mu_0 m_1 g \lambda/(\pi(1+\lambda^2 v^2))) \tag{15}$$
$$c_{22}=c_1+c_2+(2\mu_0 m_2 g \lambda/(\pi(1+\lambda^2 v^2)))$$

It is evident from (15) that the eigenvalues of the system matrix **A** (defined in equation (10)) depend on a number of system parameters, especially, the set P : = [*k, c,* μ_0*, v,* λ]. The parameters in the set P are varied one at a time and the eigenvalues of the linearized system are calculated. It is observed that while varying *c* from 1 to 50 and keeping other parameters constant, the eigenvalues of the linearized system split up at two critical values of *c* i.e. 5.77 and 10. For $c \geq 10$, both the masses exhibit overdamped motion and the 4 eigenvalues are found to be in the left-hand plane on the real axis. So, the system is stable and is attracted towards the equilibrium point. For $c \leq 5.77$, both the masses exhibit underdamped motion, whereas, for $c \in (5.77, 10)$, the motion of one of the mass is overdamped whereas the other shows underdamped behavior. The system remains structurally stable at all times for the variation in the damping coefficient *c*. Similarly, the

system remains structurally stable for $\mu_0 \in (0, 0.75]$, $v \in [-10, 10] \subseteq \Re$, and $k > 0$. However, it is important to note that the parameter-space defined by the set P is a 5-dimensional space (a variation in *c* could be simultaneously accompanied by variations in *v*, *k*, etc.). So, it is difficult to conclude that the linearized system is globally structurally stable unless stability analyses are done for each and every point of the 5-dimensional parameter-space. Figure 4.10 illustrates the dynamics of a system expressed by equation (11) for the parameter set P (P: = [*k, c,* μ_0*, v,* λ] = [25, 1, 0.25, 3.5, 10^4]) and different sets of initial conditions.

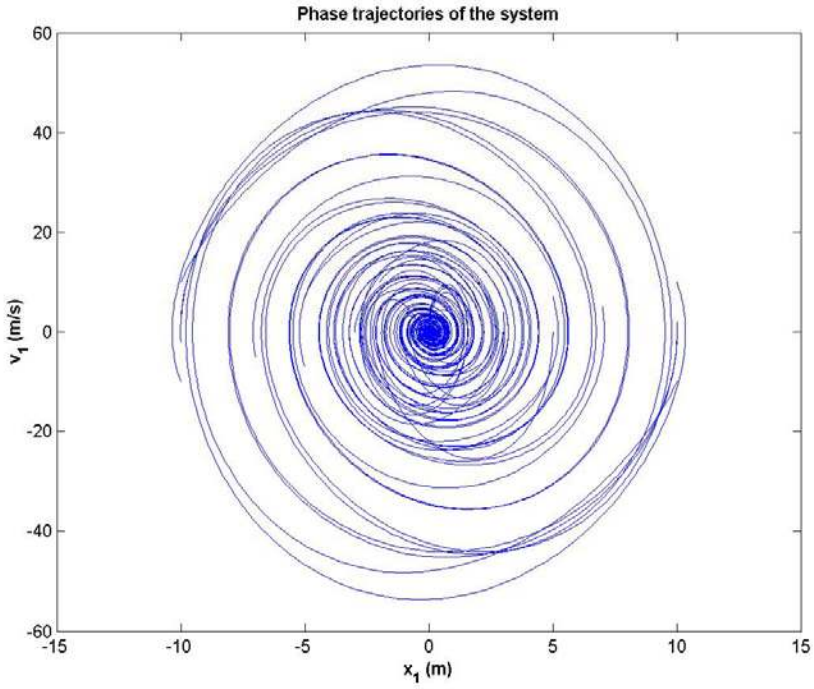

(a) Phase portrait for mass m_1

Figure 4.10: Dynamic indicators for Case 1

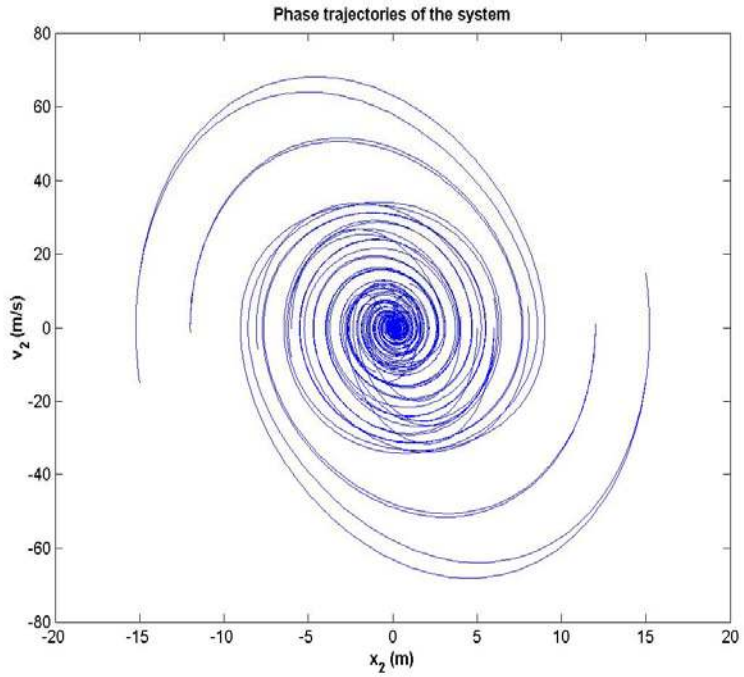

(b) Phase portrait for mass m_2

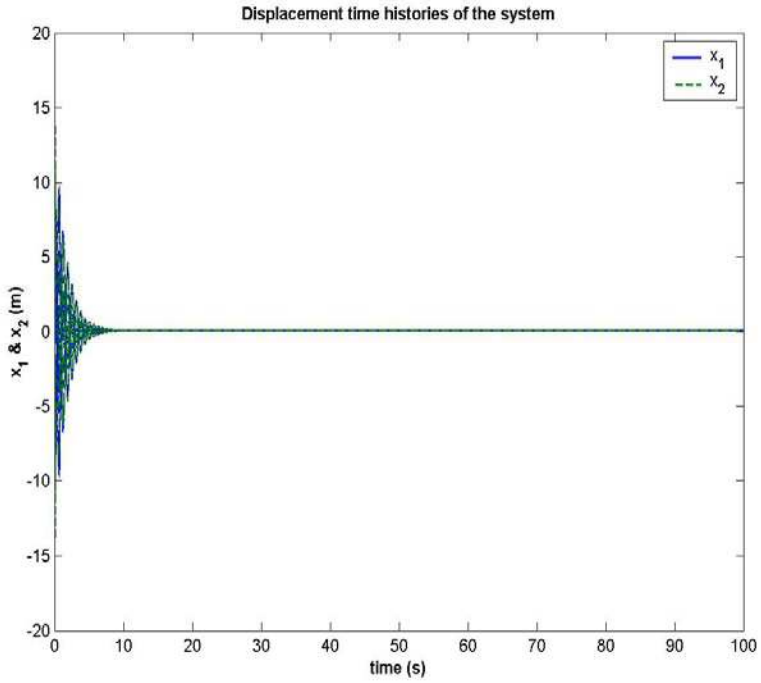

(b) Displacement profiles (x_1, x_2) for various initial conditions

Figure 4.10: Dynamic indicators for Case 1 (contd.)

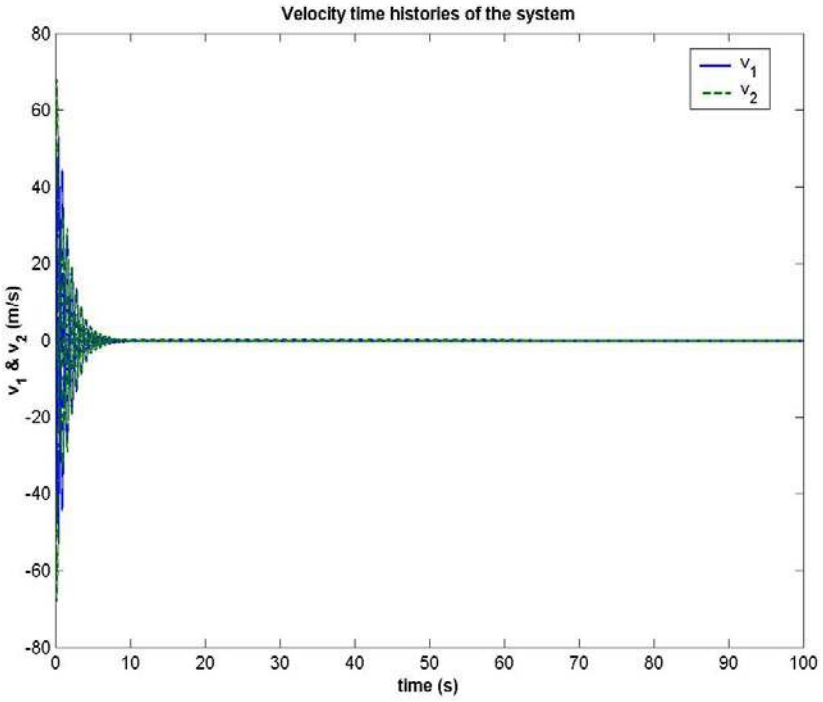

(c) Velocity profiles (v_1, v_2) for various initial conditions

Figure 4.10: Dynamic indicators for Case 1 (contd.)

It is evident from the phase trajectories and the time histories of the system that the equilibrium point i.e. (x_1^*, x_2^*) = (0.098, 0.098) is a stable attractor. No matter whatsoever initial conditions the system is exposed to, the system is always driven towards to the equilibrium point. It can also be noted that the phase trajectories of the system intersect each other for some of the initial conditions. However, these intersections may not necessarily be homoclinic or heteroclinic intersections as the phase-space of the concerned system is multidimensional. The phase portrait in Figure 4.10 is the projection of the time-evolution parameters of the system onto a two-dimensional surface; hence, the intersections in the two-dimensional portrait may represent folding or unfolding of the trajectory in a multi-dimensional space. Moreover, since (11) has 4-dimensional phase-space representation, it is likely that the system undergoes chaotic behavior. Hence, it is

necessary to conduct further analyses on the system to determine whether the system behaves chaotically or not.

A large number of tools have been developed to identify chaotic behavior in dynamical systems [154, 156]. Among such tools, Lyapunov-exponent analysis is one of the most powerful diagnostic for chaotic systems, especially in higher dimensions. However, other commonly used nonlinear tools like power spectral density plots, Poincaré maps, bifurcation diagrams, etc. also give valuable insight into understanding the chaotic behavior of a system. Chaos in a deterministic system, as discussed earlier, implies a sensitive dependence on initial conditions. This means that if two trajectories start close to one another in phase space, they will move exponentially away from each other for small times on the average (refer to Figure 4.7). This sensitivity to initial conditions can be quantified as,

$$| \delta x(t) | \approx e^{\bar{\lambda} t} \, | \delta x(0) |$$

where $\bar{\lambda}$ is called the Lyapunov exponent. So, Lyapunov exponents are related to the exponentially fast divergence and convergence of nearby orbits in phase space. A system with one or more positive exponents is defined to be chaotic. Lyapunov exponents can thus also be considered as analogues to the eigenvalues of a linear system since both of them govern the system stability to a large extent. However, the trajectories of chaotic motion do not escape to infinity, but preserve a recurrence property. Extensive research has been done on developing algorithms for computing the Lyapunov exponents of a dynamical system. Wolf *et al.* [157] developed an efficient algorithm for computing Lyapunov exponents of an *N*- dimensional continuous dynamical system. Müller [158] developed a generalized algorithm for computing the spectrum of Lyapunov exponents of

a nonlinear system with discontinuities. For a 4- dimensional system, the attractor can only be non-chaotic if none of the Lyapunov exponents are positive. Figure 4.11 depicts the growth of Lyapunov exponents with time for the smoothened system (11) with classical Coulomb friction model.

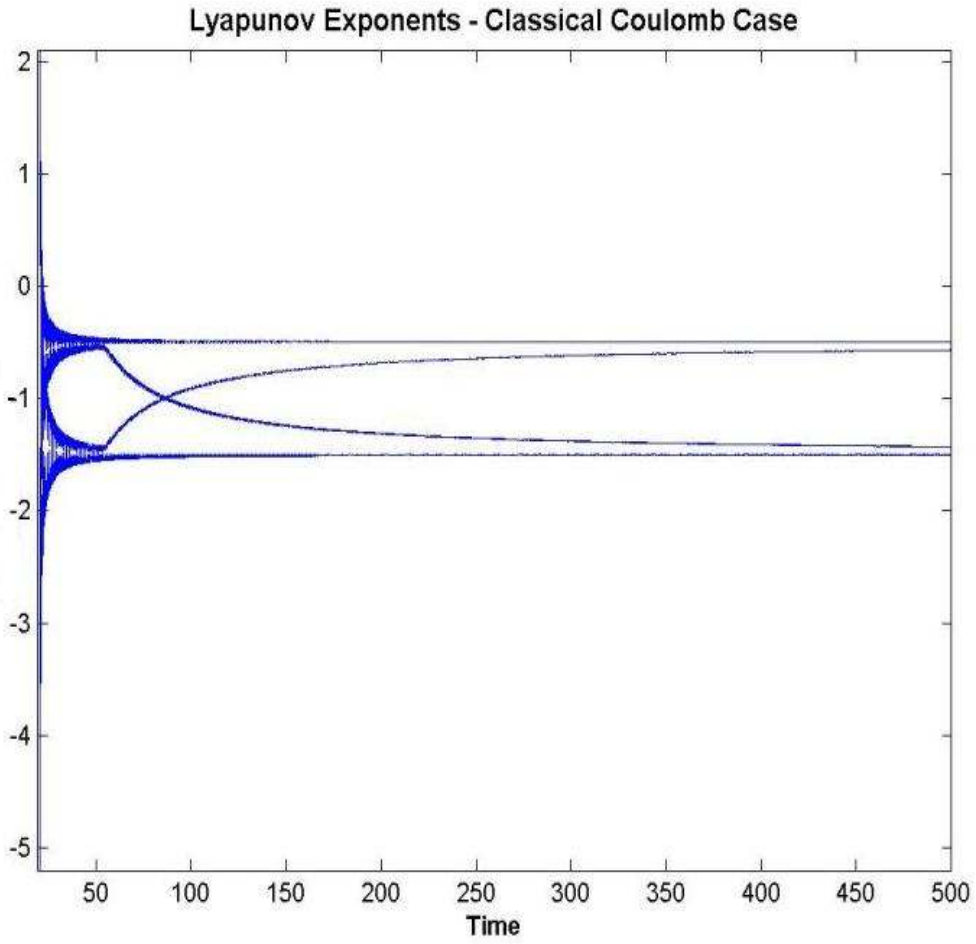

Figure 4.11: Lyapunov Exponent Spectrum for Case 1

For a number of initial conditions close to the basin of attraction, the following Lyapunov exponents were obtained: (-0.49791 -0.56974 -1.4286 -1.5038). Since all the Lyapunov exponents are negative, the equilibrium point of the system is asymptotically stable, and all the trajectories are attracted towards it.

Case 2: $\mu = \mu_0 \left(1 - e^{-b|v_{rel}|}\right)\left(1 + (f_r - 1)e^{-a|v_{rel}|}\right)$

The friction characteristic, unlike the previous case, varies continuously with the relative velocity between the masses and the belt. Moreover, the difference between static and kinetic friction is also taken into account in this model through the parameter f_r. In addition to describing kinetic-friction dynamics, this friction model captures not only the effects due to stiction, but also those due to boundary lubrication (Stribeck-like effects). The equilibrium point of the smoothened system is obtained by setting the time derivatives of the states in (11) to zero. The equilibrium point for the system defined by the aforementioned parameters is given by (x_1^*, x_2^*) = (0.114, 0.114). Figure 4.12 illustrates the dynamics of a system with Stribeck-like friction model for different sets of initial conditions.

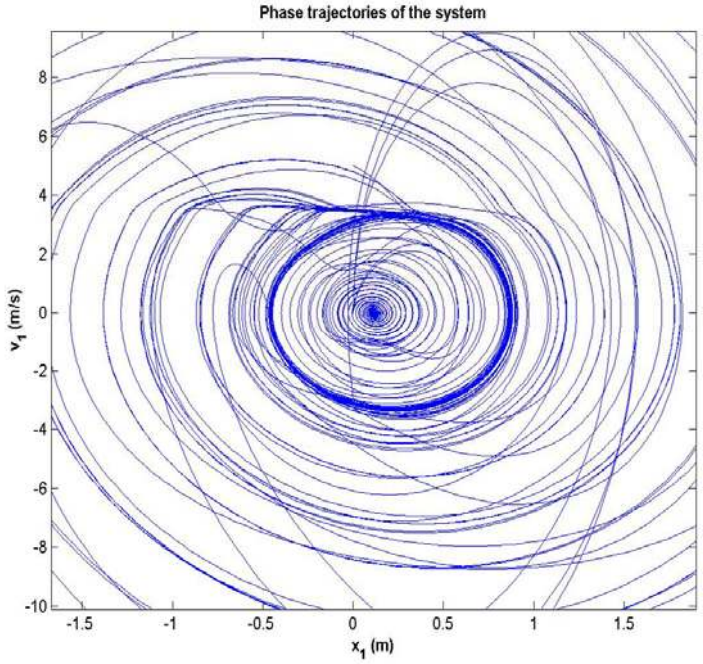

(a) Phase portrait for mass m_1

Figure 4.12: Dynamic indicators for Case 2

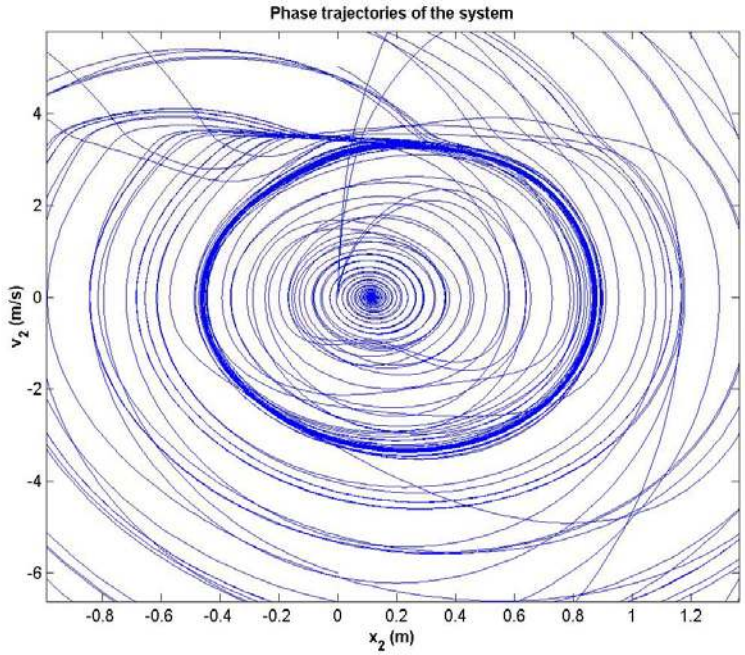

(b) Phase portrait for mass m_2

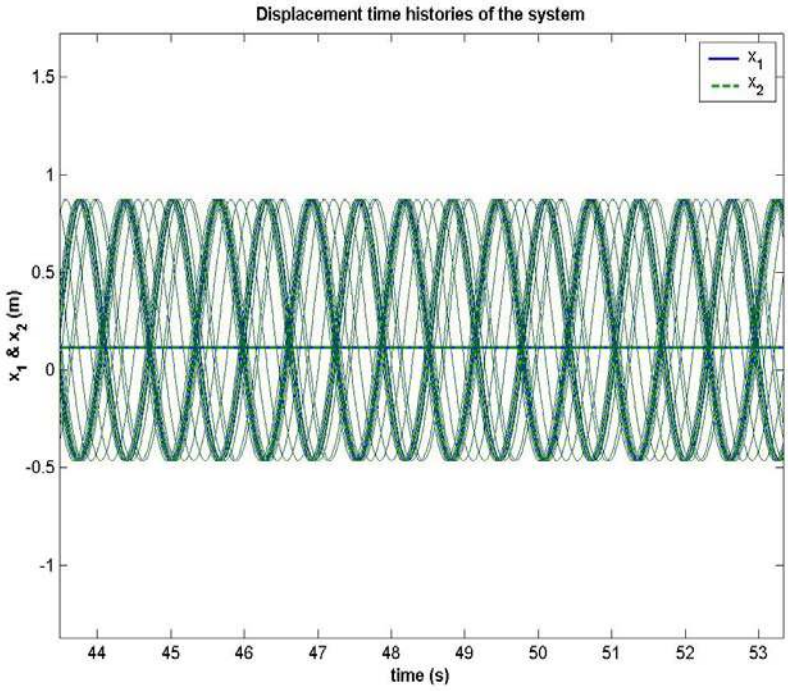

(c) Displacement profiles (x_1, x_2) for various initial conditions

Figure 4.12: Dynamic indicators for Case 2 (contd.)

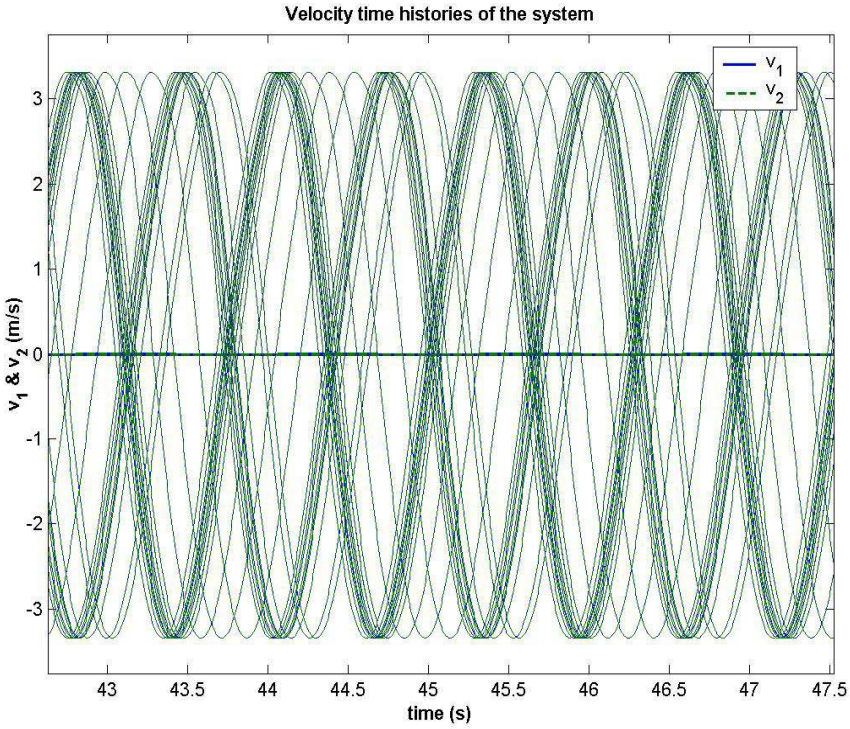

(d) Velocity profiles (v_1, v_2) for various initial conditions

Figure 4.12: Dynamic indicators for Case 2 (contd.)

Linearizing the smoothened system about the equilibrium point (x_1^*, x_2^*) yields the following system of equations:

$$
\begin{bmatrix} m_1 & 0 \\ 0 & m_2 \end{bmatrix}\begin{Bmatrix} \ddot{\hat{x}}_1 \\ \ddot{\hat{x}}_2 \end{Bmatrix}+\begin{bmatrix} k_1+k_2 & -k_2 \\ -k_2 & k_1+k_2 \end{bmatrix}\begin{Bmatrix} \hat{x}_1 \\ \hat{x}_2 \end{Bmatrix}+\begin{bmatrix} c_1+c_2+m_1 p & -c_2 \\ -c_2 & c_1+c_2+m_2 p \end{bmatrix}\begin{Bmatrix} \dot{\hat{x}}_1 \\ \dot{\hat{x}}_2 \end{Bmatrix}=\begin{Bmatrix} 0 \\ 0 \end{Bmatrix}
$$

$$
p = 2\mu_0 g(p_1+p_2+p_3)/\pi
$$

$$
p_1 = \left(1-e^{-b|v|}\right)\left(1+(f_r-1)e^{-a|v|}\right)\lambda/(1+\lambda^2 v^2)
$$

$$
p_2 = \frac{2b\left(1+(f_r-1)e^{-a|v|}\right)\tan^{-1}(-\lambda v)}{\pi}e^{-b|v|}\left(\tan^{-1}(-\lambda v)-\frac{\lambda v}{1+\lambda^2 v^2}\right) \qquad (16)
$$

$$
p_3 = -\frac{2a(f_r-1)e^{-a|v|}\tan^{-1}(-\lambda v)}{\pi}\left(\tan^{-1}(-\lambda v)-\frac{\lambda v}{1+\lambda^2 v^2}\right)\left(1-e^{-b|v|}\right)
$$

The parameter set P: = [k, c, μ_0, v, λ, f_r, a, b] on which the eigenvalues of the linearized system depend belongs to an 8- dimensional space. Similar to Case 1, the parameters in

the set P are varied one at a time and the eigenvalues of the linearized system are calculated. It is observed that while varying v from -10 to 10 and keeping other parameters constant, the eigenvalues of the linearized system exhibit transitions, as depicted in Figure 4.13, from the left-hand plane to the right-hand plane for certain values of v. This implies that there is a range of values of the belt velocity $v \in [0.81, 2.6]$ for which the system becomes structurally unstable, which was not observed when the friction characteristic was treated in the classical Coulomb sense. Such phenomenon is known as *bifurcation behavior* as the qualitative behavior of the system (or its fixed points) changes as one of the system parameters is varied. Moreover, within the stable region, the system is capable of exhibiting different dynamic behavior depending on the value of v. For instance, both the masses exhibit overdamped motion for $v \in [-0.26, 0.26]$. It can also be noted from Figure 4.13 that the fixed points of the system, for some values of v, can be stable or unstable focus, thereby causing the system to undergo damped-periodic or self-excited motion respectively. The system remains structurally stable for $c > 0$ and $k > 0$. However, it exhibits bifurcation behavior as $\mu_0 \in (0, 0.75]$. Figure 4.13 also depicts the path of the eigenvalues of the linearized system when the coefficient of friction μ_0 is varied. The system becomes structurally unstable, i.e. the eigenvalues cross the left-hand plane, when $\mu_0 \in [0.62, 0.75]$. As mentioned before, it is difficult to assess the structural stability of the system globally as the parameter space is 8- dimensional (a variation in one of the parameters could be simultaneously accompanied by variations in the others.). For instance, the same system is structurally stable for $v = 3.5$ when $\mu_0 = 0.25$, but is unstable for $v = 3.5$ when $\mu_0 = 0.62$.

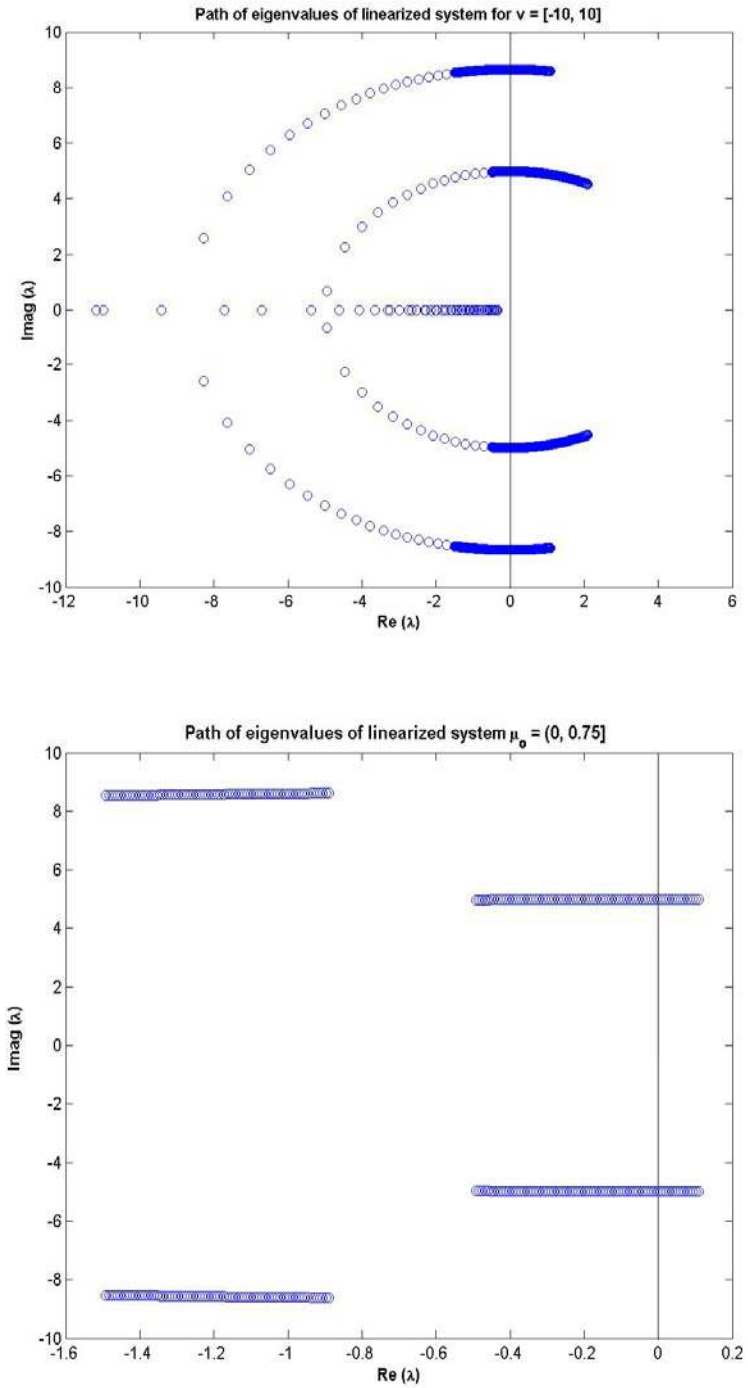

Figure 4.13: Path of eigenvalues of the linearized system – Case 2

It can also be observed from the phase portrait and the time histories of the system that there is a set of initial conditions for which the system exhibits limit cycle behavior and another set for which the trajectories are driven towards the equilibrium point. This is

further corroborated by conducting a Lyapunov exponent analysis for some initial conditions in the basin of attraction.

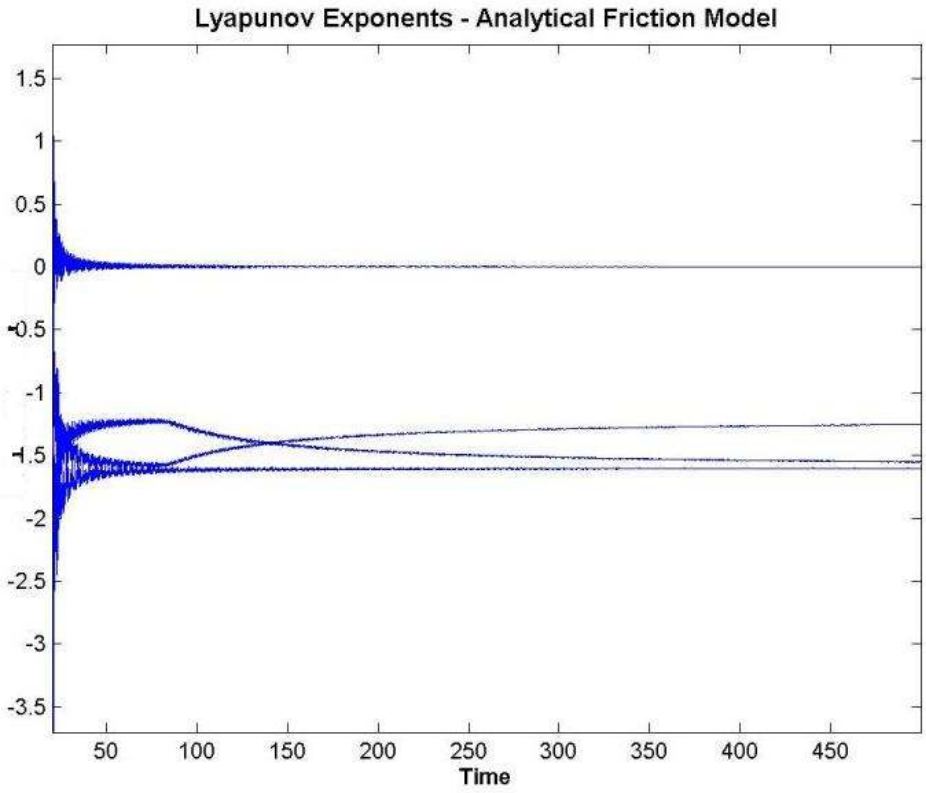

Figure 4.14: Lyapunov Exponent Spectrum for Case 2

The Lyapunov spectrum is plotted, as shown in Figure 4.14, for one such set of initial condition that drives the system towards the limit cycle behavior. For a 4- dimensional system to exhibit limit cycle behavior, one of the Lyapunov exponents must be zero. The Lyapunov exponents for the system with initial conditions: $[x_1^0, v_1^0, x_2^0, v_2^0] = [0\ 3\ 0\ 6]$ are found to be: (0.001187 -1.2535 -1.5535 -1.6016). Moreover, for another set of initial condition, such as $[x_1^0, v_1^0, x_2^0, v_2^0] = [0\ 0\ 0\ 0]$, all of the Lyapunov exponents are negative, consequently, the system is driven towards the fixed point. It can be noted that the system subjected to the aforementioned initial conditions (i.e. $[x_1^0, v_1^0, x_2^0, v_2^0] = [0\ 3\ 0\ 6]$), in fact, exhibits mild chaotic behavior instead of a regular periodic motion, as the first Lyapunov

exponent is slightly greater than zero. So, the Lyapunov exponent analysis highlights that the apparent limit-cycle behavior of system in case 2 is, in fact, not a regular periodic motion, as illustrated by Figure 4.12 (c) and (d), but it is a mild chaotic behavior. It is clear from this analysis that for a higher dimensional phase-space, time-histories and phase-portraits of a system are not the sole factors for analyzing its stability. It is, thus, necessary to incorporate other tools from nonlinear and chaotic analysis to characterize a system's stability.

4.6 Closure

Dry friction is an inevitable nonlinear phenomenon present in most mechanical systems. It is crucial to study the implications of different friction characteristics on the dynamics of a system. The friction phenomenon in most of the systems can be adequately described by Coulomb's law, which is inherently discontinuous in nature. It is a common engineering practice to introduce a smoothening function to represent the set-valued Coulomb friction law. However, certain friction-related phenomena like chaos, limit-cycles, hysteresis, etc., are neither easy to detect nor easy to explain on the basis of Coulomb friction theory. Since it is difficult to monitor friction experimentally during the running conditions of a complex nonlinear system, the mathematical models of friction give insight into the different dynamic maneuvers that a system can undergo. Moreover, it has been well-documented in literature [159-161] that friction-based systems undergo not only self-excited vibrations, but also chaotic vibrations, which might be perilous to the system. Moreover, since friction can initiate chaos in a system, a controller based on

the basic principles of nonlinear control may not be able to get rid of the chaotic behavior. A simple 2- DOF stick-slip oscillator shows a mild chaotic behavior which would not have been detected had the friction not been modeled with a negative slope with respect to the relative velocity between the contacting surfaces. The stick-slip oscillator system, discussed in this chapter, rudimentarily simulates the possible dynamic interactions in a CVT system as the belt/chain traverses either of the two pulleys.

CHAPTER 5

RESULTS AND DISCUSSION

5.1 Introduction

The previous chapters outlined the development of mathematical models for two different types of continuously variable transmissions (CVT): metal V-belt- type and chain- type. A detailed transient-dynamic model of a metal pushing V-belt CVT was developed taking the inertial effects and pulley flexibility into account. A model of chain CVT was also developed using multibody formalisms. Moreover, as discussed in the previous chapter, it is incumbent on the designer or the engineer to study the influence of different friction characteristics on the dynamic performance of a CVT. The response of a CVT also changes considerably under the influence of certain nonlinearities, which may be inherent or may arise during its continual operation (e.g. clearance effects). So, the CVT-models were further modified in order to encompass the nonlinear effects induced by friction, pulley flexibility, and clearance.

The belt-CVT model was developed on the MATLAB / SIMULINK platform, whereas the chain-CVT model was developed on the Visual C++ platform. It was preferable to develop chain-CVT model in the Visual C++ platform because of the discrete multibody nature of chain CVT, which could be readily implemented using object-oriented programming approach. The Runge-Kutta method is used to integrate the state equations in order to get the time histories of the system states. The computer programs used for simulating the dynamics of these CVTs are outlined in the

Appendices. The results pertaining to these models will be discussed subsequently. The results provide valuable insight into the dynamics of a CVT subjected to different loading conditions (i.e. axial forces and torques). The models can also be readily exploited to observe the influence of different configuration parameters on the performance of the system.

5.2 Results from Chain CVT Model

The simulation of a chain-CVT model starts off with an initial condition and a specific design configuration and computes different dynamic performance indices i.e. axial forces, angular velocities, tension, etc. Moreover, the driver pulley is subjected to a high input torque (200 Nm) whereas a low resisting load torque (100 Nm) is applied to the driven pulley. The assumptions and the modeling conditions have already been discussed in the previous chapter on model development. As mentioned earlier, the smooth approximation of the stick-phase in dry-friction phenomenon obviates the use of event-detection integration methods and linear complementarity problem formulations in a chain CVT model, which consequently leads to time-efficient calculations of the dynamic performance indices. The chain-CVT model is subjected to various smoothened friction characteristics which describe the contact conditions between the chain links and the pulleys. Moreover, clearance-induced nonlinearities are also integrated into the model by using piecewise stiffness elements between the chain links. The simulation of a chain-CVT model starts off with an initial condition of rest and a specific design configuration and computes different dynamic performance indices i.e. axial forces, angular velocities,

tension, etc. The results germane to this model are discussed in the subsequent sections. Table 5.1 lists the numerical values of selected parameters used in all the chain CVT simulations.

Table 5.1: Chain CVT simulation parameters and values

Parameters	**Values**
Half sheave angle, β_0	15 deg
Mass of chain link, m	0.112 kg
Moment of inertia of pulley, J_p	2.358 kg-m^2
Length of chain link	0.03 m
Total number of chain links	34
Bolt stiffness, K_b	200 kN/m
Coefficient of kinetic friction between link and the pulley, μ_o	0.25

5.2.1 Influence of different friction characteristics

The chain CVT model is subjected to the following three different friction characteristics that describe the friction, μ, in the contact region between the chain links and the pulley sheaves:

Case 1: Continuous Coulomb friction, $\mu = a + (\mu_0 - a)(1 - e^{-|v_{rel}|/b})$

Case 2: Boundary lubrication- type friction, $\mu = \mu_0\left(1 - e^{-\kappa|v_{rel}|}\right)\left(1 + (f_r - 1)e^{-\bar{\lambda}|v_{rel}|}\right)$

Case 3: Stribeck- like friction, $\mu = \alpha_0 + \alpha_1 e^{-\left(v_{rel}/v_0\right)^2} + \alpha_2 v_{rel}$

The coefficient of friction mentioned in Case 1 describes the classical Coulomb-Amonton friction law which aptly captures the dynamics associated with kinetic friction and is most commonly referenced in literature. However, the coefficient of friction mentioned in Cases 2 and 3 is more detailed as it not only captures the dynamics associated with kinetic friction, but also captures the dynamics associated with stiction- and Stribeck-effects (which are prominent under dry and lubricated contact conditions respectively).

The model also takes into account the effects associated with clearance between the chain links by using piecewise stiffness elements to model the link interaction forces. Table 5.2 lists the parameter values that define two different clearance models (refer to Figure 3.16) used in the CVT simulation. Moreover, Table 5.3 lists the parameters that define the friction characteristics for the abovementioned three cases.

Table 5.2: Parameter Values for the Clearance Model

	k_1	b_1	k_2	b_2	k_3	b_3	ε_{min}	ε_{max}
Clearance-I	35	1.2	70	2.4	93	3.0	0.00005	0.0001
Clearance-II	0.001	2.5e-4	1	0.05	93	3.0	0.0003	0.0006
Units of k: kN/m Units of b: kNs/m Units of ε: m								

Table 5.3: Parameter Values for the Friction Characteristics

	a	b	μ_0	f_r	κ	$\overline{\lambda}$	α_0	α_1	α_2	v_0
Case 1	0.003	0.01	0.25	-	-	-	-	-	-	-
Case 2	-	-	0.25	1.5	100	5	-	-	-	-
Case 3	-	-	-	-	-	-	0.25	0.1	0.001	0.8

The driver and driven pulleys have constant radii of r_p = 3 in. and r'_p = 4.5 in. respectively. However, the links traverse around the pulley grooves in different pitch radii, thereby, causing a variation in the transmission ratio. Figure 5.1 depicts the time histories of the distance of a link from the center of the driver pulley for the three different cases. The variation in link distance is computed by tracing the position of a link from the center of the driver pulley as the link traverses the different section of the chain CVT, i.e. the free-strands, the driver pulley, and the driven pulley. It can be readily observed from Figure 5.1 that the chain-link pitch radius on the driver pulley is not the same for all the cases.

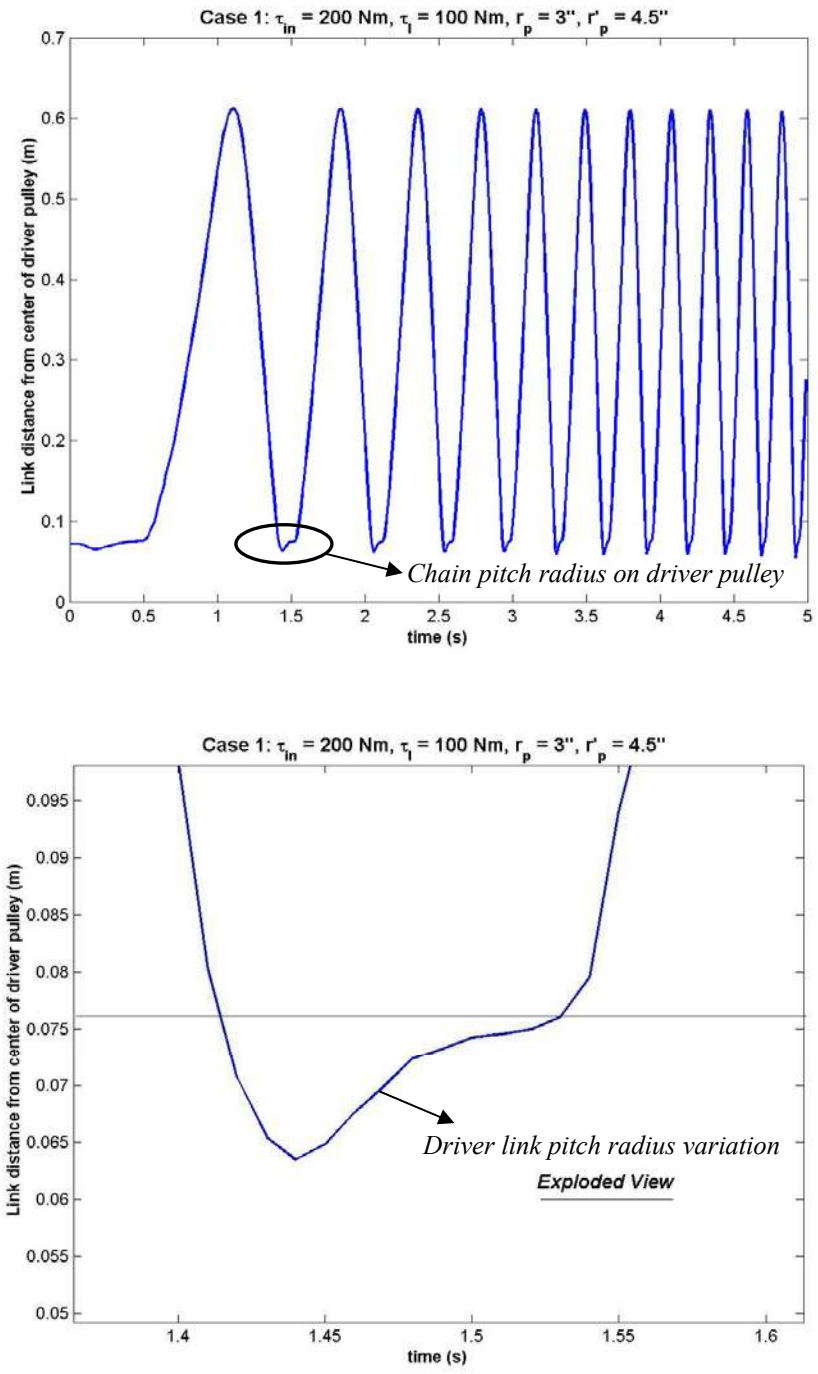

(a) Link Distance variation for Case 1

Figure 5.1: Time history of link distance from the center of driver pulley

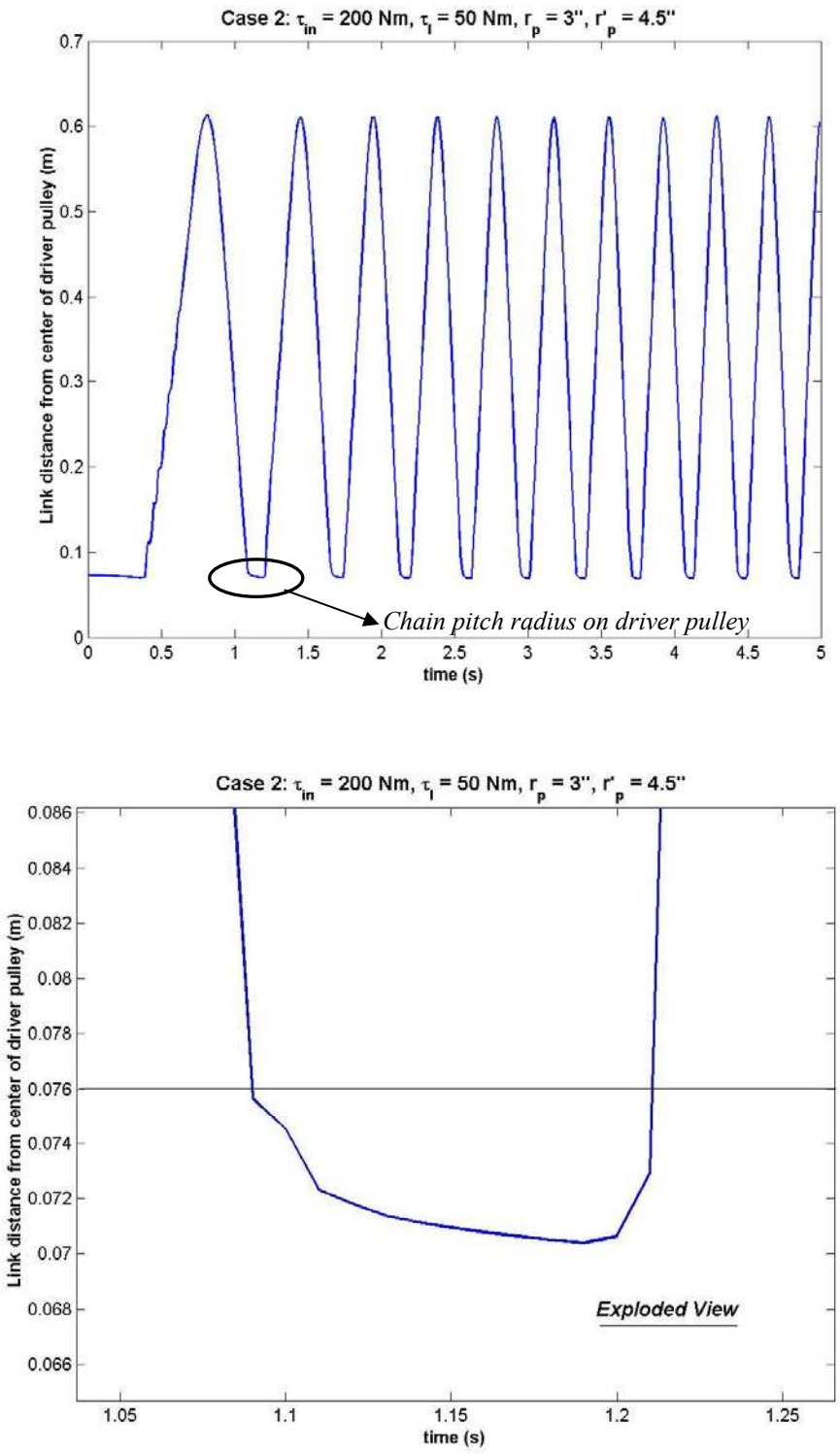

(b) Link Distance variation for Case 2

Figure 5.1: Time history of link distance from the center of driver pulley (contd.)

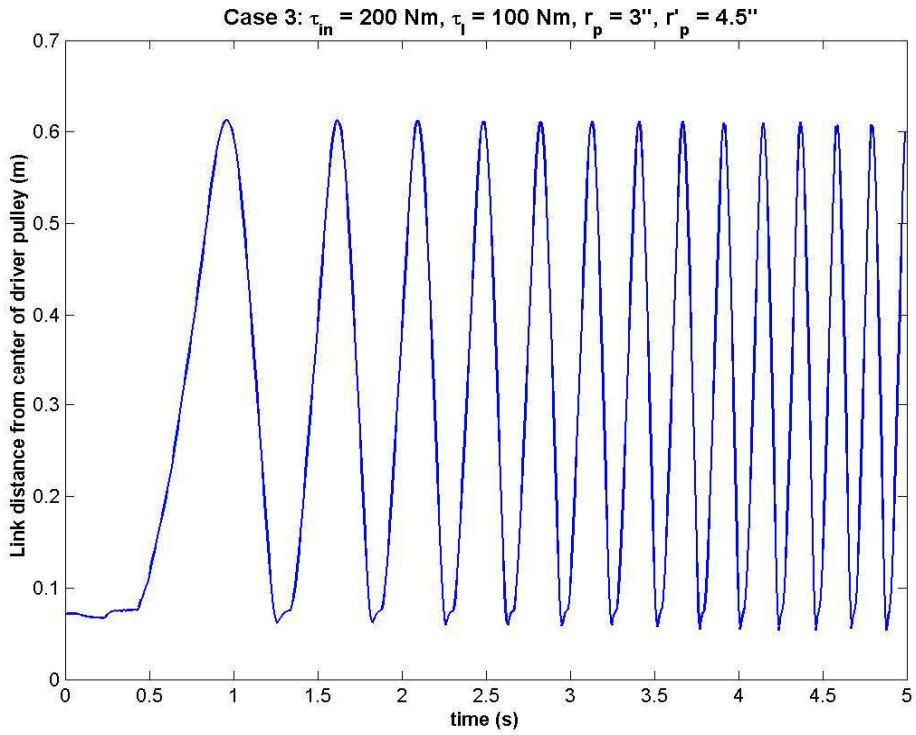

(c) Link Distance variation for Case 3

Figure 5.1: Time history of link distance from the center of driver pulley (contd.)

However, the variations in the chain pitch radius on the driver pulley for case 1 are similar to those for case 3. As the chain link enters the driver pulley groove, the chain pitch radius decreases. This phenomenon can be attributed to the wedging action between the link and the pulley. However, as the link traverses the pulley wrap, the chain pitch radius increases till the link exits the pulley. This can be attributed to the drop in the tensile force of the link as it moves from the entrance to the exit of the driver pulley. It can also be noted from the figure that with passage of time, the chain links come in contact with the pulley much more rapidly. The large radial path of the links over the pulleys can also be attributed to the dynamic effects associated with the flexibility of the pulley. So, pulley flexibility allows for greater motion of the links in the pulley sheaves, thereby yielding higher dissipative power. It can be noted from the figure that the chain

links wedge earlier with the pulleys in case 2 than in cases 1 and 3 owing to the presence of a lower resisting load torque (50 Nm) on the driven pulley for case 2. However, with passage of time, the chain links travel faster for cases 1 and 3 as depicted in the figure by the increasing number of revolutions (or cycles) of the chain for cases 1 and 3. It was observed (refer to Figure 5.2) that a chain CVT under the presence of a friction characteristic governed by case 2 was unable to sustain a higher load torque of 100 Nm, which was contrary to the load carrying capacity predicted by the classical continuous Coulomb friction law and Stribeck law (i.e. under cases 1 and 3).

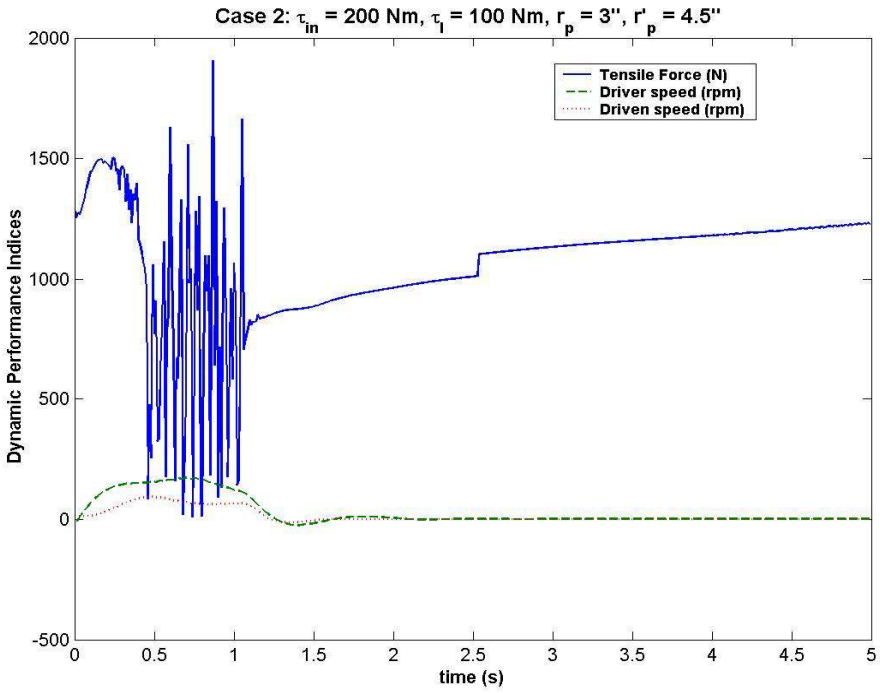

Figure 5.2: Dynamic Performance Indices (Tension and Pulley Speeds) - Case 2

Moreover, owing to larger normal force generation in case 1, the radial path traversed by a chain link in the driver pulley groove is greater in this case than in case 2. A chain link contacting the driven pulley also shows complementary behavior in the entry and exit phases of its motion.

Normal Force:

Figure 5.3 illustrates the time histories of the normal force between a chain link and the pulleys. Whenever a chain link comes in contact with the pulley sheave, it exerts a normal force on the sheave, which tends to move the pulley sheaves apart. The pulley normal force has a nonuniform distribution over the contact arc. The normal force increases from the entrance to the exit of the pulley, which is in consonance with the observations made by Ide *et al.* [50] and Pfeiffer *et al.* [7]. Moreover, the normal force between the driver pulley and the chain link is higher than the normal force generated between the link and the driven pulley. As the chain link wedges into the pulley groove, a significant amount of radial friction force is generated to prevent the inward radial motion of the chain link. Since during the wedging the pitch radius of the chain link decreases on the driver pulley, the link exerts a large normal force on the pulley in order to generate enough torque to compensate for the resisting load on the driven pulley. As the chain links traverse the pulley wrap, the tensile force in the links also builds up. Since the variations in the pitch radius of the chain on the driven pulley are higher than those over a driver pulley, an adequate amount of normal force between the link and the pulley generates enough friction torque to meet the resisting load torque. It can also be observed from the figure that the normal force generated is lower for case 2 than for cases 1 and 3 because of the lower load torque requirements on the driven pulley for case 2 as well as due to the presence of lubrication-related dynamic effects.

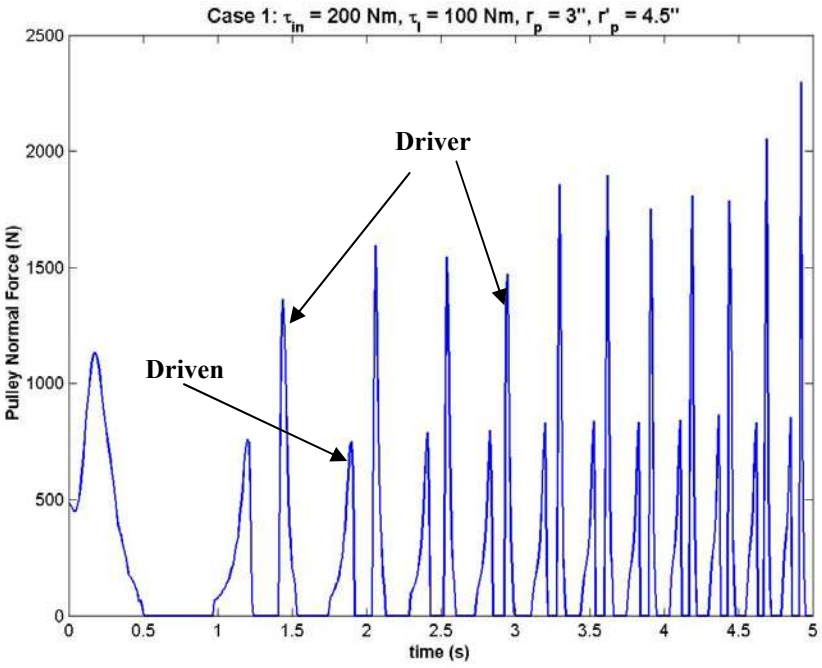

(a) Normal Force variation for Case 1

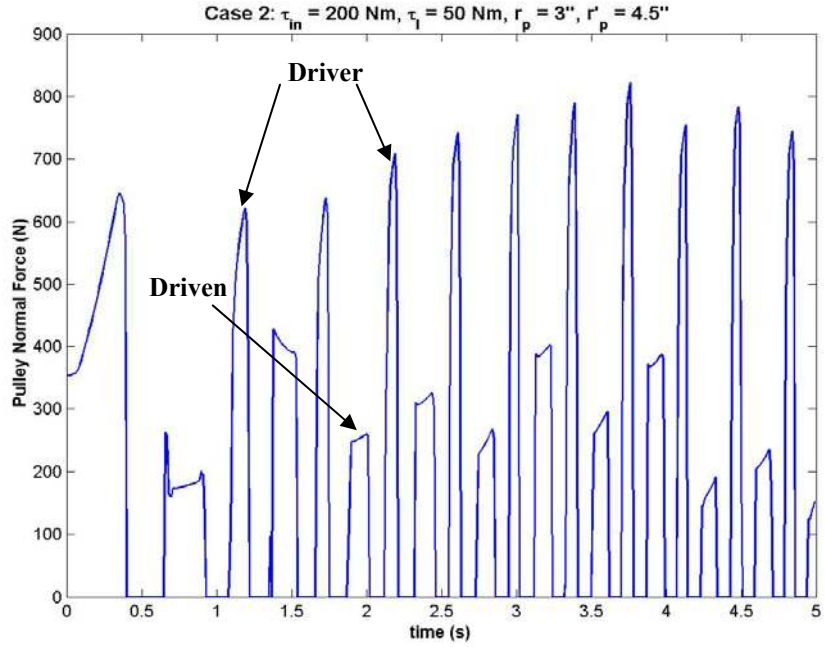

(b) Normal Force variation for Case 2

Figure 5.3. Time history of Pulley Normal Force

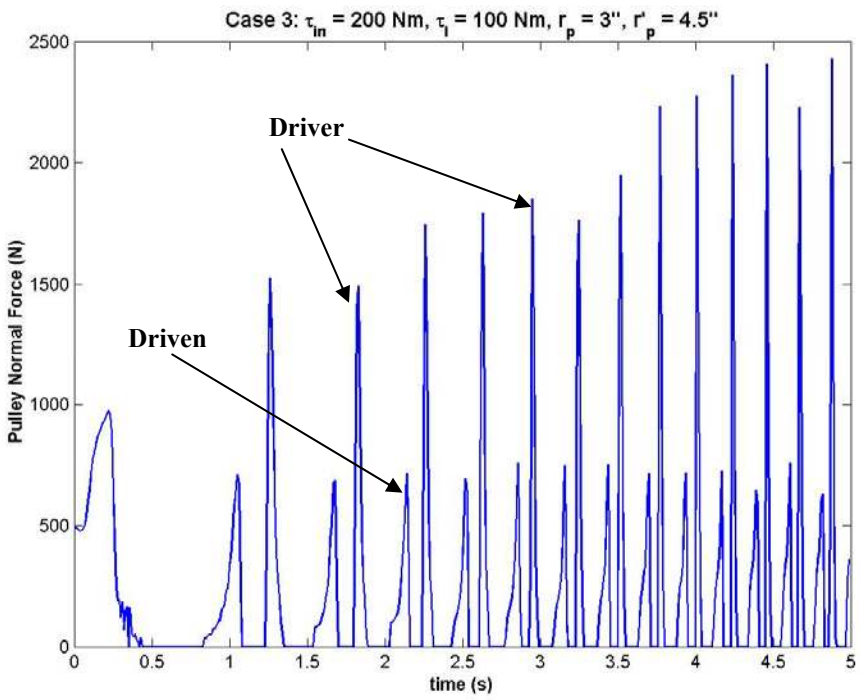

(c) Normal Force variation for Case 3

Figure 5.3: Time history of Pulley Normal Force (contd.)

It can be also be noted from Figure 5.3 that with passage of time, the links come in contact with the pulleys faster for case 1 and case 3 than for case 2. So, the losses due to clearance and vibration are more prominent in the system with boundary lubrication- like friction than in other systems, as is evident from a noisy wedging action in the driven pulley (refer to Figure 5.3 (b)). Moreover, as mentioned before, the load sustaining capacity of such a system is also lower than the system with friction characteristics defined by cases 1 and 3.

Friction Force:

Since one of the pulley sheaves is movable, the chain link is capable of exhibiting both tangential and radial motions when it traverses the pulley wrap angle. Consequently, a friction force is generated in the sliding plane that opposes the relative velocity between

the chain link and the pulley. Knowing the sliding direction and the sheave angle, the friction force in the sliding plane can be readily decomposed into radial and tangential components. Figure 5.4 illustrates the time histories of radial and tangential friction force components for all the three cases. It can be noted from the figure that the time histories of friction forces for case 1 and case 3 are similar to each other. As the chain link wedges into the pulley, it tends to move radially inwards in the pulley groove. This leads to the development of a high radial friction force at the entrance of the pulley. Moreover, it is apparent from Figure 5.4 that the variation in the radial friction force is similar to the variation in the normal force between the pulley and the link. The slight difference in the variations can be attributed to the dependence of radial friction force on a velocity-dependent friction coefficient between the link and the pulley. The radial friction force drops as the link exits the pulley. In fact, the friction force acts to retain the link within the pulley. On the other hand, the tangential friction force acts as the transmitting force and causes the variations in the tensile force in the chain links. It can be observed from Figure 5.4 that the tangential friction force between the driver pulley and the link is in anti-phase to the tangential friction phase between the driven pulley and the link. This relationship, in fact, aptly describes the energy transfer interactions between the chain link and the pulleys. It is to be noted that the transmitting force in case 2 is higher than in cases 1 and 3. Since the chain links traverse greater radial path in these cases than in case 2, the transmitting force required to overcome the resisting load torque is not high enough for cases 1 and 3. It is to be noted from the time histories of normal force and friction force that the chain CVT system exhibit greater wedging losses in case 2 owing to noisy entrance and exit dynamics over the pulley wraps. So, in addition to the

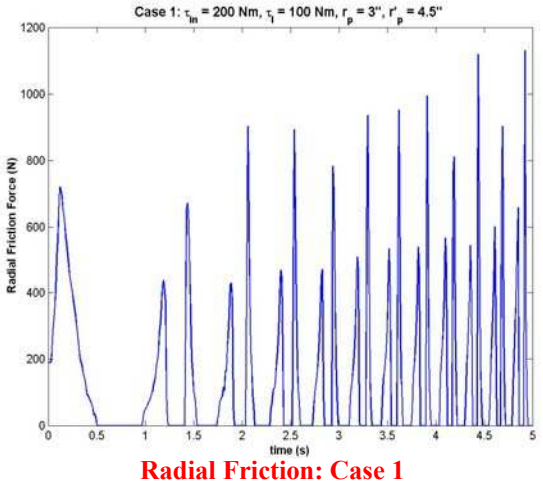

Radial Friction: Case 1

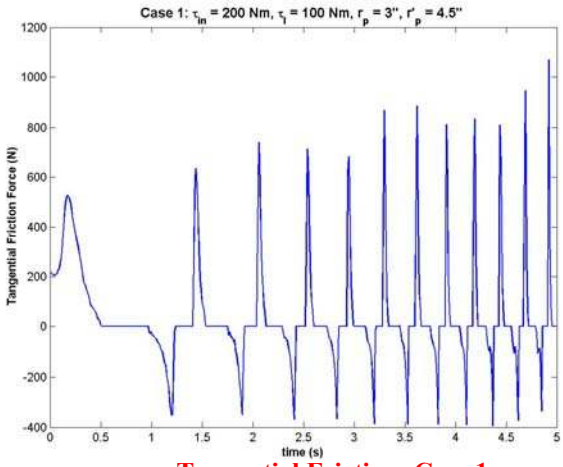

Tangential Friction: Case 1

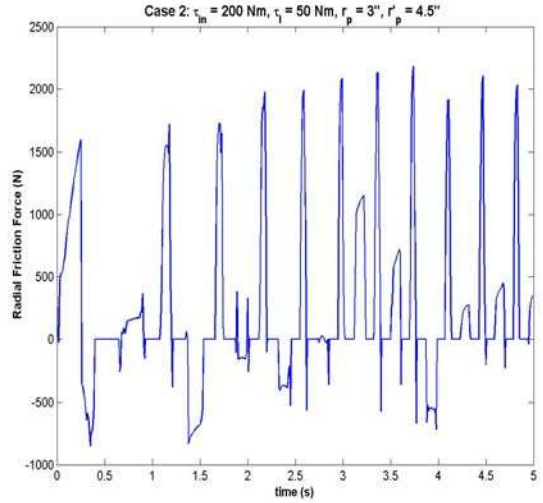

Radial Friction: Case 2

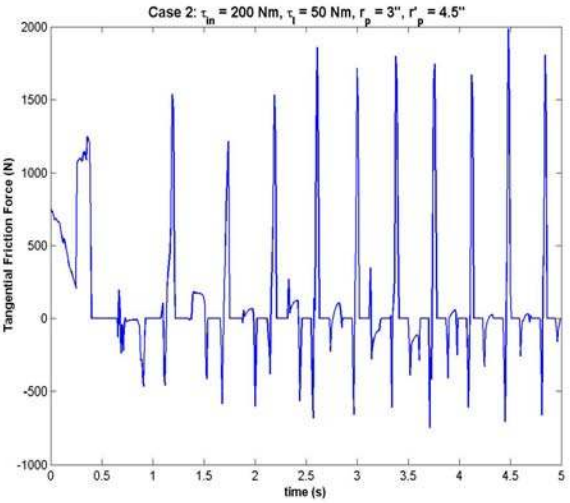

Tangential Friction: Case 2

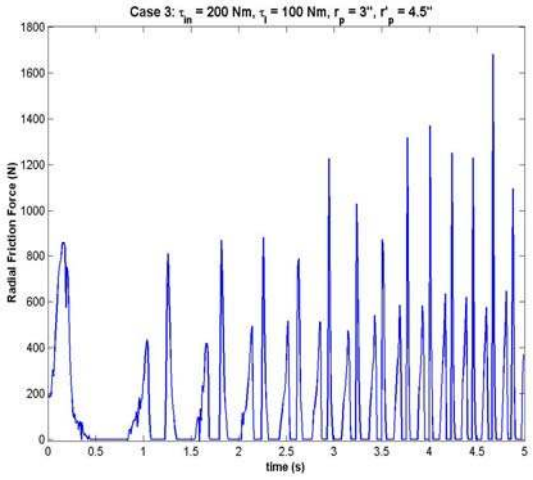

Radial Friction: Case 3

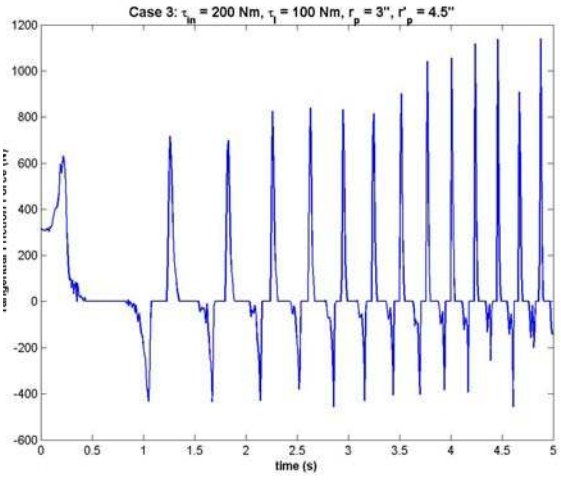

Tangential Friction: Case 3

Figure 5.4: Time histories of Friction Force

losses due to clearance between the links, further transmission losses are registered as the links wedge in and out of the pulleys.

Tensile Force:

Figure 5.5 illustrates the time history of the tensile force in the chain links for all the three cases. It can be observed that the chain tensile force decreases over the driver pulley wrap and increases over the driven pulley wrap as the chain links move from the inlet to the exit of the pulleys. Moreover, the free span of the chain undergoes vibrations, consequently, enhancing the transmission losses. With the passage of time, the tension in the chain links also increases. This can be attributed to the increase in the stiffness between the links as the joint clearance closes with time.

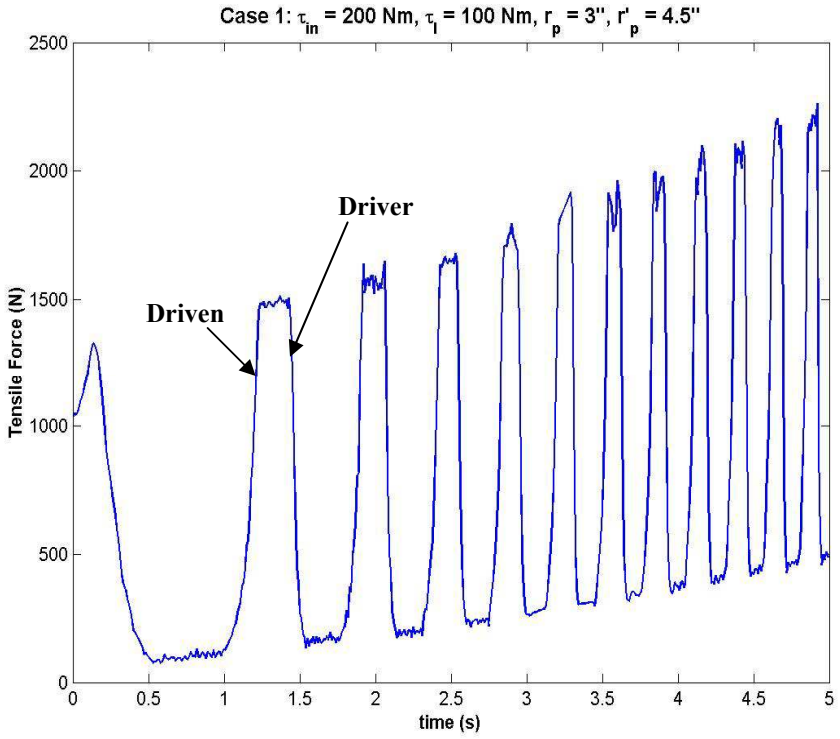

(a) Link Tension – Case 1

Figure 5.5: Time history of Link Tensile Force

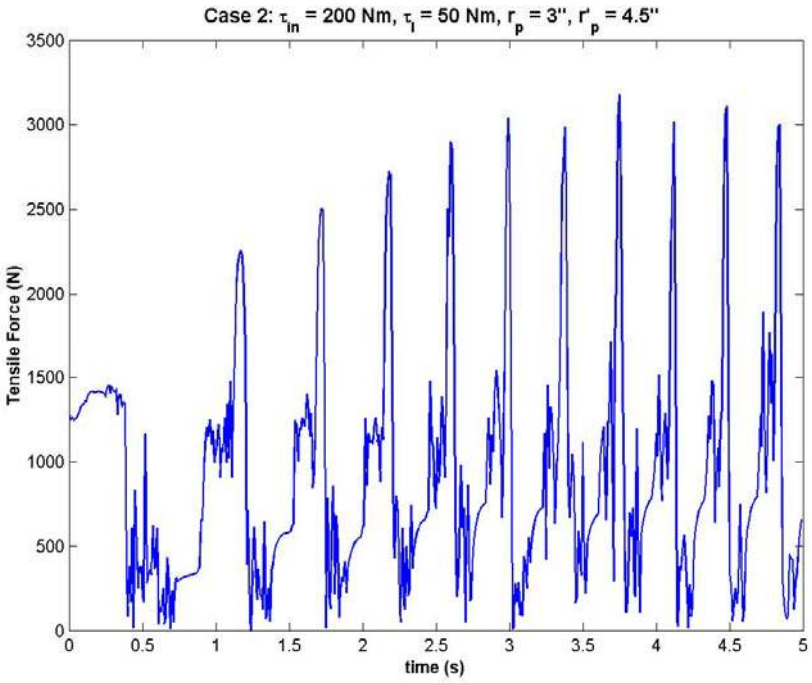

(b) Link Tension – Case 2

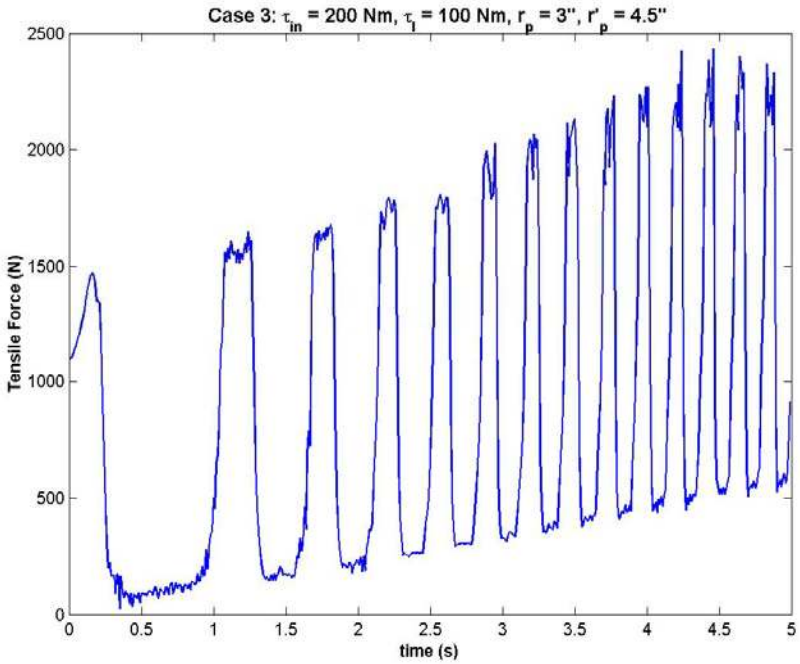

(b) Link Tension – Case 3

Figure 5.5: Time history of Link Tensile Force (contd.)

It can also be noted from the figure that the link tension exhibits significant variations as the link passes through the entry and exit regions of the pulleys for a CVT system with friction described by case 2. This not only degrades the system performance, but also induces chaoticity in the system, which might be difficult to control. Moreover, since the transmitting force required to meet the load torque is higher for case 2, the tensile force in the chain links with friction described by case 2 is higher is in comparison to the tensile force generated in the other two cases. It is plausible from the plots that a CVT system with continuous Coulomb friction characteristic is able to transmit torque much more smoothly than CVT systems with friction characteristics described by cases 2 and 3.

Pulley speed:

The pulleys are subjected to the torque loading conditions. An input torque is applied to the driver pulley, whereas the driven pulley is subjected to an opposing load torque. The links and the pulleys start off from a zero initial velocity configuration. Figure 5.6 depicts the time histories of pulley speeds for all the three cases. It is obvious from the plots that for each case, the system is able to successfully meet the load torque. It can also be inferred from the plots that the CVT system entails greater losses in case 2 than in cases 1 and 3, as in spite of a low load torque of 50 Nm, it is not able to generate enough friction torque to rev up the driven pulley. However, there is a greater difference between the driver and driven pulley speeds for cases 1 and 3 than for case 2. This can be attributed to the greater radial penetration of chain links in the pulley groove under the friction characteristic described by cases 1 and 3. Consequently, the friction torque on the driver pulley decreases (thereby, increasing the driver pulley speed), whereas it increases on the driven pulley (thereby, increasingly opposing the load torque on the driven pulley). It is

plausible from the plots that the system runs most efficiently under the friction characteristic defined by case 3.

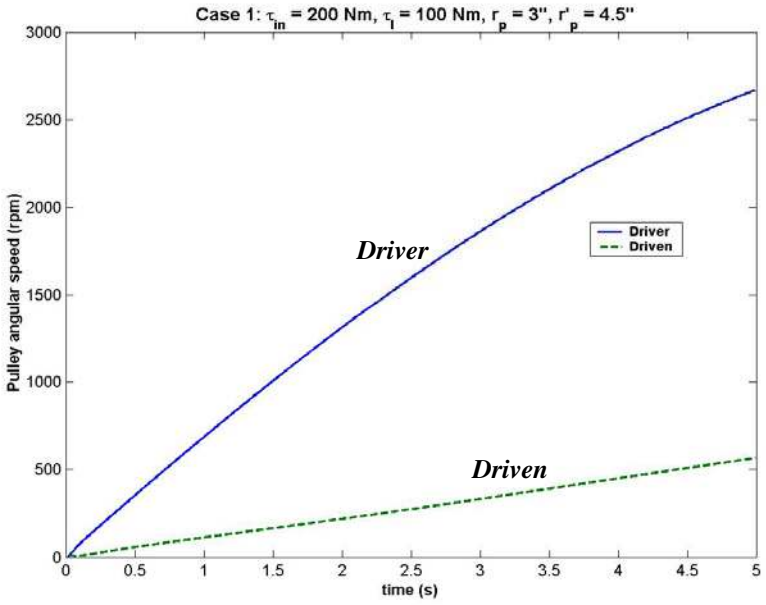

(a) Case 1 - Pulley speeds

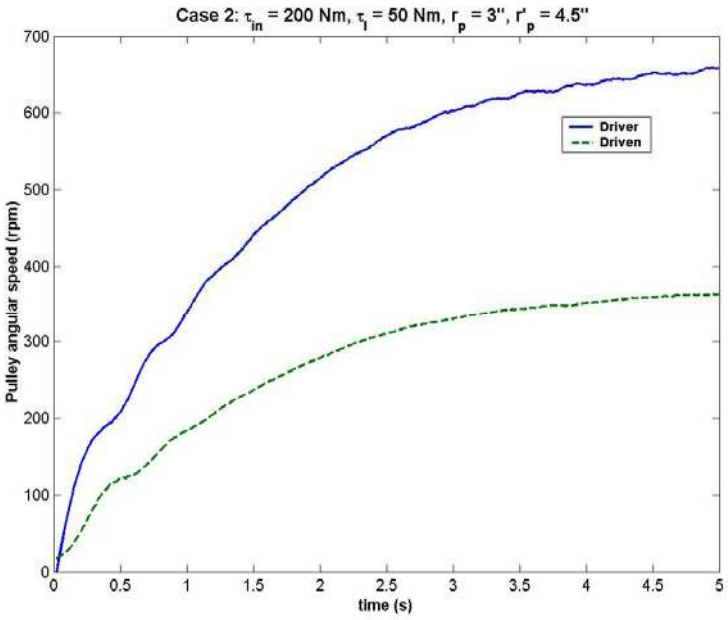

(b) Case 2 – Pulley speeds

Figure 5.6: Time histories of Pulley Speed

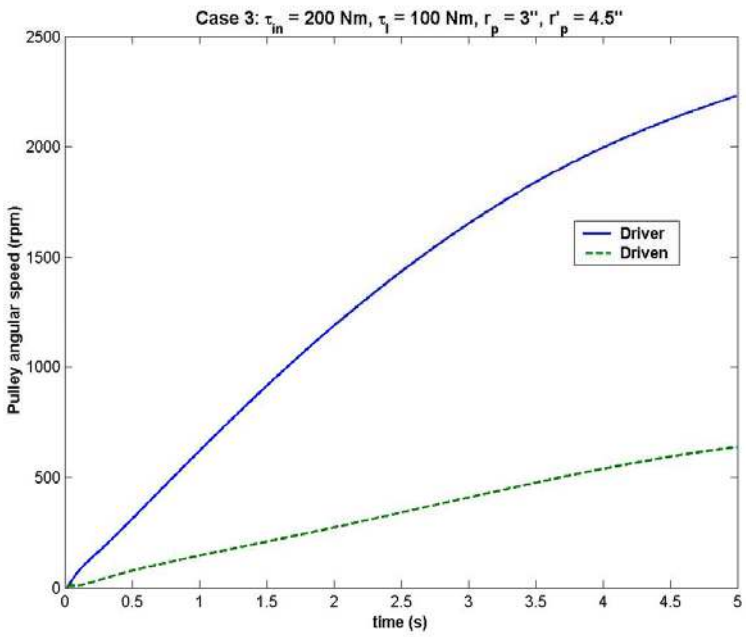

(c) Case 3 – Pulley speed

Figure 5.6: Time histories of Pulley Speed (contd.)

Pulley Axial Force:

As the link moves around the pulleys, it exerts a force in the axial direction on the pulley sheave. The link moves radially inwards and outwards within the pulley groove, which causes variations in the transmission ratio. The axial force directed along the pulley shaft axis is computed from the bolt force of the chain, as discussed in the previous chapters. Figure 5.7 illustrates the time histories of the axial forces on the driver and driven pulleys for all the three cases. Among all the three cases, the system generates the maximum amount of axial force under the influence of Stribeck- friction characteristic (i.e. Case 3). Consequently, the range of variation in the transmission ratio is the maximum for case 3. It can be noted from the figure that the system is unable to generate more axial force after some time for case 2. The pulley sheaves, in fact, begin to experience medium-amplitude high-frequency oscillations which degrade the system performance.

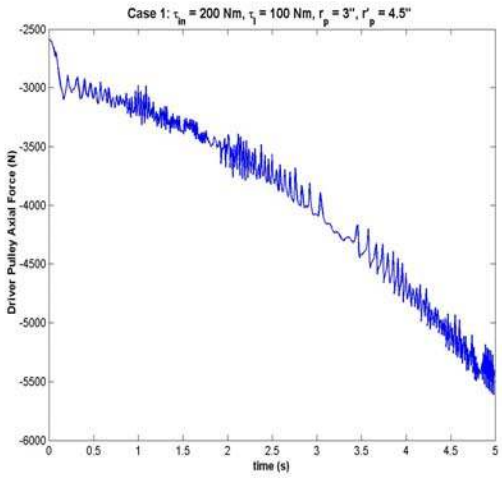

Case 1: Driver Axial Force

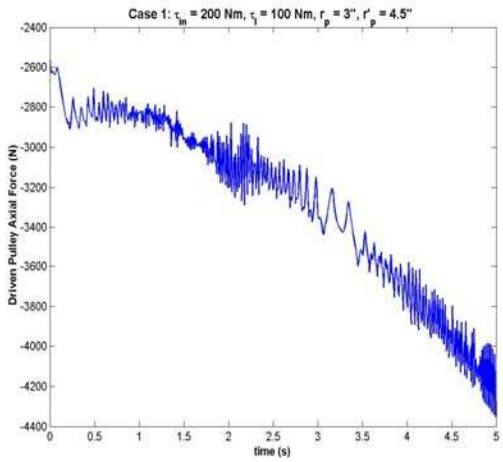

Case 1: Driven Axial Force

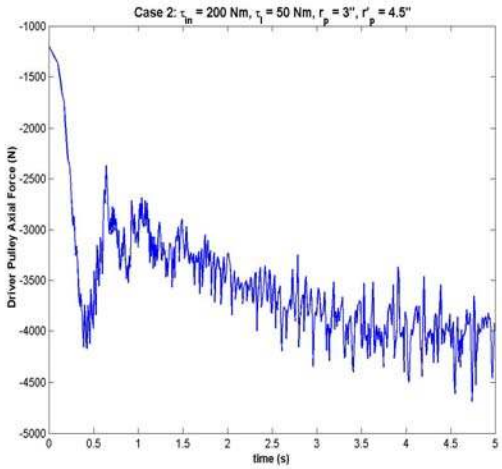

Case 2: Driver Axial Force

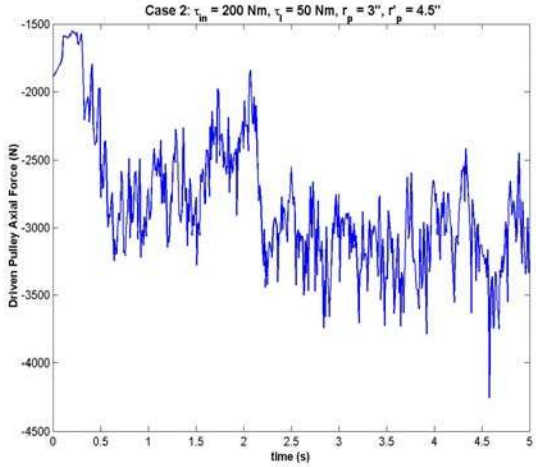

Case 2: Driven Axial Force

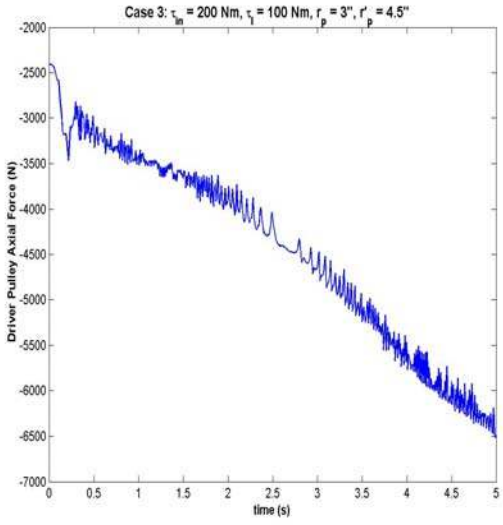

Case 3: Driver Axial Force

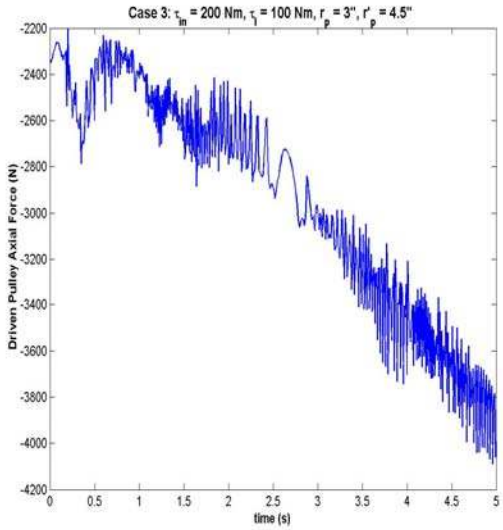

Case 3: Driven Axial Force

Figure 5.7: Time histories of pulley axial force

5.2.2 Influence of clearance between chain links

The response of a CVT changes considerably under the influence of clearance between the chain links, which may be inherent or may arise during its continual operation. As discussed previously, clearance-induced nonlinearities are taken into account through the piecewise stiffness elements between the chain links. The two significant parameters in the clearance model that drastically influence the system dynamics are: (*k, b*) and ε**.** The results presented in the previous section were obtained under the influence of different friction characteristics and clearance-I (refer to Table 5.2) model parameters. In order to understand the impact of clearance on system dynamics, clearance-II model parameters are now introduced in the chain CVT model. As can be noted from Table 5.2, clearance-II model parameters manifest system dynamics under high clearance. It was observed that in spite of increasing the clearance parameter (as in clearance-II, refer to Table 5.2), ε, the dynamic performance indices did not exhibit significant deviations from the previous case of lower clearance parameter. This could be attributed to the high stiffness of the interconnecting force elements between the chain links. Even though the links are able to generate sufficient forces to meet the load torque, the pulley sheaves undergo chattering due to high-frequency chaotic or quasi-periodic oscillations, which are perilous to the CVT system. It was observed that as the slope parameters of the clearance-model were increased, such high frequency chattering phenomena were circumvented, the transmission efficiency increased, and torque transmissibility also enhanced (Srivastava *et al.* [162]). It was also observed that under certain simulation conditions, a clearance-model with lower slope parameters and higher ε (say, ε_{min} being more than two millimeters) drastically lowers the torque capacity and performance of the CVT system,

as illustrated by some of the dynamic performance indices in Figure 5.8. So, owing to higher clearance effects, the same CVT system under the influence of continuous Coulomb friction characteristic has a torque carrying capacity lower than it had earlier. Thus, it is the combined nonlinear effect of friction and clearance that influences the torque transmitting capacity of a chain CVT system.

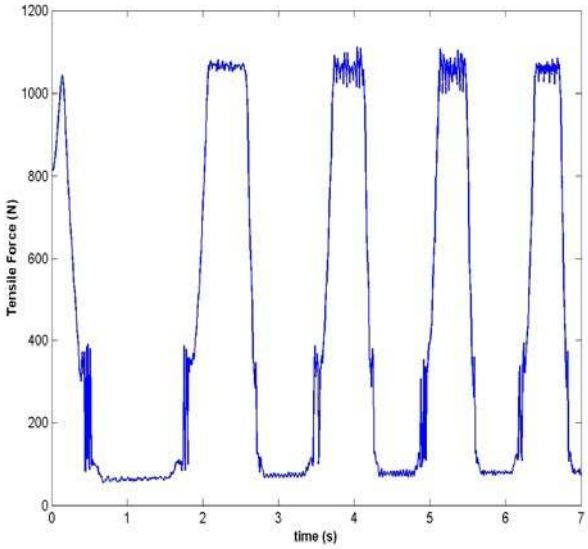

Tensile Force vs. Time

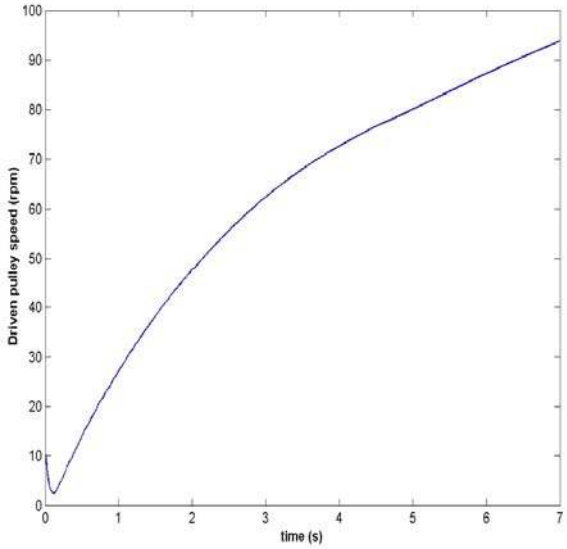

Driven Pulley Speed vs. Time

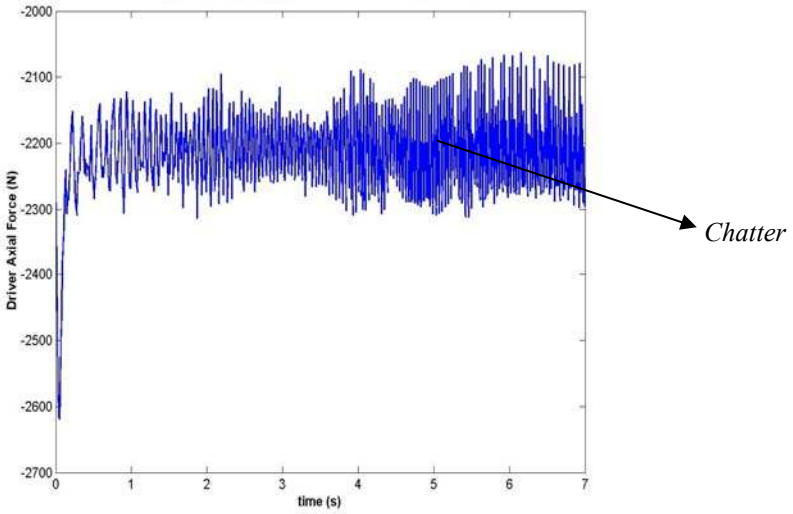

Driver Pulley Axial Force vs. Time

Figure 5.8: Dynamic performance indices under clearance (high ε, low k_1, b_1) – Case 1

5.3 Results from Belt CVT model

The simulation of a belt-CVT model starts off with an initial condition and a specific design configuration. The initial operating conditions required for the model, to successfully transmit torque, are: belt pretension and precompression at the inlet of the pulleys. In addition to these operating conditions, the model is also subjected to torque loading conditions. The driver pulley is subjected to a high input torque (200 Nm), whereas a low resisting load torque (100 Nm) is applied on the driven pulley. Moreover, the driver pulley speed is maintained constant (2000 rpm) throughout the simulation. The program uses these data to calculate the time histories of forces, displacements, velocities, slip, and etc. that describe the dynamic interactions between the belt and the pulleys. The belt CVT model was developed on the MATLAB/SIMULINK platform. The time-histories of the system states were obtained by integrating the state equations using the Runge-Kutta algorithm. The simulation tracks a belt element from the inlet to the exit of the pulley and records the various dynamic performance indicators. It stops as soon as the belt element moves past the exit of either of the two pulleys.

So, the CVT model, subjected to initial operating conditions and loading conditions, records the dynamic interactions between the belt element and the pulleys as the belt element completes one cycle (i.e., from the inlet to the exit of the pulley). In reality, the operating conditions at the driven pulley inlet are known as soon as the operating conditions at the driver pulley inlet are specified. This can be attributed to the continuity of the belt and the dynamics in the free section of the belt. Since this model captures the dynamic interactions for one cycle, the inertial dynamics in the free section of the belt have been ignored. However, the coupling between the driver and the driven

pulley systems still exists through the constraint of constant belt length. Owing to the absence of belt dynamics in the free-section, it is necessary to specify operating conditions at the inlet of the driven pulley. It is extremely cumbersome for the user to make a knowledgeable guess of the operating regime. Without real world experiments, it is difficult to estimate the operating values consistent with the behavior of a real production CVT.

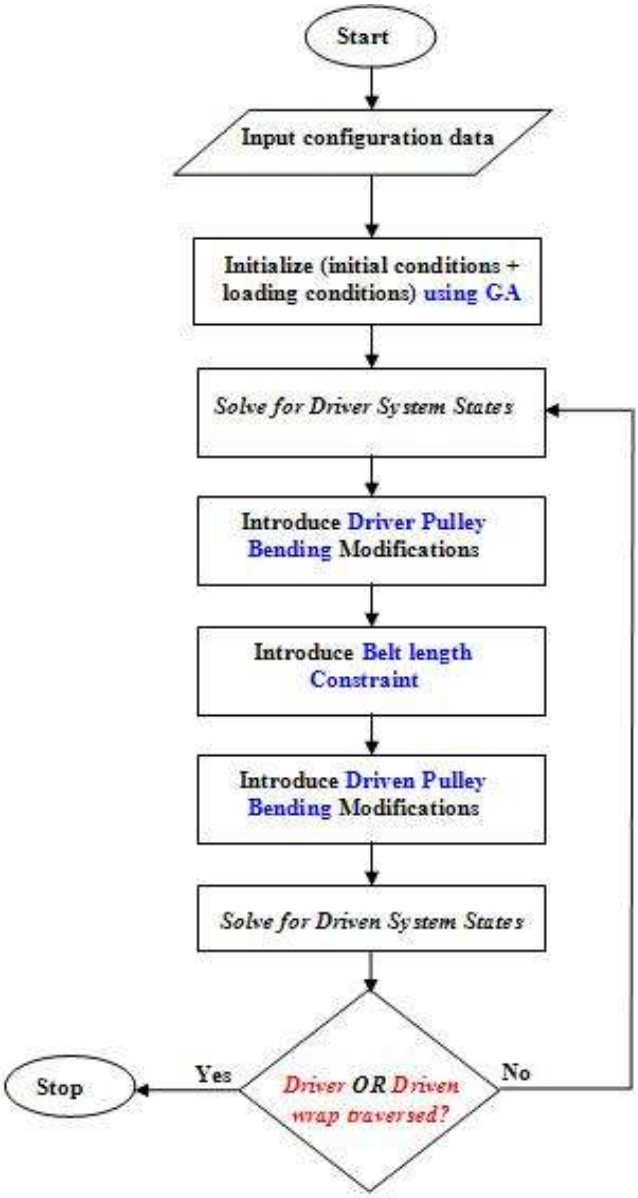

Figure 5.9: Flowchart for Transient belt-CVT model

Srivastava *et al.* [76-77] highlighted the significance of using Genetic Algorithms (GA) in a transient dynamic CVT model for estimating operating conditions necessary for successful torque transmission. Figure 5.9 depicts the flowchart of transient dynamic model of a belt CVT. The algorithm flow begins with the driver analysis and uses the constraint of constant belt length and pulley-bending effects to proceed with the driven analysis. The simulation stops as soon as a belt element goes past the exit of either of the pulleys. Table 5.4 lists the numerical values of selected parameters used in all belt CVT simulations.

Table 5.4. Simulation parameters and values for belt CVT model

Parameters	**Values**
Half sheave angle, β_0	15 deg
Linear Band pack density, σ_b	1.5 kg/m
Linear Element density, σ_e	2 kg/m
Starting transmission ratio, r/r'	0.0118 / 0.0177 (m/m)
Coefficient of kinetic friction between band pack and element, μ_a or μ_{ao}	0.25
Coefficient of kinetic friction between element and pulley, μ_{bo}	0.25
Center distance, d	0.5 m

5.3.1 Influence of different friction characteristics

The belt CVT model is subjected to the following friction characteristics that describe the friction in the contact region between a belt element and the pulley surfaces:

Case 1: Continuous Coulomb friction, $\mu_b = a + (\mu_{bo} - a)(1 - e^{-|v_s|/b})$

Case 2: Boundary lubrication- type friction, $\mu_b = \mu_{bo}\left(1 - e^{-\kappa|v_s|}\right)\left(1 + (f_r - 1)e^{-\bar{\lambda}|v_s|}\right)$

It is to be noted that v_s is the actual slip velocity of the belt element in the sliding plane of the pulley sheave (refer to Figure 3.3 (a)). The driver pulley runs at a constant speed (2000 rpm) and is subjected to a high input torque, whereas an opposing load torque is

applied on the driven pulley. The dynamics in a belt CVT seem to be more complex in nature in comparison to the chain CVT because of the presence of both band pack-element and element-pulley interactions. The belt CVT can transmit torque not only by the push action of the steel elements, but also by the pull action of the bands. It is a combined push-pull mechanism that decides the maximum torque transmitting capacity [41, 61, 76-78] of a metal V-belt CVT.

Radial Variations

Figure 5.10 illustrates the time histories of the belt pitch radii on the driver and driven pulleys for both the cases. The belt element, while traversing the pulley wrap, accelerates under the influence of radial and tangential forces. Consequently, the relative velocity between a belt element and the pulley varies over the pulley wrap. Figure 5.11 depicts the relative velocity diagram where the components of the relative velocity vector in the radial and tangential directions are plotted with respect to each other. It is plausible from the plots that the friction characteristic of the contact zone between the belt element and pulley plays a significant role in the variation of the transmission ratio in a CVT system. It is to be noted from Figure 5.11 that there are certain transition points (*a*, *b*, and *c* for case 1) in the system (*marked by thick black lines in the figure*) where the relative velocity between the belt element and the pulley is either completely radial or completely tangential. For instance, the belt element moves radially at the transition point *a,* whereas at transition points *b* and *c*, the belt does not undergo any relative radial motion. Moreover, at the transition point *a*, the belt element only moves tangentially with the same speed as that of the pulley. It can also be noted from the plots the variations in the belt pitch radii are in consonance with the constraint of constant belt length. It is apparent

from the relative-velocity diagrams that the belt element follows a complex noncircular path over the pulley wraps.

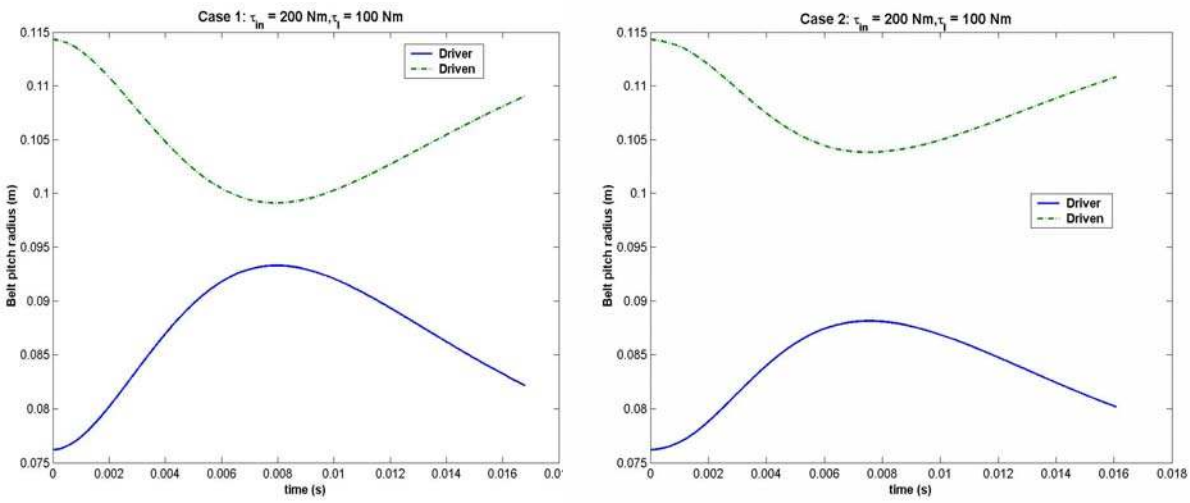

(a) Case 1 **(b) Case 2**

Figure 5.10: Time histories of Belt Pitch Radius

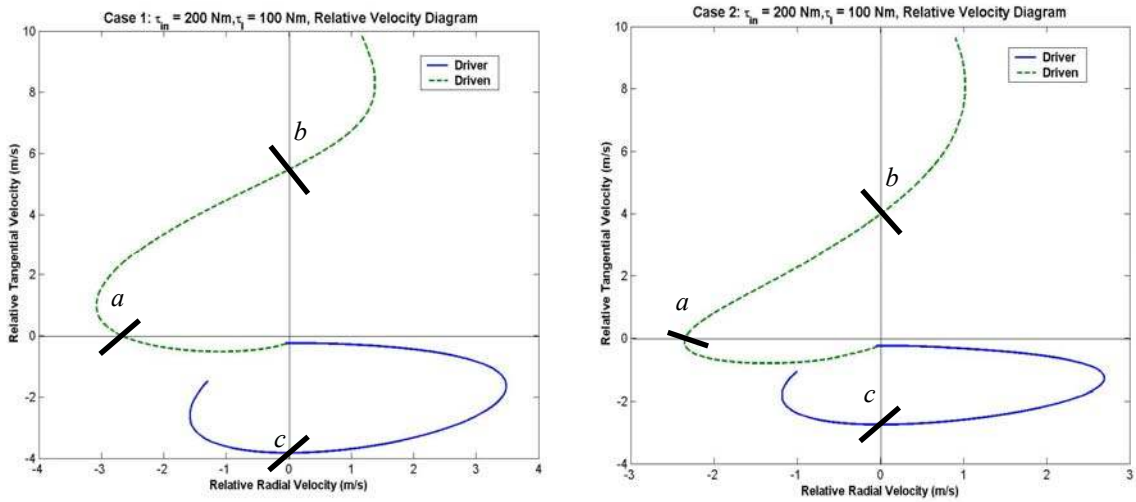

(a) Case 1 **(b) Case 2**

Figure 5.11: Relative Velocity Diagrams

Pulley sheave angle:

As the belt elements traverse the pulley wrap, they exert forces on the pulley sheave in the axial direction. Since these forces can be considerably high under transient conditions, the pulley sheaves experience bending torques, which further leads to

variations in the pulley sheave angle. Moreover, since the belt pitch radii and the forces on the driver and the driven pulleys differ from each other, the pulleys undergo asymmetrical pulley deformation. Figure 5.12 illustrates the time histories of pulley half-sheave angle for both the cases.

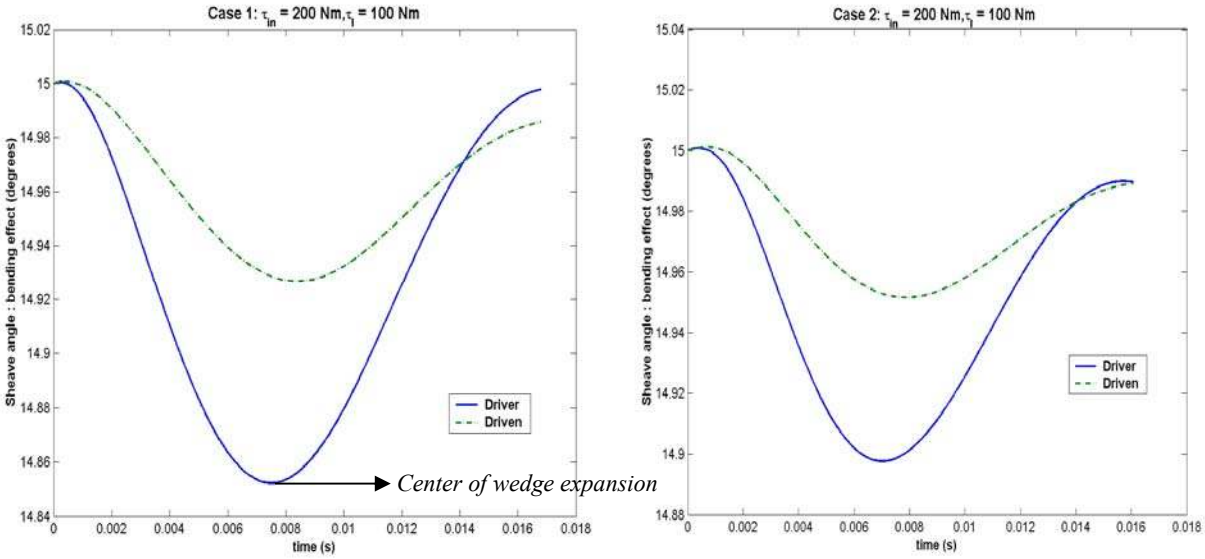

(a) Case 1 **(b) Case 2**

Figure 5.12: Time histories of pulley half-sheave angle

It can be observed from the figure that the continuous Coulomb friction model predicts greater bending of pulley sheaves than the boundary lubrication- like friction model. This can be attributed to the reduction in the force transfer due to greater lubrication (Stribeck-related) effects in the contact zone of the belt element and the pulley. As the belt element wedges into the pulley groove, it tends to move the pulley sheaves apart. This allows the belt element to slide radially inwards into the pulley groove. However, since the driver pulley runs at a constant speed at all times, the pulley exerts a large normal force which, on the contrary, increases the belt pitch radius. This is inevitable as the belt needs to generate a large enough opposing friction torque on the driver pulley to overcome the acceleration effects arising from the constant input torque. At the onset of the motion, the

belt slips relative to the pulley; however, it soon begins to catch up with the driver pulley speed (as noted by transitions *b* and *c* in Figure 5.11). It is during this phase of motion that the belt element crosses the center of wedge expansion and the pulley sheave angle starts to increase, as can be observed in the figure.

Belt Compressive Force:

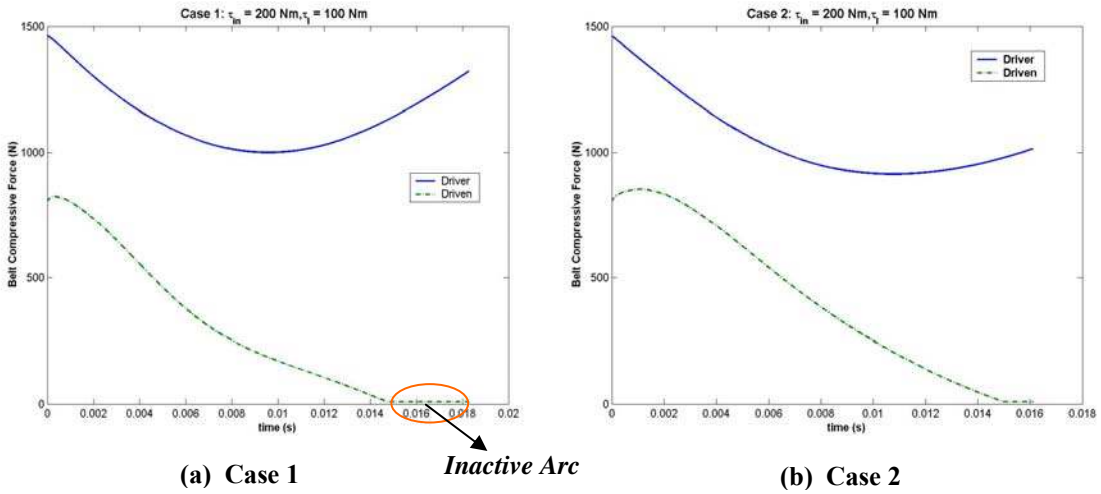

(a) Case 1 **(b) Case 2**

Figure 5.13: Time histories of belt compressive force

As the belt moves around the pulleys, the steel elements push against each other in order to generate compressive forces. The pushing mechanism of belt elements plays a significant factor in the torque transmission characteristic of a metal V-belt CVT. Figure 5.13 illustrate the time histories of the compressive force that is generated in the belt due to the push action of the steel elements. For both the cases, as the belt element wedges into the driver pulley, the compressive force decreases as the elements begin to move at a larger pitch radius in order to maintain constant driver pulley speed. However, as the belt element passes through the center of pulley-wedge expansion (where the sheave angle is minimum), the compressive force tends to build up. This can be attributed to a decrease in the belt pitch radius on the driver pulley as less compressive force is now required to

overcome the resisting load torque. On the contrary, the belt compressive force on the driven pulley wrap decreases from the inlet to the exit of the pulley. It can also be noted from the figure that there are certain regions of the driven pulley wrap which do not contribute effectively to the torque transmission. Such regions are called inactive or idle arcs where the belt compressive force is negligible. The inactive arcs need not necessarily form at the exit of the driven pulley. They can also form at the inlet of the driven pulley, as observed by Srivastava and Haque [76-77]. Since the belt compressive force does not exhibit strict monotonicity (as seen for driver pulley in Case 1) over the pulley wrap, the gaps between the elements begin to redistribute themselves. The redistribution of gaps among the steel elements leads to microslip phenomena in the belt [41, 43, 76-78], which contribute to the transmission losses. The gaps among the belt elements exist due to manufacturing or assembly defects. They can also arise with time due to wear and fatigue of the elements due to continual operation of a CVT. The compressive force profiles seemingly do not differ much from each other. However, it is to be noted that the losses in the CVT system with continuous Coulomb friction is more in comparison to the CVT system in case 2. In addition to the push mechanism, the pulling action in the band pack also contributes to the torque transmission. Srivastava *et al.* [78], Fujii *et al.* [61-62, 65], Kobayashi *et al.* [43], have highlighted the significance of tensile force in the band pack in determining the maximum torque transmitting capacity of a metal V-belt CVT under steady-state conditions. Moreover, it is the combined effect of the tensile force in the band pack and the compressive force in the elements that determines the redistribution of inter-element gaps in the belt, which consequently influences the belt slip and the pulley axial force.

Pulley Speed:

Figure 5.14 illustrates the time histories of the angular speeds of the driver and driven pulleys for both the cases. The driver pulley speed, as seen from the plots, remains constant at all times. In addition to the pulley speeds, Figure 5.14 depicts the angular speed with which a belt element traverses the driver and the driven pulley wraps. It can be observed that the angular speed of a belt element traversing the driver pulley decreases

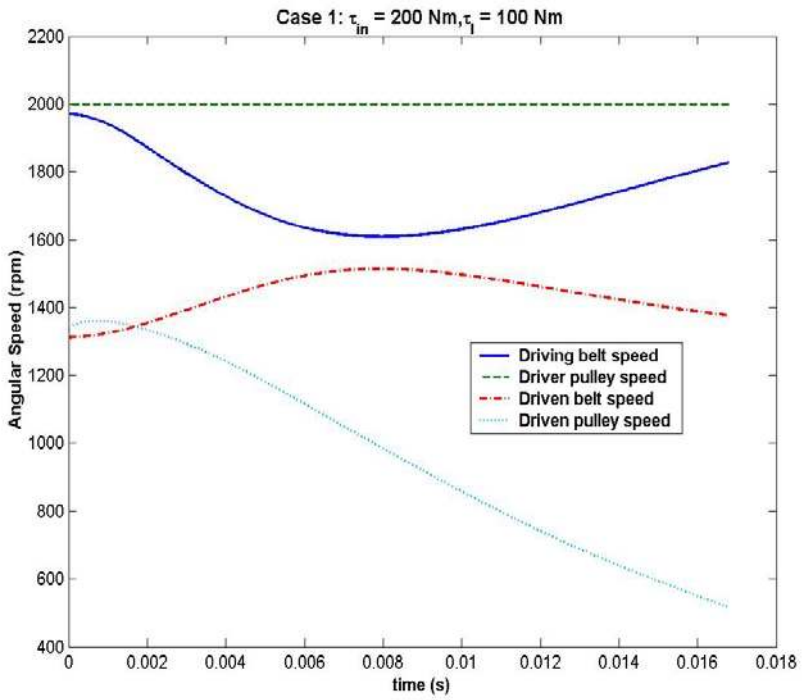

(a) Case 1

Figure 5.14: Time histories of pulley and belt speeds

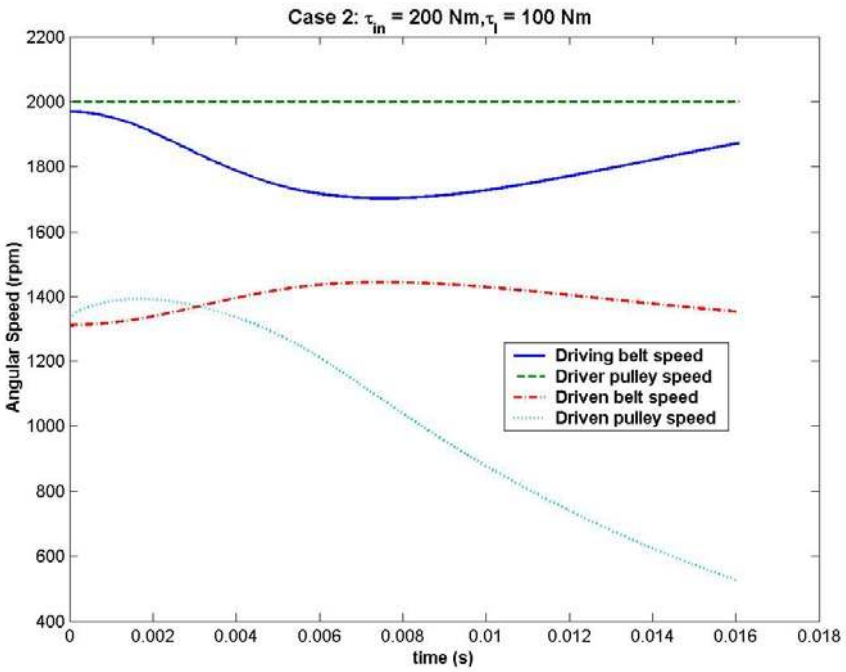

(b) Case 2

Figure 5.14: Time histories of pulley and belt speeds (contd.)

at the onset of the motion because of a higher frictional torque that prevents the driver pulley from accelerating. As the belt element gathers momentum, higher forces are generated in the belt, which overcome the load torque. Moreover, after having crossed the center of pulley-wedge expansion, the belt element moves at a lower pitch radius, which lowers the frictional torque on the belt element. This phenomenon, consequently, leads to an increase in the angular speed of the driver belt element. The belt element traversing the driven pulley wrap undergoes a complementary phenomenon. It can be observed the CVT system is able to meet the load torque successfully over a cycle as the driven pulley rotates in the forward direction. However, since the driven pulley speed decreases with time, the speed of the final drive is also reduced. In order to ensure that the CVT system meets load requirements at all times, the dynamics in the free-section of the belt needs to be modeled and the initial operating conditions need to be changed continuously with

time. It can also be observed from the plots that the angular speeds of the belt elements are higher for case 2 than for case 1. This can be attributed to higher losses encountered by the belt in case 1 in comparison to Case 2.

It is quite a common practice, as cited in most of the literature, to neglect the influence of inertial effects on the performance of a metal belt CVT. However, Srivastava *et al.* [76-77], Pfeiffer *et al.* [7, 122, 126], Fujii *et al.* [63-65] have developed detailed transient dynamic models of CVTs which highlight the role of inertial effects on the performance of a CVT system. Figure 5.15 depicts the time history of belt acceleration as a belt element moves around driver and driven pulleys for Case 1. In addition to the plots of total belt acceleration, the figure also includes time histories of belt acceleration arising from centripetal effects at steady-state.

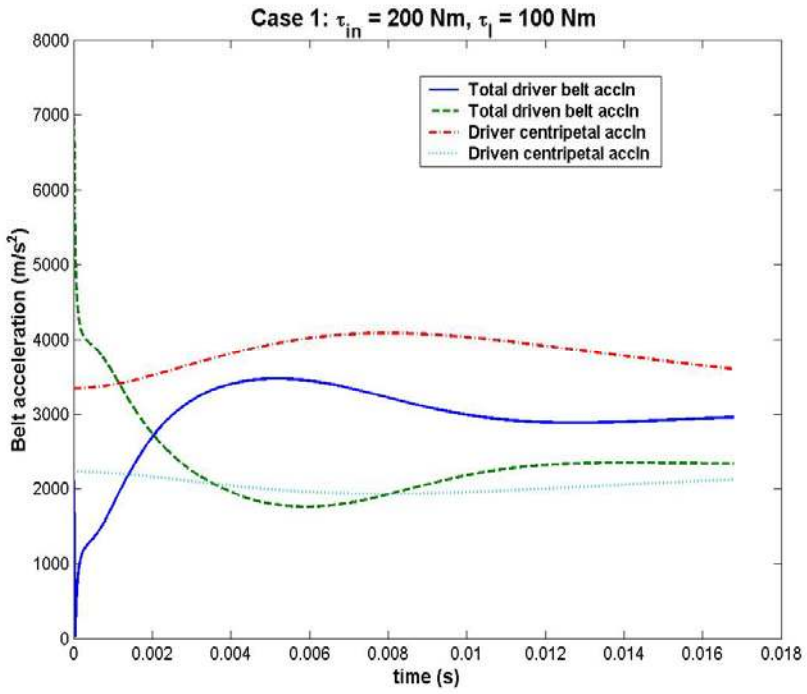

Figure 5.15: Time histories of belt acceleration – Case 1

It has been commonly assumed in the CVT models mentioned in most of the literature that the belt element only experiences centripetal acceleration. However, as can be noted

from Figure 5.15, the total belt acceleration is much different from the belt centripetal acceleration. The belt centripetal acceleration, as shown in the figure, over the driver and driven pulley wraps is computed by assuming the driver and driven pulley speeds to be unaffected by the inertial interactions between the belt and the pulley as the belt moves within the pulley sheaves. The inertial effects arising from a model based on centripetal acceleration are not able to realistically capture the dynamic interactions that possibly take place at the onset of the motion. Since acceleration directly influences the forces and vice-versa, it is necessary to predict the total belt acceleration which in turn governs the control strategies for pulley axial forces and belt slip.

Pulley Axial Force:

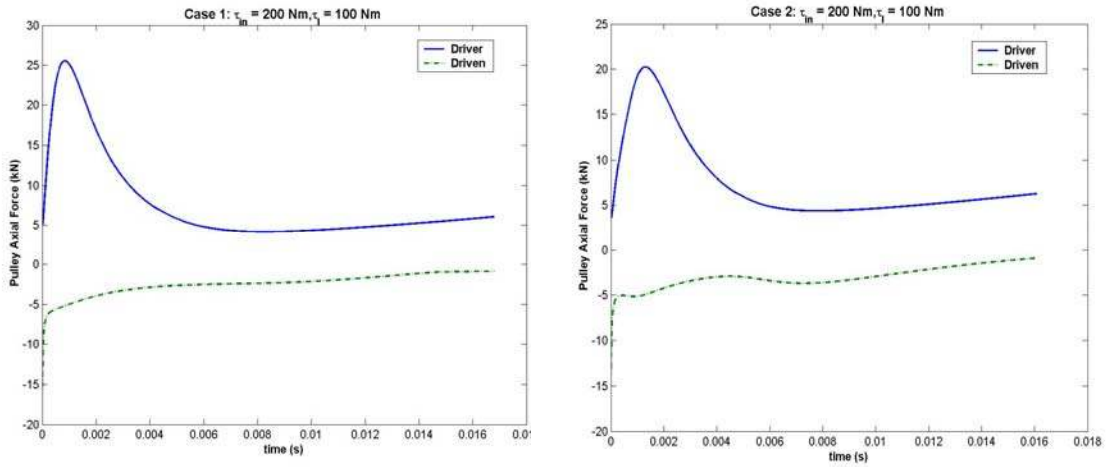

(a) Case 1 **(b) Case 2**

Figure 5.16: Time histories of pulley axial forces

Figure 5.16 illustrate the time histories of the axial forces on the driver and the driven pulleys. It can be observed from the figure that higher axial forces need to be applied to the pulley sheaves at the onset of the belt motion. Moreover, the axial force requirement required for the system under case 1 is more than that for system in Case 2. This is inevitable as the belt slips more in the radial and tangential directions for the system in

Case 1 than it does for the system in Case 2. It can also be noted from the figure that the axial forces required for varying the transmission ratio and meeting the load torque are higher for a metal V-belt CVT than for a chain CVT.

5.3.2 Influence of band pack slip

Most of the metal-belt CVT models mentioned in the literature ignore the influence of dynamic interactions between the band pack and the belt element. However, Srivastava *et al.* [76-78], Fujii *et al.* [60-65], Kobayashi *et al.* [43-44] had previously reported the influence of band pack tensile force on the torque capacity and slip behavior of the CVT system. These models were either based on steady-state experiments or quasi-static equilibrium conditions with impending slip conditions between the band and the belt element. The present belt CVT model, as described in section 3.3 of chapter 3, allows the band to slip relative to the belt element and, hence, is able to capture the influence of slip dynamics due to the inertial coupling between the band and the element on the performance of a belt-CVT system. The results discussed in this section are for the same loading conditions as mentioned before and the friction characteristic between different contacting surfaces is governed by Case 2 (i.e. boundary lubrication- type friction).

The performance of a CVT is highly dependent on the wedging action of the belt element in the pulley sheaves. The belt element, while traversing the pulley wrap, accelerates under the influence of radial and tangential forces. Owing to this wedging action, there exists a time lag between the element motion and the pulley motion. Consequently, the relative velocity between the belt element and the pulley builds up. Since the bands are allowed to slip on the surface of the belt elements, the relative

velocity between the band pack and the belt element also begins to vary with time. Figure 5.17 illustrates the time history of the belt pitch radius on the driver and driven pulleys. The figure not only depicts variations in the pitch radius of a belt element, but also illustrates variations in the radial motion of the band pack. It is to be noted from the plot that the variations in the belt pitch radius are in consonance with the constraint of constant belt length. Figure 5.18 depicts the relative velocity diagram where the components of the relative velocity vector in the radial and tangential directions are plotted with respect to each other.

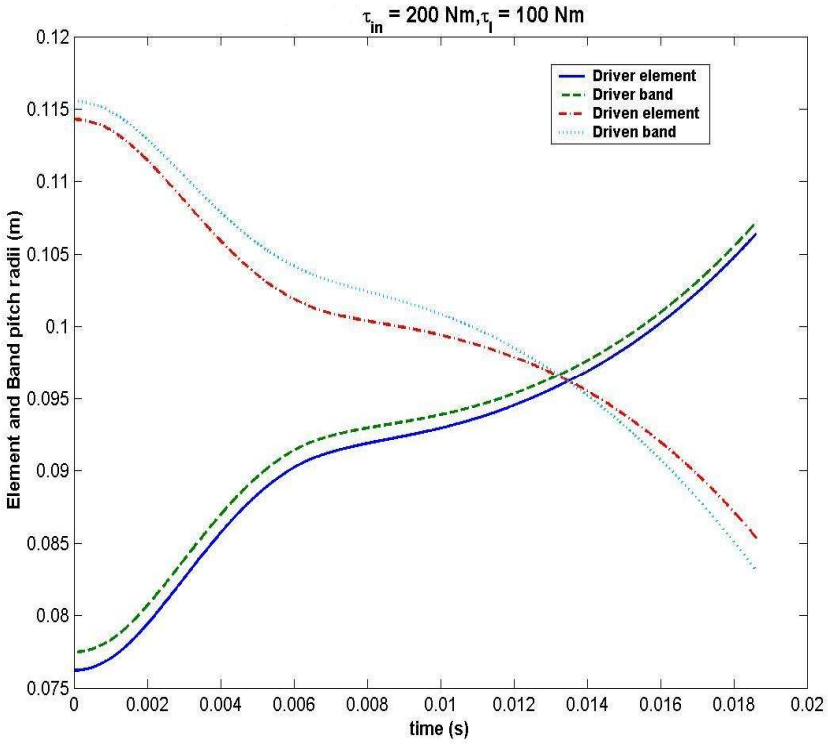

Figure 5.17: Time histories of Belt and Band Pitch Radius – Case 2

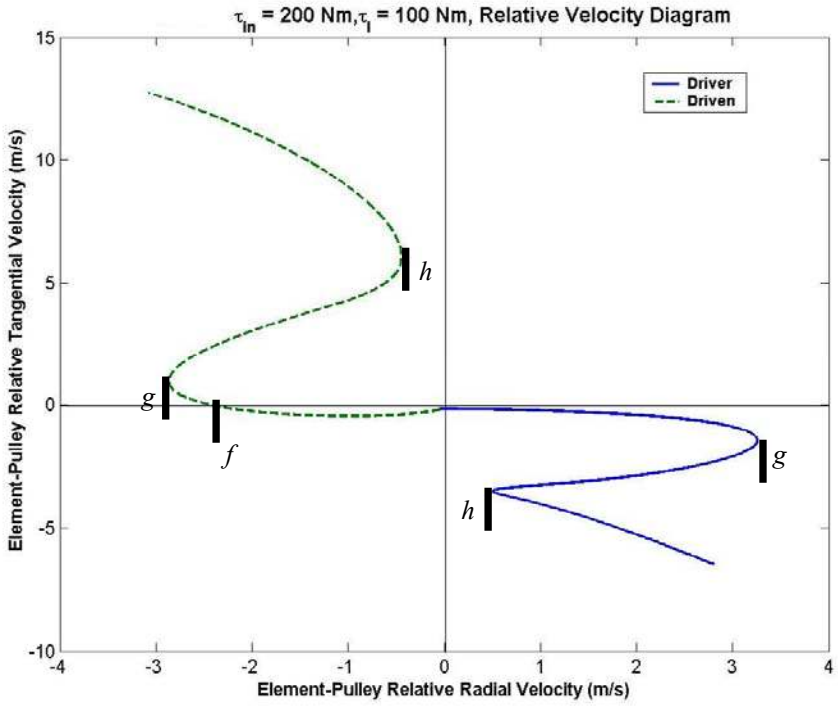

Figure 5.18: Relative velocity diagram for the belt element – Case 2

Figure 5.19 illustrates the time history of the relative velocity between the element and the band pack on the driver and driven pulleys. The relative velocity between the element and the band and between the element and the pulley depends not only on the radial and angular motions of the belt, but also on the angular motion of the pulley. It is apparent from these relative-velocity diagrams that the belt element follows a complex noncircular path over the pulley wraps. It can also be noted that these relative velocity diagrams feature certain transition points (extrema or crossing points) where the relative velocity is either maximum or minimum or completely radial (asserting the observations made by Carbone *et al.* [55], Gerbert [24]). For instance, in Figure 5.18, a belt element engaged with the driven pulley moves radially at the transition point *f*. Moreover, at the transition point *f*, the belt element moves with the same speed as that of the driven pulley.

Similarly, labels *g* and *h* in the figure signify time transitions where the radial velocity of the belt element reaches maximum and minimum respectively.

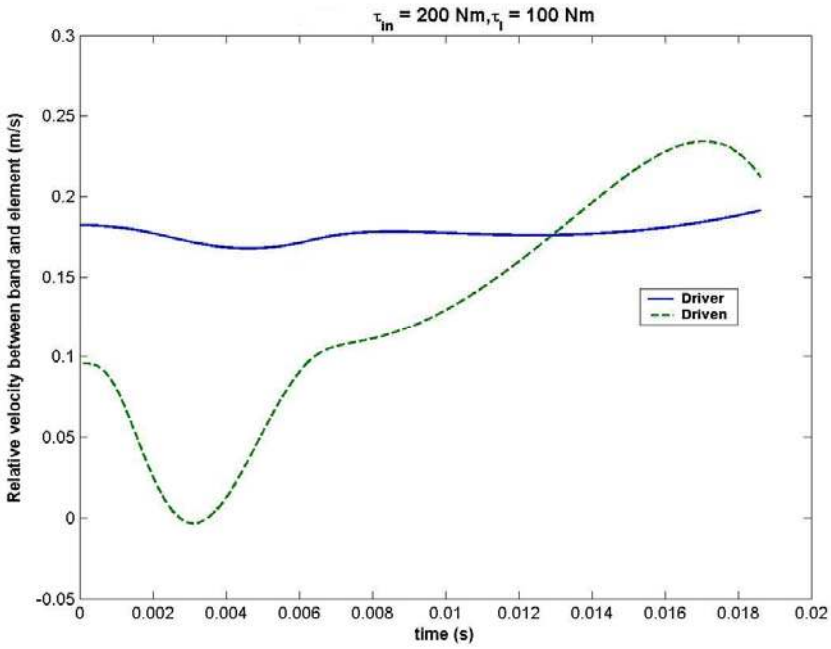

Figure 5.19: Time history of relative velocity between the band pack and the belt element – Case 2

Contrary to the results from the previous model (refer to Figure 5.11, conditions of impending slip between the band pack and the belt element), it is interesting to note that the transition points where the relative velocity between the belt element and the pulley is completely tangential disappear in this case. It can also be observed from Figure 5.19 that for most of the time, band pack travels faster than the belt element as the belt moves around the pulleys (asserting the observations made by Micklem *et al.* [6] and Sun [41]). However, there also exists a small time transition (2-4 ms in the plot) when the relative velocity between the band pack and the belt element becomes negligible, thereby inducing stiction-related dynamics on the driven pulley. The friction force between the driven band pack and the driven belt element, being continuously dependent on the relative velocity, also lowers during this time transition. Since the belt is constantly under

the influence of torque loading conditions, the relative velocity soon begins to grow due to the effects of belt acceleration. Thus, the presence of a constant load torque on the driven pulley creates a shock section at the element-band interface that enables the motion to be resumed in the slip mode. This shock section divides the pulley wrap into regions of active and inactive arcs where the inactive arc, in this case, represents that region of the pulley wrap where the band pack tensile force remains almost constant or varies at a quasi-static rate. Figure 5.20 illustrates the time history of the band pack tensile force over the driven pulley wrap. It can be noted from the plot that the band pack tensile force exhibits quasi-static variations over the region of inactive arc that spans a period of 4 ms.

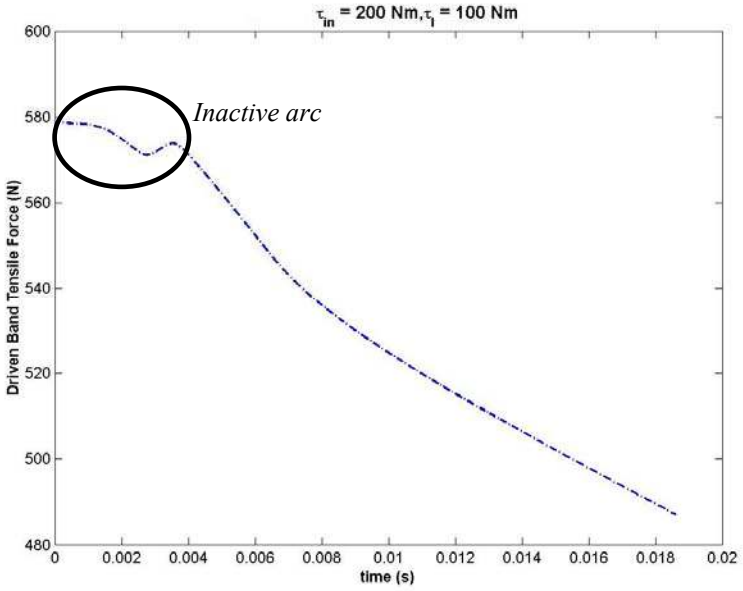

Figure 5.20: Time history of tensile force in driven band pack – Case 2

Moreover, it is interesting to note that the inactive arcs, i.e. those regions of the pulley wrap that do not contribute significantly to the torque transmission, for the band pack and the belt element differ from each other (discussed subsequently). This implies that the losses that the transmission encounters due to band and element motion can occur in

different phases as the belt traverses the pulley wraps. It is also to be noted that this shock section at the element-band interface is a newly observed phenomenon in the driven system dynamics, whereas Srivastava *et al.* [76-77], Carbone *et al.* [56], etc., previously reported shock-section related dynamics only at the belt element-driver pulley interface. Thus, the slip between the band pack and the belt element further enhances the transmission losses and reduces torque carrying capacity of the CVT system.

The compressive force arises in the belt due to the pushing action of the steel elements against each other. In addition to the push mechanism, the pulling action in the band pack also contributes to the torque transmission. The pulling action of the bands causes the tensile force in the band pack to vary, as observed in Figure 5.20. Over the driver pulley wrap, the band pack aids in positive torque transmission whereas the belt elements impede torque transmission as they transmit negative torque. However, over the driven pulley wrap, since the band pack transmits torque negatively, the belt elements transmit more torque in order to successfully meet the load requirements. The total power transmitted by the band pack under the current loading conditions, as it traverses the driver and driven pulley wraps, is higher than that generated by the belt elements. Thus, it is the combined effect of tensile force in the band pack and the compressive force in the belt elements that determine the redistribution of inter-element gaps in the belt, which consequently influences the belt slip, the torque carrying capacity, and the pulley clamping forces. Figure 5.21 illustrates the time history of the compressive force that is generated in the belt due to the push action of the steel elements. As the belt element wedges into the driver pulley sheave, the compressive force decreases as the elements begin to move at a larger pitch radius in order to maintain constant driver pulley speed. It

can be noted from the figure that the inactive arcs exist not only over the driven pulley wrap, but also over the driver pulley wrap (contrary to the result depicted by Figure 5.13).

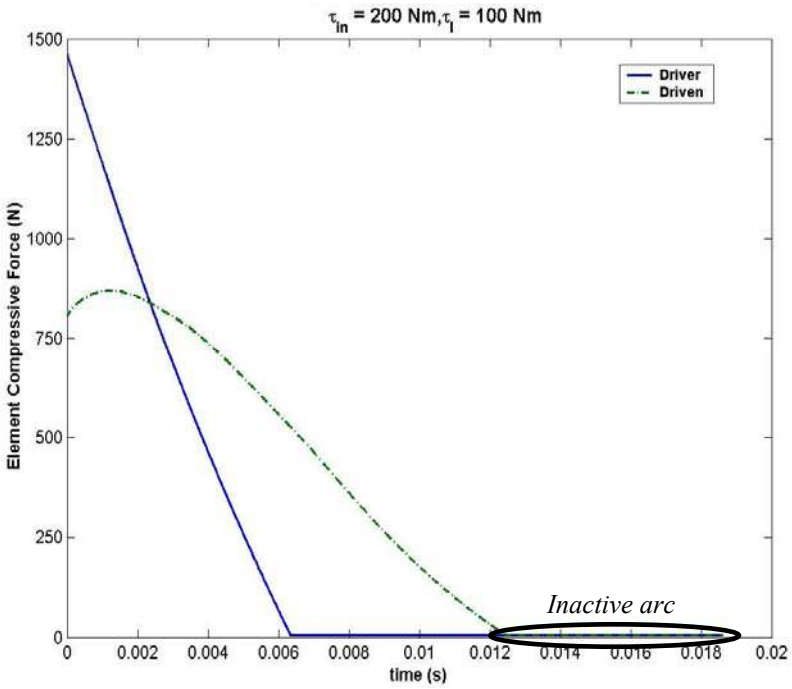

Figure 5.21: Time history of belt element compressive force – Case 2

Since the belt fails to generate enough compressive force in the region of inactive arcs, the gaps between the elements tend to redistribute among them. The redistribution of gaps among the steel elements leads to microslip phenomena in the belt [41, 43, 78], which further enhance the transmission losses. These gaps among the belt elements exist due to manufacturing or assembly defects. They can also arise with time due to wear and fatigue of the belt elements owing to the continual operation of a CVT. Moreover, since the gaps among the belt elements increase over the region of inactive arc, it is quite plausible for the band pack to traverse the pulley wrap at a pitch radius lower than that of the belt element. Figure 5.17 illustrates this phenomenon as the driven band pack begins to traverse the pulley wrap at a lower pitch radius than the driven belt element after 13-14 ms. Thus, it is not only feasible for the band pack to travel at a pitch radius higher than

that of a belt element (which is the most commonly observed phenomenon), but also to move at a lower pitch radius (owing to gap redistribution between the belt elements).

Figure 5.22 illustrates the time histories of the angular speeds of the driver and driven pulleys for both the cases. The driver pulley speed, as seen from the plots, remains constant at all times. In addition to the pulley speeds, Figure 5.23 depicts the angular speeds with which a belt element and the band pack traverse the pulley wraps. It can be observed that the angular speed of a belt element traversing the driver pulley decreases with time because of the presence of a higher frictional torque that prevents the driver pulley from accelerating. The belt element traversing the driven pulley wrap undergoes a complementary phenomenon as it moves around the pulley at a decreasing pitch radius. It can also be observed from Figure 5.23 that there is a small amount of tangential slip that continuously exists between the belt element and the band pack. However, there is a considerable amount of slip between the belt element and the pulley. The bands initially move slower than the element; however, with passage of time (i.e. about 13-14 ms), they begin to catch up with the angular speed of the element. It can be observed the CVT system is able to meet the load torque successfully over a cycle as the driven pulley rotates in the forward direction. However, since the driven pulley speed decreases with time, the speed of the final drive is also reduced. Moreover, since the losses due to slip are higher in this case, the axial forces required to actuate the pulley sheaves in order to ensure successful torque transmission are higher than those observed in the previous model, as depicted by Figure 5.24.

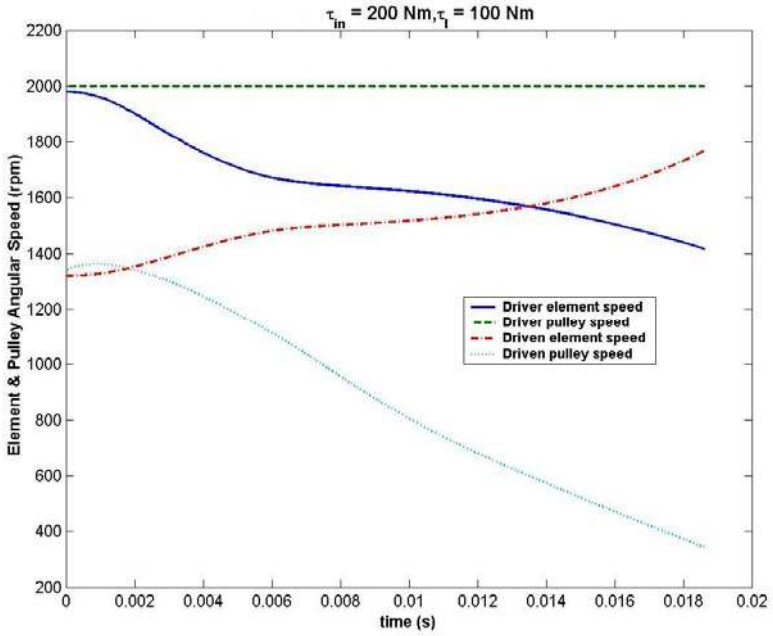

Figure 5.22: Time histories of element and pulley angular speeds – Case 2

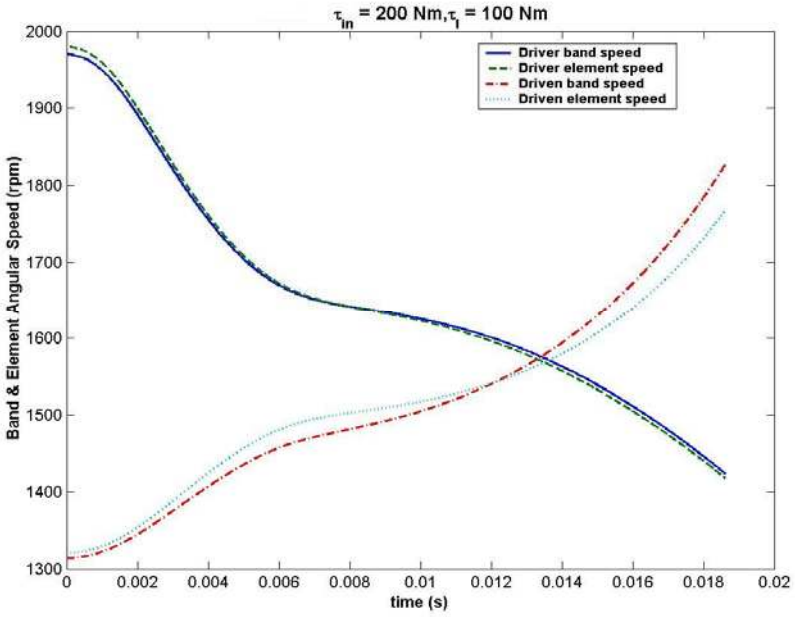

Figure 5.23: Time histories of element and band pack angular speeds – Case 2

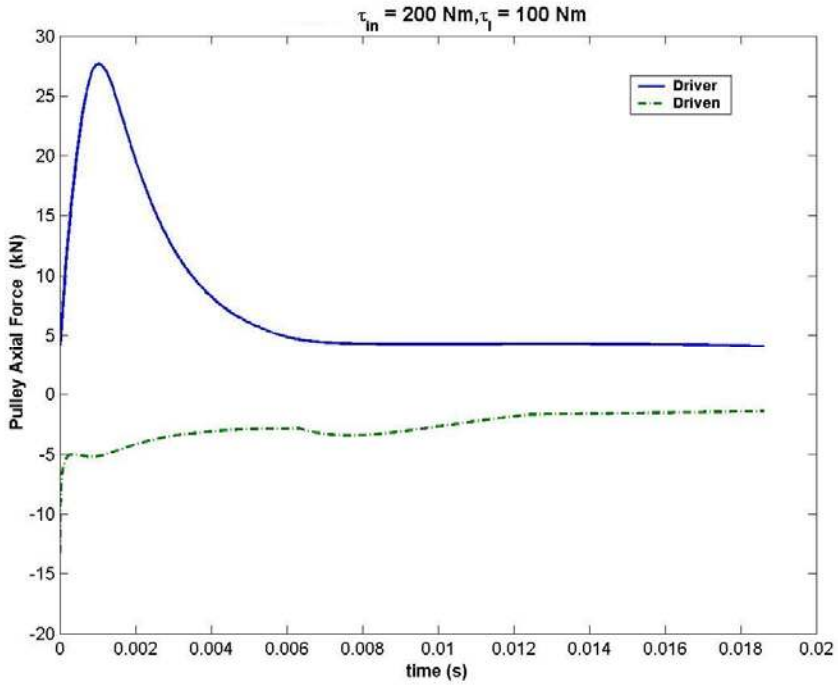

Figure 5.24: Time histories of pulley axial force – Case 2

5.4 Closure

The results describing the dynamic interactions in two different types of CVTs, chain-type and metal belt-type, have been discussed. The models were subjected to different friction characteristics that described the friction conditions between the chain/belt and the pulley sheaves. The models describe detail dynamic interactions between the various components of a CVT. The system performance was observed to vary with respect to these friction characteristics. For instance, the chain CVT model plausibly behaves chaotically under the influence of boundary lubrication- like friction characteristic. Moreover, the torque transmissibility also varies with these characteristics. The chain CVT model was able to transmit much more torque for cases 1 and 3 than for case 2. The bending of pulley sheaves further enhances the transmission losses. Although a belt CVT

guarantees faster response to the loading conditions than a chain CVT, by smoothly but rapidly varying the transmission ratio, the axial forces needed to perform such task are much higher in comparison to those for chain CVT. The torque carrying capacity for a belt CVT is also observed to be higher than that for a chain CVT under the influence of boundary-lubrication friction characteristic. The belt CVT is able to meet the load torque of 100 Nm under the friction characteristic described by case 2, whereas the chain CVT, under the same contact conditions, fails to transmit enough torque to compensate for the resisting load torque. In addition to varying friction characteristics of the contact zone, clearance between CVT components significantly affect the torque capacity and the dynamic performance of a CVT system, as was observed in the case of chain CVT model.

CHAPTER 6

CONCLUSIONS AND RECOMMENDATIONS

6.1 Concluding Remarks

Continuously variable transmission is an emerging automotive technology that offers a continuum of gear ratios between two extremes, which consequently allows better matching of the engine operating conditions to the variable driving scenarios. The CVT technology has aroused tremendous interest in the vehicle industry for the last two decades. The advantages it offers over an automatic transmission, as discussed in the introductory chapter, makes it an exciting area of research. Several automotive manufacturers have already started implementing the CVT technology, along with a planetary gear train, in the driveline of a real production vehicle. In spite of some of the associated transmission losses, a CVT indubitably plays a crucial role in the plan to improve fuel economy. Among all the different types of CVTs, metal-belt and chain CVTs are the most commonly used. These CVTs fall under the category of friction-limited drives as their performance and torque capacities rely significantly on the friction characteristic of the contacting surface between the belt/chain and the pulley sheave.

In order to maximize the potential benefits of a CVT, it is incumbent upon the researchers to understand the dynamic interactions between the various components of a CVT in detail. Two different models were developed in order to capture the detailed dynamic interactions in a metal V-belt and chain CVT system. Since belt and chain CVTs are friction-limited drives, it is crucial to study the influence of different friction

characteristics on the dynamic performance of such systems. A friction-limited drive is governed by a set-valued friction law; however, it is a common engineering practice to introduce smoothening functions to approximate the inherent discontinuity in the stick-phase of the friction law. Owing to continual operation, different components of a system usually undergo wear and fatigue, which further introduce various nonlinearities in the system. These nonlinearities, which possibly emerge as a change in the friction characteristic or as clearance between the different components, significantly affect the performance of a CVT system. The belt and the chain CVT models were subjected to torque loading conditions and different friction characteristics. The clearance effect between the chain links was modeled using a piecewise stiffness element between two links. Moreover, since the pulley sheaves in a CVT system experience high thrusts in the axial direction (i.e. along the shaft axis), a bending model based on Sferra's work [48] was incorporated in the models to capture the influence of pulley flexibility on the dynamic performance of a CVT system.

Chain CVT:

The chain CVT model was subjected to the conditions of a high input-torque on the driver pulley and a low load torque on the driven pulley. The model was also subjected to three different friction characteristics that simulated its behavior under continuous Coulomb friction characteristic, boundary lubrication-like friction, and Stribeck-like friction. It was observed that the chain CVT system, under the given loading conditions, runs most efficiently under the influence of Stribeck-friction characteristic. The links, in this case, were able to travel faster into and out of the pulley grooves; however, the axial forces on the pulley sheaves required to ensure such motion were considerably high.

Consequently, the losses due to pulley bending also increase. The chain CVT exhibited lower torque transmitting capacity under boundary lubrication-like friction characteristic. The pulley sheaves, in this case, underwent medium amplitude oscillations in addition to their gross rigid body motions. It is plausible that this phenomenon marks the onset of chaoticity in the system, which severely degrades the system performance. Moreover, the CVT system with boundary lubrication-like friction characteristic exhibited huge wedging losses as the links moved in and out of the pulleys. It was also observed during the analysis that the chain CVT system under continuous Coulomb friction characteristic ensured much smoother torque transmission in comparison to the other friction characteristics. However, it also exhibited a transmission lag as the driven pulley took time to rev-up to meet the load torque. Moreover, the losses due to slip between the chain link and the pulley are plausibly more in the case of continuous Coulomb friction characteristic than in the other cases. It was observed that increasing the clearance, ε, between the links and reducing the slope, (k_1, b_1) in the clearance model (refer to Figure 3.16) foster chaoticity in the system and also cause chattering of the pulley sheaves.

Metal V-belt CVT:

The metal V-belt CVT model was also subjected to the conditions of a high input-torque on the driver pulley and a low load torque on the driven pulley. Moreover, the driver pulley was constrained to run at a constant speed at all times. Two different friction characteristics were incorporated to simulate the model's behavior under continuous Coulomb friction regime and boundary lubrication-like friction regime. It was observed that the belt CVT had higher torque transmission capacity than the chain CVT in the case of boundary lubrication-like friction. Moreover, the axial force requirements for the belt

CVT were lower in the case of boundary lubrication-like friction than in the case of continuous Coulomb friction characteristic. This was attributed to lower slip between the belt and the pulley in the case of a system with boundary lubrication-like friction. Moreover, it was observed that the axial forces experienced by the pulley sheaves in the belt CVT were also higher than those in the chain CVT system. Since the axial forces are high, transmission losses due to pulley flexibility are also predictably high in a system with continuous Coulomb friction characteristic. The belt transmits torque due to the combined action of the tensile and compressive forces that arise in the band pack and the steel elements respectively. Inactive arcs were also found to exist over certain regions of the pulley wrap where the belt does not contribute effectively to torque transmission. The belt CVT system was also observed to transmit torque at a much lower noise level than a chain CVT. Although a belt CVT guaranteed faster response to the loading conditions than a chain CVT, by smoothly but rapidly varying the transmission ratio, the axial forces needed to perform such task were much higher in the case of a belt CVT than in the case of a chain CVT. The variations in the belt/chain pitch radii under the contact conditions of boundary lubrication (i.e. case 2) were also observed to be smaller than those under continuous Coulomb friction conditions (i.e. case 1). This can be attributed to the reduction in the force transfer due to greater lubrication-related effects in the contact zone of the belt/chain and the pulley. Moreover, it was observed that not only the inertial coupling between the belt element and the pulley, but also the slip dynamics between the band pack and the belt element significantly affect the torque transmission behavior of a belt CVT system. Owing to the slip dynamics between the band pack and the element, inactive arcs were even noted to exist on certain regions of the band pack. Thus, the

redistribution of gaps between the belt elements is dependent not only on the negligible compressive force in the inactive arc of the element-pulley wrap, but also on the low tensile force that exists in certain regions of the band pack. Since the losses associated with the band pack slip are higher, the axial forces required to meet the load torque on the driven pulley also increase. It was also noted that the torque carrying capacity of a belt CVT system is higher than that of the chain CVT drive under the same contact conditions of boundary lubrication.

It is quite evident from the aforementioned results that the performance of a belt/chain CVT varies in response to a variation in the friction characteristic of the contact zone between the belt/chain and the pulley. Since the friction characteristics used in the present research are mathematical models, it is necessary to study the influence of variations in friction parameters on the behavior of a CVT system. The three important parameters which govern the aforementioned friction characteristics are: the rising slope ($1/b, \bar{\kappa}$), the Stribeck parameter ($\bar{\lambda}, 1/v_0$), f_r (which is related to the ratio of static friction to kinetic friction), and α_0, α_1 (stiction-related parameters). It was observed that the lower the rising slope, the higher are the losses encountered in the CVT system. However, from a physics point of view, lower rising slope in the friction model does not represent the stick-phase dynamics accurately. So, in order to accurately represent the stick-slip dynamics exhibited by a CVT system, it is preferable to choose a high value for the rising slope in the friction model. The parameters, $\bar{\lambda}, 1/v_0$, aim to capture the Stribeck effects that occur in the contact-zone of the belt/chain-pulley interface due to lubrication. The lower the values of $\bar{\lambda}, 1/v_0$, the greater is the influence of lubrication on the system dynamics. The higher the value of f_r, the greater is the effect of stiction on the system

dynamics. So, under the conditions of enhanced Stribeck effects (high lubrication) and high stiction, higher axial forces are required to achieve a desired variation in the transmission-ratio (Srivastava *et al.* [163-164]).

It is evident from the results that a CVT, being a highly nonlinear system, is capable of exhibiting varied performance under different friction characteristics of the contact zone between the belt/chain and the pulley. It is also plausible for the system to undergo self-excited vibrations [105] which not only hampers the torque transmission, but also makes it difficult to be controlled. So, the performance of a CVT can vary drastically from the condition of dry friction to a fully-lubricated condition. It is thus crucial to study the influence of different friction characteristics on the performance of a CVT system. A CVT, like any other dynamical system, is susceptible to form clearances among its components, which can drastically influence its dynamic behavior. It is important to note that although an exact knowledge of the friction characteristic and clearance in a CVT system can only be obtained by real-time monitoring of both the contact patch dynamics and the motion of individual elements/links in a production CVT, these mathematical models still give profound insight into the probable behavior of a CVT system under different operating/loading conditions. This knowledge can be further exploited to design efficient CVT controllers, to analyze the noise and vibration behavior of a CVT-loaded powertrain or vehicle, to identify various loss mechanisms in a CVT, to characterize the operating regime of a CVT for maximum load carrying capacity, etc. The detailed dynamic models presented in this dissertation characterize the friction-driven CVTs in a broader context by taking into account the effects of various nonlinearities on their performance.

6.2 Recommendations for Future Work

The research reported in this dissertation significantly contributes towards providing a detailed understanding of the various dynamic interactions among the different components of a CVT. The results are not only in consensus with the physics of the transmission, but also in agreement with some of the trends mentioned in the literature on CVT dynamics. For instance, some of the results from the chain CVT model are analogous to those reported by Pfeiffer *et al.* [7, 122-123]. Some of the results obtained from the belt CVT model agree with those mentioned in literature [6, 59, 76-77]. However, since most of the newly observed phenomena, as reported in this dissertation, are based on the theoretical models of belt and chain CVT drives, an experimental investigation is necessary to corroborate the trends associated with such friction- and clearance- related dynamics. Moreover, a more accurate analysis of the torque transmissibility of a belt/chain CVT system can be done by modeling the belt/links/pulleys as elastic bodies under unilateral contact, accounting for spatial orientation of the chain links, and developing a finite element model for elastic deformations in the pulley sheave. It is to be noted that the results from the belt CVT model are valid for one cycle i.e. till a belt element moves past the exit of either of the two pulleys. The continuity of the belt can be incorporated in the present model by modeling the dynamics in the free-section of the belt. Extensive literature is available on vibrations of belt [103], however, a detail vibration analysis of the coupled pulley and metal-belt/chain motion is still keenly being pursued. As mentioned earlier, since literature on vibrations and noise of CVT systems is scarce [95, 98, 132], the present models could be further extended to understand the vibration-related effects in a CVT

drive. Although the friction characteristics mentioned in the present models are able to capture the effects of stiction and lubrication, a more accurate description of friction can be obtained by using the theory of Elastohydrodynamic lubrication [165], which relates the coefficient of friction not only to the relative velocity between the two surfaces, but also to the normal force (or pressure) between those two surfaces. It is to be noted that the friction models presented in this research are static-based friction models as the stiction phase of the motion is represented approximately by the conditions of negligible relative velocity. A more accurate analysis of the sticking-phase contact conditions can be done using a dynamic friction model, like Lugre friction model, that accounts for not only the effects of relative velocity, but also the effects of relative acceleration between two contacting surfaces. Moreover, these detailed transient dynamic models of belt/chain CVT (as discussed in this research) can be further exploited to characterize a CVT drive from a system (or macroscopic) point of view, which may enable easy integration into a powertrain/vehicle model for future research studies on fuel economy and vehicle efficiency. These recommendations, if incorporated along with the present concepts, will provide a profound insight towards understanding or identifying important parameters for improving the CVT efficiency, and consequently the vehicle performance.

APPENDICES

Appendix A

<u>MATLAB codes for running the SIMULINK models of metal V-belt CVT</u>

The following two MATLAB files are used as model initialization functions for the SIMULINK models of belt CVT:

- **design_variables.m** provide the initial operating conditions (compressive and tensile forces at the pulley inlets) for the model to meet load torque requirements
- **input_data.m** provide the parameter values and loading conditions for the model

There are 3 SIMULINK models for the belt CVT

- **<u>MODEL 1</u>: cvt_belt_v2.mdl** with constant driver angular speed + time-rates of bending-model parameters + continuous Coulomb friction model
- **<u>MODEL 2</u>: cvt_belt_v2_B.mdl** with constant driver angular speed + time-rates of bending-model parameters + boundary lubrication-like friction model (Case-2 friction, *refer to the text*)
- **<u>MODEL 3</u>: cvt_belt_band_B1.mdl** with constant driver angular speed + time-rates of bending- model parameters + boundary lubrication-like friction model (Case-2 friction, *refer to the text*) + slip between band pack and belt element

```
%%%%%%%%%%%%%%%%%%%%%%%%%%%%%%%%%%%%%%%%%%
% input_data.m
format long
clc                 % Comment it out if running GA
clear all           % Comment it out if running GA
time_step =   1e-5;            % 1e-5 for simulation, 1e-4 for GA
```

```
rpm_init =      2000;                % initial driver pulley speed in rpm

Stop_time  =  1.0;

pi =           3.14159265358979;

in2m =         2.54/100;

rpm2rads =     pi/30;

center_dist = 0.5;       % in meters


half_sheave = 15*pi/180;       %  non-deformed pulley half sheave angle (in radians)

mu_a_bp = 0.25;        %  friction between band pack and element (for MODELS 1 and 2)


Driver_inertia = 0.01452;       % Pulley inertia (kg-m^2)

Driven_inertia = 0.03275;


% Friction between the element and pulley

% MODEL 1 friction parameters

% (Uncomment the following 3 lines if you want to run MODEL 1)

% a = 0.0003;              % initial friction offset

% b = 0.05;                % slope with which friction rises

% mu_b_sat = 0.25;    % saturation limit of friction

%

% MODEL 2 friction parameters

% (Uncomment the following 4 lines if you want to run MODEL 2)

% mu_b_sat = 0.25;
```

```
% a = 4;          % Stribeck-slope of friction
% b = 250;        % Rising slope of friction
% ff = 1.85;      % relates static to kinetic friction
%
% MODEL 3 friction parameters
%  Lubrication-related friction between the element and the pulley, and between the
%  element and the band pack
% (Uncomment the following 8 lines if you want to run MODEL 3)
% mu_b_sat = 0.25;
% a = 2;
% b = 250;
% ff = 1.3;
% a_bp = 10;
% b_bp = 250;
% ff_bp = 1.15;
% mu_a_sat = 0.25;
%
density_bp = 1.5;        % linear mass density of band pack
density_ele = 2.0;       % linear density of element
rho_red = (density_ele+density_bp)/(density_ele*density_bp);
del_sheave_init = 0.001;
% del_sheave = 0.001;
```

```
const1 = (1+(cos(half_sheave))^2)/(sin(half_sheave)*cos(half_sheave));
%
% Driver pulley loading and initial conditions
pulley_dot_init = rpm_init*rpm2rads;
theta_dot_init = 0.99*pulley_dot_init;
gam_dot_init = 0.985*pulley_dot_init;
theta_init =  0.0001;
gam_init = 0.00005;
r_dot_init =    -0.001;
r1_dot_init =  -0.001;
r_init =        3*in2m;    %  in inches
r1_init =       3.05*in2m;
N_init = 1000;            % in N
F_init = 1000;
Input_torque = 200;   % in Nm
%
% Driven pulley loading and initial conditions
r_dot2_init = 0.001;
r1_dot2_init = 0.001;
r2_init = 4.5*in2m;
r1_2_init = 4.55*in2m;
pulley2_dot_init = pulley_dot_init*r_init/r2_init;
theta_dot2_init = 0.99*pulley2_dot_init;
```

```
gam_dot2_init = 0.985*pulley2_dot_init;

theta2_init = 0.0001;

gam2_init = 0.00005;

N2_init = 2750;

F2_init = 2250;

Load_torq = 100;   % in Nm

%%%%%%%%%%%%%%%%%%%%%%%%%%%%%%%%%%%%%%%%%%%%%%%%%

% design_variables.m

% This file is obtained using a Genetic-Algorithm for the parameters and loading

% conditions mentioned in input_data.m

% Driver initial inlet operating conditions

T_init = 2019;

Q_init = 1461;

% Driven initial inlet operating conditions

Q2_init = 802;

T2_init = 578;
```

Appendix B

<u>MATLAB codes for implementing Genetic Algorithm on a metal V-belt CVT model</u>

As mentioned in the text and by Srivastava *et al.* [77], the belt CVT model requires a feasible set of initial operating conditions (pretension and precompression) for the belt to traverse the entire pulley wrap and successfully meet the load torque requirements. The subsequent pages outline the MATLAB-based GA (Genetic Algorithm) codes. Out of these, the most important ones are "**prega.m**" and "**fct.m**", where the users can make changes to the objective function, the fitness function, and the number of optimization/design variables. The main program to be executed for implementing the GA on belt CVT model is "**prega**".

```
%%%%%%%%%%%%%%%%%%%%%%%%%%%%%%%%%%%%%%%%%%%%%%
% prega.m
%
clear all
nvars = 4;      % Number of design variables
nbits(1) = 11;
nbits(2) = 11;
nbits(3) = 11;
nbits(4) = 11;
N = 50;         % Number of individuals in a population
max_generations = 120;
freq_conv_check = 20;
mutation_parameter = 0.15;
```

```
epsilon = 0.0001;

gene_size = 0;
for i=1:nvars
   gene_size = gene_size+nbits(i);
end

[evolution,pop_dec] =
GA(nvars,nbits,gene_size,N,mutation_parameter,max_generations,epsilon,
freq_conv_check)

plot(evolution)

fid = fopen('results.m','w');
s = size(evolution);
fprintf(fid,'%s\n','Number of generations = ');
fprintf(fid,'%s\n',num2str(s(1)));
fprintf(fid,'%s\n','evolution = ');
for i=1:s(1)
   fprintf(fid,'%s\n',num2str(evolution(i,:)));
end
fprintf(fid,'%s\n','population = ');
```

```
for i=1:N
   fprintf(fid,'%s\n',num2str(pop_dec(i,:)));
end
fclose(fid);
%%%%%%%%%%%%%%%%%%%%%%%%%%%%%%%%%%%%%%%%%%%%%%%%%%%%%%%%%%%%%%%%%%%%%%%%
% fct.m
function y = fct(x)
clear design_variables
if (x(1) > 10 & x(2) > 10 & x(3) > 10 & x(4) > 10)
        fid = fopen('design_variables.m','w');
        fprintf(fid,'T_init = %s;\n',num2str(x(1)));
        fprintf(fid,'Q_init = %s;\n',num2str(x(2)));
        fprintf(fid,'Q2_init = %s;\n',num2str(x(3)));
        fprintf(fid,'T2_init = %s;\n',num2str(x(4)));
        fclose(fid);
        open_system('cvt_belt_band_B1');  % input SIMULINK model file name
        [timeVector,stateVector,outputVector] = sim('cvt_belt_band_B1');
        y = 1/length(R);
else
        y = 1000000;
end
%%%%%%%%%%%%%%%%%%%%%%%%%%%%%%%%%%%%%%%%%%%%%%%%%%%%%%%%%%%%%%%%%%%%%%%%
% ga.m
```

```
function [evolution,pop_dec] =
GA(nvars,nbits,gene_size,N,mutation_parameter,max_generations,epsilon,freq_conv_ch
eck)
%
% Initialize population
%
[pop_bin,pop_dec] = initialize_pop(N,gene_size,nbits);
pop_dec
%---------------------------
% START EVOLUTION
%---------------------------
convergence = 0;
count = 1
evolution = [];
while (convergence == 0 & count < max_generations)
%
% Analyze population
%
[fitness,keep_track] = analyze(pop_dec,nbits);
evolution = [evolution;keep_track];
%
% SELECTION: Select individuals to fill up the mating pool based on merit
pool_1 = selection(pop_bin,fitness);
```

```
% CROSSOVER (one-point crossover)
pool_2 = crossover(pool_1);
%
% MUTATION
pool_3 = mutation(pool_2,mutation_parameter);


for i=1:N
   pop_dec(i,1:nvars) = bin2dec(pool_3(i,:),gene_size,nbits);
end


pop_bin = pool_3;
count = count+1;
%
% Convergence check
if (mod(count,freq_conv_check) == 0)
   pop_dec
   [num2str(count),' / ',num2str(max_generations)]
   convergence = convergence_check(pop_dec,epsilon);
end
end
convergence
```

%%% *For brevity purposes, the implementation of the standard algorithms for mutation, crossover, etc. are not included in the text*

Appendix C

Visual C++ - based modules for the simulation of a chain CVT model

```
// Bolt class:
#ifndef BOLT_H
#define BOLT_H
#pragma warning( disable : 4786 )
class Pulley;
class Link;
class Spring;
#include "Rigid.h"
class Bolt
{
protected:
        double m_K;
        //double m_orgLength;
        Pulley *m_pPulley[2];
        Link *m_pLink;
        Spring *m_pSpring;
        int m_refIndex;
        struct Vector m_relativeVelocity;
        struct Vector m_frictionForce;
        double m_magnitude;
        double m_radialRelaVelocity;
```

```
        double m_tangentialRelaVelocity;
        double m_radialRelaFriction;
        double m_tangentialRelaFriction;
        double m_slipAngle;
        double m_pulleyDeformPhi;
        double m_currMu;
public:
        Bolt(double K, Link *m_pLink, int refIndex, Spring *pSping = NULL);
        ~Bolt(){};
public:
        double m_dist2Pulley[2];
public:
        void SetSpring(Spring *pSpring);
        void SetPulley(Pulley *pPulley1, Pulley *pPulley2);
        void SetDeformPulleyPhi(double phi)
        {
                m_pulleyDeformPhi = phi;
        }
        void GetForce(struct Vector *pForce, Pulley **contactPulley);
        struct Vector *GetFrictionForce();
        struct Vector *GetRelativeVelocity();
```

```
        void GetRelativeVelocity(double *radial, double *tangential)
        {
                *radial = m_radialRelaVelocity;
                *tangential = m_tangentialRelaVelocity;
        }
        void GetRelativeFriction(double *radial, double *tangential)
        {
                *radial = m_radialRelaFriction;
                *tangential = m_tangentialRelaFriction;
        }
        double GetNormalForce();
        double GetSlipAngle() { return m_slipAngle; }
        double GetMu() { return m_currMu; }
        void GetPosition(struct Vector *pos);
protected:
        void CalRadialTangentialRelative(
                Vector *center,
                Vector *pos,
                double dist,
                Vector *relaVector,
                double *radialRela,
                double *tangentialRela);
                double CalSlipAngle(double radial, double tangential);
```

```
};
#endif
////////////////////////////////////////////////////////////////////////////////////////////////////////////////////////
// CVT Class:
#ifndef CVT_H
#define CVT_H


class Link;
class Bolt;
class Pulley;
class Spring;
class EventCenter;
struct LinkList
{
	struct LinkList *pNext;
	Link *pLink;
};
struct SpringList
{
	struct SpringList *pNext;
	Spring *pSpring;
};
```

```
struct BoltList
{
	struct BoltList *pNext;
	Bolt *pBolt;
};

class CVT
{
protected:
	int m_linkNum;
	Pulley *m_pPulley[2];
	struct LinkList *m_pLinkList;
	struct SpringList *m_pSpringList;
	struct BoltList *m_pBoltList;
	EventCenter *m_eventCenter;
public:
	CVT();
	~CVT();
public:
	void AddPulley(Pulley *pPulley1, Pulley *pPulley2);
	void AddLink(Link *pLink);
	void AddSpring(Spring *pSpring);
	void AddBolt(Bolt *pBolt);
```

```
        Pulley* GetPulley(int index);

        int GetLinkNum();
        LONG GetFirstLink(Link **pLink);
        LONG GetNextLink(LONG index,  Link **pLink);

        LONG GetFirstBolt(Bolt **);
        LONG GetNextBolt(LONG index, Bolt **);

        LONG GetFirstSpring(Spring **);
        LONG GetNextSpring(LONG index, Spring **);
public:
        void SetRotateSpeed(int index, double velocity);
        void InputTorque(int index, double torque);
        void OutputTorque(int index, double torque);

        void MovePulley(int index, double x, double y, double z);
        void Update();
        void Step(double time);
        //void Save(FILE *out);
        //void Read(FILE *in);
        double GetCenterDistance();
```

```
        //void RecordLinkInfo(FILE *fp, char type, double time, int index);
        /*interface for the user*/
        double GetOutputAngle(){    return 0.0; }
        double GetOutputVelocity() {          return 0.0 ; }
};
#endif
////////////////////////////////////////////////////////////////////////////////////////////////////////////////////////
// CVT Parameters Listener Class
#include "factory.h"
#include "deformhelper.h"

class CVTCfgParamListener : public ParamListener
{
protected:
        CVTCreateParam m_param;
        DeformParam m_deformParam;
        int m_deformParamSet;
public:
        CVTCfgParamListener();
        virtual ~CVTCfgParamListener();
public:
        virtual int NewItemAttribute(OLECHAR *nodeName, OLECHAR *attrName,
OLECHAR *value);
```

```
        CVTCreateParam *GetFilledParam() { return &m_param; }
        DeformParam *GetDeformParam() { if (m_deformParamSet) return
&m_deformParam; else return NULL; }
protected:
        int FillLinkParam(OLECHAR *attrName, OLECHAR *value);
        int FillSpringParam(OLECHAR *attrName, OLECHAR *value);
        int FillPulley1Param(OLECHAR *attrName, OLECHAR *value);
        int FillPulley2Param(OLECHAR *attrName, OLECHAR *value);
        int FillBoltParam(OLECHAR *attrName, OLECHAR *value);
        int FillCfgParam(OLECHAR *attrName, OLECHAR *value);
        int FillSimulationParam(OLECHAR *attrName, OLECHAR *value);
        int FillTorqueParam(OLECHAR *attrName, OLECHAR *value);
        int CVTCfgParamListener::FillDeformParam(OLECHAR *attrName, OLECHAR
*value);
};
#endif
////////////////////////////////////////////////////////////////////////////////////////////////////////////////////
// CVT Create Parameter Class
#ifndef OBJECT_FACTORY_H
#define OBJECT_FACTORY_H
#include <list>
#include <vector>
```

```
class Pulley;
class Link;
class Spring;
class Bolt;
class CVT;
class CVTFactory;
// #include <fstream.h>
#define MAX_LINK_NUMBER       200
#define CONTINUOUS_COULOMB_FRICTION_MODEL 0
#define SELF_EXCITED_FRICTION_MODEL                1
#define SELF_EXCITED_FRICTION_MODEL2      2
#define LUGRE_FRICTION_MODEL              3
#define ELASTO_FRICTION_MODEL             4
#define FACTORY_EVENT_ON_CVT_CREATED      0

struct CVTCreateParam
{
        int linkNum;
        double linkWidth, linkLength, linkMass, linkJ, boltDist2Center;
        double springK, springB, springK2, springB2, springK3, springB3;
        double radius1, minRadius1, pulleyPhi1;
        double radius2, minRadius2, pulleyPhi2;
        double pulleyMass1, pulleyMass2, pulleyJ1, pulleyJ2;
```

```
        double centerDistance;
        double mu, mu_a, mu_b;
        double boltK;
        int IsLinearSpring;
        double nonLinearSpringClearance, nonLinearSpringClearance2;
        unsigned char simuMode;
        unsigned char frictionModel;
        double inputTorque, outputTorque;
        double inputSpeed;
        double aa, bb, ff;
        double cc, dd;
        // parameters for Lugre friction model
        double sigma0, sigma2;
        double mus, muk, vs;
        // parameters for elasto friction modeml
        double sigma1, fc, fe, zba;
};
class CVTFactoryEvent
{
public:
   virtual void OnCVTFactoryEvent(unsigned long id, CVTFactory *sender, void
*param) = 0;
};
```

```
class CVTFactory
{
protected:
        struct CVTCreateParam m_CVTParam;
   std::vector<std::list<CVTFactoryEvent *> *> m_EventListenerList;
public:
        CVTFactory();
        ~CVTFactory();
public:
        CVT *CreateCVT(struct CVTCreateParam *param, struct DeformParam
*deformParam);
        //CVT *CreateCVTFromStream(FILE *in);
        void ArrangeCVTInitialPosition(CVT * pCVT, struct CVTCreateParam *param);
        struct CVTCreateParam GetCVTCreateParam() { return m_CVTParam; }
         void RegisterCVTFactoryEvent(unsigned long EventID, CVTFactoryEvent
*listener);
protected:
        void IsInPulley(int pulleyIndex, Link *pLink);
        void ArrangeCVTInitialPosition2(CVT *pCVT, struct CVTCreateParam
*param);
        void CalculateInitialAngle(CVT *pCVT, struct CVTCreateParam *param);
```

```
        void CalculateNextPosition(struct Vector *pos, double *angle, CVT *pCVT,
struct CVTCreateParam *param);
        void TestAndSetState(CVT *pCVT, struct CVTCreateParam *param);
protected:
        double m_beltMiddleAngle;
        double m_pulleyContactAngle[2][2];
        int m_initialized;
        struct Vector *m_linkPrePos;
        double m_linkPreAngle;
        int m_linkState;
        double m_linkCalculatedLength;
};
#endif
////////////////////////////////////////////////////////////////////////////////////////////////////////////////////
// Classes related to CVT Events
// EventCenter.h: interface for the EventCenter class.
#if
!defined(AFX_EVENTCENTER_H__4B724A2F_9C73_475E_BB18_0F30C5E4ED90_
_INCLUDED_)
#define
AFX_EVENTCENTER_H__4B724A2F_9C73_475E_BB18_0F30C5E4ED90__INCLU
DED_
```

```
#if _MSC_VER > 1000
#pragma once
#endif // _MSC_VER > 1000

#pragma warning( disable : 4786 )
#include <map>
#include <list>
class RigidBody;

#define LINK_ENTER_DRIVING_PULLEY		100
#define LINK_LEAVE_DRIVING_PULLEY		101
#define LINK_ENTER_DRIVEN_PULLEY		102
#define LINK_LEAVE_DRIVEN_PULLEY		103
class CVTEvent
{
public:
	CVTEvent(RigidBody *sender, int msg, void *arg)
	{
		m_sender = sender;
		m_msg = msg;
		m_arg = arg;
	}
```

```
protected:
        RigidBody *m_sender;
        int m_msg;
        void *m_arg;

public:
        RigidBody *GetSender() { return m_sender; }
        int GetMsg() { return m_msg; }
        void *GetArgument() { return m_arg;}
};

class CVTEventObserver
{
public:
        virtual int Notify(CVTEvent *pEvent) = 0;
};

class EventCenter
{
private:
        EventCenter();
        virtual ~EventCenter();
```

```
public:
        static EventCenter *CreateInstance();
        int Delete();
public:
        int DispatchEvent(CVTEvent *event);
        int RegisterObserver(int msg, CVTEventObserver *pObserver);
protected:
        static EventCenter *m_this;
        std::map<int, std::list<CVTEventObserver *>* >m_listeners;
        static int m_ref;
};
#endif
//////////////////////////////////////////////////////////////////////////////////////////////////////////////////////
// CVTInput.h: interface for the CVTInput class.
//
#if
!defined(AFX_CVTINPUT_H__FD7A3A3E_1FAD_4381_AE43_83E59377837A__IN
CLUDED_)
#define
AFX_CVTINPUT_H__FD7A3A3E_1FAD_4381_AE43_83E59377837A__INCLUDED
_

#if _MSC_VER > 1000
```

```
#pragma once
#endif // _MSC_VER > 1000

#include "CVTSimulator.h"

class CVTInput : public CVTSimuObserver
{
public:
	CVTInput(double inputTorque, double outputTorque)
	{
		m_input = inputTorque;
		m_output = outputTorque;
	}

	virtual ~CVTInput();
public:
	virtual int Operation(CVT *pCVT, double time);
protected:
	double m_input, m_output;
};
#endif
//////////////////////////////////////////////////////////////////////////////////////////////////////////////////////
// CVTPositionRecorder.h: interface for the CVTPositionRecorder class.
```

```
#if
!defined(AFX_CVTPOSITIONRECORDER_H__308AFA03_33B0_4789_BEED_84BE
389D6E97__INCLUDED_)
#define
AFX_CVTPOSITIONRECORDER_H__308AFA03_33B0_4789_BEED_84BE389D6E
97__INCLUDED_

#if _MSC_VER > 1000
#pragma once
#endif // _MSC_VER > 1000

#include "COMPONENT\CVTSimulator.h"

class CVTPositionRecorder : public CVTSimuObserver
{
protected:
        FILE *m_OutputFile;
        double m_NextTime;
        double m_Interval;
public:
        CVTPositionRecorder(const char *fileName, double interval);
        virtual ~CVTPositionRecorder();
```

```
public:
        virtual int Operation(CVT *pCVT, double time);
};
#endif
//////////////////////////////////////////////////////////////////////////////////////////////////////////////////////
// CVTSimulator.h: interface for the CVTSimulator class.
//
#if
!defined(AFX_CVTSIMULATOR_H__9DEAD3BB_A0E2_4F53_BF82_5224F31EEC3
0__INCLUDED_)
#define
AFX_CVTSIMULATOR_H__9DEAD3BB_A0E2_4F53_BF82_5224F31EEC30__INC
LUDED_
#if _MSC_VER > 1000
#pragma once
#endif // _MSC_VER > 1000
#include <list>

class CVT;
class CVTSimuObserver
{
public:
        virtual ~CVTSimuObserver() {};
```

```
public:
        virtual int Operation(CVT *pCVT, double time) = 0;
};
class CVTSimulator
{
public:
        CVTSimulator(CVT *pCVT);
        virtual ~CVTSimulator();
public:
        void Simulate(double initTime = 0.05, double step = 0.01, double time = 10.0);
public:
        int RegisterPreSimuObserver(CVTSimuObserver *pObserver);
        int RegisterPostSimuObserver(CVTSimuObserver *pObserver);
protected:
        std::list<CVTSimuObserver *> m_preList;
        std::list<CVTSimuObserver *> m_postList;
        CVT *m_pCVT;
protected:
        int PostSimuOperation(double t);
        int PreSimuOperation(double t);
};
#endif
////////////////////////////////////////////////////////////////////////////////////////////////////////////////////////
```

```
// CVTStateRecorder.h: interface for the CVTStateRecorder class.
//
#if
!defined(AFX_CVTSTATERECORDER_H__3F101D6C_9DAE_47ED_9DAD_1A9BF
2A3A067__INCLUDED_)
#define
AFX_CVTSTATERECORDER_H__3F101D6C_9DAE_47ED_9DAD_1A9BF2A3A06
7__INCLUDED_

#if _MSC_VER > 1000
#pragma once
#endif // _MSC_VER > 1000

#include "CVTSimulator.h"
#include <list>

struct CVTStat
{
        double m_pulleyAxleForce[2];
        double m_pulleyTorque[2];
        double m_pulleyRotateSpeed[2];
        double m_toPulleyDist[2];
        double m_linkForce;
```

```
        double m_time;
        double m_relativeVelocity;
        double m_friction;
        double m_mu;
        double m_normalForce;
        double m_springForce;
        double m_radialRelaVelocity;
        double m_tangentialRelaVelocity;
        double m_radialRelaFriction;
        double m_tangentialFriction;
        double m_relaVelX;
        double m_relaVelY;

        double m_tension;
};
class CVTStateRecorder : public CVTSimuObserver
{
public:
        CVTStateRecorder(double recordInterval);
        virtual ~CVTStateRecorder();
public:
        virtual int Operation(CVT *pCVT, double time);
        std::list<struct CVTStat *> *GetStateList() { return &m_statList; }
```

```
protected:
        double m_interval;
        std::list<struct CVTStat *> m_statList;
        double m_nextTime;
};
#endif
////////////////////////////////////////////////////////////////////////////////////////////////////////////////////
// Class for different friction models
// FrictionModel.h: interface for the FrictionModel class.
//
#if
!defined(AFX_FRICTIONMODEL_H__4C31864D_2F9D_48C1_A53F_B5C1B776CB
FB__INCLUDED_)
#define
AFX_FRICTIONMODEL_H__4C31864D_2F9D_48C1_A53F_B5C1B776CBFB__INC
LUDED_

#if _MSC_VER > 1000
#pragma once
#endif // _MSC_VER > 1000

#include "factory.h"
class Link;
```

```
class FrictionModel
{
protected:
   unsigned long m_Ref;
public:
   FrictionModel()
   {
      m_Ref = 0;
   }
public:
   unsigned long AddRef()
   {
      m_Ref++;
      return m_Ref;
   }
   unsigned long Release()
   {
      unsigned long ref;
      if (m_Ref != 0)
         m_Ref--;
      ref = m_Ref;
      if (m_Ref == 0)
         delete this;
```

```
        return ref;
    }
protected:
        virtual ~FrictionModel(){};
public:
        virtual double CalculateMu(double relaVelocity, Link *link) = 0;
        virtual double CalculateMu(double relaVx, double relaVy, Link *link);
};

class CoulombFrictionModel : public FrictionModel
{
protected:
        double m_a, m_b, m_mu;
public:
        CoulombFrictionModel(double a, double b, double mu)
        {
                m_a = a;
                m_b = b;
                m_mu = mu;
        }
        virtual double CalculateMu(double relaVelocity, Link *link);
};
```

```
class SelfExcitedFrictionModel : public FrictionModel
{
protected:
	double m_a, m_b, m_f, m_mu;
public:
	SelfExcitedFrictionModel(double a, double b, double f, double mu)
	{
		m_a = a;
		m_b = b;
		m_f = f;
		m_mu = mu;
	}
	virtual double CalculateMu(double relaVelocity, Link *link);
};

class SelfExcitedFrictionModel2 : public FrictionModel
{
protected:
	double m_a, m_b, m_c, m_d;
public:
	SelfExcitedFrictionModel2(double a, double b, double c, double d)
	{
		m_a = a;
```

```
            m_b = b;
            m_c = c;
            m_d = d;
        }
        virtual double CalculateMu(double relaVelocity, Link *link);
};

class FrictionModelFactory
{
private:
   static FrictionModel *m_FrictionModel[10];
public:
        static FrictionModel *CreateFrictionModel(CVTFactory *factory,
CVTCreateParam *param);
};
#endif
////////////////////////////////////////////////////////////////////////////////////////////////////////////////////
// Class for Spring
#ifndef LINEAR_SPRING_H
#define LINEAR_SPRING_H

#include "spring.h"
class LinearSpring : public Spring
```

```
{
protected:
        double m_K, m_orgLength, m_B;
        struct
        {
                RigidBody *pRigid;
                int refPoint;
        }m_rigid[2];
public:
        LinearSpring(double K, double B, RigidBody *pRigid1, int refPoint1, RigidBody
*pRigid2, int refPoint2);
        virtual ~LinearSpring(){};

public:
        virtual int GetForce(struct Vector *force, struct Vector *springForce, struct
Vector* dampForce, RigidBody *pRigid);
};
#endif
////////////////////////////////////////////////////////////////////////////////////////////////////////////////////
// Link class
#ifndef LINK_H
#define LINK_H
```

```
#pragma warning( disable : 4786 )

class Spring;
class Bolt;
class DeformHelper;
class Pulley;
class LinkExternalState;

#include "rigid.h"

#define LINK_IN_DRIVING_PULLEY      0
#define LINK_IN_MIDDLE              1
#define LINK_IN_DRIVEN_PULLEY       2
#define LINK_STATE_UNDEFINED            -1

class Link : public RigidBody
{
protected:
        double m_length, m_width;
        Spring *m_pSpring;
        Bolt *m_pBolt;
        double m_bolt1Dist, m_bolt2Dist;
        double m_springForce;
```

```
        double m_tension;
        DeformHelper *m_DeformHelper;
        Pulley *m_ContactPulley;
        LinkExternalState *m_ExternalState;
public:
        Link(double length, double width,double mass, double J);
        virtual ~Link();
public:
        void AddSpring(Spring *pSpring);
        void AddBolt(Bolt *pBolt);

        // link context, currently only used by Lugre friction model
        void InstallExternalState(LinkExternalState *externalState)
        {
                m_ExternalState = externalState;
        }
        LinkExternalState* GetExternalState()
        {
                return m_ExternalState;
        }
public:
        double GetBoltDistance();
        double GetSpringForce() { return m_springForce; }
```

```
double GetTension() { return m_tension; }
void GetDistanceToPulley(double *dist);
Bolt *GetBolt() { return m_pBolt; }
Spring *GetSpring() { return m_pSpring; }
double GetRelativeVelocity();
double GetFrictionForce();
void InformContact(int isContact, int refIndex, int pulleyIndex, double contactLen);
int GetForce(int refIndex, Vector *force);
double GetBolt2CenterDistance(int index)
{
    if (index == 0)
    {
        return m_bolt1Dist;
    }
    else
    {
        return m_bolt2Dist;
    }
}

void DoDeformAdjustment(DeformHelper *deformHelper);
```

```
public:
        virtual void Update();
        virtual int PostUpdate();
        virtual int AddPoint(double distance, double angle);
        virtual void Step(double time);
        //virtual void RecordInfo(FILE *fp, char type, double time);
        void DoDeformAdjustment(struct DeformParam *deformParam);
protected:
        int m_state;
        Vector m_force[2];
};
#endif
////////////////////////////////////////////////////////////////////////////////////////////////////////////////////
// LinkEventHandler.h: interface for the LinkEventHandler class.
//
#if
!defined(AFX_LINKEVENTHANDLER_H__9514C40A_556E_4C2D_9F46_16E098E6
3262__INCLUDED_)
#define
AFX_LINKEVENTHANDLER_H__9514C40A_556E_4C2D_9F46_16E098E63262__I
NCLUDED_

#if _MSC_VER > 1000
```

```
#pragma once
#endif // _MSC_VER > 1000

class Link;
#include "EventCenter.h"

class LinkEventHandler : public CVTEventObserver
{
public:
	LinkEventHandler();
	virtual ~LinkEventHandler();
public:
	virtual int Notify(CVTEvent *pEvent);

public:
	double GetTension();
	double GetDistance();
protected:
	Link *m_link[2];
	int m_refIndex[2];
};
#endif
//////////////////////////////////////////////////////////////////////////////////////////////////////////////////////
```

```
// Clearance model parameters defined in this Class
// NonlinearSpring.h: interface for the NonlinearSpring class.
#if
!defined(AFX_NONLINEARSPRING_H__E3892130_CF22_4847_8EE6_4A66D8EB3
AE6__INCLUDED_)
#define
AFX_NONLINEARSPRING_H__E3892130_CF22_4847_8EE6_4A66D8EB3AE6__IN
CLUDED_

#if _MSC_VER > 1000
#pragma once
#endif // _MSC_VER > 1000

#include "spring.h"

class NonlinearSpring : public Spring
{
public:
        NonlinearSpring(double K1, double B1, double K2, double B2, double K3,
double B3, double clearanceDist, double clearanceDist2, RigidBody * pRigid1, int
refPoint1, RigidBody * pRigid2, int refPoint2);
        virtual ~NonlinearSpring();
```

```
protected:
        double m_K[3], m_orgLength, m_B[3], m_clearance[2];
        struct
        {
                RigidBody *pRigid;
                int refPoint;
        }m_rigid[2];


public:
        virtual int GetForce(struct Vector *force, struct Vector *springForce, struct
Vector* dampForce, RigidBody *pRigid);
};
#endif
//////////////////////////////////////////////////////////////////////////////////////////////////////////////////////
// ParamListener.h: interface for the ParamListener class.
//
#if
!defined(AFX_PARAMLISTENER_H__58B4345E_843E_41CB_8F71_56C116BA30D
1__INCLUDED_)
#define
AFX_PARAMLISTENER_H__58B4345E_843E_41CB_8F71_56C116BA30D1__INCL
UDED_
```

```
#if _MSC_VER > 1000
#pragma once
#endif // _MSC_VER > 1000
#include <atlbase.h>


class ParamListener
{
// Uncomment the following lines of code (i.e. between /* an */) to run the program
/ * public:
        ParamListener();
        virtual ~ParamListener();
public:
        virtual int NewItemAttribute(OLECHAR *nodeName, OLECHAR *attrName,
OLECHAR *value); */
};
#endif
////////////////////////////////////////////////////////////////////////////////////////////////////////////////////////
// Pulley Class
#ifndef PULLEY_H
#define PULLEY_H
#include "rigid.h"
class FrictionModel;
class Link;
```

```
class Pulley : public RigidBody
{
protected:
        double m_radius, m_slotRadius; //, m_contactRadius;
        double m_phi;
        double m_torque;
        //double m_boltLength;
        double m_axleForce;
        double m_savedTorque;
        double m_inputTorque;
        double m_outputTorque;
        double m_saveAxleForce;
        FrictionModel *m_friction;
public:
        Pulley(double radius, double slotRadius, double phi,
                double mass, double J, FrictionModel *frictionModel);
        virtual ~Pulley();

public:
        void GetForce(double magnitude, struct Vector *pos, struct Vector *velocity,
                struct Vector *force, double *mu, struct Vector *relaVelocity, Link *link);
        BOOL GetSpace(struct Vector *pos, double *length, double deformPhi);
        void SetRotationVelocity(double velocity);
```

```
        void AddForce (struct Vector* force, Vector *pos);
        void SetRotateSpeed(double velocity) {  m_angleVelocity = velocity; }
        double GetRotateSpeed() { return m_angleVelocity; }
        double GetRadius() { return m_radius; }
        double GetTorque() { return m_savedTorque; }
        double GetAxleForce() { return m_saveAxleForce; }
        void InputTorque(double inputTorque);
        void OutputTorque(double output);
public:
        virtual void Step(double time);
        virtual void Update();
};
#endif
////////////////////////////////////////////////////////////////////////////////////////////////////////////////////////
// Rigid body Class
#ifndef RIGIDBODY_H
#define RIGIDBODY_H

#include "def.h"
#include <fstream>
#include <stdio.h>

#define MAX_REFERENCE_POINT_NUM          10
```

```
#define RECORD_SPRING_FORCE          1
#define RECORD_PIN_DISTANCE1 2
#define RECORD_PIN_DISTANCE2 3

struct Vector
{
        double x, y, z;
};

class RigidBody
{
protected:
        double m_time;
        double m_mass, m_J;
        struct Vector m_center;
        struct Vector m_velocity;
        struct Vector m_acceleration;
        double m_angle, m_angleVelocity, m_angleAcceleration;
        struct {
                int used;
                double distance;
                double angle;
```

```
    }m_point[MAX_REFERENCE_POINT_NUM];
public:
    RigidBody(double mass, double J);
    virtual ~RigidBody(){};
public:
    void Rotate(double angle)  { m_angle += angle; }
    void RotateTo(double angle) { m_angle = angle; }
    void Move(struct Vector *displacement);
    void MoveTo(struct Vector *pos) { m_center = *pos; }
    BOOL GetPointCurrentPos(int refIndex, Vector *pos);
    BOOL GetPointCurentVelocity(int refIndex, Vector *velocity);
    Vector* GetCenterVelocity() { return &m_velocity; }
    double GetAngle() { return m_angle; }
    double GetRotationVelocity() { return m_angleVelocity;}
    void SetRotationVelocity(double w) { m_angleVelocity = w;}
    double GetRotationAcceleration() { return m_angleAcceleration;}
    void SetRotationAcceleration(double w) { m_angleAcceleration = w;}
    Vector *GetCenterAcceleration() { return &m_acceleration; }
    struct Vector &GetPosition() const;
public:
    int virtual AddPoint(double distance, double angle);
    void virtual Step(double time) { m_time += time; };
    void virtual Update() {};
```

```
        int virtual PostUpdate() { return 0; }
        //void virtual Save(FILE *out);
        //void virtual Read(FILE *in);
        void virtual RecordInfo(FILE *fp, char type, double time) {};
};
#endif
////////////////////////////////////////////////////////////////////////////////////////////////////////////////////
// Spring.h: interface for the Spring class.
//
#if
!defined(AFX_SPRING_H__466A627F_18B5_4027_8F34_B5F3C5B84D08__INCLU
DED_)
#define
AFX_SPRING_H__466A627F_18B5_4027_8F34_B5F3C5B84D08__INCLUDED_

#if _MSC_VER > 1000
#pragma once
#endif // _MSC_VER > 1000

class RigidBody;

class Spring
{
```

```
public:
        Spring();
        virtual ~Spring();


public:
        virtual int GetForce(struct Vector *force, struct Vector *springForce, struct
Vector* dampForce, RigidBody *pRigid) = 0;
};
#endif
//////////////////////////////////////////////////////////////////////////////////////////////////////////////////////
// TensionObserver.h: interface for the TensionObserver class.
//
#if
!defined(AFX_TENSIONOBSERVER_H__2BA9008F_D9A6_4379_A4C6_8B60722B
5564__INCLUDED_)
#define
AFX_TENSIONOBSERVER_H__2BA9008F_D9A6_4379_A4C6_8B60722B5564__IN
CLUDED_


#if _MSC_VER > 1000
#pragma once
#endif // _MSC_VER > 1000
```

```
#pragma warning( disable : 4786 )


#include "CVTSimulator.h"
#include <list>
class LinkEventHandler;
class TensionObserver : public CVTSimuObserver
{
public:
	TensionObserver(double recordInterval);
	virtual ~TensionObserver();
public:
	virtual int Operation(CVT *pCVT, double time);
public:
	std::list<double> *GetResultList() { return &m_KList; }
	std::list<double> *GetTimeList() { return &m_timeList; }
protected:
	double m_interval;
	std::list<double> m_KList;
	std::list<double> m_timeList;
	double m_nextTime;
	LinkEventHandler *m_observer;
};
#endif
```

```
////////////////////////////////////////////////////////////////////////////////////////////////////////////////////////
// XmlCfgReader.h: interface for the XmlCfgReader class.
#if
!defined(AFX_XMLCFGREADER_H__36C9C376_3B3B_4437_BC25_325A1E30B35
6__INCLUDED_)
#define
AFX_XMLCFGREADER_H__36C9C376_3B3B_4437_BC25_325A1E30B356__INCL
UDED_

#if _MSC_VER > 1000
#pragma once
#endif // _MSC_VER > 1000
#include "ParamListener.h"

class XmlCfgReader
{
public:
        XmlCfgReader();
        virtual ~XmlCfgReader();
public:
        virtual int Read(BSTR fileName, ParamListener *pListener);
};
```

```
#endif                                                                  //
!defined(AFX_XMLCFGREADER_H__36C9C376_3B3B_4437_BC25_325A1E30B35
6__INCLUDED_)
////////////////////////////////////////////////////////////////////////////////////////////////////////////////////
// CVT Main Executable Class
#include "XmlCfgReader.h"
#include "CVTCfgParamListener.h"
#include "CVTSimulator.h"
#include "cvt.h"
#include "CVTStateRecorder.h"
#include "CVTInput.h"
#include "tensionobserver.h"
#include "deformhelper.h"
// #include "cvtpositionrecorder.h"

typedef struct _StatOutputInfo
{
        _StatOutputInfo(char *fileName, char *varName, int offset)
        {
                this->offset = offset;
                strcpy_s(this->fileName, fileName);
                strcpy_s(this->varName, varName);
                //strcpy(this->fileName, fileName);
```

```
		//strcpy(this->varName, varName);
	}
	char fileName[256];
	char varName[20];
	int offset;
}StatOutputInfo;

int OutputTension(std::list<double> *list, std::list<double> *time)
{
	std::list<double>::iterator iter;
	FILE *fp;

	fopen_s(&fp, "tension.txt", "w");

	fprintf(fp, "tension=[\n");

	for (iter = list->begin(); iter != list->end(); iter++)
	{
		fprintf(fp, "%f, \n", (*iter));
	}
	fprintf(fp, "]\n");
	fclose(fp);
```

```
	return 0;
}
void OutputSelectedInfo(std::list<StatOutputInfo *>* selectedList, std::list<struct CVTStat *> *dataList)
{
	FILE *fp;
	std::list<StatOutputInfo *>::iterator i;
	std::list<struct CVTStat *>::iterator j;

	for (i = selectedList->begin(); i != selectedList->end(); i++)
	{
		fopen_s(&fp, (*i)->fileName, "w");
		fprintf(fp, "%s=[\n", (*i)->varName);
		for (j = dataList->begin(); j != dataList->end(); j++)
		{
			fprintf(fp, "%f, \n", *(double *)((char *)(*j) + (*i)->offset));
		}
		fprintf(fp, "]\n");
		fclose(fp);
	}

}
void OutputInfo(std::list<struct CVTStat *> *list)
```

```
{
        std::list<StatOutputInfo *>::iterator i;
        std::list<StatOutputInfo *>selectedList;
        selectedList.push_back(new StatOutputInfo("dist.txt", "dist", offsetof(CVTStat, m_toPulleyDist[0])));
        selectedList.push_back(new StatOutputInfo("time.txt", "time", offsetof(CVTStat, m_time)));
        selectedList.push_back(new StatOutputInfo("friction.txt", "friction", offsetof(CVTStat, m_friction)));
        selectedList.push_back(new StatOutputInfo("spring.txt", "spring", offsetof(CVTStat, m_springForce)));
        selectedList.push_back(new StatOutputInfo("NormalForce.txt", "normalForce", offsetof(CVTStat, m_normalForce)));
        selectedList.push_back(new StatOutputInfo("Radial.txt", "RadialVelocity", offsetof(CVTStat, m_relativeVelocity)));
        selectedList.push_back(new StatOutputInfo("Tangential.txt", "TangentialVelocity", offsetof(CVTStat, m_tangentialRelaVelocity)));
        selectedList.push_back(new StatOutputInfo("Tension.txt", "Tension", offsetof(CVTStat, m_tension)));
        selectedList.push_back(new StatOutputInfo("pulley1rad.txt", "pulley1_speed.txt", offsetof(CVTStat, m_pulleyRotateSpeed[0])));
        selectedList.push_back(new StatOutputInfo("pulley2rad.txt", "pulley2_speed.txt", offsetof(CVTStat, m_pulleyRotateSpeed[1])));
```

```
        selectedList.push_back(new StatOutputInfo("pulley1torq.txt",
"pulley1_force.txt", offsetof(CVTStat, m_pulleyTorque[0])));
        selectedList.push_back(new StatOutputInfo("pulley2torq.txt",
"pulley2_force.txt", offsetof(CVTStat, m_pulleyTorque[1])));
        selectedList.push_back(new StatOutputInfo("friction_rad.txt", "FrictionRadial",
offsetof(CVTStat, m_radialRelaFriction)));
        selectedList.push_back(new StatOutputInfo("friction_tan.txt",
"FrictionTangential", offsetof(CVTStat, m_tangentialFriction)));
        selectedList.push_back(new StatOutputInfo("axle1.txt", "axleForce1",
offsetof(CVTStat, m_pulleyAxleForce[0])));
        selectedList.push_back(new StatOutputInfo("axle2.txt", "axleForce2",
offsetof(CVTStat, m_pulleyAxleForce[1])));
        selectedList.push_back(new StatOutputInfo("mu.txt", "mu", offsetof(CVTStat,
m_mu)));
        selectedList.push_back(new StatOutputInfo("RelaVelX.txt", "RelaVelX",
offsetof(CVTStat, m_relaVelX)));
        selectedList.push_back(new StatOutputInfo("RelaVelY.txt", "RelaVelY",
offsetof(CVTStat, m_relaVelY)));
        OutputSelectedInfo(&selectedList, list);

        for (i = selectedList.begin(); i != selectedList.end(); i++)
        {
                delete *i;
```

```
        }
}
CVT *CreateCVT(OLECHAR *file, CVTCreateParam *param)
{
        XmlCfgReader reader;
        CVTCfgParamListener listener;

        BSTR fileName = ::SysAllocString(file);
        if (reader.Read(fileName, &listener) != 0)
        {
                ::SysFreeString(fileName);
                return NULL;
        }
        ::SysFreeString(fileName);

        CVTFactory factory;
        *param = *listener.GetFilledParam();

        return factory.CreateCVT(param, listener.GetDeformParam());
}

void RunCVT(CVT *pCVT, double recordTime, double step, double timeSpan,
CVTCreateParam *param)
```

```
{
        CVTSimulator simu(pCVT);
        CVTStateRecorder recorder(recordTime);
        CVTPositionRecorder posRecorder("CVTPosition.txt", recordTime);

        CVTInput input(param->inputTorque, param->outputTorque);
        TensionObserver tension(recordTime);

        simu.RegisterPostSimuObserver(&recorder);
        simu.RegisterPostSimuObserver(&posRecorder);
        //simu.RegisterPostSimuObserver(&tension);
        simu.RegisterPreSimuObserver(&input);
        simu.Simulate(0.05, step, timeSpan);

        std::list<struct CVTStat *> *list = recorder.GetStateList();

        OutputInfo(list);
        //OutputTension(tension.GetResultList(), tension.GetTimeList());
}
void main(int argc, char *argv[])
{
        CoInitialize(0);
        OLECHAR *fileName;
```

```
int strLen, i;
double recordTime, timeSpan, step;
CVTCreateParam param;

if (argc != 5)
{
    printf("Usage: CVTSimu [configuration file] [record time interval] [time step] [simulation time duration]\n");
    return;
}

strLen = strlen(argv[1]);
fileName = new OLECHAR[strLen + 1];

for (i = 0; i < strLen; i++)
{
    fileName[i] = argv[1][i];
}
fileName[i] = 0;

recordTime = atof(argv[2]);
step = atof(argv[3]);
timeSpan = atof(argv[4]);
```

```
	CVT *pCVT = CreateCVT(fileName, &param);
	delete []fileName;

	if (pCVT)
	{
		RunCVT(pCVT, recordTime, step, timeSpan, &param);
		delete pCVT;
	}
	else
	{
		printf("Failed to create CVT simulator. Please check your configuration file\n");
	}
	CoUninitialize();
}
```

//

Command line: *executable file* [configuration file.txt] [recording time] [integration time step] [final time] > output.txt

Use integration time step of 1e-6 seconds.

The configuration file contains parameters for clearance, friction characteristics, loading conditions, and CVT component dimensions.

An example configuration file is given as:

```
<CVT>
    <Items>
        <Link Num="34" Width="0.02" Length="0.030035" Mass="0.1125" J="1.5026e-005" BoltDistance2Center="0.02"/>
        <Spring IsLinear="0" K="35000" B="1200" K2="70000" B2="2400" K3="93000" B3="3000" ClearanceDistance="0.00005" ClearanceDistance2="0.0001"/>
        <Pulley1 Mass="1" J="1.4516" MinRadius="0.0" Radius="0.0762" SlopeAngle="15.0"/>
        <Pulley2 Mass="1" J="3.2661" MinRadius="0.0" Radius="0.1143" SlopeAngle="15.0"/>
        <Bolt K="200000"/>
    </Items>
    <Configure>
        <Param name="PullyDistance">0.5</Param>
        <Param name="FrictonModel">Continuous Coulomb Friction</Param>
        <Param name="FrictionRate">0.25</Param>
        <Param name="Friction_a">0.003</Param>
        <Param name="Friction_b">0.01</Param>
    </Configure>
    <Simulation Mode="0">
        <Torque Input="200" Output="100"/>
    </Simulation>
</CVT>
```

APPENDIX D

MATLAB codes for plotting the results from belt and chain CVT models

```
% plotcvt.m - used for belt CVT models 1 and 2
acclnE1_r = r_accln-R.*theta_dot.^2;
acclnE1_t = R.*theta_accln+2*R_dot.*theta_dot;
acclnE1 = sqrt(acclnE1_r.^2+acclnE1_t.^2);
acclnE2_r = r_accln2-R2.*theta_dot2.^2;
acclnE2_t = R2.*theta_accln2+2*R_dot2.*theta_dot2;
acclnE2 = sqrt(acclnE2_r.^2+acclnE2_t.^2);
acclnE1_id = R*(pulley_dot_init)^2;
acclnE2_id = R2*(pulley2_dot_init)^2;

figure(1)
plot(time,theta,time,alpha,'--',time,theta2,'-.',time,alpha2,':','Linewidth',1.5)

figure(2)
plot(time,theta_dot*30/pi,time,pspeed1*30/pi,'--',time,theta_dot2*30/pi,'-
.',time,pspeed2*30/pi,':','Linewidth',1.5)
legend('Driving belt speed','Driver pulley speed','Driven belt speed','Driven pulley speed')
xlabel('time (s)','Fontweight','bold','FontSize',10)
ylabel('Angular Speed (rpm)','Fontweight','bold','FontSize',10)
title('Case 1: \tau_i_n = 200 Nm,\tau_l = 100 Nm','Fontweight','bold','Fontsize',12)
```

```
figure(3)
plot(time,Q,time,Q2,'-.','Linewidth',1.5)
legend('Driver','Driven')
xlabel('time (s)','Fontweight','bold','FontSize',10)
ylabel('Belt Compressive Force (N)','Fontweight','bold','FontSize',10)
title('Case 1: \tau_i_n = 200 Nm,\tau_l = 100 Nm','Fontweight','bold','Fontsize',12)

figure(4)
plot(time,R,time,R2,'-.','Linewidth',1.5)
legend('Driver','Driven')
xlabel('time (s)','Fontweight','bold','FontSize',10)
ylabel('Belt pitch radius (m)','Fontweight','bold','FontSize',10)
title('Case 1: \tau_i_n = 200 Nm,\tau_l = 100 Nm','Fontweight','bold','Fontsize',12)

figure(5)
plot(time,beta*180/pi,time,beta2*180/pi,'-.','Linewidth',1.5)
legend('Driver','Driven')
xlabel('time (s)','Fontweight','bold','FontSize',10)
title('Case 1: \tau_i_n = 200 Nm,\tau_l = 100 Nm','Fontweight','bold','Fontsize',12)
ylabel('Sheave angle : bending effect (degrees)','Fontweight','bold','FontSize',10)

figure(6)
plot(time,Fz_1/1000,time,Fz_2/1000,'-.','Linewidth',1.5)
```

```
legend('Driver','Driven')
xlabel('time (s)','Fontweight','bold','FontSize',10)
ylabel('Pulley Axial Force (kN)','Fontweight','bold','FontSize',10)
title('Case 1: \tau_i_n = 200 Nm,\tau_l = 100 Nm','Fontweight','bold','Fontsize',12)

figure(7)
plot(R_dot,R.*(theta_dot-pspeed1),R_dot2,R2.*(theta_dot2-pspeed2),'--','Linewidth',1.5)
xlabel('Relative Radial Velocity (m/s)','Fontweight','bold','FontSize',10)
ylabel('Relative Tangential Velocity (m/s)','Fontweight','bold','FontSize',10)
legend('Driver','Driven')
title('Case 1: \tau_i_n = 200 Nm,\tau_l = 100 Nm, Relative Velocity Diagram','Fontweight','bold','Fontsize',12)

figure(8)
plot(time,fric1,time,fric2,'--')
xlabel('time (s)','Fontweight','bold','FontSize',10)
ylabel('Frictional Force (N)','Fontweight','bold','FontSize',10)
legend('Driver','Driven')
title('Case 1: \tau_i_n = 200 Nm,\tau_l = 100 Nm','Fontweight','bold','Fontsize',12)

figure(9)
plot(time,mu_b,time,mu_b2,'--')
xlabel('time (s)','Fontweight','bold','FontSize',10)
```

```
ylabel('Coefficient of Friction','Fontweight','bold','FontSize',10)
legend('Driver','Driven')
title('Case 1: \tau_i_n = 200 Nm,\tau_l = 100 Nm','Fontweight','bold','Fontsize',12)

figure(10)
plot(time,theta,time,theta2,'--','Linewidth',1.5)
xlabel('time (s)','Fontweight','bold','FontSize',10)
ylabel('Element angular location on pulleys (rad)','Fontweight','bold','FontSize',10)
title('Case 1: \tau_i_n = 200 Nm,\tau_l = 100 Nm','Fontweight','bold','Fontsize',12)
legend('Driver','Driven')

figure(11)
plot(time,phi*180/pi,time,phi2*180/pi,'-.','Linewidth',1.5)
legend('Driver','Driven')
xlabel('time (s)','Fontweight','bold','FontSize',10)
ylabel('Element slope angle (degrees)','Fontweight','bold','FontSize',10)
title('Case 1: \tau_i_n = 200 Nm,\tau_l = 100 Nm','Fontweight','bold','Fontsize',12)

figure(12)
plot(time,acclnE1,time,acclnE2,'--',time,acclnE1_id,'-
.',time,acclnE2_id,':','Linewidth',1.5)
xlabel('time (s)','Fontweight','bold','FontSize',10)
ylabel('Belt element acceleration (m/s^2)','Fontweight','bold','FontSize',10)
```

```
title('Case 1: \tau_i_n = 200 Nm,\tau_l = 100 Nm','Fontweight','bold','Fontsize',12)
legend('Total driver element accln','Total driven element accln','Driver element centripetal accln','Driven element centripetal accln')
%
%%%%%%%%%%%%%%%%%%%%%%%%%%%%%%%%%%%%%%%%%%
% plotcvt_band.m: used for plotting belt CVT model 3 results
FricE = mu_b.*N;
FricE2 = mu_b2.*N2;
FricB = mu_a.*F;
FricB2 = mu_a2.*F2;

acclnE1_r = r_accln-R.*theta_dot.^2;
acclnE1_t = R.*theta_accln+2*R_dot.*theta_dot;
acclnE1 = sqrt(acclnE1_r.^2+acclnE1_t.^2);
acclnE2_r = r_accln2-R2.*theta_dot2.^2;
acclnE2_t = R2.*theta_accln2+2*R_dot2.*theta_dot2;
acclnE2 = sqrt(acclnE2_r.^2+acclnE2_t.^2);

acclnB1_r = r1_accln-R1.*gam_dot.^2;
acclnB1_t = R1.*gam_accln+2*R1_dot.*gam_dot;
acclnB1 = sqrt(acclnB1_r.^2+acclnB1_t.^2);
acclnB2_r = r1_accln2-R1_2.*gam_dot2.^2;
acclnB2_t = R1_2.*gam_accln2+2*R1_dot2.*gam_dot2;
```

```
acclnB2 = sqrt(acclnB2_r.^2+acclnB2_t.^2);

acclnE1_id = R*(pulley_dot_init)^2;
acclnE2_id = R2*(pulley2_dot_init)^2;
acclnB1_id = R1*(pulley_dot_init)^2;
acclnB2_id = R1_2*(pulley2_dot_init)^2;

figure(1)
plot(time,theta,time,alpha,'--',time,theta2,'-.',time,alpha2,':','Linewidth',1.5)
title('Theta-Alpha Plot','Fontweight','bold','Fontsize',12)
legend('\theta','\alpha','\theta_2','\alpha_2')

figure(2)
plot(time,gamma,time,alpha,'--',time,gamma2,'-.',time,alpha2,':','Linewidth',1.5)
title('Gamma-Alpha Plot','Fontweight','bold','Fontsize',12)
legend('\gamma','\alpha','\gamma_2','\alpha_2')

figure(3)
plot(time,theta_dot*30/pi,time,pspeed1*30/pi,'--',time,theta_dot2*30/pi,'-
.',time,pspeed2*30/pi,':','Linewidth',1.5)
legend('Driver element speed','Driver pulley speed','Driven element speed','Driven pulley
speed')
xlabel('time (s)','Fontweight','bold','FontSize',10)
```

```
ylabel('Element & Pulley Angular Speed (rpm)','Fontweight','bold','FontSize',10)
title('Case 1: \tau_i_n = 200 Nm,\tau_l = 100 Nm','Fontweight','bold','Fontsize',12)

figure(4)
plot(time,gam_dot*30/pi,time,theta_dot*30/pi,'--',time,gam_dot2*30/pi,'-
.',time,theta_dot2*30/pi,':','Linewidth',1.5)
legend('Driver band speed','Driver element speed','Driven band speed','Driven element
speed')
xlabel('time (s)','Fontweight','bold','FontSize',10)
ylabel('Band & Element Angular Speed (rpm)','Fontweight','bold','FontSize',10)
title('Case 1: \tau_i_n = 200 Nm,\tau_l = 100 Nm','Fontweight','bold','Fontsize',12)

figure(5)
plot(time,Q,time,Q2,'-.','Linewidth',1.5)
legend('Driver','Driven')
xlabel('time (s)','Fontweight','bold','FontSize',10)
ylabel('Element Compressive Force (N)','Fontweight','bold','FontSize',10)
title('Case 1: \tau_i_n = 200 Nm,\tau_l = 100 Nm','Fontweight','bold','Fontsize',12)

figure(6)
plot(time,T,time,T2,'-.','Linewidth',1.5)
legend('Driver','Driven')
xlabel('time (s)','Fontweight','bold','FontSize',10)
```

```
ylabel('Band Tensile Force (N)','Fontweight','bold','FontSize',10)
title('Case 1: \tau_i_n = 200 Nm,\tau_l = 100 Nm','Fontweight','bold','Fontsize',12)

figure(7)
plot(time,R,time,R1,'--',time,R2,'-.',time,R1_2,':','Linewidth',1.5)
legend('Driver element','Driver band','Driven element','Driven band')
xlabel('time (s)','Fontweight','bold','FontSize',10)
ylabel('Element and Band pitch radii (m)','Fontweight','bold','FontSize',10)
title('Case 1: \tau_i_n = 200 Nm,\tau_l = 100 Nm','Fontweight','bold','Fontsize',12)

figure(8)
plot(time,beta*180/pi,time,beta2*180/pi,'-.','Linewidth',1.5)
legend('Driver','Driven')
xlabel('time (s)','Fontweight','bold','FontSize',10)
title('Case 1: \tau_i_n = 200 Nm,\tau_l = 100 Nm','Fontweight','bold','Fontsize',12)
ylabel('Sheave angle : bending effect (degrees)','Fontweight','bold','FontSize',10)

figure(9)
plot(time,Fz_1/1000,time,Fz_2/1000,'-.','Linewidth',1.5)
legend('Driver','Driven')
xlabel('time (s)','Fontweight','bold','FontSize',10)
ylabel('Pulley Axial Force  (kN)','Fontweight','bold','FontSize',10)
title('Case 1: \tau_i_n = 200 Nm,\tau_l = 100 Nm','Fontweight','bold','Fontsize',12)
```

```
figure(10)
plot(R_dot,R.*(theta_dot-pspeed1),R_dot2,R2.*(theta_dot2-pspeed2),'--','Linewidth',1.5)
xlabel('Element-Pulley Relative Radial Velocity (m/s)','Fontweight','bold','FontSize',10)
ylabel('Element-Pulley Relative Tangential Velocity (m/s)','Fontweight','bold','FontSize',10)
legend('Driver','Driven')
title('Case 1: \tau_i_n = 200 Nm,\tau_l = 100 Nm, Relative Velocity Diagram','Fontweight','bold','Fontsize',12)

figure(11)
plot(time,V_be,time,V_be2,'--','Linewidth',1.5)
xlabel('time (s)','Fontweight','bold','FontSize',10)
ylabel('Relative velocity between band and element (m/s)','Fontweight','bold','FontSize',10)
legend('Driver','Driven')
title('Case 1: \tau_i_n = 200 Nm,\tau_l = 100 Nm','Fontweight','bold','Fontsize',12)

figure(12)
plot(V_be,R.*(theta_dot-pspeed1),V_be2,R2.*(theta_dot2-pspeed2),'--','Linewidth',1.5)
xlabel('Band-element relative velocity (m/s)','Fontweight','bold','FontSize',10)
ylabel('Element-pulley relative tangential velocity (m/s)','Fontweight','bold','FontSize',10)
legend('Driver','Driven')
```

```
title('Case 1: \tau_i_n = 200 Nm,\tau_l = 100 Nm, Relative Velocity Diagram','Fontweight','bold','Fontsize',12)

figure(13)
plot(time,FricE,time,FricE2,'--','Linewidth',1.5)
xlabel('time (s)','Fontweight','bold','FontSize',10)
ylabel('Element-Pulley Frictional Force (N)','Fontweight','bold','FontSize',10)
legend('Driver','Driven')
title('Case 1: \tau_i_n = 200 Nm,\tau_l = 100 Nm','Fontweight','bold','Fontsize',12)

figure(14)
plot(time,FricB,time,FricB2,'--','Linewidth',1.5)
xlabel('time (s)','Fontweight','bold','FontSize',10)
ylabel('Band-Element Frictional Force (N)','Fontweight','bold','FontSize',10)
legend('Driver','Driven')
title('Case 1: \tau_i_n = 200 Nm,\tau_l = 100 Nm','Fontweight','bold','Fontsize',12)

figure(15)
plot(time,mu_b,time,mu_b2,'--','Linewidth',1.5)
xlabel('time (s)','Fontweight','bold','FontSize',10)
ylabel('Element-Pulley Coefficient Of Friction','Fontweight','bold','FontSize',10)
legend('Driver','Driven')
title('Case 1: \tau_i_n = 200 Nm,\tau_l = 100 Nm','Fontweight','bold','Fontsize',12)
```

```
figure(16)
plot(time,mu_a,time,mu_a2,'--','Linewidth',1.5)
xlabel('time (s)','Fontweight','bold','FontSize',10)
ylabel('Band-Element Coefficient Of Friction','Fontweight','bold','FontSize',10)
legend('Driver','Driven')
title('Case 1: \tau_i_n = 200 Nm,\tau_l = 100 Nm','Fontweight','bold','Fontsize',12)

figure(17)
plot(time,theta,time,gamma,'--',time,theta2,'-.',time,gamma2,':','Linewidth',1.5)
xlabel('time (s)','Fontweight','bold','FontSize',10)
ylabel('Element and Band angular location on pulleys
(rad)','Fontweight','bold','FontSize',9)
title('Case 1: \tau_i_n = 200 Nm,\tau_l = 100 Nm','Fontweight','bold','Fontsize',12)
legend('Driver element','Driver band','Driven element','Driven band')

figure(18)
plot(time,phi*180/pi,time,phi1*180/pi,'--',time,phi2*180/pi,'-
.',time,phi1_2*180/pi,':','Linewidth',1.5)
legend('Driver element','Driver band','Driven element','Driven band')
xlabel('time (s)','Fontweight','bold','FontSize',10)
ylabel('Element and Band slope angles (degrees)','Fontweight','bold','FontSize',10)
title('Case 1: \tau_i_n = 200 Nm,\tau_l = 100 Nm','Fontweight','bold','Fontsize',12)
```

```
figure(19)
plot(time,acclnE1,time,acclnE2,'--',time,acclnE1_id,'-
.',time,acclnE2_id,':','Linewidth',1.5)
xlabel('time (s)','Fontweight','bold','FontSize',10)
ylabel('Belt element acceleration (m/s^2)','Fontweight','bold','FontSize',10)
title('Case 1: \tau_i_n = 200 Nm,\tau_l = 100 Nm','Fontweight','bold','Fontsize',12)
legend('Total driver element accln','Total driven element accln','Driver element
centripetal accln','Driven element centripetal accln')

figure(20)
plot(time,acclnB1,time,acclnB2,'--',time,acclnB1_id,'-
.',time,acclnB2_id,':','Linewidth',1.5)
xlabel('time (s)','Fontweight','bold','FontSize',10)
ylabel('Band pack acceleration (m/s^2)','Fontweight','bold','FontSize',10)
title('Case 1: \tau_i_n = 200 Nm,\tau_l = 100 Nm','Fontweight','bold','Fontsize',12)
legend('Total driver band accln','Total driven band accln','Driver band centripetal
accln','Driven band centripetal accln')
%
%%%%%%%%%%%%%%%%%%%%%%%%%%%%%%%%%%%%%%%%%%%%%%%%%%%%%%%
% plot_chain.m: used for plotting chain CVT model results
clc
clear
```

```
format long
time = [];         % insert data from time.txt which is an output file from chain CVT model
Tension = [];   % insert data from tension.txt which is an output file from the model
figure(1)
plot(time,Tension,'Linewidth',1.25)
xlabel('time (s)','Fontweight','bold','FontSize',10)
ylabel('Tensile Force (N)','Fontweight','bold','FontSize',10)
title('Case 1: \tau_i_n = 200 Nm, \tau_l = 100 Nm','Fontweight','bold','Fontsize',11)
legend('Driver','Driven')
%%%%%%%%%%%%%%%%%%%%%%%%%%%%%%%%%%%%%%%%%%%%%%%%%
```

APPENDIX E

SIMULINK models of metal V-belt CVT

Since models 1 and 2 differ only in the friction characteristic, system level block diagram of only model 1 will be subsequently illustrated. Model 3 accounts for slip dynamics between band pack and the belt element.

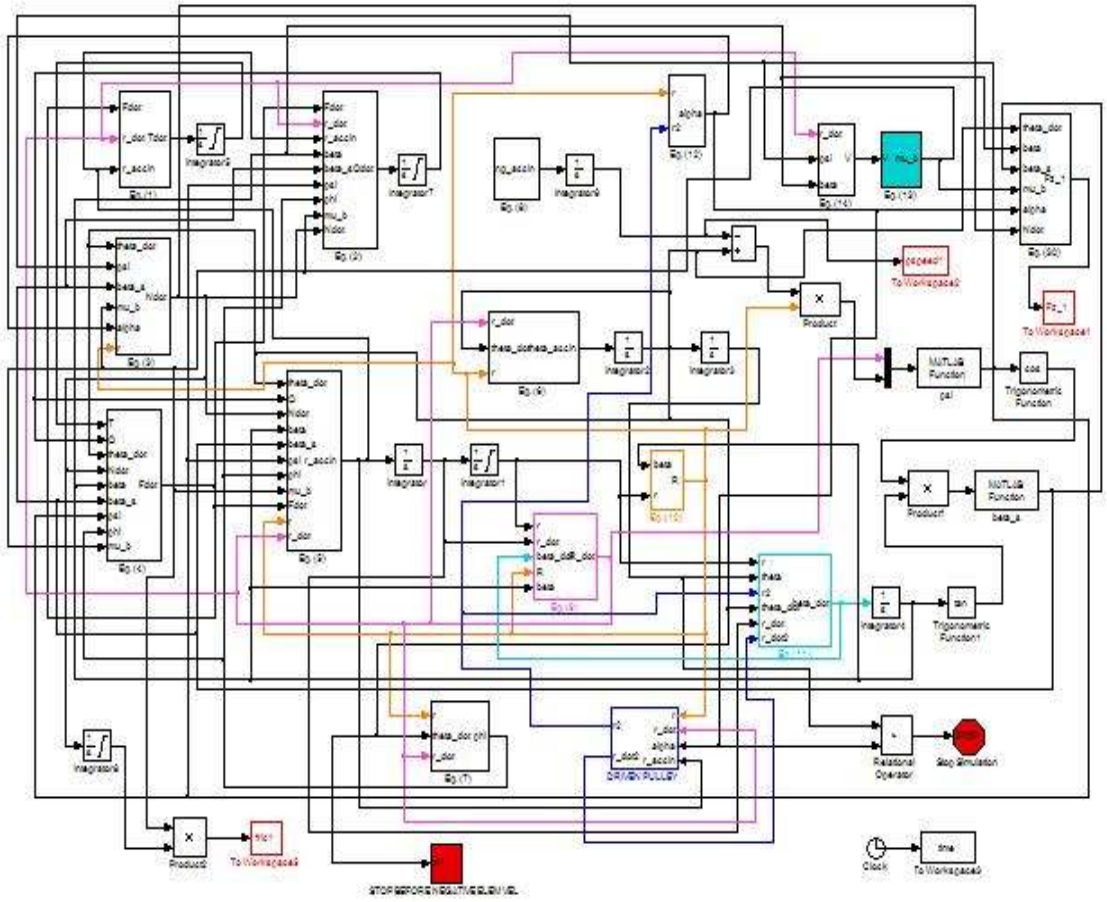

(a) Driver System Block Diagram

Figure E.1: SIMULINK block diagram of belt CVT model 1

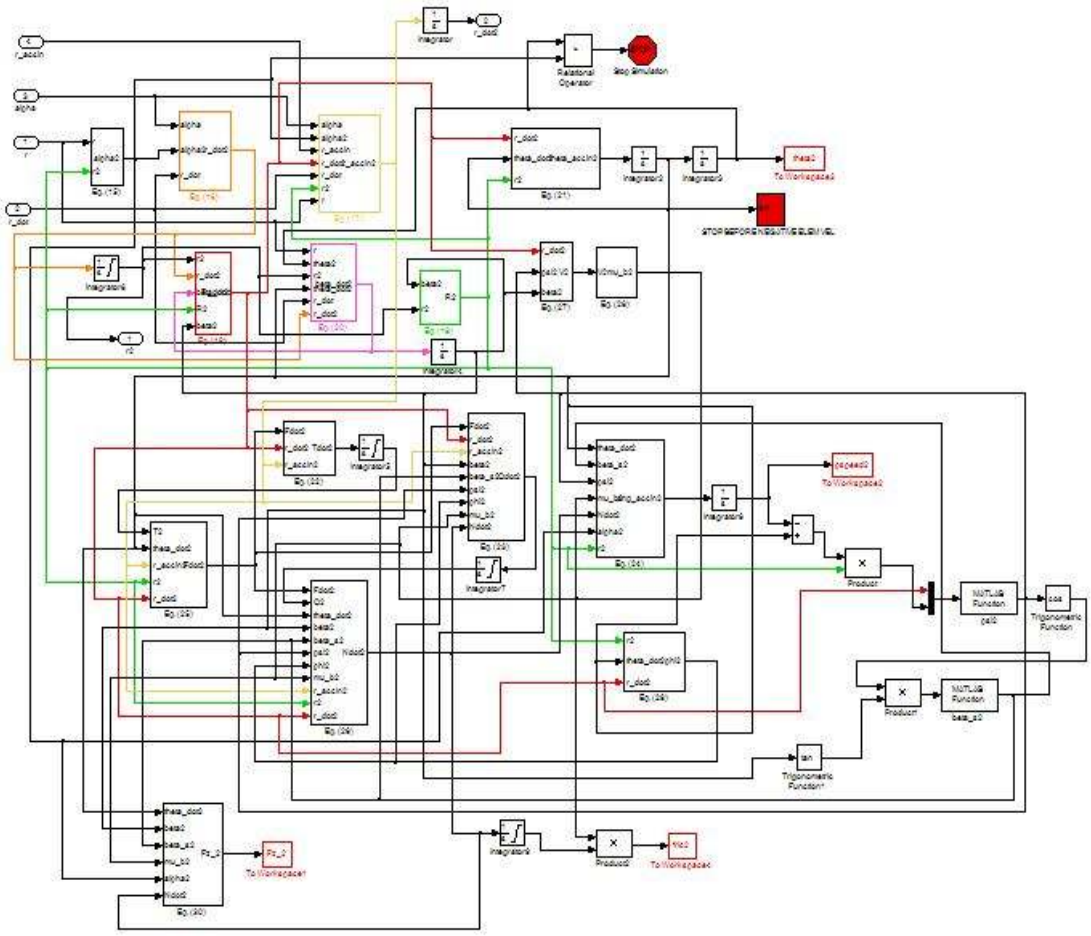

(b) Driven System Block Diagram

Figure E.1: SIMULINK block diagram of belt CVT model 1 (contd.)

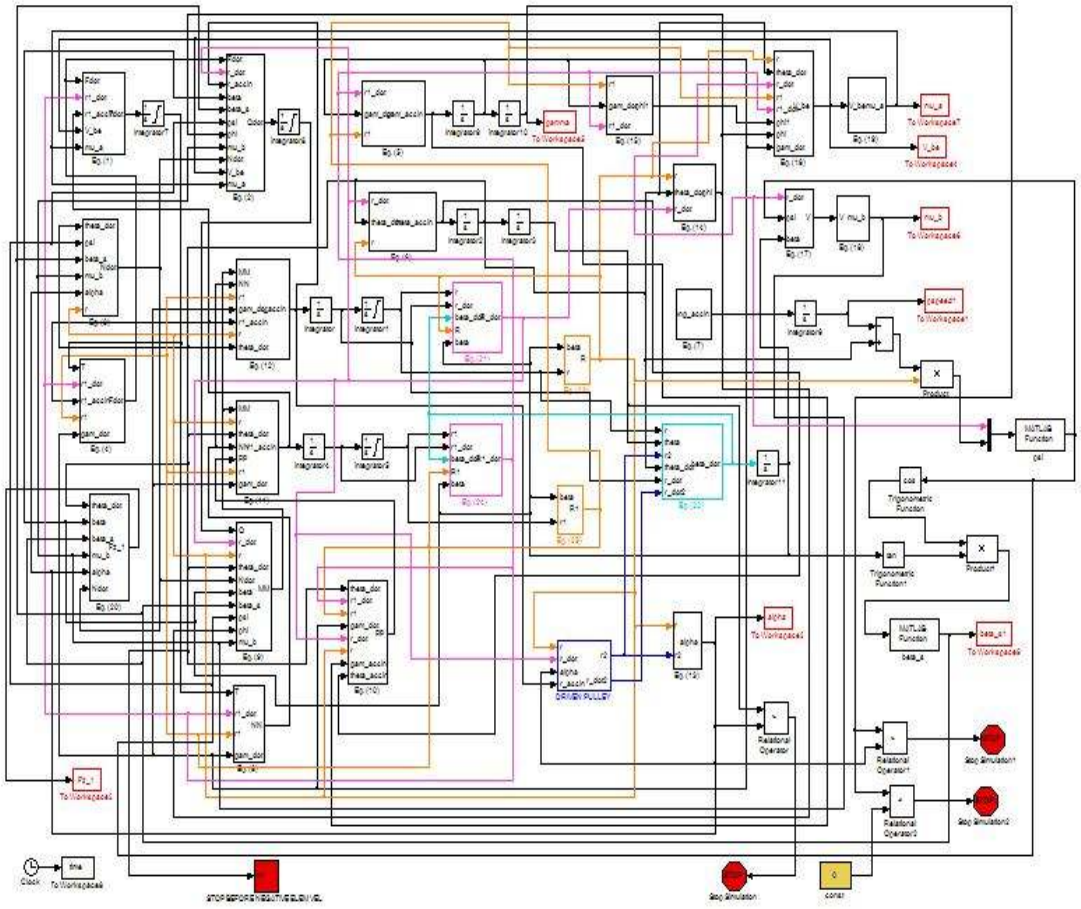

(a) Driver System Block Diagram

Figure E.2: SIMULINK block diagram of belt CVT model 3

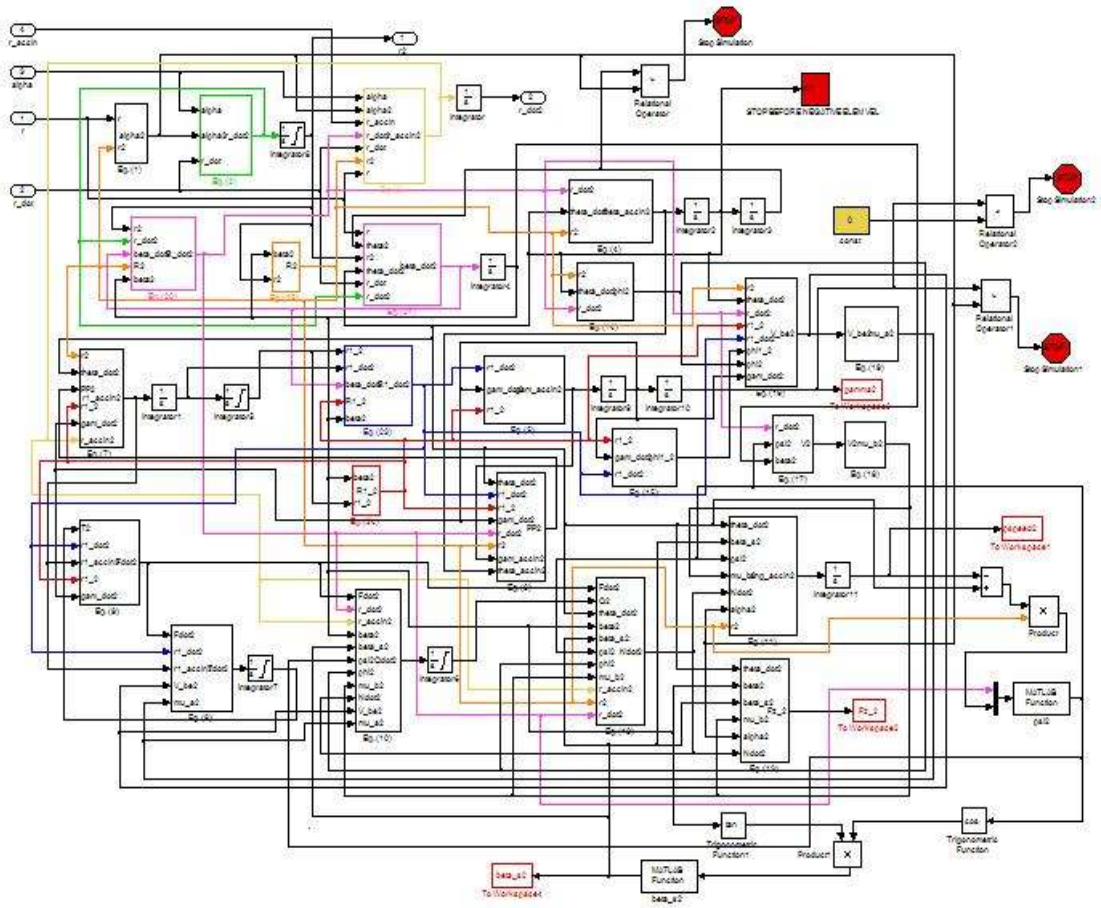

(b) Driven System Block Diagram

Figure E.2 SIMULINK block diagram of belt CVT model 3 (contd.)

Appendix F

MATLAB / SIMULINK modeling of 2-DOF stick-slip oscillator

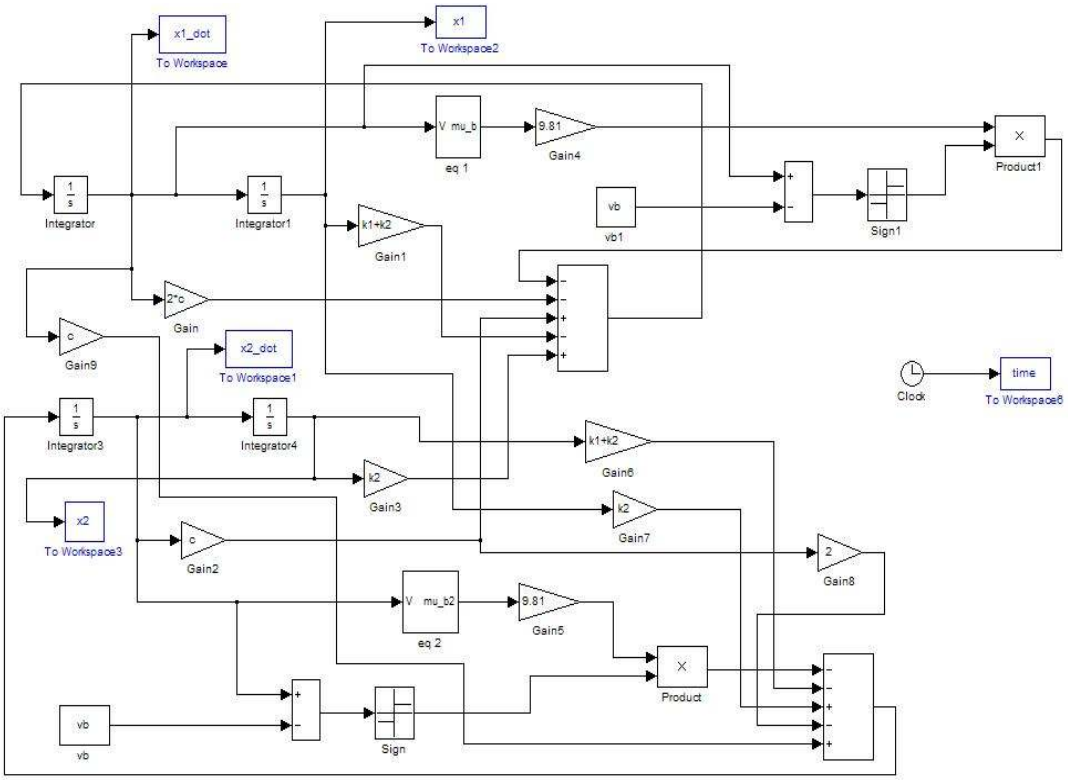

Figure F.1: SIMULINK block diagram for 2-DOF stick-slip oscillator

% ***vibr_two.m***: *calls the above SIMULINK model to plot the time histories*

% 2-DOF system with different friction characteristics

% mass m1 & m2 = 1 (unit mass)

clc

clear all

close all

format long

tstep = 0.005;

```
tfinal = 100;

Fs = 1/tstep;

k = 25;

k1 = 25;

k2 = 25;

c = 1;

vb = 3.5;

cl = 1;

% Uncomment the following 3 lines for continuous Coulomb friction characteristic

% a = 0.003;

% b = 1e-3;

% mu_b_sat = 0.25;

% Uncomment the following 4 lines for Stribeck-like friction characteristic

% a = 1;

% b = 5;

% ff = 6.5;

% mu_b_sat = 0.25;


IC_data = [0 0 0 0

5 0 0 0

0 5 0 0

0 0 5 0

0 vb 0 0
```

0 0 0 vb

0 0 0 5

3 0 6 0

0 3 0 6

3 4 0 0

0 0 4 3

-3 0 -6 0

0 -3 0 -6

3 0 0 6

0 -3 6 0

10 2 12 1

2 10 1 12

-10 2 -12 1

-2 10 -1 12

-10 -2 -12 -1

-2 -10 -1 -12

10 -2 12 -1

5 7 6 8

7 5 8 6

-5 -7 -6 -8

-7 -5 -8 -6

-5 7 -6 8

5 -7 6 -8

```
10 10 15 15
-10 -10 -15 -15
-10 10 -15 15
10 -10 15 -15];

[row,col] = size(IC_data);

for i=1:row,
   ic = IC_data(i,:);
   x1_init = ic(1);
   x1_dot_init = ic(2);
   x2_init = ic(3);
   x2_dot_init = ic(4);
%   sim('vibr3')              % Coulomb friction model
     sim('vibr3_b')           % Stribeck-like friction model

   figure(1)
   plot(x1,x1_dot)
   title('Phase trajectories of the system')
   xlabel('x_1 (m)')
   ylabel('v_1 (m/s)')
%    pause
   hold on
```

```
   figure(2)
   plot(x2,x2_dot)
   title('Phase trajectories of the system')
   xlabel('x_2 (m)')
   ylabel('v_2 (m/s)')
%    pause
   hold on
%
   figure(3)
   plot(time,x1,time,x2,'--')
   title('Displacement time histories of the system')
   ylabel('x_1 & x_2 (m)')
   xlabel('time (s)')
   legend('x_1','x_2')
%    pause
   hold on

   figure(4)
   plot(time,x1_dot,time,x2_dot,'--')
   title('Velocity time histories of the system')
   xlabel('time (s)')
   ylabel('v_1 & v_2 (m/s)')
```

```
    legend('v_1','v_2')
    hold on
%     pause
end
disp('Program terminated successfully')
```

BIBLIOGRAPHY

1. Ottis, C., and Hartman, R., "*Hybrid Electric Vehicles: Pursuing Automotive Efficiency*," Paper #189, Conference Session C2, Fifth Annual Freshman Conference, April 9, 2005, Pittsburgh, PA, USA

2. Greene, David L., Schafer, Andreas, "*Reducing Greenhouse Gas Emissions From U.S. Transportation*," Report Prepared for the Pew Center on Global Climate Change, May 2003

3. "*Continuously variable transmission*", accessed on October 16, 2006, http://en.wikipedia.org/wiki/Continuously_variable_transmission

4. "*How Manual Transmissions Work*," accessed on October 16, 2006, http://auto.howstuffworks.com/transmission5.htm

5. "*How Automatic Transmissions Work*," accessed on October 16, 2006, http://auto.howstuffworks.com/automatic-transmission4.htm

6. Micklem, J. D., Longmore, D. K., Burrows, C. R., "*Modelling of the Steel Pushing V-belt Continuously Variable Transmission*," Proceedings Inst. Mech. Engineers Vol. 208 Part C: pp 13-27, 1994

7. Srnik, J. and Pfeiffer, F., "*Dynamics of CVT chain drives*," Int. J. of Vehicle Design, Vol. 22, Nos. 1/2, pp. 54-72, 1999

8. "*Traction Modelling for a toroidal CVT*," accessed on October 16, 2006, http://www.imperial.ac.uk/tribology/Nikas/project6.htm

9. Ashley, Steven, "*Is CVT the car transmission of the future?*" , Mechanical Engineering-CIME, 116(11), pp. 64-68, November, 1994

10. Kim, J., Park, F. C., Park, Y., and Shizuo, M., "*Design and analysis of a spherical continuously variable transmission*," ASME Journal of Mechanical Design, Vol. 124, Issue 1, pp. 21-29, March 2002

11. "*Hybrid Synergy Drive (HSD/E-CVT)*," accessed on October 16, 2006, http://en.wikipedia.org/wiki/Hybrid_Synergy_Drive

12. Belfiore, N. P., Stefani, G. De, "*Ball toroidal CVT: a feasibility study based on topology, kinematics, statics and lubrication*," International Journal of Vehicle Design, Vol. 23, No. 3/4, pp. 304-331, 2003

13. Cretu, O. S., Glovnea, R. P., "*Constant Power Continuously Variable Transmission (CP-CVT): Operating Principle and Analysis*," ASME Journal of Mechanical Design, Vol. 127, Issue 1, pp. 114-119, January 2005

14. "*Mazda Nextourer Concept Technical Specifications*," accessed on October 16, 2006, http://media.ford.com/nextourer

15. "*Torotrak: Infinitely Variable Transmission*," accessed on October 16, 2006, http://histomobile.com/histomob/tech/2/108.htm

16. Berkepile, D., and Drudy, M., "*A stepless future with the continuously variable transmission*," Paper #114, Conference Session C2, Fifth Annual Freshman Conference, April 9, 2005, Pittsburgh, PA, USA

17. Simner, D., "*The Contribution of Transmissions to Vehicle Fuel Economy*," presented at IMechE AUTOTECH 95 Conference, C498/34/135

18. Akehurst, S., "*An investigation into the loss mechanisms associated with a pushing metal V-belt continuously variable transmission*," University of Bath, School of Mechanical Engineering, PhD Thesis, 2001

19. Gerbert, G., "*Traction Belt Mechanics: Flat belts, V-belts, V-rib belts*," Chalmers Univ. of Technology, Gotebörg, Sweden, 1999. ISBN: 9163078856

20. Kimmich, E. G., Roesler, W. Q., "*Variable speed V-belt drives for farm machines*," Agricultural Engineering, Vol. 31, No. 7, pp. 334-340, 1950

21. Gutyar, E. M., "*Radial slip of V-belts*," *Vestnik Mashinostroenia* (Soviet Engineering Research), Vol. 39, No. 8, pp. 26-31, 1959

22. Amijima, S., "*Some problems associated with the friction between belt and pulley*," The science and engineering review of Doshisha University, Vol. 3, Nos. 3/4, pp. 9-21, 1962

23. Gerbert, G., "*Belt Slip-A Unified Approach*," ASME Journal of Mechanical Design, Vol. 118, No. 3, pp. 432-438, 1996

24. Gerbert, G., "*Force and Slip Behavior in V-belt Drives*," No. 67 in Mechanical Engineering Series, Acta Polytechnica Scandinavica, Lund Technical University, Lund, Sweden, 1972

25. Gerbert, G., "*Skew V-belt pulleys*," In Proceedings of International Conference on Continuously Variable Power Transmission, Paper No. 101 (9636259), pp. 1-9, Japanese Society of Automotive Engineers, September 11-12, Yokohama, Japan, 1996

26. Ciavatti, V., Dragoni, E., Strozzi, A., "*Mechanical analysis of an annular plate transversely loaded at an arbitrary point by a concentrated force*," Trans. ASME, Journal of Mechanical Design, Vol. 114, No. 3, pp. 335-342, 1992

27. Sorge, F., "*A Qualitative-Quantitative Approach to V-belt Mechanics*," ASME Journal of Mechanical Design, Vol. 118, pp. 15-21, 1996

28. Worley, W. S., Dolan, J. P., "*Closed-form approximations to the solution of V-belt force and slip equations*," Trans. ASME, Journal of Mechanical Design, Vol. 107, No. 2, pp. 292-300, 1985

29. Sorge, F., "*Transient Mechanics of V-belt Variators*," 2004 International Continuously Variable and Hybrid Transmission Congress, Paper No. 04CVT-45, September 23 – 25, San Francisco, USA, 2004

30. Gerbert, G., Sorge, F., "*Full Sliding Adhesive-Like Contact of V-belts*," Trans. ASME, Journal of Mechanical Design, Vol. 124, No. 4, pp.706-712, 2002

31. Sorge, F., "*Influence of Pulley Bending on Metal V-Belt Mechanics*," In Proceedings of International Conference on Continuously Variable Power Transmission, Paper No. 102 (9636268), pp. 9-15, Japanese Society of Automotive Engineers, September 11-12, Yokohama, Japan, 1996

32. Robertson, A. J., Tawi, K. B.., "*Misalignment equation for the Van Doorne metal pushing V-belt continuously variable transmission*," Proc. IMechE, Part D, Vol. 211, pp. 121-128, 1991

33. Sattler, H., "*Efficiency of Metal Chain and V-belt CVT*," Int. Congress on Continuously Variable Power Transmission CVT' 99, pp. 99-104, September 16-17, Eindhoven, The Netherlands, 1999

34. Micklem J. D., Longmore D. K., Burrows C. R., "*Modelling of the Van Doorne, metal V-belt, continuously variable transmission system*," JSME Conference on Motion and Power Transmissions, Paper No. 3C2, pp. 400-404, Hiroshima, Japan, 1991

35. Gerbert G., "*Metal V-belt Mechanics*," ASME paper 84-DET-227, presented at Design Engineering Technology Conference (Conference Code: 05902), 1984

36. Karam, A., Play, D., "*A Discrete Analysis of Metal V-belt Drive*," Trans. ASME, International Power Transmission and Gearing Conference, DE-Vol. 43-1, pp. 319-327, 1992

37. Asayama H., Kawai J., Tonohata A., Adachi M., "*Mechanism of metal pushing belt*," JSAE Review, volume 16, pp. 137-143, 1995

38. Kim H., Lee J., "*Analysis of Belt Behavior and Slip Characteristics for a Metal V-Belt CVT*," Mechanism & Machine Theory, Vol. 29, No. 6, pp. 865-876, 1994

39. Lee H., Kim H., "*Analysis of Primary and Secondary Thrust for a metal CVT Part 1: New Formula for Speed Ratio-Torque-Thrust Relationship Considering Band Tension and Block Compression*," SAE Paper, 2000-01-0841, SAE special publication (SP-1522), Transmission and Driveline Symposium 2000, pp. 117-125

40. Choi, Byung-Dae, and Kim, Hyun-Soo, "*Analysis of Belt Behavior for an Automotive V-belt CVT*," SAE Paper No. 912482, pp. 263-269, 1991

41. Sun D. C., "*Performance analysis of a variable speed-ratio metal V-belt drive*," Trans. ASME, Mechanisms, Transmission and Automotive Design, V110, pp 472-481, 1988

42. Massouros, G., "*Elastic Creep Velocity of V-Belts*," ASME Spring National Design Engineering Conf. And Show, Chicago, USA, Paper 87-DE-10, March 1987

43. Kobayashi D., Mabuchi Y., Katoh Y., "*A study on the Torque Capacity of a Metal Pushing V-belt for CVTs*," SAE Paper 980822, 1998

44. Shimizu H., Kobayashi D., Kawashima J., Kato Y., "*Development of 3-D Simulation for Analyzing the Dynamic Behavior of a Metal Pushing V-Belt for CVTs*," SAE Paper No. 2000-01-0828, SAE special publication (SP-1522), Transmission and Driveline Symposium 2000, pp. 31-36

45. Browne, V. D., "*Metal Belt CVT's – Torque Capacity*," ASME Proceedings of the International Power Transmission and Gearing Conference, Vol. 7, pp. 453-457, October 6-9, 1996

46. Bonsen, B., Klaassen, T. W. G. L., van de Meerakker, K. G. O., Steinbuch, M., Veenhuizen, P. A., "*Analysis of Slip in a Continuously Variable Transmission*," Proceedings of IMECE' 03, 2003 ASME International Mechanical Engineering Congress, Paper No. IMECE2003-41360, November 15-21, 2003

47. Amijima, S., Fujii, T., Matsuoka, H. and Ikeda, E., "*Study on axial force and its distribution of a new CVT belt for cars*," Int. J. of Vehicle Design, Vol. 13, No. 2, pp. 168-181, 1992

48. Sferra, D., Pennestri, E., Valentini, P. P., and Baldascini, F., "*Dynamic Simulation of a Metal-Belt CVT Under Transient Conditions*," Proceedings of the DETC02, 2002 ASME Design Engineering Technical Conference, Paper No. DETC02/MECH-34228, Vol. 5A, pp. 261-268, September 29-October 2, Montreal, Canada, 2002

49. Chung, Y. Y., Sung, C. K., "*The Contact Behavior of a Rubber V-belt Drive*," In Proceedings of International Conference on Continuously Variable Power Transmission, Paper No. 201 (9636376), Japanese Society of Automotive Engineers, September 11-12, Yokohama, Japan, 1996

50. Ide, T., Tanaka, H., "*Contact Force Distribution between Pulley Sheave and Metal Pushing V-belt*," Proceedings of CVT 2002 Congress, VDI-Berichte, Vol. 1709, pp. 343-355, Düsseldorf, Germany, 2002

51. Ferrando, F., Martin, F., Riba, C., "*Axial Force Test and Modelling of the V-belt Continuously Variable Transmission for Mopeds*," Trans. ASME, Journal of Mechanical Design, Vol. 118, pp. 266-273, June 1996

52. Worley, W. S., "*Designing Adjustable Speed V-belt Drives for Farm Implements*," SAE Transactions, Vol. 63, pp. 321-333, 1955

53. Gerbert, G., "*Some notes on V-belt drives*," Trans. ASME, Journal of Mechanical Design, Vol. 103, No. 1, pp. 8-18, 1981

54. Bullinger, M., Pfeiffer, F., "*An elastic model of a metal V-belt CVT*," Proc. Appl. Math. Mech. (PAMM), Vol. 2, pp. 112-113, 2003

55. Carbone, G., Mangialardi, L., Mantriota, G., "*Theoretical Model of Metal V-belt Drives during Rapid Ratio Changing*," Trans. ASME, Journal of Mechanical Design, Vol. 123, pp. 111-117, March 2001

56. Carbone, G., Mangialardi, L., Mantriota, G., "*Influence of Clearance between plates in metal pushing V-belt dynamics*," Trans. ASME, Journal of Mechanical Design, Vol. 124, pp. 543-557, September 2002

57. Carbone, G., Mangialardi, L., "*CVT Behavior in "Slip Mode" and "Creep Mode" Phases*," Proceedings of CVT 2002 Congress, VDI-Berichte, Vol. 1709, pp. 357-369, Düsseldorf, Germany, 2002

58. Carbone, G., Mangialardi, L., Mantriota, G., "*EHL visco-plastic friction model in CVT shifting behaviour*," International Journal of Vehicle Design, Vol. 32, Nos. 3/4, pp. 333-357, 2003

59. Carbone, G., Mangialardi, L., Mantriota, G., "*The Influence of Pulley Deformations on the Shifting Mechanism of Metal Belt CVT*," Trans. ASME, Journal of Mechanical Design, Vol. 127, pp. 103-113, January 2005

60. Fujii, T., Kurokawa, T., Kanehara, S., "*A Study of a Metal Pushing V-Belt type CVT, Part 1: Relationship between Transmitted Torque and Pulley Thrust*," SAE Transactions, Paper 930666, pp. 989-999, 1993

61. Fujii, T., Kurokawa, T., Kanehara, S., "*A Study of a Metal Pushing V-Belt Type CVT Part 2: Compression Force Between Metal Blocks and Ring Tension*," SAE Transactions, Paper 930667, pp. 1000-1009, 1993

62. Kanehara, S., Fujii, T., Kitagawa, T., "*A Study of a Metal Pushing V-Belt Type CVT (Part 3: What Forces Act on Metal Blocks?)*", SAE Transactions, Paper 940735, pp. 942-952, 1994

63. Fushimi, Y., Kanehara, S., Fujii, T., "*A Numerical Approach to Analyze the Power Transmitting Mechanisms of a Metal Pushing V-Belt Type CVT,*" SAE Transactions, Paper 960720, pp. 161-172, 1996

64. Kitagawa, T., Fujii, T., Kanehara, S., "*A study of a Metal Pushing V-Belt Type CVT (Part 4: Forces Act on Metal Blocks when the Speed Ratio is Changing)*," SAE Transactions, Paper 950671, pp. 1344-1353, 1995

65. Kuwabara, S., Fujii, T., Kanehara, S., "*Power Transmitting Mechanism of CVT Using a Metal V-Belt and Load Distribution in the Steel Ring*," SAE Transactions, Paper 980824, 1998

66. Katsuya, A., Sato, T., and Kurimoto, K., "*An Analytical Study on the Behavior of CVT Belt (in Japanese)*," Proceedings of Japanese Society of Automotive Engineers (JSAE), Paper No. 891041, 1989

67. Kanehara, S., Fujii, T., Oono, S., "*A study on a Metal Pushing V-Belt Type CVT Macroscopic Consideration for Coefficients of Friction between Belt and Pulley*," International Conference on Continuously Variable Power Transmissions, CVT'96, Paper No. 9636277, pp. 15-22, September 11-12, Yokohama, Japan, 1996

68. Kanehara, S., Fujii, T., Fujimura, O., "*Characterization of a CVT using a Metal V-Belt at Transitional States*," International Conference on Continuously Variable Power Transmissions, CVT'99, pp. 58-64, September 16-17, Eindhoven, The Netherlands, 1999

69. Fujimura, O., Okubo, K., Fujii, T., Kanehara, S., "*Shifting Mechanism and Variation of Frictional Coefficients for CVT using Metal Pushing V-Belts*," SAE Paper 2000-01-0840, SAE special publication (SP-1522), Transmission and Driveline Symposium, pp. 107-116, 2000

70. Kataoka, R.,, Okubo, K., Fujii, T., Kanehara, S., "*A Study on a Metal Pushing V-belt type CVT – A Novel Approach to Characterize the Friction between Blocks and a Pulley, and Shifting Mechanisms*," SAE Transactions, Paper No. 2002-01-0697, pp. 49-59, 2002

71. Miyawaza, T., Fujii, T., Nonaka, K., Takahashi, M., "*Power Transmitting Mechanism of a Dry Hybrid V-Belt for a CVT – Advanced Numerical Model Considering Block Tilting and Pulley Deformation*," SAE Transactions, Paper No. 1999-01-0751, pp. 143-153, 1999

72. Shieh, C. J., Chen, W. H., "*Three-Dimensional Finite Element Analysis of Frictional Contact for Belt Transmission Systems*," The Chinese Journal of Mechanics, Vol. 17, No. 4, pp. 189-199, December 2001

73. Chen, W. H., Yeh, J. T., "*Three-Dimensional Finite Element Analysis of Static and Dynamic Contact Problems with Friction*," Computers and Structures, Vol. 35, No. 5, pp. 541-552, 1990

74. Wilson, E. L., Taylor, R. L., Doherty, W. P., Ghaboussi, J., "*Incompatible Displacement Modes*," in Numerical and Computer Methods in Structural Mechanics, pp. 43-57, 1973

75. Shieh, C. J., Chen, W. H., "*Effect of angular speed on behavior of a V-belt drive system*," International Journal of Mechanical Sciences, Vol. 44, pp. 1879-1892, 2002

76. Srivastava, N., Haque, I., "*On the transient dynamics of a metal pushing V-belt CVT at high speeds*," International Journal of Vehicle Design, Vol. 37, No. 1, pp. 46-66, 2005

77. Srivastava, N., Blouin, V. Y., Haque, I. U., "*Using Genetic Algorithms to Identify Initial Operating Conditions for a Transient CVT Model*," 2004 ASME International Mechanical Engineering Congress, Paper No. IMECE2004-61999, November 13-19, Anaheim, CA, USA, 2004

78. Srivastava, N., Haque, I. U., "*On the operating regime of a metal pushing V-belt CVT under steady state microslip conditions*," 2004 International Continuously Variable and Hybrid Transmission Congress, Paper No. 2004-34-2851, September 23 – 25, San Francisco, USA, 2004

79. Hsieh, L., and Yan, H., "*On the Mechanical Efficiency of Continuously Variable Transmissions with Planetary Gear Trains*," International Journal of Vehicle Design, Vol. 11, No. 2, pp. 177-187, 1990

80. Huang, Y. M., and Hu, B. S., "*Minimum Fuel Consumption and CO Emission and Optimum Speed of the Motorcycle with a CVT*," Journal of Energy Resources Technology, Vol. 125, Issue 4, pp. 311-317, December 2003

81. Hanachi, S., "*A study of the Dynamics of a Split-Torque, Geared-Neutral Transmission Mechanism*," ASME Journal of Mechanical Design, Vol. 112, No. 3, pp. 261-270, 1990

82. Vahabzadeh, H., and Linzell, S. M., "*Modeling, Simulation, and Control Implementation for a Split-Torque, Geared Neutral, Infinitely Variable Transmission*," SAE Transactions, Paper No. 910409, Vol. 100, Section 6, pp. 546-557, 1991

83. Mucino, V. H., Smith, J. E., Cowan, B., and Kmicikiewicz, M., "*A Continuously Variable Power Split Transmission for Automotive Applications*," SAE Special Publications, Paper No. 970687, Vol. 1241, pp. 75-80, 1997

84. Kluger, M. A., Long, D. M., "*An Overview of Current Automatic, Manual and Continuously Variable Transmission Efficiencies and Their Projected Future Improvements*," SAE Transactions, Paper No. 1999-01-1259, pp. 653-658, 1999

85. Kluger, M. A., Fussner, D. A., "*An Overview of Current CVT Mechanisms, Forces and Efficiencies*," SAE Transmission and Driveline Systems Symposium (SP-1241), Paper No. 970688, pp. 81-88, Detroit, MI, USA, 1997

86. Singh, T., Nair, S. S., "*A Mathematical Review and Comparison of Continuously Variable Transmissions*," SAE Transactions, Paper No. 922107, pp. 1-10, 1992

87. Gerbert, G., "*New Arc Correction Factors in V-Belt Transmission Design*," Proc. of the 1989 Int. Power Transmission and Gearing Conf., Chicago, IL, pp. 71-80, April 25-28, 1989

88. Micklem J. D., Longmore D. K., Burrows C. R., "*Belt Torque Losses in a Steel V-belt Continuously Variable Transmission*," Proceedings Inst. Mech. Engineers Part D, Vol. 208, pp. 91-97, 1993

89. Saito, T., "*Development of Metal Pushing V-Belt Stress Simulation for CVT*," Proceedings of CVT 2002 Congress, VDI-Berichte, Vol. 1709, pp. 371-381, Düsseldorf, Germany, 2002

90. Childs, T.H.C., Cowburn, D., "*Power Transmission Losses in V-Belt Drives Part 1: Mismatched Belt and Pulley Groove Wedge Angle Effects*," Proc. Instn. Mech. Engineers, Vol. 201, No. D1, pp 33-40, 1987

91. Childs, T.H.C., Cowburn, D., "*Power Transmission Losses in V-Belt Drives Part 2: Effects of Small Pulley Radii*," Proc. Instn. Mech. Engineers, Vol. 201, No. D1, pp 41-53, 1987

92. Abo, K., Takahara, H., "*Heat Generation of a Metal V-belt for CVTs*," Int. Congress on Continuously Variable Power Transmission CVT'99, pp. 148-152, September 16-17, Eindhoven, The Netherlands, 1999

93. Peiffer, R., Kraneburg, P., "*Functionality of New CVTs – the Fluid Question*," Int. Congress on Continuously Variable Power Transmission CVT'99, pp. 172-176, September 16-17, Eindhoven, The Netherlands, 1999

94. Narita, K., Deshimaru, J., Kato, M., "*The Influence of Lubricating Oil on the Performance of a Metal V-Belt-Type Continuously Variable Transmission*," Lubrication Science, Vol. 16, No. 2, pp. 139-151, February 2004

95. Yue, G., "*Belt Vibration Considering Moving Contact between Belt and Pulley*," JSME Conference on Motion and Power Transmissions, Paper No. 4C1, pp. 411-416, November 23-26, Hiroshima, Japan, 1991

96. Kong, L., Parker, R. G., "*Vibration of an axially moving beam wrapping on fixed pulleys*," Journal of Sound and Vibration, Vol. 280, pp. 1066-1074, 2005

97. Thurman, A. L., Mote Jr. , C. D., "*Free, Periodic, Nonlinear Oscillation of an Axially Moving Strip*," Trans. of ASME, Journal of Applied Mechanics, Vol. 36, pp. 83-91, March 1969

98. Chung, Y. Y., and Sung, C. K., "*Belt Vibration of a Continuously Variable Transmission (CVT) during Speed-Ratio Change*," Journal of Chinese Society of Mechanical Engineers, Vol. 18, No. 5, pp. 407-414, 1997

99. Wasfy, T. M., Leamy, M., "*Effect of bending stiffness on the dynamic and the steady-state responses of belt-drives*," Proceedings of DETC'02, ASME 2002 Design Engineering Technical Conferences, Paper No. DETC2002/MECH-34223, pp. 217-224, September 29- October 2, Montreal, Canada, 2002

100. Leamy, M. J., Barber, J. R., Perkins, N. C., "*Dynamics of Belt/Pulley Frictional Contact*," IUTAM Symposium on Unilateral Multibody Contacts, pp. 277-286, August 3-7, Munich, Germany, 1998

101. Moon, J., Wickert, J. A., "*Radial Boundary Vibration of Misaligned V-Belt Drives*," Journal of Sound and Vibration, Vol. 225, No. 3, pp. 527-541, 1999

102. Moon, J., Wickert, J. A., "*Non-linear vibration of power transmission belts*," Journal of Sound and Vibration, Vol. 200, pp. 419-431, 1997

103. Abrate, S., "*Vibrations of belts and belt drives*," Mech. Machine Theory, Vol. 27, No. 6, pp. 645-659, 1992

104. Abrate, S., "*Noise and Vibration in Power Transmission Belts*," SAE Paper No. 860428, pp. 12-21, 1986

105. Lebrecht, W., Pfeiffer, F., and Ulbrich, H., "*Analysis of self-induced vibrations in a pushing V-belt CVT*," 2004 International Continuously Variable and Hybrid Transmission Congress, Paper No. 04CVT-32, September 23 – 25, San Francisco, USA, 2004

106. Takemoto, Y., Imamura, K., Shozaki, A., Yoneda, Y., Hiraoka, M., "*Noise Reduction on Continuously Variable Transmission*," Proceedings of the 16th International Modal Analysis Conference, pp. 855-861, February 2-5, Santa Barbara, CA, USA, 1998

107. "*Continuous Variable Transmission – CVT*," accessed on October 16, 2006, http://cvt.com.sapo.pt/toc_en.htm

108. Takiyama, T., Morita, S., "*Analysis of improvement of fuel consumption by Engine-CVT consolidated control*," Proc. of AVEC'96, International Symposium on Advanced Vehicle Control, pp. 1159-1167, June 1996

109. Takiyama, T., "*Engine-CVT-A/F consolidated control using decoupling control theory*," JSAE Review, Vol. 22, No. 1, pp. 9-14, January 2001

110. Sakaguchi, S., Kimura, E., Yamamoto, K., "*Development of an Engine-CVT Integrated Control System*," SAE Special Publications (SP-1440), Transmission and Driveline Symposium, Paper No. 1999-01-0754, pp. 171-179, 1999

111. Yasuoka, M., Uchida, M., Katakura, S., Yoshino, T., "*An Integrated Control Algorithm for an SI Engine and a CVT*," SAE Special Publications (SP-1440), Transmission and Driveline Symposium, Paper No. 1999-01-0752, pp. 155-160, 1999

112. Kim, T., Kim, H., "*Performance of an Integrated Engine-CVT Control, Considering Powertrain Loss and CVT Response Lag*," Proceedings of IMechE Part D: Journal of Automobile Engineering, Vol. 216, No. 7, pp. 545-553, July 2002

113. Yeo, H., Song, C. H., Kim, C. S., Kim, H. S., "*Hardware in the loop simulation of hybrid vehicle for optimal engine operation by CVT ratio control*," International Journal of Automotive Technology, Vol. 5, No. 3, pp. 201-208, 2004

114. Bonsen, B., Pulles, R. J., Simons, S. W. H., Steinbuch, M., Veenhuizen, P. A., "*Implementation of a slip controlled CVT in a production vehicle*," IEEE Conference on Control Applications, Toronto, Canada, 2005

115. Bonsen, B., Klaassen, T. W. G. L., Pulles, R. J., Simons, S. W. H., Steinbuch, M., Veenhuizen, P. A., "*Performance optimization of the push-belt CVT by variator slip control*," International Journal of Vehicle Design, Vol. 39, No. 3, pp. 232-256, 2005

116. Saito, T., Lewis, A. D., "*Development of a Simulation Technique for CVT Metal Pushing V-Belt with Feedback Control*," SAE Transmissions and Driveline Symposium, Paper No. 2004-01-1326, pp. 353-359, March 2004

117. Setlur, P., Wagner, J., Dawson, D., and Samuels, B., "*Nonlinear Control of a Continuously Variable Transmission for Hybrid Vehicle Powertrains*," Proceedings of the American Controls Conference, pp. 1304-1309, June 25-27, Arlington, VA, 2001

118. Kim, T., Kim, H., Yi, J., and Cho, H., "*Ratio Control of Metal Belt CVT*," SAE Paper No. 2000-01-0842, 2000

119. Pfiffner, R., Guzzella, L., Onder, C. H., "*A Control-Oriented CVT Model with Nonzero Belt Mass*," Trans. of ASME, Journal of Dynamic Systems, Measurement, and Control, Vol. 124, pp.481-484, 2002

120. Pfiffner, R., Guzzella, L., "*Optimal Operation of CVT-Based Powertrains*," International Journal of Robust Nonlinear Control, Vol. 11, No. 11, pp. 1003-1021, 2001

121. Fawcett, J. N., "*Chain and Belt Drives – A Review*," Shock and Vibration Digest, Vol. 13, No. 5, pp. 5-12, 1981

122. Srnik, J., Pfeiffer, F., "*Simulation of a CVT Chain Drive as a Multibody System with Variant Structure*," Proceedings of the 1st Joint Conference of International Simulation Societies, pp. 241-245, August 22-25, Zurich, Switzerland, 1995

123. Srnik, J., Pfeiffer, F., "*Dynamics of CVT Chain Drives: Mechanical Model and Verification*," Proceedings of DETC'97, 1997 ASME Design Engineering Technical Conferences, Paper No. DETC97/VIB-4127, September 14-17, Sacramento, CA, USA, 1997

124. Fritz, P., Pfeiffer, F., "*Dynamics of High Speed Roller Chain Drives*," DE-Vol. 84-1, 1995 ASME Design Engineering Technical Conferences, Volume 3- Part A, pp. 573-584, September 17-21, Boston, MA, USA, 1995

125. Pfeiffer, F., Glocker, C., "*Multibody Dynamics with Unilateral Contacts*," Wiley-Interscience, June 1, 1996. ISBN: 0471155659

126. Pfeiffer, F., Sedlmayr, M., "*Spatial Motion of CVT Chains*," Proceedings of IUTAM Symposium on chaotic dynamics and control of systems and processes in mechanics, pp. 81-95, June 8-13, Rome, Italy, 2003

127. Sedlmayr, M., Bullinger, M., Pfeiffer, F., "*Spatial Dynamics of CVT Chain Drives*," Proceedings of CVT 2002 Congress, VDI-Berichte, Vol. 1709, pp. 511-552, Düsseldorf, Germany, 2002

128. Pfeiffer, F., Sedlmayr, M., "*Spatial Contact Mechanics of CVT Chain Drives*," Proceedings of DETC'01, ASME 2001 Design Engineering Technical Conference, Paper No. DETC2001/VIB-21511, pp. 1789-1795, September 9-12, Pittsburgh, PA, USA, 2001

129. Pfeiffer, F., Sedlmayr, M., "*Force reduction in CVT Chains*," Int. J. of Vehicle Design, Vol. 32, Nos. 3/4, pp. 290-303, 2003

130. Pfeiffer, F., Lebrecht, W., Geier, T., "*State-of-the-Art of CVT-Modelling*," 2004 International Continuously Variable and Hybrid Transmission Congress, Paper No. 04CVT-46, September 23 – 25, San Francisco, USA, 2004

131. Pausch, M., Pfeiffer, F., "*Nonlinear Dynamics of a chain drive CVT*," Proceedings of the 3rd international conference on nonlinear mechanics, pp. 336-341, August 1998

132. Maier, S. K., Pfeiffer, F., "*CVT Gear Noise in the Hybrid Car Drive Train*," Proceedings of DETC'01, ASME 2001 Design Engineering Technical Conference, Paper No. DETC2001/VIB-21506, pp. 1747-1753, September 9-12, Pittsburgh, PA, USA, 2001

133. Stepanenko, Y., Sankar, T. S., "*Vibro-impact analysis of control systems with mechanical clearance and its application to robotic actuators*," Trans. of ASME, Journal of Dynamic Systems, Measurement and Control, Vol. 108, No. 1, pp. 9-16, March 1986

134. Tenberge, P., "*Efficiency of Chain-CVTs at Constant and Variable Ratio: A new mathematical model for a very fast calculation of chain forces, clamping forces, clamping ratio, slip, and efficiency*," 2004 International Continuously Variable and Hybrid Transmission Congress, Paper No. 04CVT-35, September 23 – 25, San Francisco, USA, 2004

135. Canudas de Wit, C., Olsson. H., Åström, K. J., Lischinsky, P., "*Dynamic friction models and control design*," Proceedings of the 1993 American Control Conference, pp. 1920-1926, San Francisco, California, USA, 1993

136. Togai, K., Takeuchi, T., "*CVT Drive Train Vibration Analysis and Active Control System Design*," Mitsubishi Motors Technical Review, No. 17, pp. 11-22, 2005

137. Leine, R. I., Van Campen, D. H., De Kraker, A., and Van Den Steen, L., "*Stick-slip vibrations induced by alternate friction models*," Nonlinear Dynamics, Vol. 16, No. 1, pp. 41-54, 1998

138. Friedland, B., Haessig Jr., D. A., "*On the Modeling and Simulation of Friction*," Journal of Dynamic Systems, Measurement, and Control, Vol. 113, No. 3, pp. 354-362, September 1991

139. Hess, D. P., Soom, A., "*Friction at a lubricated line contact operating at oscillating sliding velocities*," Journal of Tribology, Vol. 112, No. 1, pp. 147-152, 1990

140. Bliman, P. -A., Sorine, M., "*Friction modelling by hysteresis operators: application to Dahl, Stiction, and Stribeck effects*," Proceedings of the Conference "Models of Hysteresis", Trento, Italy, 1991

141. Armstrong-Hélouvry, B., Dupont, P., and Canudas de Wit, C., "*A survey of models, analysis tools, and compensation methods for the control of machines with friction*," Automatica, Vol. 30, No. 7, pp. 1083-1138, 1994

142. Filippov, A. F., "*Differential Equations with Discontinuous Righthand Sides*," Kluwer Academic Publishers, 1988. ISBN: 902772699X

143. Leine, R., Nijmeijer, H., "*Dynamics and Bifurcations of Non-Smooth Mechanical Systems*," Lecture Notes in Applied and Computational Mechanics, Vol. 18, Springer, 2004. ISBN: 3540219870

144. Stewart, D. E., and Trinkle, J. C., "*An implicit time-stepping scheme for rigid body dynamics with inelastic collisions and Coulomb friction*," International Journal for Numerical Methods in Engineering, Vol. 39, No. 15, pp. 2673-2691, 1996

145. Anitescu, M., and Potra, F. A., "*Formulating dynamic multi-rigid-body contact problems with friction as solvable linear complementarity problems*," Nonlinear Dynamics, Vol. 14, No. 3, pp. 231-247, 1997

146. Simo, J. C., and Laursen, T. A., "*An Augmented Lagrangian treatment of contact problems involving friction*," Computers and Structures, Vol. 42, Issue 1, pp. 97-116, 1992

147. Murty, K. G., "*Linear Complementarity, Linear and Nonlinear Programming*," Vol. 3 of Sigma Series in Applied Mathematics, Heldermann Verlag, Berlin, 1988

148. Dankowicz, H., and Nordmark, A. B., "*On the origin and bifurcations of stick-slip oscillations*," Physica D, Vol. 136, No. 3, pp. 280-302, 2000

149. Stelter, P., and Sextro, W., "*Bifurcations in dynamical systems with dry friction*," International Series of Numerical Mathematics, Vol. 97, pp. 343-347, 1991

150. Ibrahim, R. A., "*Friction-Induced Vibration, Chatter, Squeal, and Chaos, Part I: Mechanics of Contact and Friction*," ASME Applied Mechanics Reviews, Vol. 47, No. 7, pp. 209-226, 1994

151. Ibrahim, R. A., "*Friction-Induced Vibration, Chatter, Squeal, and Chaos, Part II: Modeling and Dynamics*," ASME Applied Mechanics Reviews, Vol. 47, No. 7, pp. 227-253, 1994

152. Awrejcewicz, J. and Delfs, J., "*Dynamics of a self-excited stick-slip oscillator with two-degrees-of-freedom. Part II: Slip-stick, slip-slip, stick-slip transitions, periodic and chaotic orbits*," European Journal of Mechanics A. Solids, Vol. 9, No. 5, pp. 397-418, 1990

153. Galvanetto, U., "*Bifurcations and Chaos in a Four-Dimensional Mechanical System with Dry Friction*," Journal of Sound and Vibration, Vol. 204, No. 4, pp. 690-695, 1997

154. Moon, F. C., "*Chaotic Vibrations: An Introduction for Applied Scientists and Engineers*," Wiley-Interscience, June 2004. ISBN: 0471679089

155. Slotine, J. J., Li, W., "*Applied Nonlinear Control*," Prentice Hall, October 1990. ISBN: 0130408905

156. Parker, T. S., and Chua, L. O., "*Practical Numerical Algorithms for Chaotic Systems*," Springer-Verlag, September 1989. ISBN: 0387966887

157. Wolf, A., Swift, J. B., Swinney, H. L., and Vastano, J. A., "*Determining Lyapunov exponents from a time series*," Physica D, Vol. 16, pp. 285-317, 1985

158. Müller, P. C., "*Calculation of Lyapunov exponents for dynamic systems with discontinuities*," Chaos, Solitons and Fractals, Vol. 5, No. 9, pp. 1671-1681, 1995

159. Awrejcewicz, J., and Lamarque, Claude-Henri, "*Bifurcation and Chaos in Nonsmooth Mechanical Systems*," World Scientific Series on Nonlinear Science, Series A, Vol. 45, 2003. ISBN: 9812384596

160. Awrejcewicz, J., "*Bifurcation and Chaos in Coupled Oscillators*," World Scientific, June 1991. ISBN: 9810205791

161. Wiercigroch, M., and De Kraker, B., "*Applied Nonlinear Dynamics and Chaos of Mechanical Systems with Discontinuities*," World Scientific Series on Nonlinear Science, Series A, Vol. 28, 2000. ISBN: 9810229275

162. Srivastava, N., Miao, Y., Haque, I., "*Influence of Clearance on the Dynamics of Chain CVT Drives*," 2006 ASME International Mechanical Engineering Congress, Paper No. IMECE2006-14059, November 5-10, Chicago, IL, USA, 2006

163. Srivastava, N., Haque, I., "*Transient dynamics of metal V-belt CVT: Effects of pulley flexibility and friction characteristic*," ASME Journal of Computation and Nonlinear Dynamics, Paper No. CND-06-1084, 2006

164. Srivastava, N., Haque, I., "*Transient dynamics of metal V-belt CVT: Effects of band pack slip and friction characteristic*," Journal of Mechanism and Machine Theory, 2006 (*under review*)

165. Gohar, Ramsey, "*Elastohydrodynamics,*" World Scientific Publishing Co., 2nd edition, 2002. ISBN: 1860941702

166. Srivastava, N., "*Dynamic modeling of slip in a metal pushing V-belt CVT*," Clemson University, Department of Mechanical Engineering, M.S. Thesis, December 2002

167. Zakhariev, E., "*Dynamics of Rigid Multibody Systems with Clearances in the joints*," Mechanics of Structures and Machines, Vol. 27, No. 1, pp. 63-87, February 1999

168. Flores, P., Ambrosio, J., Claro, J. C. P., Lankarani, H. M., Koshy, C. S., "*A study on dynamics of mechanical systems including joints with clearance and lubrication*," Mechanism and Machine Theory, Vol. 41, No. 3, pp. 247-261, March 2006

169. Bauchau, O. A., Rodriguez, J., "*Modeling of joints with clearance in flexible multibody systems*," International Journal of Solids and Structures, Vol. 39, No. 1, pp. 41-63, December 2002

170. Amirouche, F. M. L., Jia, T., "*Modelling of clearances and joint flexibility effects in multibody systems dynamics*," Computers and Structures, Vol. 29, No. 6, pp. 983-991, 1988